FEASIBILITY OF *IN-SITU* REMOVAL OF HEAVY METALS BY ELECTROREMEDIATION OF OFFSHORE MUDS

by

Muhammad Haroun

A Dissertation Presented to the
FACULTY OF THE GRADUATE SCHOOL
UNIVERSITY OF SOUTHERN CALIFORNIA
In Partial Fulfillment of the
Requirements for the Degree
DOCTOR OF PHILOSOPHY
(ENVIRONMENTAL ENGINEERING)

August 2009

Dedication

For the *late,* Malak Kabara, *may she rest in peace*,
One of the first female lawyers in the Arab World.
A pioneer in her field and in the region.
My grandmother.

For, Sahar Al Halabi,
The UAE's first practicing Architect.
A self-made woman, who is respected and looked up to by peers,
Whose dreams have been translated into tall and proud structures.
For my mother, for pushing me to build my own dream.

For the memory of the late H.H. Sheikh Zayed bin Sultan Al Nahyan, *may he rest in peace*,
The founder and first president of the U.A.E. who has embraced education and technology based on his tremendous vision, for all the citizens of the U.A.E.
Our Founder and Father.

You have been instrumental in my life, my drive and my ambition.
I have always looked up to you and always will.

I would also like to dedicate this to four distinguished U.A.E. statesmen, H.H. Sheikh Khalifa bin Zayed Al Nahyan, the president of the U.A.E. and H.H. Sheikh Mohamed bin Zayed Al Nahyan, the Crown Prince of Abu Dhabi and Deputy Supreme Commander of the UAE Armed Forces, H.E. Ahmad Khalifa Al Suwaidi and H.E. Youssef Omeir Al Youssef, all have supplied me with uninterrupted support to reach the highest levels of education.

Acknowledgements

My thanks for their help and support. This Doctoral Dissertation would not have been possible without the support and guidance of three groups of individuals: my family; my professors at USC and Lehigh, and my friends and supervisors in the U.A.E.

First and foremost, my family, without, whom this would not have been possible.

For her inspiration, my late grandmother, Malak Kabbara, one of the first female practicing lawyers in the Arab world. She was the first person in my life that kept on pushing me hardest and further into the biggest challenges while reminding me that one has to make a positive change in this world.

For his motivation, my late grandfather, Dr. Mohammed Saeed Al Halabi, who was the first U.A.E. practicing surgeon since the late sixties.

For her unwavering support, my mother, Sahar Al Halabi, who was the first practicing Architect from the U.A.E., she always been a big source of inspiration and motivation. The sacrifices of my mother, and prayers were the main driving force behind this effort,

For the rest of the women in my family, my sister Reem and aunt Maha. Not only has their support and encouragement been instrumental in concluding this phase of my life, but being given the opportunity to look up to so many strong women in my life, and so

close to my path only reinforced in me the need to push and strive to better myself and set my aims higher.

For my Uncle Hamdi, whose words of wisdom have helped guide me.

I would like to acknowledge the continuous support and guidance of my PhD committee members, Dr. Meshkati, Dr. Chilingar, Dr. Ershaghi, and Dr. Pamukcu, for making this Environmental Engineering PhD at USC a reality.

Dr. N. Meshkati has always guided me to organize my thoughts and helped me polish my presentation style. He has advised me on how best to keep digging through my research allowing me to stay on target.

Dr. G.V. Chilingar has always been there at all the oddest times of the day and night with his door open offering me with his generous help, motivation and fuel to feed on my curiosity in the field of Electrokinetics. This research would have never been possible without Dr. Chilingar’s meticulous efforts in preparing me to be an independent thinker while boosting my confidence.

Dr. I. Erhshaghi has provided me with the capability to address all the questions related to electrokinetics and highlight the originality of this work. He has been there for me from the very beginning with the generous guidance to ensure the highest quality of work. He provided me with a clear vision of what is remains to be investigated.

Dr. S. Pamukcu has spent countless hours in enlightening me about electroremediation. She has thoroughly trained me in her lab at Lehigh University, while closely monitoring my lab performance. She provided me with all the necessary apparti developed through her electrokinetic lab.

The help extended by Dr. J. P. Bardet, Chairman of The Sonny Astani Civil and Environmental Engineering at USC, and Dr. T. F. Yen for their motivation and support.

I am also very appreciative for Dr. M. Sahimi, his Ph.D students and lab assistants, who have been very curteous in giving me access to their ICP-MS at the Chemical Engineering labs at USC.

I would like to also extend my thanks and appreciation to everyone at USC Viterbi School of Engineering.

I would also like to extend my appreciation to everyone at The Petroleum Institute, Abu Dhabi, U.A.E. Starting with Dr. M. Ohadi up to the entire Petroleum Engineering faculty, research assistants and technicians, and all my friends at ADNOC including Mr. Rashed Al Zahmi, for all their help and support.

I am also grateful for the full support of the government of the UAE in sponsoring this research work and for establishing the Electrokinetic Research Center (ERC) at the

Petroleum Institute in Abu Dhabi, U.A.E. This technology will result in further breakthrough in the fields of enhanced petroleum recovery, ground stabilization, soil and groundwater remediation, and other possible applications.

Table of Contents

List of Tables

List of Figures

Abstract

The present experimental work is directed towards investigation of the electokinetically-enhanced transport of soil contaminants (specifically heavy metals) in clay media and offshore muds.

The electrokinetic process is an emerging technology for *in-situ* soil decontamination, in which chemical species, both ionic and nonionic, are transported to electrode sites in soil. Electrokinetics refers to movement of water, ions and charged particles relative to one another under the action of an applied direct current electric field. In a porous compact matrix of surface-charged particles such as soil, the pore fluid containing ions are made to flow to the collection sites under the applied electric field (Pamukcu et al., 1993).

Remediation of anthropogenically contaminated clay-soil media were conducted by Dr. Pamukcu at Lehigh University. Experiments of high concentrations of heavy metals in clay-soil media were conducted at the University of Southern California by the writer. Water containing acids were used for pH control.

The EK tests were performed for 24 hrs, and the initial and final concentrations were analyzed using an ICP-MS equipment. The removal efficiency, initial and final pH of slurry at 3 positions was recorded.

The effectiveness of the process demonstrated that up to 99% of initial concentrations of metals can be removed from soil. In this process, the pH and contaminant type was found to influence the removal rather than the electroosmotic flow.

In the absence of pH control mechanisms, the basic conditions developed at the cathode, causing most of the metals to precipitate near the cathode as carbonates and hydroxides. pH adjustment at the cathode appeared to minimize such precipitation and to enhance the removal of some heavy metals.

Applicability of this electrokinetic technology in remediating offshore muds from heavy metals was not evaluated to date. Tests were made using 22 different offshore mud samples from different locations in Abu Dhabi, U.A.E., contaminated with 29 different heavy metals. The experimental work was performed by the writer at the newly-established Electrokinetic laboratories at the Petroleum Institute in Abu Dhabi, U.A.E. In the process it was determined that D.C. current can be used to decontaminate the offshore muds from heavy metals.

Preface: Introduction to Study Area and Heavy Metals in the Environment

Anthropogenic input of toxic contaminants into the environment has lead to detrimental effects to the health of humans and animals. Contamination of soil and ground water is also of great concern. The writer concentrated on inorganic contaminants.

The inorganic group, specifically heavy metals, exist in nature in very small concentrations and are known as trace metals. Certain regions around the world are rich in specific heavy metals present in water, e.g., Arsenic in South East Asia and Strontium in the U.A.E. Certain industries, including oil and gas, petrochemical, mining, metallurgy, landfills, and sewage systems contribute a significant increase in their concentration in soils and offshore muds, in many cases augmenting the concentrations by several orders of magnitude.

Certain heavy metals at low concentrations, however, may benefit life within our ecosystems, e.g., chromium which accelerates the growth of plants. Once the pre-existing trace concentrations are significantly increased, all forms of life are subjected to toxic levels causing detrimental health problems, including cancer.

Among the leading emerging technologies for *in-situ* soil and ground decontamination is Electrokinetics technology. As a result of application of DC current, cations move towards the cathode, whereas anions move towards the anode.

Electrokinetics technology has been proven to be a viable method for environmental restoration, i.e., the removal of soil contaminants *in-situ* (Chilingar et al., 1952-2008; Pamukcu el al., 1991- 2008). The results obtained by the writer for heavy metals confirm the above conclusion. The viability of using this technology to remediate the large volumes of offshore muds of Abu Dhabi, U.A.E., contaminated with heavy metals, appears to be feasible.

In electrobioremediation, a term coined by Professor George V. Chilingar, the function of D.C. current is mainly to drive bacteria and nutrients to considerable distances inside the formation to be treated. Otherwise, bioremediation alone is not as effective because one cannot inject bacteria and nutrients deep enough due to low permeability of soils. Electrobioremediation would be considered in the future testing phases together with the upscaling for pilot tests.

Offshore muds are composed of clays, which are predominantly negatively charged and, therefore, act as storage "sponges" for positively charged heavy metals, which can be absorbed and adsorbed in muds. Offshore muds are being deposited daily across the coastlines worldwide, acting as toxic supply to the marine environment. This is affecting the ecosystem due the suddenly significant concentrations of toxic and carcinogenic compounds, leading to adverse health effects to all the coastline communities. Whereas people whose diet is heavily focused on seafood are the most affected, epidemiological studies conducted are showing evidence that water sources and agriculture are affected by the sudden increase in the heavy metal concentration, leading to detrimental health effects.

Most of the presence of heavy metals present in the offshore muds is due to unregulated industrial discharges and lack of environmental proactive technology. For example, in the Arabian-Persian Gulf area there is a very heavy oil/gas traffic, which contributes heavily to both organic and inorganic contaminations. The increasing health concerns are due to both the industrial toxic and carcinogenic heavy metals. Complex combinations of heavy metals, e.g., strontium plus chromium, leads to bone cancer among other diseases.

The Euphrates and Tigris rivers discharge large volumes of sediments into the Gulf waters that are deposited all across the Gulf on both the Arabian and Iranian coastlines. Together with most refineries and aluminum, petrochemical and desalinization plants, 40% (with projections of up to 70% of the world oil production by 2030) of the daily world oil production is being shipped out continuously through the Gulf. Thus, there exists a critical problem of frequent spills and contaminant discharge into the relatively stagnant large water body. The United Arab Emirates is located at the outlet of the Gulf waters leading to the Arabian Sea at the neck of the Gulf. Abu Dhabi, U.A.E. stretches across the narrowest passage of the Gulf waters across from the straits of Hormoz at the outlet of the Gulf water. Therefore, large quantities of offshore muds are deposited along its coastline. (www.eia.doe.gov).

In addition, the hydrodynamic water current of the Arab-Persian Gulf follows a counterclockwise direction that could be increasing further the contamination by heavy metals of offshore muds. Therefore, Abu Dhabi, U.A.E. was selected as a prime candidate for conducting the World’s first electrokinetic tests to attempt to decontaminate the large quantities of offshore muds from toxic and carcinogenic heavy metals.

Figure PreF-1 A & B: U.A.E. and Arab-Persian Gulf region. (World Atlas)

EUPHRATES

Rising in the Caucasus Mountains of Armenia, it flows southwesterly across west-central Turkey, then generally southeast through Syria and Iraq, ending in the waters of the Persian Gulf.

It joins with the Tigris in southern Iraq, and from that junction continues on as the Shatt al Arab. Overall it's (2,235 miles) (3,596 km) in length, and is certainly the longest river in the Middle East. Historically important in ancient history, the once great city of Babylon stood on its banks.

TIGRIS

Rising in the mountains of southern Turkey, the Tigris flows southeast through Iraq, where in the southern part of that country it merges with the Euphrates to become the Shatt al Arab, which then flows to the Persian Gulf. The river has numerous small tributaries running from it's eastern bank, and is (1,180 miles) (1,899 km) in length.

Figure PreF-2: Map of Euphrates and Tigris river discharge into the Arab-Persian Gulf region (World Atlas).

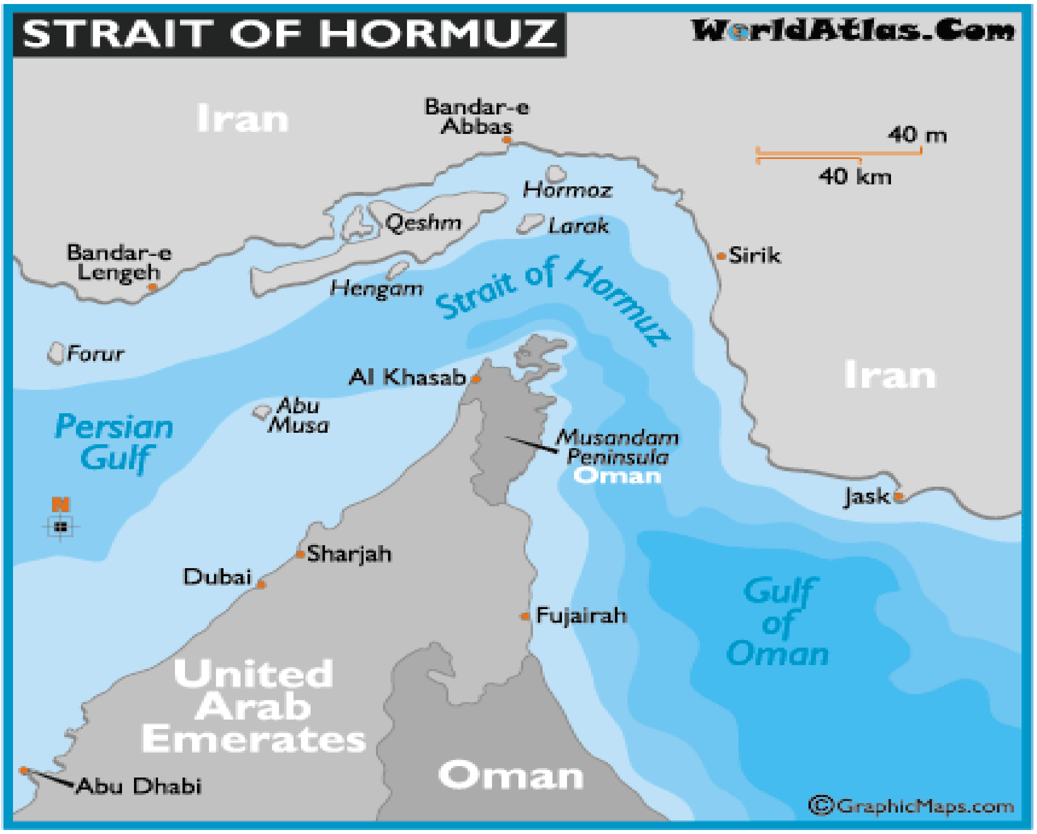

Figure PreF-3: Map of U.A.E. across from Iran along the Starit of Hormuz, leading though the narrowest width of the Arab-Persian Gulf region (GraphicMaps.com).

Persian Gulf, arm of the Arabian Sea, is in southwestern Asia, between the Arabian Peninsula on the southwest and Iran on the northeast. The Gulf extends Northwest 970 km (600 mi) from the Strait of Hormuz to the Shatt al Arab, a river formed by the confluence of the Tigris and Euphrates rivers. The Gulf is connected to the Arabian Sea by the Strait of Hormuz and the Gulf of Oman. The Persian Gulf varies in width from 47 to 370 km (29 to 230 mi). The area is 230,000 sq. km (89,000 sq. mi) and the greatest depth is 102 m (335 ft). The chief islands in the Gulf are Qeshm (belonging to Iran) and the Island nation of Bahrain. The United Arab Emirates, Saudi Arabia, Qatar, and Kuwait are on the south and Southwestern shores; Iraq is on the Northern tip; Iran is on the Northeastern shore; and the Northern tip of Oman is to the West. (Encyclopedia).

The Iranian shore of the Persian Gulf is largely mountainous and fringed with cliffs. Sandy beaches line the Arabian shore, which is broken by many small islands and lagoons. Large banks of pearl-producing mollusks are found off the Arabian coast. Spectacular cliffs rise from the shore around the Musandam Peninsula near the Strait of Hormuz at the Southeastern end of the Gulf. The Tigris, Euphrates, and Kārūn rivers deposit large amounts of silt as they empty into the Gulf in the Northwest. The Persian Gulf region is known for its high temperatures, uncomfortable humidity, and low rainfall. (Encyclopedia).

The Persian Gulf and its surrounding countries contain about 66 percent of the world’s proven reserves of oil and about 36 percent of total natural gas reserves (Year 2000 estimate). New reserves are still being discovered, both on land and offshore. Large amounts of oil are refined in the area, and oil tankers carry oil from marine terminals to all parts of the world. Major offshore oil fields include Safaniyah (belonging to Saudi Arabia), the largest offshore oil field in the world; and Khafji and Hout, divided between Saudi Arabia and Kuwait. Principal offshore gas fields include the North Field (Qatar), the largest gas field in the world; Dorra (Saudi Arabia and Kuwait); and South Pars (Iran). In 2000 the Persian Gulf region produced almost 29 percent of the world's oil. The principal ports on the Persian Gulf include Kuwait, in Kuwait; Ad Dammām and Al Jubayl, in Saudi Arabia; Būshehr, in Iran; and Mīnā’ Salmān, near Manama, in Bahrain. Major oil spills in 1983, during the Iran-Iraq War, and in 1991, during the Persian Gulf

War, have adversely affected the Gulf environment, as has oil pollution from routine tanker operations. (Encyclopedia).

Heavy metals in our environment:

There are 35 metals that are of concern because of occupational or residential exposure; 23 of these are the heavy elements or "heavy metals": antimony, arsenic, bismuth, cadmium, cerium, chromium, cobalt, copper, gallium, gold, iron, lead, manganese, mercury, nickel, platinum, silver, tellurium, thallium, tin, uranium, vanadium, and zinc (Glanze, 1996). Interestingly, small amounts of these elements are common in our environment and diet and are actually necessary for good health, but large amounts of any of them may cause acute or chronic toxicity (poisoning). Heavy metal toxicity can result in damaged or reduced mental and central nervous function, lower energy levels, and result in damage to blood composition, lungs, kidneys, liver, and other vital organs. Long-term exposure may result in slowly progressing physical, muscular, and neurological degenerative processes that mimic Alzheimer's disease, Parkinson's disease, muscular dystrophy, and multiple sclerosis. Allergies are not uncommon and repeated long-term contact with some metals or their compounds may even cause cancer (International Occupational Safety and Health Information Centre, 1999).

For some heavy metals, toxic levels can be just above the background concentrations naturally found in nature. Therefore, it is important for to know about the heavy metals and to take protective measures against excessive exposure. In most parts of the United States, heavy metal toxicity is an uncommon medical condition; however, it is a clinically significant condition when it does occur. If unrecognized or inappropriately treated, toxicity can result in significant illness and reduced quality of life (Ferner, 2001). For persons who suspect that they or someone in their household might have heavy metal toxicity, testing is essential. Appropriate conventional and natural medical procedures may need to be pursued (Dupler, 2001).

The association of symptoms indicative of acute toxicity is not difficult to recognize because the symptoms are usually severe, rapid in onset, and associated with a known exposure or ingestion (Ferner, 2001): cramping, nausea, and vomiting; pain; sweating; headaches; difficulty breathing; impaired cognitive, motor, and language skills; mania; and convulsions. The symptoms of toxicity resulting from chronic exposure (impaired cognitive, motor, and language skills; learning difficulties; nervousness and emotional instability; and insomnia, nausea, lethargy, and feeling ill) are also easily recognized; however, they are much more difficult to associate with their cause. Symptoms of chronic exposure are very similar to symptoms of other health conditions and often develop slowly over months or even years. Sometimes the symptoms of chronic exposure actually abate from time to time, leading the person to postpone seeking treatment, thinking the symptoms are related to something else. (Life Extension on Heavy Metal Toxicology).

DEFINITION OF A HEAVY METAL

"Heavy metals" are chemical elements with a specific gravity that is at least 5 times the specific gravity of water. The specific gravity of water is 1 at 4°C (39°F). Simply stated, specific gravity is a measure of density of a given amount of a solid substance when it is compared to an equal amount of water. Some well-known toxic metallic elements with a specific gravity that is 5 or more times that of water are arsenic, 5.7; cadmium, 8.65; iron, 7.9; lead, 11.34; and mercury, 13.546 (Lide, 1992).

BENEFICIAL HEAVY METALS

In small quantities, certain heavy metals are nutritionally essential for a healthy life. Some of these are referred to as the trace elements (e.g., iron, copper, manganese, and zinc). These elements, or some of their compounds, are commonly found naturally in foodstuffs, in fruits and vegetables, and in commercially available multivitamin products (International Occupational Safety and Health Information Centre, 1999). Diagnostic medical applications include direct injection of gallium during radiological procedures, dosing with chromium in parenteral nutrition mixtures, and the use of lead as a radiation shield around x-ray equipment (Roberts, 1999). Heavy metals are also common in industrial applications such as in the manufacture of pesticides, batteries, alloys, electroplated metal parts, textile dyes, steel, and so forth. (International Occupational Safety and Heath Information Centre, 1999). (Life Extension on Heavy Metal Toxicology).

TOXIC HEAVY METALS

Heavy metals become toxic when they are not metabolized by the body and accumulate in the soft tissues. Heavy metals may enter the human body through food, water, air, or absorption through the skin when they come in contact with humans in agriculture and in manufacturing, pharmaceutical, industrial, or residential settings. Industrial exposure accounts for a common route of exposure for adults. Ingestion is the most common route of exposure in children (Roberts, 1999). Children may develop toxic levels from the normal hand-to-mouth activity of small children who come in contact with contaminated soil or by actually eating objects that are not food (dirt or paint chips) (Dupler, 2001). Less common routes of exposure are during a radiological procedure, from inappropriate dosing or monitoring during intravenous (parenteral) nutrition, from a broken thermometer (Smith et al., 1997), or from a suicide or homicide attempt (Lupton et al., 1985).

As a rule, acute poisoning is more likely to result from inhalation or skin contact of dust, fumes or vapors, or materials in the workplace. However, lesser levels of contamination may occur in residential settings, particularly in older homes with lead paint or old plumbing (International Occupational Safety and Health Information Centre 1999). The Agency for Toxic Substances and Disease Registry (ATSDR) in Atlanta, Georgia, (a part of the U.S. Department of Health and Human Services) was established by congressional mandate to perform specific functions concerning adverse human health effects and diminished quality of life associated with exposure to hazardous substances. The ATSDR is responsible for assessment of waste sites and providing health information concerning hazardous substances, response to emergency release situations, and education and training concerning hazardous substances (ATSDR Mission Statement, November 7, 2001). In cooperation with the U.S. Environmental Protection Agency, the ATSDR has compiled a Priority List for 2001 called the "Top 20 Hazardous Substances." The heavy metals arsenic (1), lead (2), mercury (3), and cadmium (7) appear on this list. (Life Extension on Heavy Metal Toxicology).

According to Life Extension, the commonly encountered Toxic Heavy Metals are as follows:

- Arsenic
- Lead
- Mercury
- Cadmium
- Iron
- Aluminum

As noted earlier, there are 35 metals of concern, with 23 of them called the heavy metals. Toxicity can result from any of these metals. This protocol will address the metals that are most likely encountered in our daily environment. Briefly covered will be four metals that are included in the ATSDR's "Top 20 Hazardous Substances" list. Iron and aluminum will also be discussed even though they do not appear on the ATSDR's list.

ARSENIC

Arsenic is the most common cause of acute heavy metal poisoning in adults and is number 1 on the ATSDR's "Top 20 List." Arsenic is released into the environment by the smelting process of copper, zinc, and lead, as well as by the manufacturing of chemicals and glasses. Arsine gas is a common byproduct produced by the manufacturing of pesticides that contain arsenic. Arsenic may be also be found in water supplies worldwide, leading to exposure of shellfish, cod, and haddock. Other sources are paints, rat poisoning, fungicides, and wood preservatives. Target organs are the blood, kidneys, and central nervous, digestive, and skin systems (Roberts 1999; ATSDR ToxFAQs for Arsenic).

LEAD

Lead is number 2 on the ATSDR's "Top 20 List." Lead accounts for most of the cases of pediatric heavy metal poisoning (Roberts 1999). It is a very soft metal and was used in pipes, drains, and soldering materials for many years. Millions of homes built before 1940 still contain lead (e.g., in painted surfaces), leading to chronic exposure from weathering, flaking, chalking, and dust. Every year, industry produces about 2.5 million tons of lead throughout the world. Most of this lead is used for batteries. The remainder is used for cable coverings, plumbing, ammunition, and fuel additives. Other uses are as paint pigments and in PVC plastics, x-ray shielding, crystal glass production, and pesticides. Target organs are the bones, brain, blood, kidneys, and thyroid gland (International Occupational Safety and Health Information Centre 1999; ATSDR ToxFAQs for Lead).

MERCURY

Number 3 on ATSDR's "Top 20 List" is mercury. Mercury is generated naturally in the environment from the degassing of the earth's crust, from volcanic emissions. It exists in three forms: elemental mercury and organic and inorganic mercury. Mining operations, chloralkali plants, and paper industries are significant producers of mercury (Goyer, 1996). Atmospheric mercury is dispersed across the globe by winds and returns to the earth in rainfall, accumulating in aquatic food chains and fish in lakes (Clarkson, 1990). Mercury compounds were added to paint as a fungicide until 1990. These compounds are now banned; however, old paint supplies and surfaces painted with these old supplies still exist. Mercury continues to be used in thermometers, thermostats, and dental amalgam. (Many researchers suspect dental amalgam as being a possible source of mercury toxicity [Omura et al., 1996; O'Brien, 2001]). Medicines, such as mercurochrome and merthiolate, are still available. Algaecides and childhood vaccines are also potential sources. Inhalation is the most frequent cause of exposure to mercury. The organic form is readily absorbed in the gastrointestinal tract (90-100%); lesser but still significant amounts of inorganic mercury are absorbed in the gastrointestinal tract (7-15%). Target organs are the brain and kidneys (Roberts 1999; ATSDR ToxFAQs for Mercury).

CADMIUM

Cadmium is a byproduct of the mining and smelting of lead and zinc and is number 7 on ATSDR's "Top 20 list." It is used in nickel-cadmium batteries, PVC plastics, and paint pigments. It can be found in soils because insecticides, fungicides, sludge, and commercial fertilizers that use cadmium are used in agriculture. Cadmium may be found in reservoirs containing shellfish. Cigarettes also contain cadmium. Lesser-known sources of exposure are dental alloys, electroplating, motor oil, and exhaust. Inhalation accounts for 15-50% of absorption through the respiratory system; 2-7% of ingested cadmium is absorbed in the gastrointestinal system. Target organs are the liver, placenta, kidneys, lungs, brain, and bones (Roberts 1999; ATSDR ToxFAQs for Cadmium).

IRON

Discussion of iron toxicity in this protocol is limited to ingested or environmental exposure. Iron overload disease (hemochromatosis), an inherited disorder, is discussed in a separate protocol. Iron does not appear on the ATSDR's "Top 20 List," but it is a heavy metal of concern, particularly because ingesting dietary iron supplements may acutely poison young children (e.g., as few as five to nine 30-mg iron tablets for a 30-lb child).

Ingestion accounts for most of the toxic effects of iron because iron is absorbed rapidly in the gastrointestinal tract. The corrosive nature of iron seems to further increase the absorption. Most overdoses appear to be the result of children mistaking red-coated ferrous sulfate tablets or adult multivitamin preparations for candy. (Fatalities from overdoses have decreased significantly with the introduction of child-proof packaging. In recent years, blister packaging and the requirement that containers with 250 mg or more of iron have child-proof bottle caps have helped reduce accidental ingestion and overdose of iron tablets by children.) Other sources of iron are drinking water, iron pipes, and cookware. Target organs are the liver, cardiovascular system, and kidneys (Roberts 1999).

ALUMINUM

Although aluminum is not a heavy metal (specific gravity of 2.55-2.80), it makes up about 8% of the surface of the earth and is the third most abundant element (ATSDR ToxFAQs for Aluminum). It is readily available for human ingestion through the use of food additives, antacids, buffered aspirin, astringents, nasal sprays, and antiperspirants; from drinking water; from automobile exhaust and tobacco smoke; and from using aluminum foil, aluminum cookware, cans, ceramics, and fireworks (ATSDR ToxFAQs for Aluminum).

Studies began to emerge about 20 years ago suggesting that aluminum might have a possible connection with developing Alzheimer's disease when researchers found what they considered to be significant amounts of aluminum in the brain tissue of Alzheimer's patients. Although aluminum was also found in the brain tissue of people who did not have Alzheimer's disease, recommendations to avoid sources of aluminum received widespread public attention. As a result, many organizations and individuals reached a level of concern that prompted them to dispose of all their aluminum cookware and storage containers and to become wary of other possible sources of aluminum, such as soda cans, personal care products, and even their drinking water (Anon., 1993).

However, the World Health Organization (WHO, 1998) concluded that, although there were studies that demonstrate a positive relationship between aluminum in drinking water and Alzheimer's disease, the WHO had reservations about a causal relationship because the studies did not account for total aluminum intake from all possible sources. Although there is no conclusive evidence for or against aluminum as a primary cause for Alzheimer's disease, most researchers agree that it is an important factor in the dementia component and most certainly deserves continuing research efforts. Therefore, at this time, reducing exposure to aluminum is a personal decision. Workers in the automobile manufacturing industry also have concerns about long-term exposure to aluminum (contained in metal working fluids) in the workplace and the development of degenerative muscular conditions and cancer (Brown, 1998; Bardin et al., 2000). The ATSDR has compiled a ToxFAQs for Aluminum to answer the most frequently asked health questions about aluminum. Target organs for aluminum are the central nervous system, kidney, and digestive system.

Selenium and Zinc

Deficiency of selenium and zinc, important antioxidant micronutrients, contributes to compromised immunity (Girodon et al., 1999) and lowered defense against free radicals (Porter et al., 1999; Schumacher, 1999). Selenium and zinc act as cofactors of antioxidant enzymes to protect against oxygen free radicals produced during oxidative stress (Leung, 1998). Selenium is often found to be deficient in persons who have experienced physical trauma. Porter et al. (1999) concluded that patients who experienced severe trauma had fewer infections and less organ dysfunction when they received selenium supplementation. Interestingly, studies on the protective benefits of selenium have implications in the management of persons receiving chemotherapy, enhancing mediation of oxygen free-radical damage to normal tissue, and decreasing side effects such as nausea, emesis, vertigo, unsteady gait, and seizures caused by the chemicals and drugs used in chemotherapy (Pakdaman, 1998). This is possibly a characteristic of persons with brain tumors who frequently have low blood levels of selenium (Pakdaman, 1998; Schumacher, 1999).

Strontium

Strontium is a soft, silver-yellow, alkaline-earth metal. It has three allotropic crystalline forms and in its physical and chemical properties it is similar to calcium and barium**.** Strontium reacts vigorously with water and quickly tarnishes in air, so it must be stored out of contact with air and water. Due to its extreme reactivity to air, this element always naturally occurs combined with other elements and compounds. Finely powdered strontium metal will ignite spontaneously in air to produce both strontium oxide and strontium nitride.

Applications

Strontium has uses similar to those of calcium and barium, but it is rarely employed because of its higher cost. Principal uses of strontium compounds are in pyrotechnics, for the brilliant reds in fireworks and warning flares and in greases. A little is used as a getter in vacuum tubes to remove the last traces of air. Most strontium is used as the carbonate in special glass for television screens and visual display units. Although strontium-90 is a dangerously radioactive isotope, it is a useful by-product of nuclear reactors from whose spent fuel is extracted. Its high-energy radiation can be used to generate an electric current, and for this reason it can be used in space vehicles, remote weather stations and navigation buoys.

Strontium in the environment

Strontium is commonly occurs in nature, formung about 0.034% of all igneous rock and in the form of the sulfate mineral celestite ($SrSO_4$) and the carbonate strontianite

($SrCO_3$). Celestite occurs frequently in sedimentary deposits of sufficient size, thus the development of mining facilities attractive. The main mining areas are UK, Mexico, Turkey and Spain. World production of strontium ores is about 140.000 tonnes per year from an unassessed total of reserves.

Foods containing strontium range from very low e.g. in corn (0.4 ppm) and orange (0.5 ppm) to high, e.g. in cabbage (45 ppm), onions (50 ppm) and lattuce (74 ppm).

Health effects of strontium

Strontium compounds that are water-insoluble can become water-soluble, as a result of chemical reactions. The water-soluble compounds are a greater threat to human health than the water-insoluble ones. Therefore, water-soluble forms of strontium have the opportunity to pollute drinking water**.** Fortunately the concentrations in drinking water are usually quite low

People can be exposed to small levels of (radioactive) strontium by breathing air or dust, eating food, drinking water, or by contact with soil that contains strontium. We are most likely to come in contact with strontium by eating or drinking.

Strontium concentrations in food contribute to the strontium concentrations in the human body. Foodstuffs that contain significantly high concentrations of strontium are grains, leafy vegetables and dairy products.

For most people, strontium uptake will be moderate. The only strontium compound that is considered a danger to human health, even in small quantities, is strontium chromate. The toxic chromium that it contains mainly causes this. Strontium chromate is known to cause lung cancer, but the risks of exposure have been greatly reduced by safety procedures in companies, so that it is no longer an important health risk. The uptake of high strontium concentrations is generally not known to be a great danger to human health. In one case someone experienced an allergic reaction to strontium, but there have been no similar cases since. For children exceeded strontium uptake may be a health risk, because it can cause problems with bone growth.

Strontium salts are not known to cause skin rashes or other skin problems of any kind. When strontium uptake is extremely high, it can cause disruption of bone development. But this effect can only occur when strontium uptake is in the thousands of ppm range. Strontium levels in food and drinking water are not high enough to be able to cause these effects.

Radioactive strontium is much more of a health risk than stable strontium. When the uptake is very high, it may cause anaemia and oxygen shortages, and at extremely high concentrations it is even known to cause cancer as a result of damage to the genetic materials in cells.

Effects of strontium on the Environment

Strontium in its elemental form occurs naturally in many compartments of the environment, including rocks, soil, water, and air. Strontium compounds can move through the environment fairly easily, because many of the compounds are water-soluble. Strontium is always present in air as dust, up to a certain level. Strontium concentrations in air are increased by human activities, such as coal and oil combustion. Dust particles that contain strontium will settle to surface water, soils or plant surfaces at some point.

When the particles do not settle they will fall back onto earth when rain or snow falls. All strontium will eventually end up in soils or bottoms of surface waters, where they mix with strontium that is already present.

Strontium can end up in water through soils and through weathering of rocks. Only a small part of the strontium in water comes from dust particles from the air. Most of the strontium in water is dissolved, but some of it is suspended, causing muddy water at some locations. Not much strontium ends up in drinking water.

When strontium concentrations in water exceed regular concentrations, this is usually caused by human activities, mainly by dumping waste directly in the water. Exceeded strontium concentrations can also be caused by settling of dust particles from air that have reacted with strontium particles from industrial processes.

Strontium concentrations in soil may also be increased by human activities, such as the disposal of coal ash and incinerator ash, and industrial wastes. Strontium in soil dissolves in water, so that it is likely to move deeper into the ground and enter the groundwater. A part of the strontium that is introduced by humans will not move into groundwater and can stay within the soil for decades. Because of the nature of strontium, some of it can end up in fish, vegetables, livestock and other animals.

One of the isotopes of strontium is radioactive. This isotope is not likely to occur naturally in the environment. It ends up in the environment, though, as a result of human activities, such as nuclear bomb testing and radioactive storage leaking. The only way to decrease concentrations of this isotope is through radioactive decay to stable zirconium. The concentrations of radioactive strontium in the environment are relatively low and the particles will always end up in soils or water-bottoms eventually, where they mix with other strontium particles. It is not likely to end up in drinking water. Certain deep-sea creatures incorporate strontium into their shells as strontium sulphate, and stony corals require it, which is why it needs to be added in the water in aquaria. (http://www.lenntech.com/Periodic-chart-elements/Sr-en.htm#ixzz0IATzpHUF&C)**.**

Maximum Limits Permissible in Drinking Water according to Canadian, U.S., WHO ad Gulf region standards

Table PreF-1: This table represents only a selection of contaminants that are posted in the guidelines. A full list is available via the websites below.

The following table is a brief selection of some contaminants and physical conditions that may be present in drinking water. A dash (-) indicates that there is no information available regarding possible limits. Units are in milligrams per liter (mg/L) unless otherwise noted. Milligrams per liter are equivalent to parts per million.

	Canadian Limit	**US limit**	**WHO limit**	**Gulf limit**
Heavy Metal	**(ppm)**	**(ppm)**	**(ppm)**	**(ppm)**
Silver	**0.05**	**0.1**	**no limit**	
	0.05	**0.1**	**no limit**	
	0.05	**0.1**	**no limit**	
	0.05	**0.1**	**no limit**	
	0.05	**0.1**	**no limit**	
Aluminum	**0.1**	**0.05 - 0.2**	**no limit**	
	0.1	**0.05 - 0.2**	**no limit**	
	0.1	**0.05 - 0.2**	**no limit**	

Arsenic	**0.01** **0.01** **0.01**	**0.01** **0.01** **0.01**	**0.01** **0.01** **0.01**	**Table 1, Continued**
Barium	**1** **1**	**2** **2**	**0.7** **0.7**	
Beryllium	**no limit** **no limit** **no limit**	**0.004** **0.004** **0.004**	**no limit** **no limit** **no limit**	
Bismuth				
Cadmium	**0.005** **0.005** **0.005** **0.005**	**0.005** **0.005** **0.005** **0.005**	**0.003** **0.003** **0.003** **0.003**	
Cesium				
Chromium	**0.05** **0.05**	**0.01** **0.01**	**0.05** **0.05**	
Cobalt	**no limit** **no limit**	**no limit** **no limit**	**no limit** **no limit**	
Copper	**1**	**1.3**	**2**	
	1	**1.3**	**2**	
	1	**1.3**	**2**	
	1	**1.3**	**2**	
Iron	**0.3**	**0.3**	**no limit**	
	0.3	**0.3**	**no limit**	
	0.3	**0.3**	**no limit**	
Gallium				
In				
Lithium				
Magnesium	**50**	**-**	**-**	
	50	**-**	**-**	
Manganese	**0.05**	**0.03**	**0.4**	
	0.05	**0.03**	**0.4**	

Sodium	**200**	**no limit**	**no limit**	**Table 1, Continued**
	200	**no limit**	**no limit**	
	200	**no limit**	**no limit**	
	200	**no limit**	**no limit**	
	200	**no limit**	**no limit**	
	200	**no limit**	**no limit**	
Nickel	**no limit**	**no limit**	**0.02**	
	no limit	**no limit**	**0.02**	
Lead	**0.01**	**0**	**0.001**	
	0.01	**0**	**0.001**	
	0.01	**0**	**0.001**	
	0.01	**0**	**0.001**	
	0.01	**0**	**0.001**	
Rubidium				
Selenium				
Strontium	**no limit**	**no limit**	**no limit**	
	no limit	**no limit**	**no limit**	
Titanium	**no limit**	**no limit**	**no limit**	
	no limit	**no limit**	**no limit**	
	no limit	**no limit**	**no limit**	
Uranium	**0.02**	**no limit**	**0.009**	
	0.02	**no limit**	**0.009**	
Vanadium	**no limit**	**no limit**	**no limit**	
	no limit	**no limit**	**no limit**	
	no limit	**no limit**	**no limit**	
	no limit	**no limit**	**no limit**	
	no limit	**no limit**	**no limit**	
Zinc	**5**	**5**	**no limit**	
	5	**5**	**no limit**	
	5	**5**	**no limit**	

* As per Canadian or BC Health Act Safe Drinking Water Regulation BC Reg 230/92, & Sch 120, 2001. Task force of the Canadian Council or Resource and Environment Ministers Guidelines for Canadian Drinking Water Quality, 1996. See their website for more information.

** As per the U.S. Environmental Protection Agency Drinking Water Standards. See their website for more information.

*** As per the WHO (1998) Guidelines for drinking water quality, 2nd edition. Geneva, World Health Organization. See their website for more information.

^ TCU = true colour unit

^^ Individual limits for some of the individual trihalomethanes & haloacetic acids:

- Trihalomethanes: bromodichloromethane (zero); bromoform (zero); dibromochloromethane (0.06 mg/L). Chloroform is regulated with this group but has no MCLG.
- Haloacetic acids: dichloroacetic acid (zero); trichloroacetic acid (0.3 mg/L). Monochloroacetic acid, bromoacetic acid, and dibromoacetic acid are regulated with this group but have no limits.

^^^ NTU = nephelometric turbidity unit. Based on conventional treatment/slow sand or diatomaceous earth filtration/membrane filtration

Statement of the problem: To decontaminate large volumes of offshore muds conatminated by toxic and carcinogenic heavy metals.

Different solutions for decontamination include:

1. Physical excavation: Time and labor intensive, requiring mining of contaminated sediments. This renders the land unusable during the treatment process.
2. Chemical treatment: Time and labor intensive, while having to deal with the complex reactions occurring *in-situ*.
3. Biological treatment: Time and labor intensive, while having to deal with both cultivating the required bacteria and the complex reactions occurring that will leach out unknown products *in-situ*.
4. Electrokinetic treatment: If successful in offshore muds as in soils and sludges, this technology will allow for a quick, cost effective remediation (*in-situ)*.

Chapter 1: Electrokinetics

Electrokinetics is a term applied to a group of physicochemical phenomena involving the transport of charges, action of charged particles, effects of applied electric potential and fluid transport in various porous media to allow for a desired migration or flow to be achieved. These phenomena include electroosmosis, ion migration, electrophoresis, streaming potential and electroviscosity. These phenomena are closely related and all contribute to the transport and migration of the desired ionic species and chemicals. The physical and electrochemical properties of a porous medium and the pore fluid, and the applied electrical potential all impact the direction and velocity of the fluid flow. Also, an electrical potential is generated upon the forced passage of fluid carrying charged particles through a capillary of porous medium.

These electrokinetic effects have been recognized for a considerable period of time, with the effects of electroosmosis and electroviscosity being studied and evaluated by many researchers.

Theory

Factors influencing electrokinetic phenomena

The theoretical development of electrokinetic phenomena and electrochemical transport has been studied historically as far back as 1879 by Helmholtz that led to the introduction of the first analytical equation. Helmholtz described the motion of the charged ionic solution from the anode to the cathode and explained it by the presence of a double layer. This double-layer theory is illustrated in Figure 1, where the negatively charged surface of the clays attracts the positive ions of aqueous medium, forming the immobile double layer. This immobile double layer is followed by a thick mobile layer with a predominanance of positively-charged ions (cations), with a few diffused negatively-charged ions (anions).

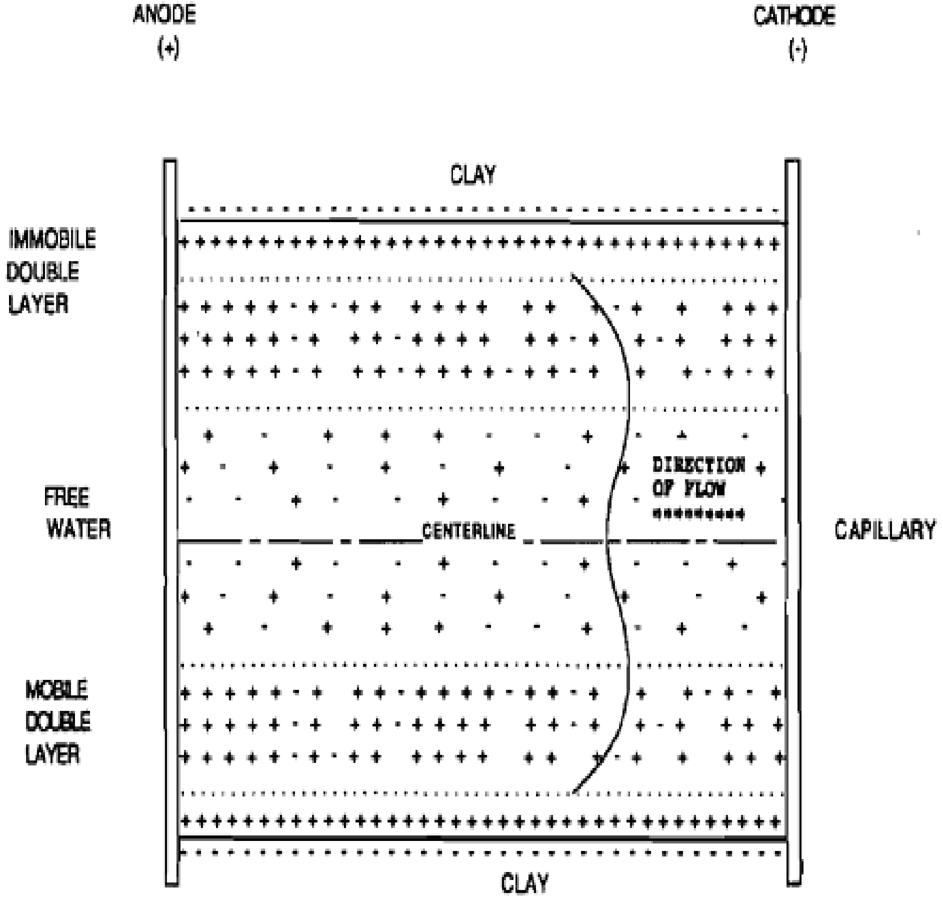

Figure 1-1: Schematic diagram of Helmholtz double-layer in an electrokinetic flow on application of direct current field. (Modified by Chilingar et al., 1997.)

Later, the analytical solution was further modified by Smoluchowski in 1921 to arrive at the Helmholtz-Smoluchowski's equation (electrokinetic permeability):

$$K_{\theta} = D\xi / 4\ \pi\eta \qquad (1\text{–}1)$$

where: D = dielectric constant

ξ = zeta potential

η = viscosity of the fluid

The proportionality constant, *D*, has been verified by several investigators for various types of liquid--solid interfaces. However, extreme sensitivity and complexity of these phenomena have lead to reports of discrepancies in the relative constancy of this term. Probstein and Hicks (1993) have shown the effects concentration of ionic species within the pore fluid, electric potential, and pH on the zeta potential (ξ). Thus, it doesn't remain constant throughout the electrically induced transport in soils that are governed by zeta potential.

Zeta potential and the Electric Double Layer Interaction

There is a region at the surface of solids that has a difference in electrical potential across just a few molecular diameters. When two dissimilar charged surfaces are contacted, electrons at the surface of each one redistribute in such a manner that one of them acquires a positive charge while the other becomes negatively charged. If a liquid and solid are brought together, an electrical potential develops across a distance of a few molecular diameters at the interface. The changes that are established are characteristic of specific phases and are the underlying cause of many natural phenomena recognized as electrophoresis, electroosmosis, colloid stability, fluid flow behavior, adsorption, catalysis, corrosion, crystal growth, etc. (Donaldson and Alam, 2008).

The separation of charges is known as the interfacial electrical double layer. It is a complex association of charges illustrated schematically in Fig. 1-2. There is a potential charge (negative or positive) at one or two molecular distances from the surface. This charge may originate from several sources such as: (1) inclusions of extraneous atoms in the lattice structure, (2) dissolution of slightly soluble atoms at the surface of water, (3) chemical reaction (chemisorption) of ions in water with surface atoms forming complex polar molecules on the surface, or (4) exposure of metallic oxides at the surface which react with water to form surface ions. These are some of the major causes of surface charges; others are recognized in suspensions of particles and flocculants in water (Hunter, 1981).

Counterions from the water solution balance the charges at the solid surface and form the immobile Stern layer, Fig. 1-2. The thickness of the Stern layer is only one or two molecular diameters consisting of ions that are adsorbed strongly enough to form an immobile layer. The outer edge of the Stern layer where the ions are mobile is known as the shear plane. There is a linear potential drop across the width of the Stern layer $(\psi_s - \psi_\zeta)$, followed by an exponential potential difference across the diffuse layer between the shear plane and the bulk solution $(\psi - \psi_\infty)$; the bulk solution is designated as the reference zero potential. This potential difference between the shear plane and the bulk fluid is known as the zeta potential (Donaldson and Alam, 2008).

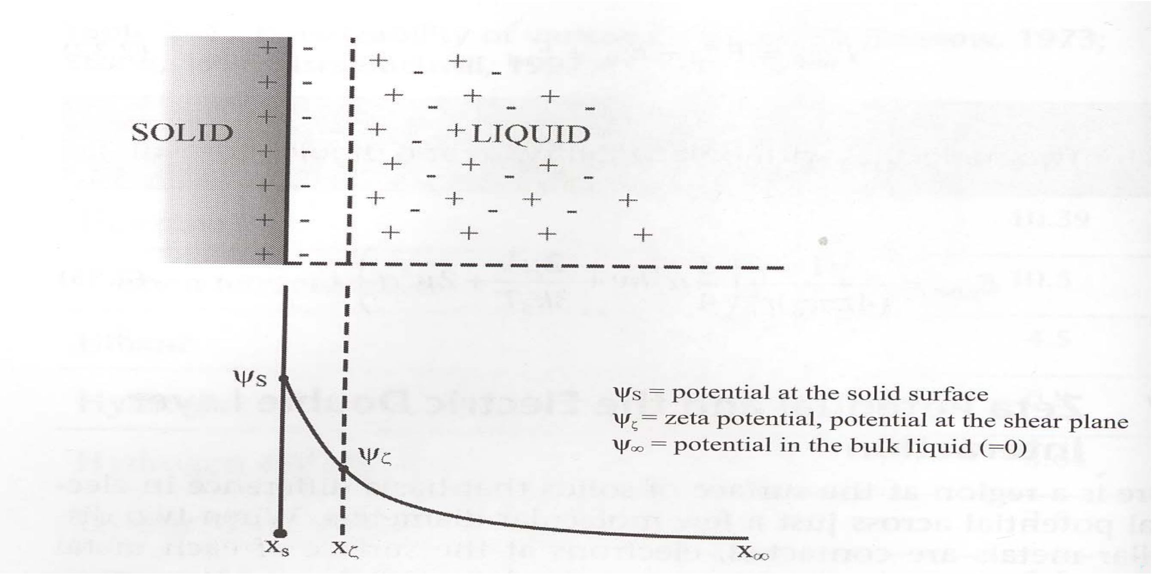

Figure 1-2 Electric double layer at the interface between a solid and liquid: x_s = surface of the solid, x_ζ = shear plane, x_∞ = bulk liquid, $x_\zeta - x_s$ = stern layer, $x_\infty - x_\zeta$ = electrical diffuse (Gouy) layer. (Debye length, *l/k*). (After Donaldson and Alam, 2008.)

Cations, anions, and molecules with electrical dipoles can be adsorbed by nonelectrical forces. Grahame has observed that anions are adsorbed by nonelectrical forces with the centers of negative charges lying on an inner plane (within the Stern layer) from the surface known as the Helmholtz inner plane (*IHP* at x_i distance from the solid surface, Fig. 1-3). The *IHP* is followed by the outer Helmholtz plane (*OHP*) drawn through the charges of the hydrated counterions.

The thickness of the Helmholtz layers thus reflects the size of the adsorbed anions and counterions within the Stern layer and is observed by the differences of the measured linear potential differences within the Stern layer.

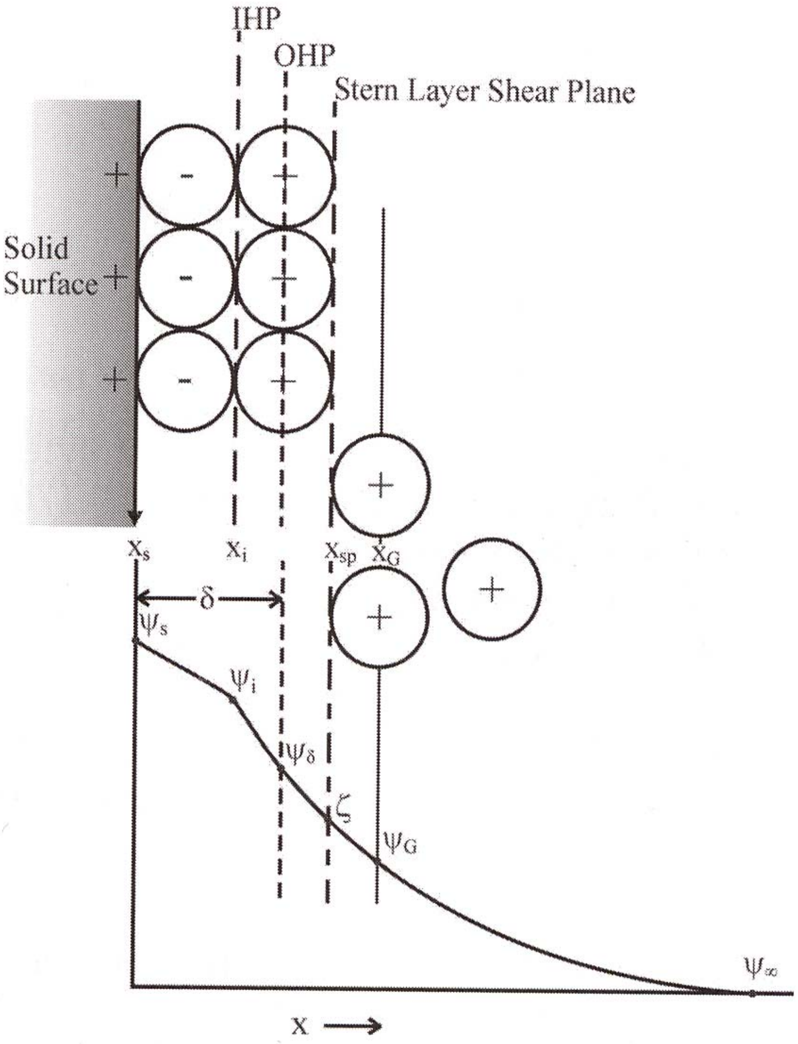

Figure 1-3 Double layer potentials showing the Helmholtz planes and their potentials. ***IHP*** **= inner Helmholtz plane** ***(x_i).*** ***OHP*** **= outer Helmholtz plane** ***($x = \sigma$)*****.** **(After Donaldson and Alam, 2008.)**

The length of the exponential electrical field decay (from the shear plane to the bulk fluid) is known as the Debye length ($1/k$). For example, if the plates of a capacitor haveequal charge densities, the zeta potential is the potential difference from the center of the separation to one of the plates (Donaldson and Alam, 2008):

$$1/k = x_o - x_s = \varepsilon\varepsilon_o\, \psi_s/\sigma_c = (\varepsilon\varepsilon_o KT/\rho_i Z^2 \varepsilon^2)^{\wedge 1/2} * [c^2/jm\ j/C\ m^2/C = m] \quad (1\text{-}2)$$

where ρ_i is the number density of ions in the solution; Eq. 1-2 also shows that the charge density of the surface (σ_c) is proportional to the surface potential (ψ_s).

With respect to an ionic solution, the Debye length is the distance from the shear plane of the Stern layer to the bulk fluid. The Debye length depends on the specific properties of the ionic solution. For aqueous solutions (Donaldson and Alam, 2008):

$$1/k = B/\surd(M) \quad (1\text{-}3)$$

where B is a constant specific to the type of electrolyte. B is equal to 0.304 for monovalent cations and anions (NaCl); 0.176 where either the cation or the anion has a valency of two ($CaCl_2$ or Na_2CO_3); and 0.152 when both ions have a valency equal to two ($CaCO_3$). M is the molarity of the pore solution.

The composition of the Stern layer varies with respect to the nature of the surface charge and ionic constituents of the electrolyte (Castellan, 1971):

1. The double layer may be entirely diffuse (no Stern layer) if ions are not adsorbed on the solid surface, Fig. 1-4 In this case the Stern layer does not exist and the

potential difference declines exponentially from the solid surface to the bulk solution.

2. If the concentration of ions in the electrolyte is sufficient to exactly balance the surface charges of the solid, the potential will decrease linearly within the Stern layer to zero at the shear plane. Thus the zeta potential is zero (equal to the potential of the bulk fluid).
3. If the adsorption of ions does not completely balance the surface charge density, the zeta potential has a finite value with respect to the bulk fluid.
4. If the surface charge is very strong, the Stern layer may contain an excess of ions from the electrolyte.

The zeta potential of mineral surfaces in contact with aqueous solutions is a function of pH. In general, acidic solutions promote positive charges at the surface with an attendant positive zeta potential and basic solutions produce an excess of negative charges at the surface from an increase of the hydroxide ion. The pH at which the zeta potential is equal to zero is defined as the zero point charge *(zpc).* When the negative and positive charges of ions in a solution are equally balanced, the solution is electrically neutral and this condition is defined as the isoelectric point *(iep).* Thomson and Pownall (1989) observed an approximate linear trend of the zeta potential with respect to pH for calcite in dilute solutions of sodium chloride and a mixed solution of sodium chloride and sodium bicarbonate, where $\zeta = -6.67*pH + 40$. The zero point charge occurred at $pH > 6$. Sharma et al. (1987) report inverted S-shaped trends where $\zeta = -20*pH + 100\ (zpc\ at\ pH \approx 5)$ for Berea cores and dilute sodium chloride solutions (Donaldson and Alam, 2008).

Zpc for most kaolinite ia at about pH = 2.

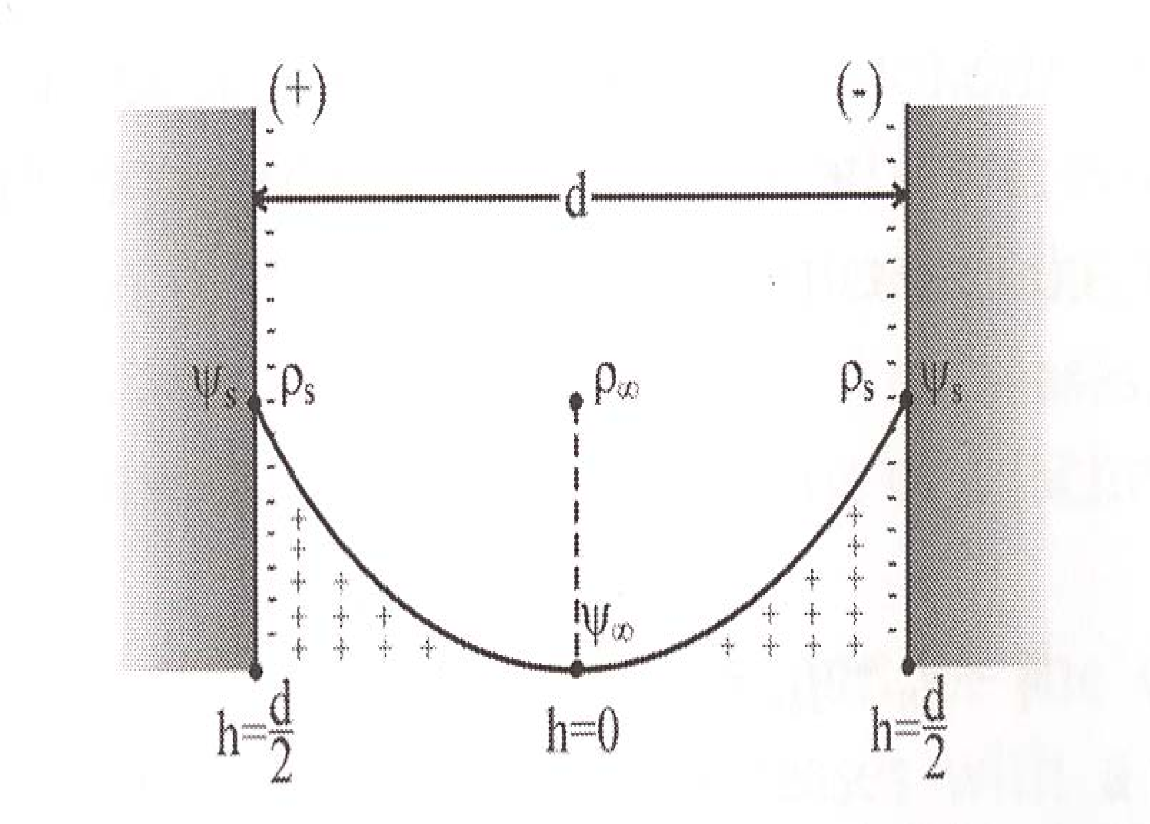

Figure 1-4 Two charged surfaces separated by distance d with a fluid between. The film thickness on each surface is h = d/2. The number density of the counter ions at the surface is ρ_s and the center is designated ρ_s which is taken as zero at the reference point in the center. The electric field, which is independent of distance is equal to the electric charge density, D, divided by the electric permittivity, $E_s = D/\varepsilon\varepsilon_o$. (After Donaldson and Alam, 2008).

Considering that the total flow rate, q, in a porous medium is composed of the flow rate where there is no electrical potential effect, q_n, and an osmotic, countercurrent flow, q_{os}:

$$q = q_n - q_{os} = k_n dP/ndx - k'_{os}(d\psi/dx) \tag{1-4}$$

where k_n is the permeability in the absence of electrical phenomena and k'_{os} is the transport coefficient resulting from the streaming potential, ψ.

The coefficient, k'_{os} is obtained from the Helmholtz equation for the velocity of electroosmotic flow in a tortuous capillary (Adamson, 1960; Scheidegger, 1974):

$$U_{os} = e\varphi\zeta d\psi/4\varphi\mu\tau^2 dx \tag{1-5}$$

When an electrolyte is passes through a porous material (rock, glass, capillaries, etc.), a potential difference develops across the ends of the core that is generally recognized as the streaming potential.

Combining Eqs. 1-4 and 1-5 into Eq. 1-4 yields the fluid flow equation that includes the effect of electroosmotic flow (Donaldson and Alam, 2008):

$$Q = (k_n/n - e^2\varphi\zeta^2 R_n/(4\pi)^2\mu t^2)dP/dx = (k_n/\mu - k_{os}/\mu)dP/dx \tag{1-6}$$

DLVO (Derjaguin, Landau, Verwey, and Overbeek) Theory

The DLVO theory (Derjaquin and Landau, 1941; Verwey and Overbeek, 1948) is the analysis of the competitive interactions of double layer forces and van der waals attractive forces they affect the stability of colloidal suspensions of particles in electrolytic solutions. Anions and cations maybe be adsorbed on surfaces by van der waal attractive forces which are not affected by variations of *pH* or the concentration of electrolytes. Curve 1, Fig. 1-5, describes the variation of the interactive potential energy that occurs from complete repulsive energy (in the absence of van der waals attractive forces); this occurs for a relatively thick double layer in a solution of high electrolyte concentration. (Donaldson and Alam, 2008).

The van der waals forces become stronger (more negative) following an exponential curve ($U_{(r)} = -r^n$) as the separation decreases and hence van der waals forces are negligible at long distances. At short distances from the wall, however, the van der waals forces exceed the repulsive double-layer forces and the result is strong attraction of the surfaces (curve 4, Fig. 1-5). (Donaldson and Alam, 2008).

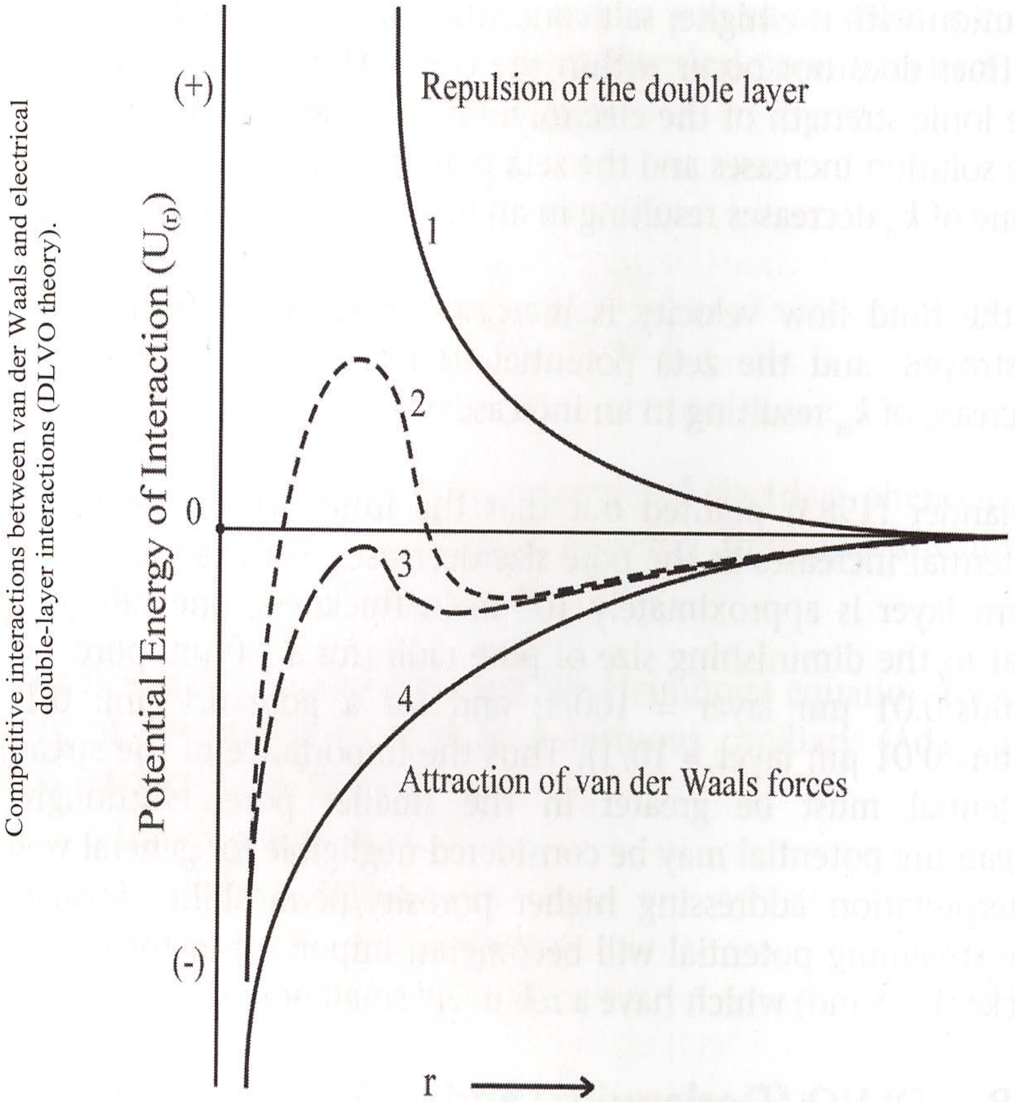

Figure 1-5 Curve 1: Repulsion of a surface caused by a double-layer Coulombic charge in the absence of van der Waals attraction. This occurs in high electrolyte concentrations. Curves 2 to 4: The increasing effect of van der Waals forces as the thickness of the double layer decreases; this results form decreasing electrolyte concentration. Curve 4: van der Waals attraction in the absence of double-layer repulsion. (After Donaldson and Alam, 2008).

Between the two extremes, as particle surfaces approach, there is an initial attractive minimum followed by a repulsive maximum that can be too great to allow actual contact of the particle surfaces (curve 2, Fig. 1-5) and the particle will remain dispersed in the electrolyte. If the surfaces have a low charge density and the repulsive maximum of the potential energy is zero or negative (curve 3), the particles will coagulate because the forces are entirely attractive. (Donaldson and Alam, 2008).

A value of 25 mV (positive or negative) can be taken as the arbitrary value that separates low-charged surfaces from highly-charged surfaces.

The significance of zeta potential is that its value can be related to the stability of colloidal dispersions. The zeta potential indicates the degree of repulsion between adjacent, similarly charged particles in a dispersion. For molecules and particles that are small enough, a high zeta potential will confer stability, i.e., the solution or dispersion will resist aggregation because the surface charge because the surface charge disperency of the particles are highly satisfied. When the potential is low, attraction exceeds repulsion and the dispersion will break and flocculate. So, colloids with high zeta potential (negative or positive) are electrically stabilized, whereas colloids with low zeta potentials tend to coagulate or flocculate as outlined below:

Zeta potential is widely used for quantification of the magnitude of the electrical charge at the double layer. However, zeta potential is not equal to the Stern potential or electric surface potential in the double layer. Such assumptions of equality should be applied with caution. Nevertheless, zeta potential is often the only available path for characterization of double-layer properties.

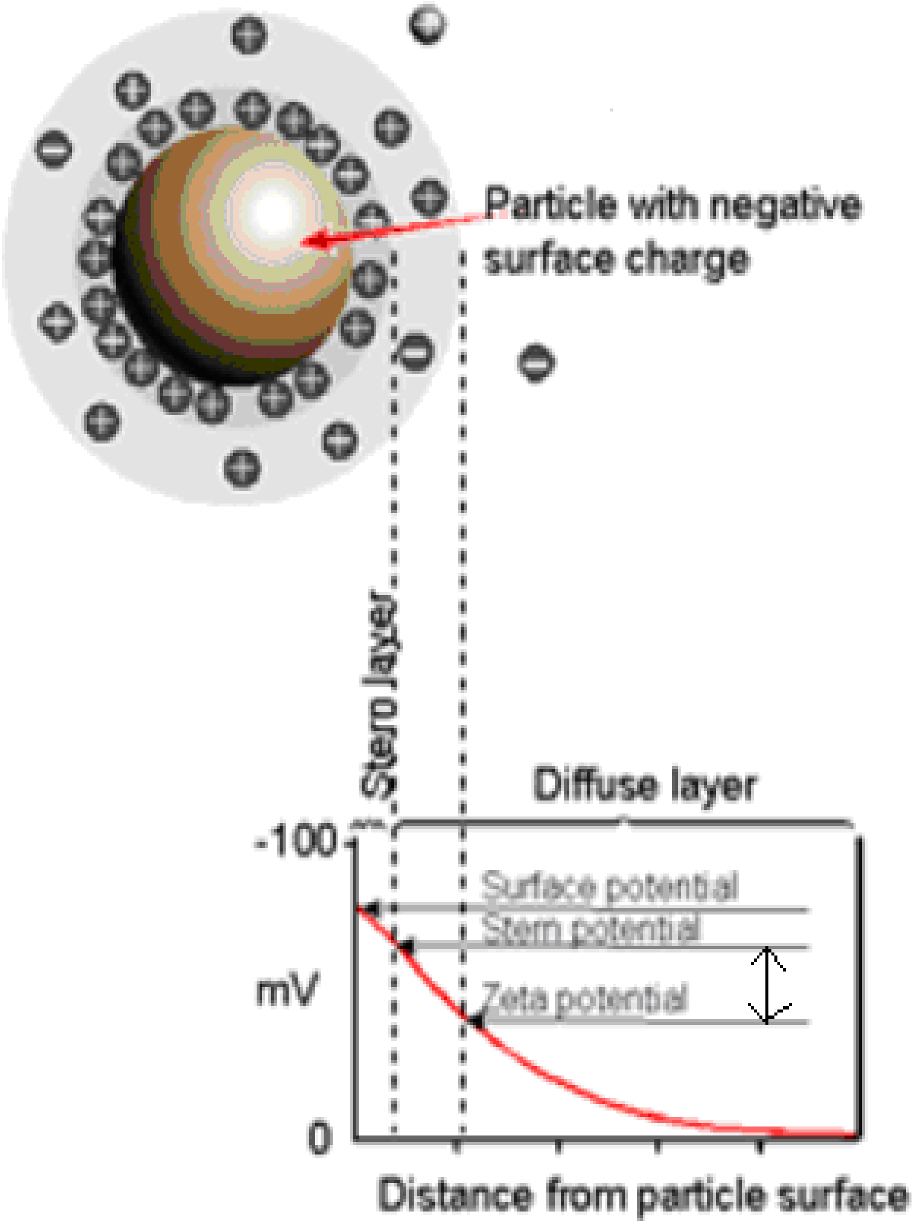

Figure 1-6: Schematic representation of zeta potential (ξ). (Modified after Zetasizer Nano series technical note, Malvern Instruments, www.nbtc.cornell.edu)

There is a surface of shear (slipping plane) between the fixed and mobile sub-regions. The zeta potential (ξ) is the potential difference between this plane and the bulk liquid. This zeta potential (ξ) is smaller than the total or thermodynamic potential (after Butler et al., 1951). The classical zeta potential (ξ) equation is as follows (after Street et al., 1961):

$$\xi = 4\pi\delta\lambda/D \tag{1-7}$$

where the double-layer thickness, λ, is equal to:

$$\lambda = f\,[1/(1/2{*}C_iZ_i^2)^{1/2}] \tag{1-8}$$

Anbah (1963) stated that the larger the ionic charge on the clay particle, the larger the electric potential between the diffuse and inner fixed layer. Thus, fewer ions are able to move in an external field. Overbeek and Liklema (1969) have shown that the higher the ion concentration, the smaller the double layer thickness and, hence, the smaller the zeta potential.

However with decreasing pH, the zeta potential (ξ) decreases until a critical pH is reached at which time a reversal in the sign of zeta potential occurs (Hunter and James, 1992). This is caused by the accumulation of H^+ ions in low--pH environments, resulting in a compression of the Helmholtz double layer due to the cation build up. The reversal of the sign of the zeta potential has been shown by Hunter and James (1992), as the concentration of hydrolyzable metal ions increase the compression of the electric double layers. This may lead to a reduction in electrokinetic flow in soils with high pore fluid electrolyte concentrations, making electromigration the dominant mechanism of electrochemical transport (Pamukcu et al., 2008). This reversal of sign of the zeta potential (ξ) has been found due to the accumulation of cations and the compression of the electric double layer. The largest effect of zeta potential (ξ) occurs during the intermediate pH, slightly higher than the value needed for precipitation of the metal hydroxide. It has been shown to be influenced by the type and concentration of electrolytes added to the suspension (Kruyt, 1952; Smith and Narimatsu, 1993).

As mentioned earlier, the pH is one of the most important factors affecting the zeta potential (ξ). Thus, the zeta potential value alone is actually meaningless without defining the solution conditions (After Zetasizer Nano series technical note, Malvern Instruments, www.nbtc.cornell.edu).

1) On assuming a negative value zeta potential, if acid is added to this suspension, a point will be reached where the charge will be neutralized. The further addition of acid will cause a buildup of positive charge. Consequently, the zeta potential (ξ) versus pH curve will be positive at low pH and lower or negative at high pH.
2) On the other hand, if more alkali is added to the system, then the accumulation and buildup of negative charge on particle will prevail. The point where the plot of the zeta potential versus pH passes through the zero zeta potential is called the isoelectric point. Usually, the colloidal system is least stable at this point.

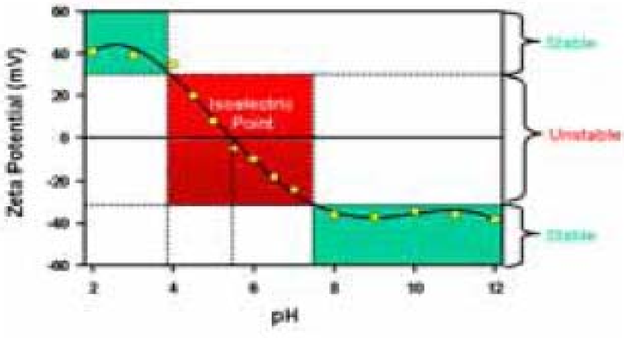

Figure 1-7: Typical plot of zeta potential (ξ) versus pH, showing the position of the isoelectric point and the pH values where the dispersion is expected to be stable (after Zetasizer Nano series technical note, Malvern Instruments, www.nbtc.cornell.edu).

In Figure 1-7, the isoelectric point of the sample is at pH ≈ 5.5. The sample is stable at pH < 4 and pH > 7.5. In the unstable region, (Fig. 1-3), the zeta potential varies from +30mV to -30mV.

Combined Flow Rate Equation

In some of the experiments performed by researchers at USC (Chilingar et al., 1970), an electric potential was applied across a core where oil was already flowing hydrodynamically. When the imposed electrical potential gradient and pressure drop are in the same direction, the oil flow rate is increased by removing some brine.

They obtained, the total flow rate equation by adding the electroosmotic relation to the Darcy equation: (Chilingar et al., 1968).

$$qt = Ak\Delta p/(\mu L) + Ak_eE/(\mu L) \tag{1-9}$$

This equation can then be presented in a dimensionless form by normalizing the flow rates and, thus, eliminating the viscosity, area and length terms:

$$q_t/q_i = 1 + k_eE/\,k\Delta p \tag{1-10}$$

and

$$(q_t - q_i)/q_i = k_eE/\,k\Delta p \tag{1-11}$$

Equation (1-10) shows that an increase in flow rate is dependent upon the zeta potential, dielectric constant, brine concentration, Darcy permeability, and pressure drop. If the dependence of k_e on k is not considered, then Eq. (1-11) would suggest that as the hydrodynamic permeability decreases, the percent increase in flow rate would become more significant. However, it should be noted that viscosity changes with temperature, and there is some heating as a result of application of an electrical potential. (see Chilingar et al., 1970.)

Calculated k_e/k, can be used as an index for predicting the probability of success and applicability of Electrically Enhanced Oil Recovery (EEOR).

The larger the ratio, the better the chance of success in dewatering sand and increasing the relative permeability to oil. In very tight formations, k_e may exceed k causing an increase in the degree of electric dewatering at the wellbore.

Two-phase Flow

When oil and brine flow simultaneously in a porous medium, and the flow is subjected to an applied electrical potential, the flow rate of the oil as well as that of the brine is affected by the electrical potential gradient. Although the electrical potential gradient affects only the brine directly, the oil flow rate is affected indirectly because the relationships that exist among the oil and water flow rates, fluid saturations, permeabilities, and pressure gradients (Chilingar et al., 1970).

In the absence of an electrical potential gradient, the initial flow rate of brine, q_{w1}, is given by an adaptation of Darcy's law to a linear flow system:

$$q_{w1} = - k_{w1}A\Delta p_{w1}/(\mu_{w1}L) \tag{1-12}$$

If an electric potential is applied across the core, the electric field will drive the cations in the mobile part of the double layer towards the cathode.

These, in turn, will drag with them water molecules and, consequently increase the water flow rate. If this increase in flow rate is to be prevented, a pressure difference ΔP_{eo} must be applied in the opposite direction. P_{eo} is defined as the electroosmotic pressure difference.

In an electroosmotic flow experiment, four variables can be controlled. These are the oil and water flow rates and the pressure and electrical potential gradients. If one elects to maintain a constant pressure gradient and a constant water flow rate and to vary the applied electrical potential, the oil flow rate will vary with potential gradient as indicated in the following derivation.

On applying an electric potential, the flow rate, q_{w2}, will become:

$$q_{w2} = - (k_{w2}A/(\mu_{w2}))[\Delta p_{w2}/L + \Delta p_{eo}/L] \tag{1-13}$$

If the inlet and outlet pressures were held constant, with the outlet pressure being atmospheric, then $\Delta P_{w1} = \Delta P_{w2} = \Delta P$. If the water is introduced into the system through a constant-rate pump, its flow rate would stabilize after the electric potential is applied for a period of time. Upon stabilization of water flow rate, $\Delta q_{w1} = \Delta q_{w2}$. Dividing,

$$q_{w1}/q_{w2} = 1 = (\mu_{w2}/\mu_{w1})(k_{w1}/k_{w2})[\Delta p/(\Delta p + \Delta P_{eo})] \tag{1-14}$$

Inasmuch as $\mu_{w1} > \mu_{w2}$ owing to an increase in temperature, and $\Delta p + \Delta p_{eo} > \Delta p$, then $k_{w1} > k_{w2}$. Because relative permeability is a function of saturation, a decrease in relative permeability to water corresponds to a decrease in water saturation. This, in turn, would result in an increase in oil saturation and thus an increase in relative permeability to oil. At constant Δp, the oil flow rate will, therefore, increase with increasing oil permeability. Thus, under the foregoing conditions, the application of an electrical potential gradient results indirectly in an increase in oil flow rate (Chilingar et al., 1970).

Coehn's rule

A general rule for the potential difference of the double layer was given by Coehn in 1909 as follows:

Substances of higher dielectric constants are positively charged in contact with substances of lower dielectric constants. The corresponding potential difference is proportional to the difference of the dielectric constants of the touching substances. Later, researchers (Smoluchowski, 1921; Fairbrother et al., 1931; Verwey, 1941; and Adamson et al., 1963) investigated this qualitative rule.

They have found that this rule does not apply to pure organic liquids with low dielectric constants, such as benzene and carbon tetrachloride. However, Coehn's rule is still used to indicate the sign of the zeta potential and, hence, the direction of movement of phases past each other.

Electrolytic concentration

The qualitative rule presented by Coehn, seems to represent a very special case where ionic liquid content is very small even when compared to dilute aqueous solutions. The electrochemical behavior of the solid--liquid interface greatly influences these electrokinetic phenomena. In the case of relatively inert surfaces, such as quartz, the electrical charge density depends primarily on the adsorbed electrolytes.

Many researchers, showed a linear logarithmic relationship between zeta potential and concentration (*c*) (Adamson et al., 1963):

$$\xi = A - B \log c \tag{1–15}$$

The zeta potential, ξ, goes through a maximum and then approaches zero, which is explained by a combination of two processes: (1) adsorption process of ions on the surface and (2) followed by a neutralization process of the charged surface with opposite sign (Kruyt, 1952.)

Rutger et al. (1945) showed the effects of the H^+ and OH^- ions on zeta potential at low concentrations. A small addition of the OH^- increased the negative zeta potential. In the case of larger concentrations, all electrolytes decreased the zeta potential, especially pronounced in the case of polyvalent ions, whereas the addition of H^+ ions decreased the zeta potential.

Although electrolytes can strongly influence the zeta potential, they have no effect on the total potential drop (Adamson et al., 1963.) The addition of multivalent ions may cause the reversal of the sign of the zeta potential. This can be explained by the adsorbability for these ions in a layer bearing a larger charge than is present on the wall. This will cause a reversal of the charge and potential in the outer part of the double layer (Kruyt, 1952) in order to maintain the electro neutrality of the system.

The theory of the diffuse double layer leads to the conclusion that the concentration of the electrolyte varies inversely with the effective thickness of the diffuse part of the double layer, (and zeta potential.) The larger the ionic charges, the few the ions needed for charge compensation, whereas the larger the ionic charges, the larger the electric forces between the diffuse layer and the inner fixed layer. The fewer ions are needed for charge compensation, the larger the valences of the adsorbed ions (Adamson et al., 1963.)

Effect of temperature

The influence of temperature on electrokinetic phenomena has been studied by many researchers [Smoluchowski, 1921; Abramson, 1934.] Cruze in 1905 [Smoluchowski, 1921] studied the effect of temperature and current through clay diaphragms. He found that constant values of electro-osmosis were obtained only after the passage of current for several hours. He also found marked dependence of the constant electro-osmotic flow on the temperature and on the current strength. According to his measurements, Wiedemann's constant *(V/i)* increases with increasing temperature, reaches a maximum and then decreases again. The quotient *(V/i)* is constant for a small current strength, increases with increasing current density to a maximum and then decreases rapidly with further increase of current. Some of Cruze's results (Adamson et al., 1963.):

Table 1-1: Cruze's (1905) measurements of Weidamann's constant *(V/i)* with increasing temperature.

$T\,^{o}C$	**9.45**	**24.16**	**30.97**	**36**	**40.21**	**49.86**	**65.81**
V/i	**6.24**	**9.26**	**9.97**	**10.27**	**9.54**	**6.17**	**4.45**

Smoluchowski (1921) calculated analogous results by using Helmoholtz-Smoluchowski's equation, and assuming zeta potential to be constant, while allowing for the variation of the viscosity and η the specific resistance R.

He indicated that the apparent dependence of the electro-osmotic transport of water on the current strength may be attributed to the heating effect of water in the diaphragm at high current strength.

Perrin (1904), and Oettinger (1912), obtained results which agree on the approximate constancy of the term, Dx, in the electrokinetic equations and its independence of temperature. Burton (Abramson, 1934) determined the electrophoretic velocity of particles of silver sol in water at different temperatures.

Some of his results are listed below:

Table 1-2: Variation of electrophoretic velocity with temperature (Burton, 1934.)

$T\,^{o}C$	**3.0**	**9.9**	**11.0**	**21.0**	**31.0**	**40.5**
$V\eta X10^{7}$	**24.5**	**24.7**	**25.1**	**25.0**	**24.0**	**24.5**

This shows that the electrophoretic velocity multiplied by the respective viscosity stays approximately constant, or where $V\eta$ is approximately a constant, known as Burton's rule for electrophoresis velocity.

This relation is known as Burton's rule for electrophoretic velocity. Some interesting research work has been done on electrophoretic velocity of kaolinite clay upon addition of NaOH (Chilingar, 1952.)

Further work, regarding the effect of temperature on electro-osmotic transmission of liquid, was reported by Winterkorn (1947.) His investigation covered a variety of clay minerals at different temperatures. It seems that he has corrected for the effect of temperature on water viscosity, yet a marked increase in the electro-osmotic transport of liquid at high temperature can be noticed. He attributed this increase to a thermal gradient causing the fluid to flow in a manner similar to electro-osmosis, and the effect was called thermo-osmosis.

Winterkorn (1947, 1955) confirmed the phenomenon of thermo-osmosis by an experiment in which a thermal gradient was set up across a hydrophilic clay sample and estimated the thermo-osmotic coefficient K_t to be equal to 1 x 10^{-7} cm/sec per degree ^oC per *cm*. By means of a potentiometer connected to two platinum electrodes fixed at the surface of the clay sample, he was able to measure a potential gradient across the sample. As mentioned earlier, Helmholtz generated the first analytical equation by assuming:

1 - The hydrodynamic equations for viscous liquids are valid for the entire region of the double layer.

2 - And laminar flow conditions prevail.

The electrokinetic velocity for a capillary tube is as follows (in Anbah et al., 1964):

$$u = i\sigma (\phi i - \phi a)/4\pi\eta \qquad (1\text{–}16)$$

where: i = current density

σ = specific resistance

η = the liquid viscosity

ϕ = electrical potential at the solid wall

Later, modifications by Smoluchowski (1921) lead to the famous Helmholtz-Smoluchowski's equations:

$$v_e = \xi DE/4\pi\eta \tag{1–17}$$

$$V = A\xi DE/4\pi\eta \tag{1–18}$$

where: A = cross-sectional area

D = dielectric constant

ξ = zeta potential

E = potential difference

v_e = electokinetic flow rate

For porous plugs, the cross-sectional area, A, was eliminated by the application of Ohm's law and by assuming no surface conductance:

$$AE = i/\lambda \tag{1–19}$$

$$v_e = D\xi i/4\pi\eta\lambda \tag{1–20}$$

where: λ = specific conductivity

i = current through capillaries

These equations were then proved to hold true for turbulent flow (Rutgers et al., 1957). If surface conductance exists in the capillaries, then:

$$AE + SE = i \tag{1–21}$$

$$v_e = D\xi i/[4\pi\eta(\lambda + (S/A)\lambda_s)] \quad (1\text{–}22)$$

where: S = circumference of capillary

λ_s = specific surface conductance

Upon measuring the conductivity or resistivity of the liquid (while present in the capillaries) necessary corrections can be made:

$$v_e = D\xi i/4\pi\eta\lambda' \quad (1\text{–}23)$$

where: λ' is the corrected specific surface conductivity. Thus, it includes the bulk conductivity, λ, and surface conductivity, λ_s.

Through experimental work, λ' can be determined experimentally from the measured resistance, R, across the core and its cell constant:

$$\lambda' = C/R \quad (1\text{–}24)$$

According to Manegold and Solf (1931):

$$C = L/[(A(1\text{-}f)\sigma] \quad (1\text{–}25)$$

where: L = length of core

A = cross sectional area

$(1\text{-}f)$ = volume fraction available for ionic migration

σ = shape factor

Thus:

$$v_e = AD\xi Ri(1\text{-}f)\sigma/4\pi\eta L = (AD\xi\sigma(1\text{-}f)/4\pi\eta)*(E/L) \quad (1\text{–}26)$$

According to Mazur and Overbeek (1951) and Lorenz (1952), a linear relation exists between the gradient and flow of current in regions and the effects of simultaneous electrical processes on the transport of liquid and electrical change in the capillary system could be considered additive (see Anbah et al., 1964):

$$i = C_{11} E + C_{12} P \tag{1–27}$$

$$V = C_{21} E + C_{22} P \tag{1–28}$$

where: i = electrical current through capillaries,

taken as positive when passing from side 1 to side 2

V = volumetric flow rate from 1 to 2, measured similarly

E = electrical potential difference, taken as positive when side 1 is positive

P = pressure difference across system, positive when side 1 is higher

C_{ij} = experimental coefficient

There are four variables and two equations only. In order to relate two variables with one coefficient, a third independent equation is needed.

This can be done by holding one variable equal to zero. For example, at P equal to zero, C_{11} represents the conductance or reciprocal of resistance. At $E = 0$, C_{22} represents the hydrodynamic permeability coefficient (Anbah et al., 1964):

Saxen's law (1892) relates electro-osmosis and streaming potential,

$[V/i = D\zeta / (4\pi\eta\lambda) = E/P]$:

$$-(E/P)_i = 0 = (V/i)_P = 0 \tag{1–29}$$

The minus sign indicates that the streaming potential and the pressure gradient act in opposite directions. Referring to Eq. 1-27, if one variable is set equal to zero and the other two variables are related, then:

$$(E/P)_i = 0 = -C_{12}/C_{11} \tag{1–30}$$

$(V/i)_P = 0 = C_{21}/C_{11}$ (1–31)

$C_{12}/C_{11} = C_{21}/C_{11}$ (1–32)

$C_{12} = C_{21} = C_e$ (1–33)

This relationship Onsager's relation (1931) can be obtained by reasoning based on the thermodynamics of irreversible processes (Overbeek, 1953).

The coefficient C_e represents the electrokinetic effect, and when interpreted in terms of zeta potential for a capillary tube, C_e is equal to $AD\zeta/4\pi\eta$, whereas for a porous plug, $C_e = AD\zeta/e\pi\eta F$.

where F = Formation factor

In the system where there is a coupling of two different transport processes, there are four different electrokinetic experiments that can be performed, namely:

(1) Electroosmotic flow at zero pressure;

(2) Electroosmotic pressure at zero flow;

(3) Streaming potential at zero current;

(4) Streaming current at zero potential.

These phenomena can be expressed as functions of current, electrical potential, flow of liquid, or pressure difference, thus leading to twelve coefficients. The coefficients for electroosmotic flow rate at $P = 0$ are (Anbah et al., 1964):

At P=0:

$(V/i)_p = 0 = C_e/C_{11}$ (1–34)

$(V/E)_p = 0 = C_e$ (1–35)

And for electroosmotic pressure at $V = 0$, can be expressed as:

$At\ V = 0:$

$$(P/E)_v = 0 = -C_e/C_{22} \tag{1–36}$$

$$(P/i)_v = 0 = -C_e/(C_{11}C_{22} - C_e^2) \tag{1–37}$$

Similarly, the coefficients for streaming potential at $i = 0$ are:

$At\ i = 0:$

$$(E/P)_i = 0 = -C_e/C_{11} \tag{1–38}$$

$$(E/V)_i = 0 = -C_e/(C_{11}C_{22} – C_e) \tag{1–39}$$

Whereas for steaming current at $E = 0$, they are:

$$(i/P)_E = 0 = C_e \tag{1–40}$$

$$(i/V)_E = 0 = C_e/C_{22} \tag{1–41}$$

The coefficients for permeability at $E =0$ and at $i = 0,$ are, respectively:

$$(V/P)_E = 0 = C_{22} \tag{1–42}$$

and

$$(V/P)_i = 0 = C_{22} - C_e^2/C_{11} \tag{1–43}$$

Finally, the coefficients for electrical conductances at $P = 0$ and $V = 0$ are equal to:

$$(i/E)_P = 0 = C_{11} \tag{1–44}$$

$$(i/E)_V = 0 = C_{11} - C_e^2/C_{22} \tag{1–45}$$

Due to existence of Onsager's relation, it appears that the absolute values of these coefficients are pairwise equal:

$$(E/P)_i = 0 = -(V/i)_P = 0 \text{ and } (i/P)_E = 0 = (V/E)_P = 0 \tag{1–46}$$

Whichever experiment is performed or whichever combination is chosen, the system is completely described by the three constants (C_{11}, C_{22} and C_e). The choice of the experiment to be performed is determined mainly by convenience and accuracy rather than by principle. In a highly conductive electrolytic solution (C_{11} is large), it is rather difficult to measure the streaming potential, whereas the streaming current will give a reasonable value and the estimated C_e will probably be more nearly accurate (Anbah et al., 1964).

It is a well-established fact (Elton, 1948; Mortada, 1952; Henniker, 1952; and Street, 1961) that when permeability is measured in the conventional way, the streaming potential has a retarding effect on the flow. This effect has been attributed to electroosmotic back flow, to electroosmotic back pressure, or to an increase in the fluid viscosity. It has been given various names, and has been referred to by such terms as electrokinetic blocking or electroviscous drag.

From Eqs. 1-42 and 1-43, the difference between the permeabilities obtained at $E = 0$ and at $i = 0$ represents the electrokinetic retardation effect and is expressed by the term C_e^2/C_{11}. This correction factor diminishes on increasing the concentration of electrolyte in the flowing solution or by allowing the electric current to flow in an outside circuit connected to the two ends of the core. It is of interest to note that, in the absence of any electrokinetic effect, the permeability will be higher than C_{22}. It could probably be obtained by coating the surface of the capillary by a conducting material. Mortada (1952) and Street (1959) related the true permeability K_t to the apparent permeability K_a for a porous plug as follows (Anbah et al., 1964):

$$K/K_a = 1 + (D^2 \xi^2 F)/(16\pi^2 \lambda \eta K) \qquad (1\text{–}47)$$

Electrokinetic Conductance Effects

From Eq. 1-45, the electrical conductance measured at $P = 0$ is given by C_{11} = $(i/E)_{p=0}$, and from Eq. 1-46, the electrical conductance, measured at $V = 0,$ is given by:

$$C_{11} - Ce^2/C_{22} = (i/E)v = o \qquad (1\text{–}48)$$

The electrical conductance, however, is ordinarily measured in the absence of any electrokinetic effects and is equal to:

$$Co = i/E \qquad (1\text{–}49)$$

Accordingly, it makes a difference whether the electrical conductance is measured at zero flow, at zero pressure, or in the absence of all electrokinetic effects.

The difference is greatest when:

(a) The radius of the capillary is small, or in the case of porous media, the permeability is low.

(b) When the specific conductivity of the electrolyte is low.

By subtracting Eq. 1-46 from 1-45, the difference Ce^2/C_{22} represents the electroosmotic conductance effect, which is comparable to the electroviscous blocking. It is due to the electroosmotic transport of excess charge of one sign by the motion of liquid, and the transmission of current takes place mainly in the form of convection.

The difference (C_{11}- C_0) represents the total surface conductance. According to Lorenz (1952), it arises from the increase of electrolyte concentration and altered ionic mobility near the wall, and an electroosmotic term, which is due to transport of surplus charge by the mobile part of the diffuse part of the double layer. The values of the different electrical conductances, as defined in Eqs. 1-44, 1-45 and 1-48, are related to each other in the following way:

$(i/E)_{p=0} > (i/E)_{v=0} > (i/E)$

The electroosmotic transmission of liquid through porous media can be given by:

$$Q_e = (AD\xi/4\pi\eta F)*(E/L) \tag{1–50}$$

$$= (AK_e/\eta)*(E/L) \tag{1–51}$$

where: K_e is electroosmotic permeability coefficient. The assumption that the electroosmotic coefficient K_e, is constant is justified if the system is under small potential gradients, the fluctuation in temperature is negligible and the solid surface is considered inert.

From Darcy's equation, the hydrodynamic flow rate:

$$Q_h = (AK/\eta)*(P/L) \tag{1–52}$$

If the two potential gradients, E/L and P/L are acting in the same direction, and the flow of current coincides with flow of liquid, then from equations 1-27 and 1-28, the total flow rate, Q_t, is the resultant addition of two separate flow rates:

$$Q_t = Q_e + Q_h = (AK_e/\eta)*(E/L) + (AK/\eta)*(P/L) \tag{1–53}$$

If the ratio Q_t/Q_h is defined as that of a normalized flow rate, then dividing equation 1-50 by 1-51, we arrive at:

$$Q_t/Q_h = 1 + Q_e/Q_h = 1 + (AD\xi E/4\pi\eta FL)*(\eta L/AKP) \tag{1–54}$$

$$= 1 + D\xi E/4\pi FKP = 1 + (Ke/K)*(E/P) \tag{1–55}$$

On excluding any formation of tiny fissures as pointed out by Cassagrande (1947), and by assuming the hydrodynamic flow rate, Q_h, is to remain constant and equal to Q_i, the normalized flow rate may be expressed as:

$$Q_t/Q_i = 1 + (K_e/K) * (E/P) = 1 + q \qquad (1\text{–}56)$$

where q is fractional increase in flow rate and equal to $(Q_t - Q_i)/ Q_i$

On using similar reasoning, one can obtain an equation for the fractional increase or percentage increase as follows:

$$(Q_t - Q_i)/Q_i * 100 = 100q \qquad (1\text{–}57)$$

Electrochemical Background

Five main mechanisms appear to be operative in EEOR, based on the available field and laboratory data (Wittle et al., 2008):

- Joule heating
- Electromigration
- Electrophoresis (movement of clay)
- Electroosmosis
- Electrochemically enhanced reactions.

All of these coupled reactions were described by the Lars Onsager (1931a, 1931b, 1969), who received the Nobel Prize in Chemistry in 1969. Mitchell (1993) and Noubehecht and Madden (1963) presented simpler representations. The matrix notation for the Onsager's relationships can be presented as follows:

$$Ji = \sum_{j=1}^{6} L_{ij} \nabla \Phi_j \qquad (1\text{–}58)$$

where: Ji = generalized flow, or flux vectors.

$\nabla \Phi_j$ = generalized potential gradient (force) vectors.

L_{ij} = generalized conductivity, or coupling coefficient (second rank) tensors.

Non-coupled fluxes are related to their potential gradients through the main diagonal terms L_{ii}, whereas the off diagonal L_{ij} relate coupled fluxes. If the products $J_i * \nabla \Phi_j$ represent free energy dissipation, then according to Onsager's principle:

$$L_{ij} = L_{ji} \tag{1–59}$$

Upon examining Eqs. 1-58, one can observe that (after Wittle et al., 2008):

- If J_1 is the electrical current density and Φ_1 is the electrical potential, then L_{11} is the electrical conductivity tensor, σ.
- If J_2 is the heat flow and Φ_2 is the temperature, then L_{22} is the thermal conductivity tensor, K, and L_{21} includes Joule heating.
- If J_3 is the ionic flux and Φ_3 is the ionic concentration, then L_{33} is the (ionic) diffusion coefficient, D_i and L_{31} includes electromigration.
- If J_4 is the charged-particle flux and Φ_4 is the charged-particle suspension density, then L_{44} is the (charged particle) diffusion coefficient, D_p, and L_{41} includes electrophoresis.
- If J_5 is the fluid flux and Φ_5 is the pressure, then L_{55} is k/μ, (k is the absolute permeability tensor and μ is the fluid viscosity) and L_{51} includes electroosmosis.

- If J_6 is the chemical reaction product flux and Φ_6 is the chemical reactant concentration, then L_{66} is the chemical reaction rate constant, and L_{61} includes electrochemically enhanced reactions.

The primary electrokinetic mechanisms are described below:

Joule Heating

The passage of the electrical current through conducting fluids and solids within a reservoir causes heating. Such Joule heating is responsible for raising the temperature and reduces the viscosity of the fluids.

Electromigration

Under the influence of an applied electric field, the cations move to cathode and anions migrate to anode. This is the basis of electroplating or electrorefining, as metallic cations migrate from anode to cathode allowing the oxidation to occur at the anode.

Electrophoresis

Similar to electromigration, the charged colloidal particles that are suspended in solution move to the electrode based on their surface charge sign. In the case of clays, being generally negatively charged, exhibits flow towards the anode. This may result in many scenarios from clearing blocked pore throats (increasing permeability), to clogging up other pore throats. However, there is a potential destruction of the double layer, therefore drastically reducing the electro-kinetics permeability. (Also see Tchilingarian, 1952).

Electroosmosis

As defined by Leo Casagrande (1952, 1959), Gray and Mitchell (1967), and Tikhomolova (1993), the Helmholtz double layers are formed in connate waters adjacent to clay minerals in narrow pore throats, allowing hydrated cations and water molecules to pass through towards cathode, but blocking anions. This mechanism can dewater expansive clays and increase permeability in petroleum reservoir rocks.

Electrochemically Enhanced Reactions

Electrochemically enhanced reactions appear to cause “cold-cracking” of heavy crudes resulting in the breakdown into lighter components, with a significant increase in the flow rate. Reactions between the pore fluids and matrix materials are enhanced by Eh/pH changes caused by the passage of direct electrical current. (Wittle et al., 2008)

Helmholtz double layer

A schematic diagram illustrating the Helmholtz double layer within a pore throat is presented in Figure 1-8.

The double layer is divided into two electrochemical regions:

- A region of fixed water molecules and cations held by strong electrostatic forces to negatively charged mineral surfaces. (stern layer)

- A region of loosely bound cations and water molecules, which are partially shielded from the negatively-charged surface charge minerals surfaces by the water molecules and cations of the Stern layer. In the presence of an external electrical field, this layer (Gouy layer) can move towards the cathode.

Distribution of negative and positive ions in formation water and distribution of hydrocarbons during flow in wide and narrow pore throats is presented in Figs. 1-8 and 1-9, as envisioned by Wittle et al. (2008).

It is important to note here that it is not really known how do oil and water flow (two-phase flow) through reservoir rocks. For example, Dr. George V. Chilingar (personal communication) believes that one phase is dispersed in another. In water-wet rocks, the discontinuous phase (non-wetting, dispersed phase—oil) is dispersed in the continuous phase (wetting, dispersion phase—water). This problem remains to be solved. The fact remains, however, that on application of DC current, both oil and water move faster towards the cathode in water-wet rocks. Whether this is true or not in the oil-wet rocks is unknown.

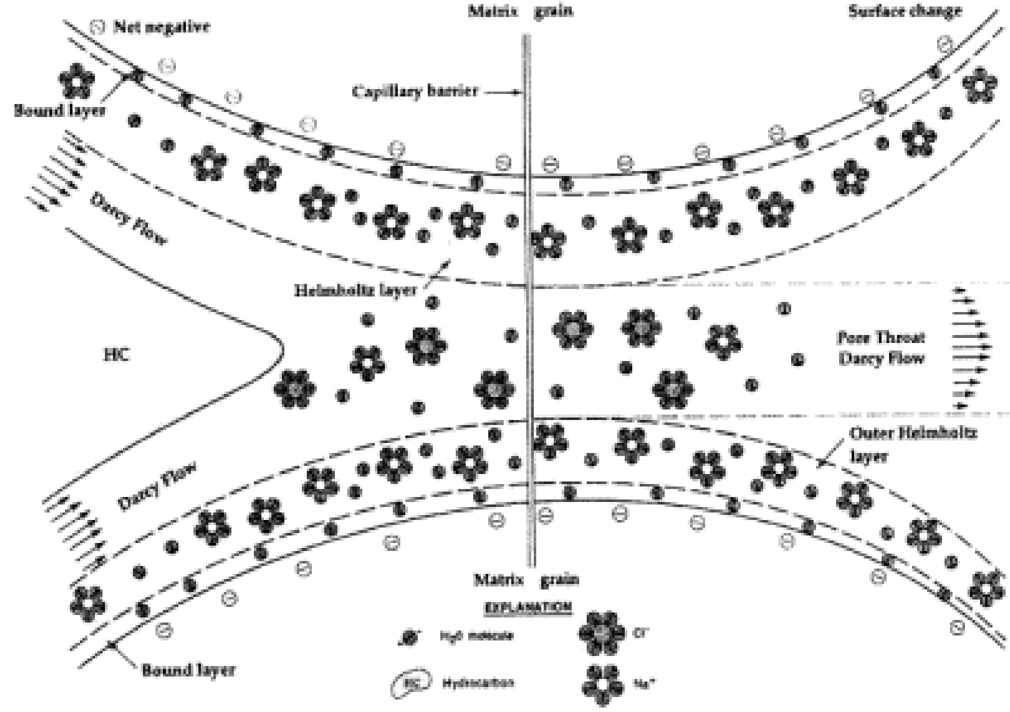

Figure 1-8: Schematic diagram of a flow through a wide pore throat of a water-wet reservoir rock showing distribution of anions and cations (double layer), as envisioned by Wittle et al. (2008). The potential difference between shear or slipping plane surface between the mobile and immobile double layers and the free fluids is the zeta potential.

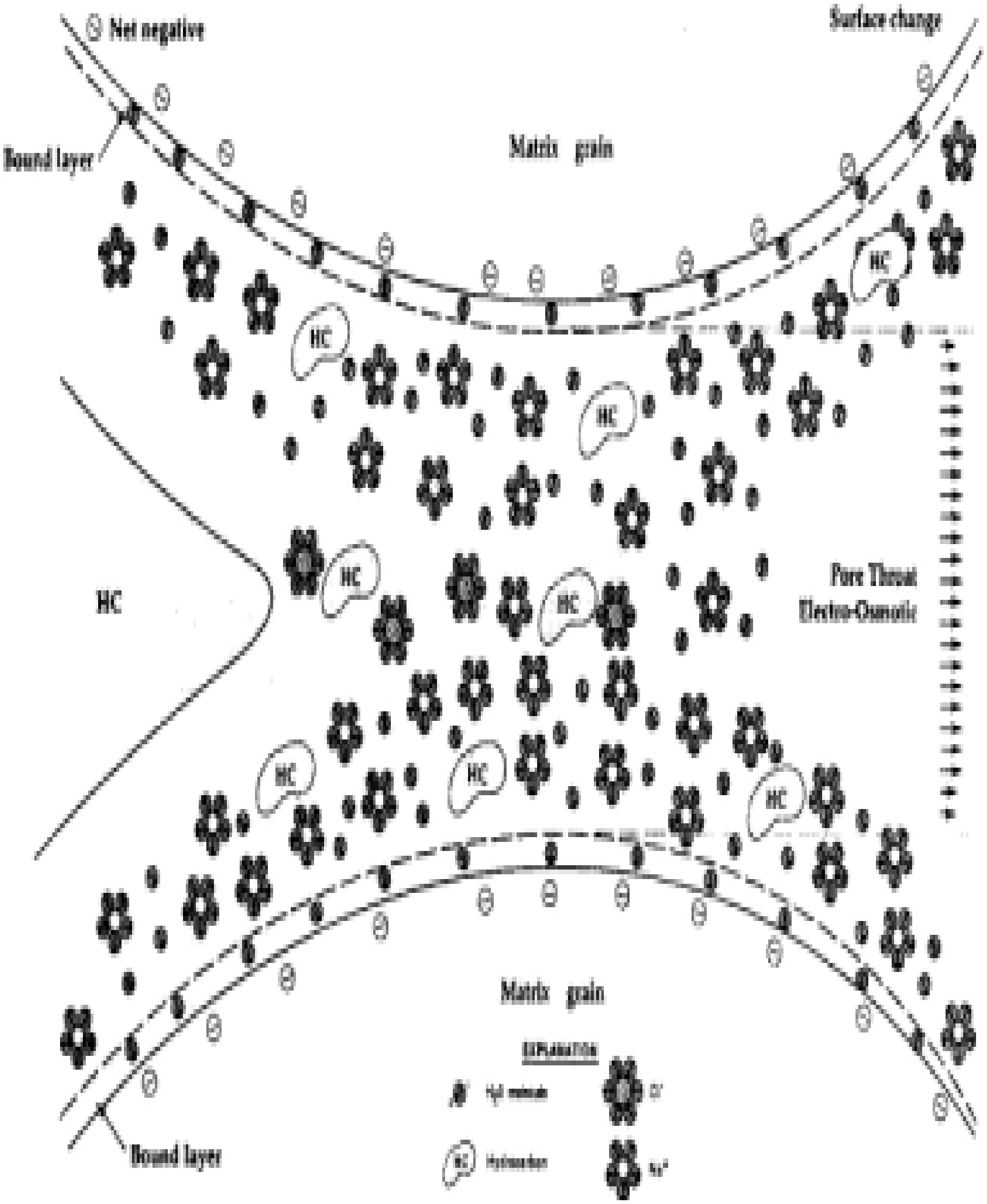

Figure 1-9: Schematic diagram of a double layer distribution in a narrow pore throat of water-wet reservoir and flow as envisioned by Wittle et al. (2008).

Figure 1-10 shows relationship between the electrical potential and normalized flow rate (qt/qi) in sand cores containing different clays (Kaolinite, illite, and montmorillonite). Test on core devoid of clays, i.e., 20-mesh silica sand, also showed a lower increase in flow rate upon application of D.C. current. Possibly, the double-layer also exists in the case of pure silica. In addition, thermal effect plays a role.

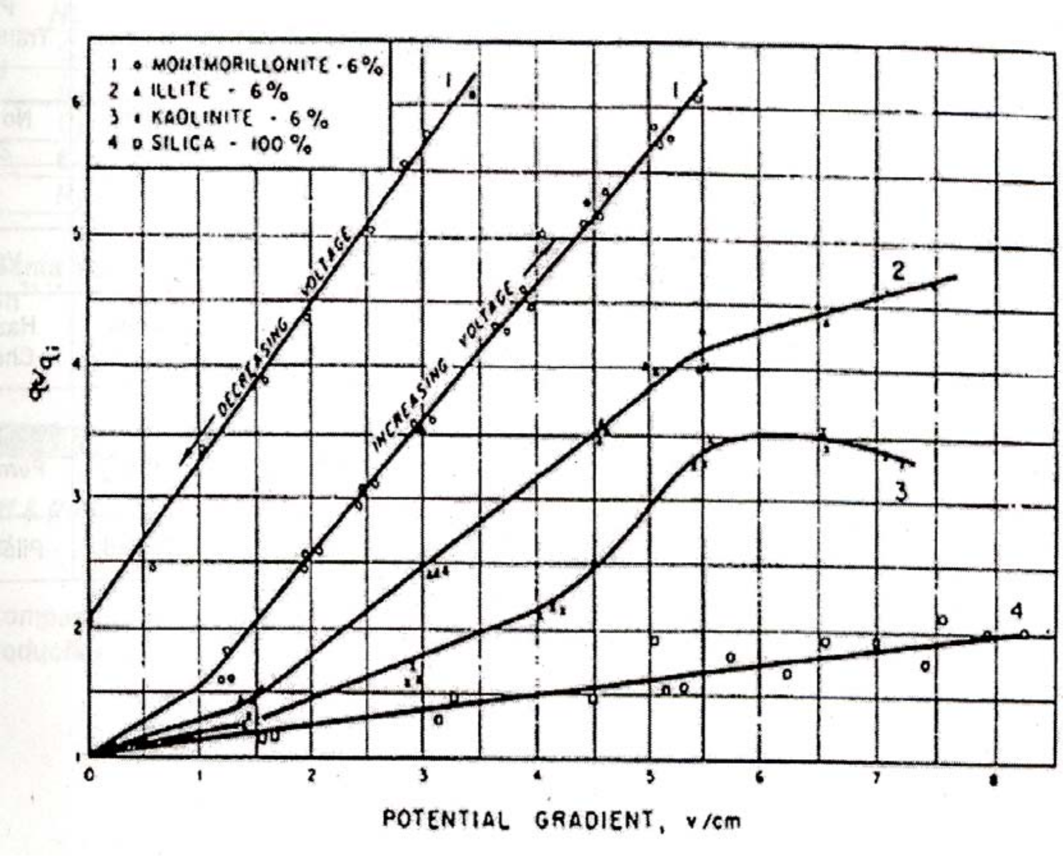

Figure 1-10: Relationship between electrical potential gradient and normalized flow rate. (After Chilingar et al., 1970.)
qi = initial flow rate before application of D.C. current.
Core no.1: 94% silica sand & 6% montmorillonite clay.
Core no.2: 94% silica sand & 6% illite clay.
Core no.3: 94% silica sand and 6% kaolinite clay.
Core no.4: 100% 20-mesh silica sand.

The following results are obtained by Anbah at al., 1964 at USC. The major variables involved here are: 1) Electric potential gradient, 2) electrical current, 3) electrolytic concentration, 4) applies pressure differential and 5) total flow rate. By holding some variables constant and they captured the effects of the varying variable with varying flow rate. The results are presented in the following figures:

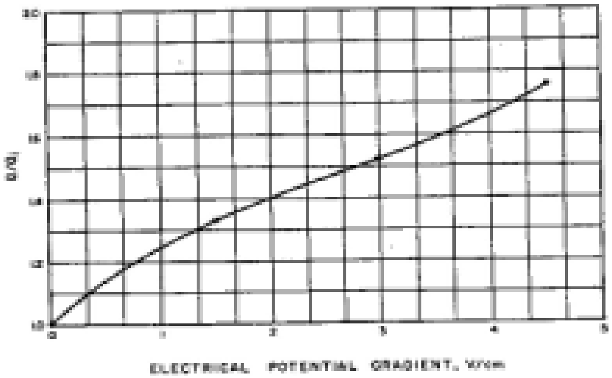

Figure 1-11: Normalized flow rate (Q/Qi) versus electrical potential gradient (E/L) showing a drop in the total flow rate due to plugging by deposited copper compounds, (after Anbah et al., 1964, p.5).

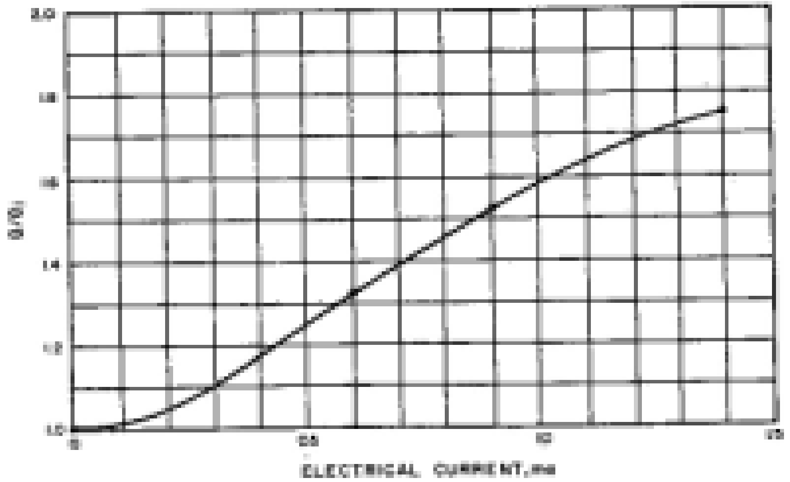

Figure 1-12: Imposed electrical potential versus q/qi (actual rate of flow/initial rate of flow) ratio. (After Anbah et al., 1964, p.5.)

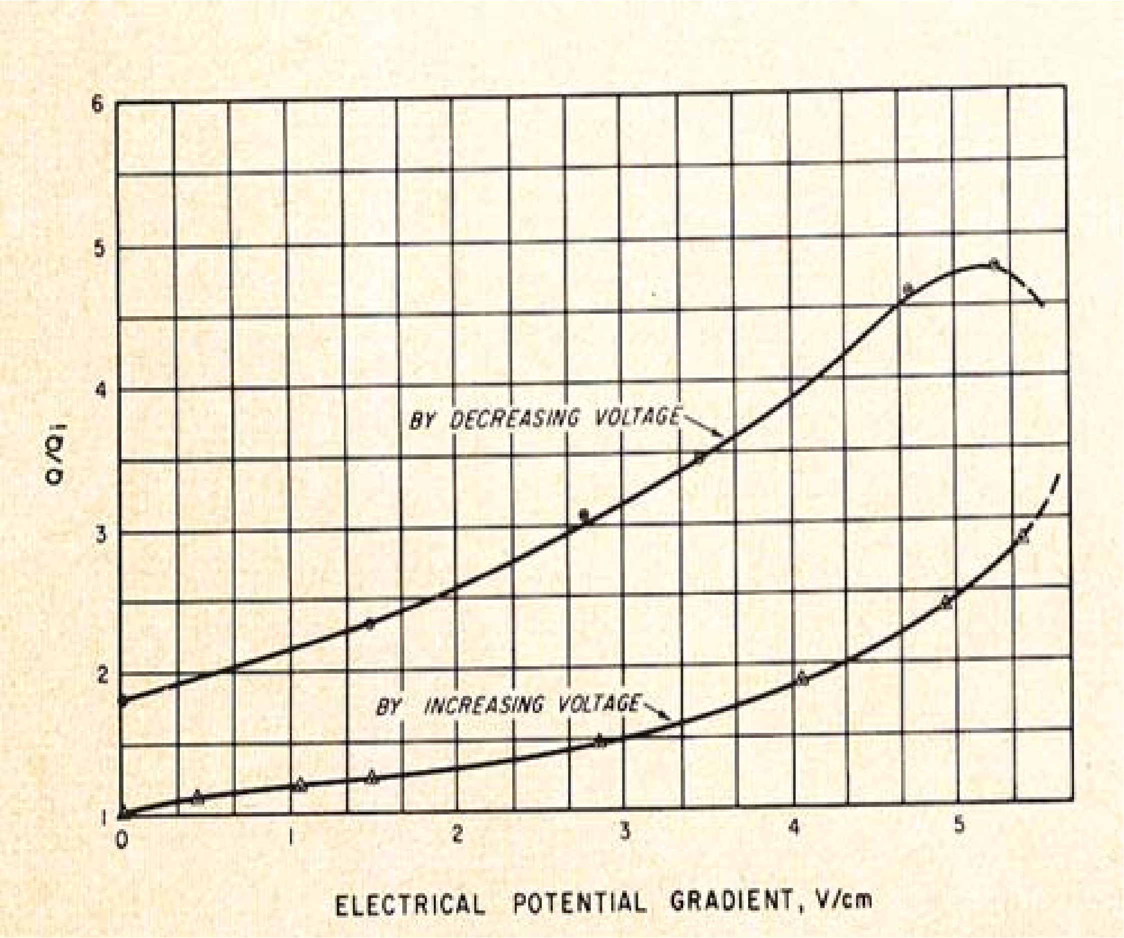

Figure 1-13: Electrical current versus normalized flow rate, q/q$_i$ (90% silica + 10% Wyo-gel synthetic core). (After Anbah et al., 1964, p.5.)

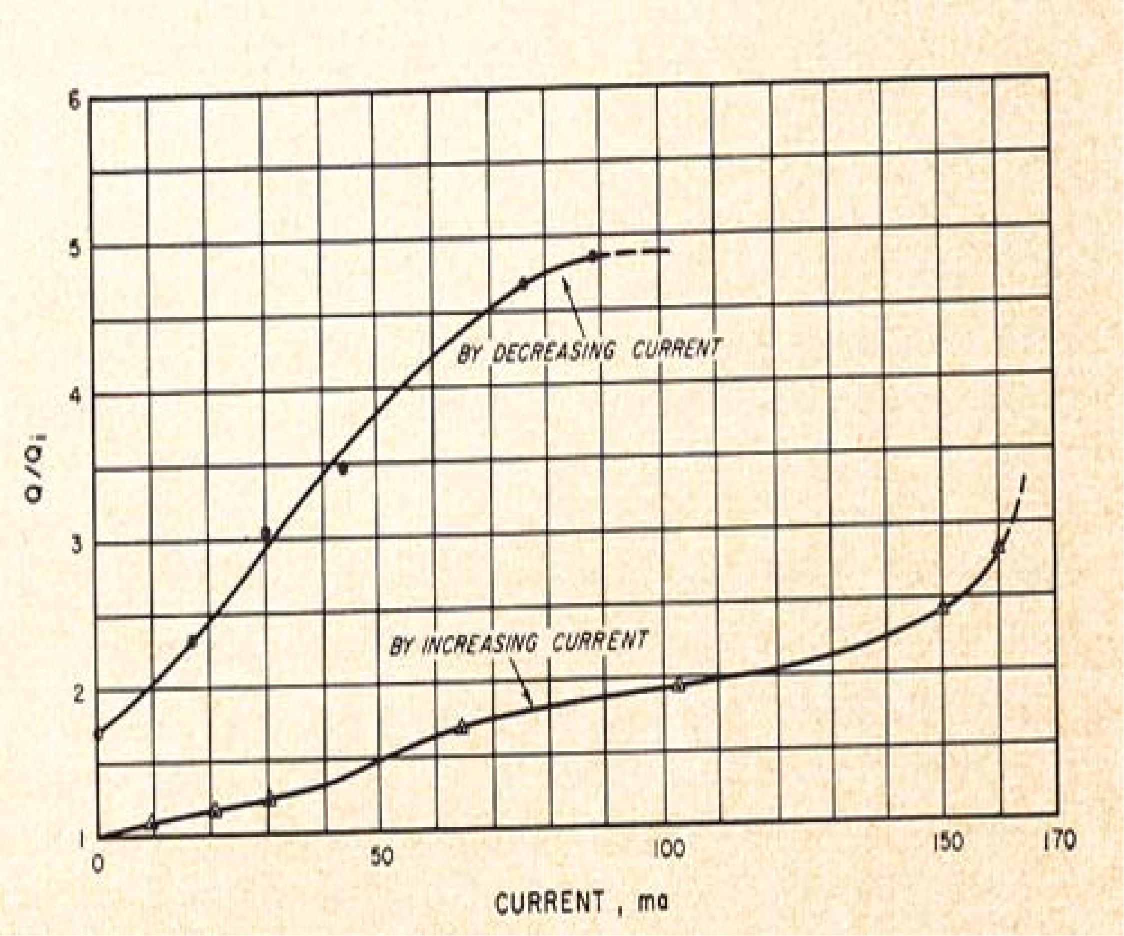

Figure 1-14: Electrical current versus flow rate, q/q_i
(95% CaCo3 + 5% Wyo-gel synthetic core). (After Anbah et al., 1964, p.5.)

Figure 1-15 through 1-18, illustrate possible field implementation, where anode(s) are placed at the ground surface and the cathode(s) are placed in or near the producing well(s). These configurations have been suggested by Chilingar. (Personal communication).

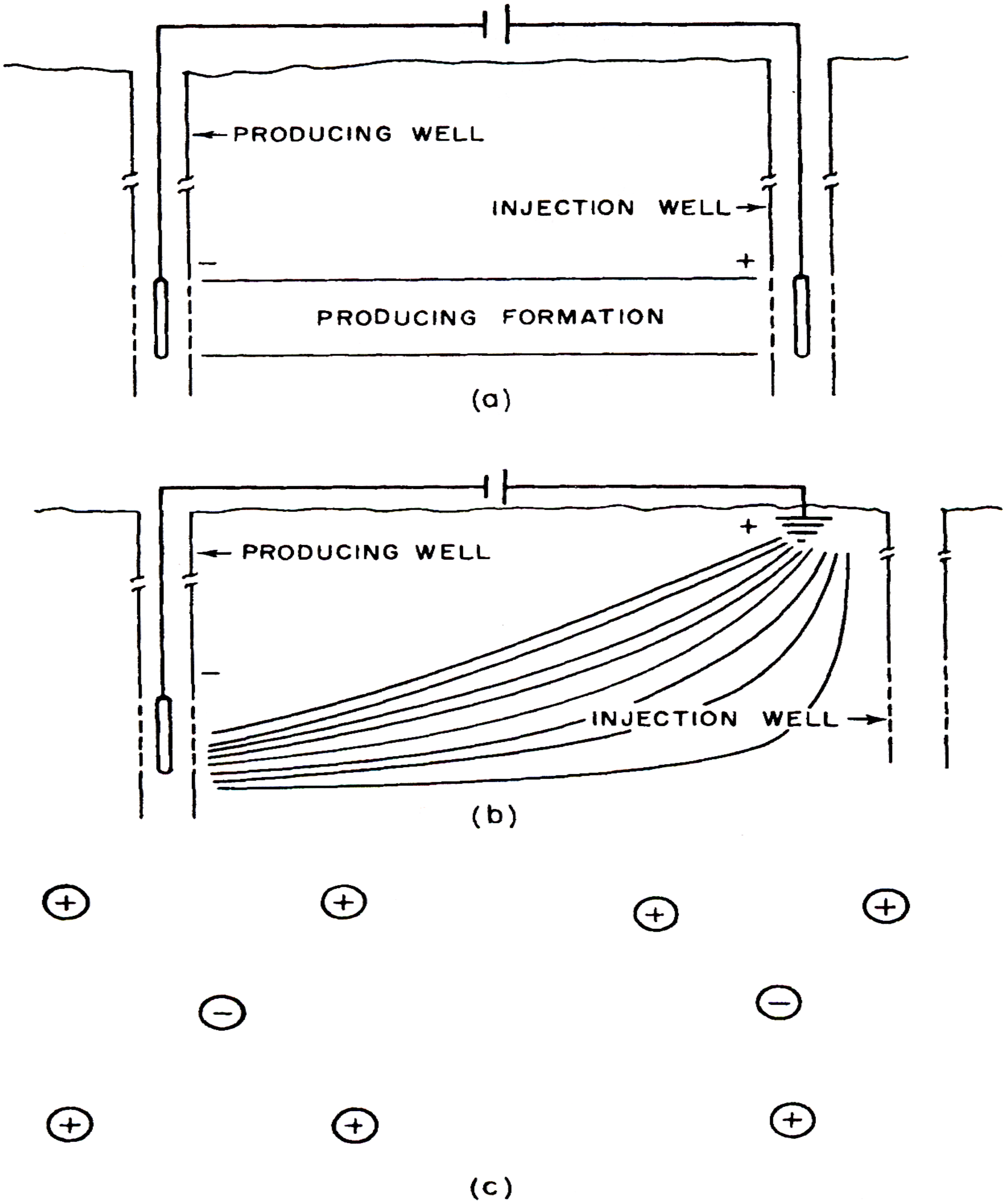

Figure 1-15: Electrode-arrangement for water flooding operation: (a) The anode is laid down in the injection well to face the producing zone. (b) The anode is driven into the wet ground near the injection well. (c) Four and five spot flooding pattern (Anbah et al. 1965).

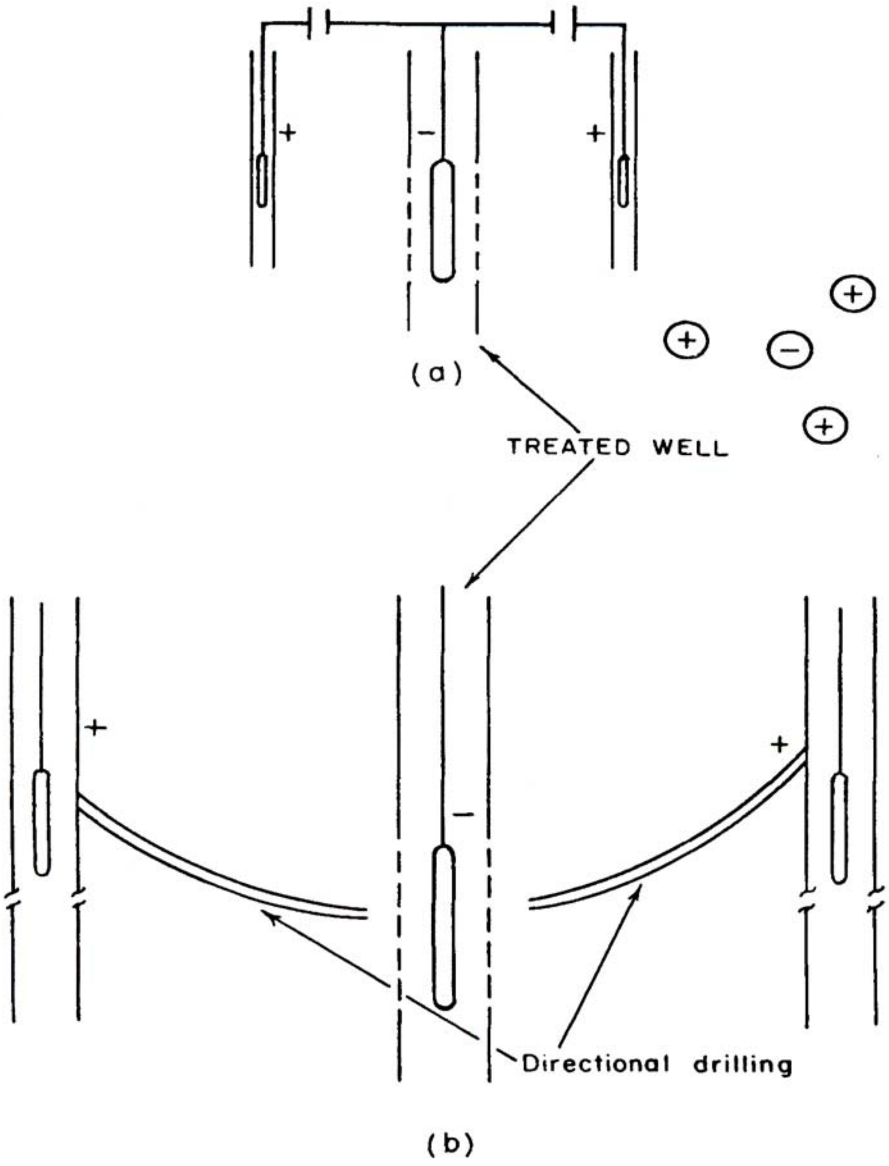

Figure 1-16: Electrode-arrangement for well stimulation. (a) Anodes are put in specially drilled small-diameter holes around the treated well. (b) Anodes are put either in shut-in wells or in directionally drilled small-diameter holes from shut-in wells (Anbah et al. 1965).

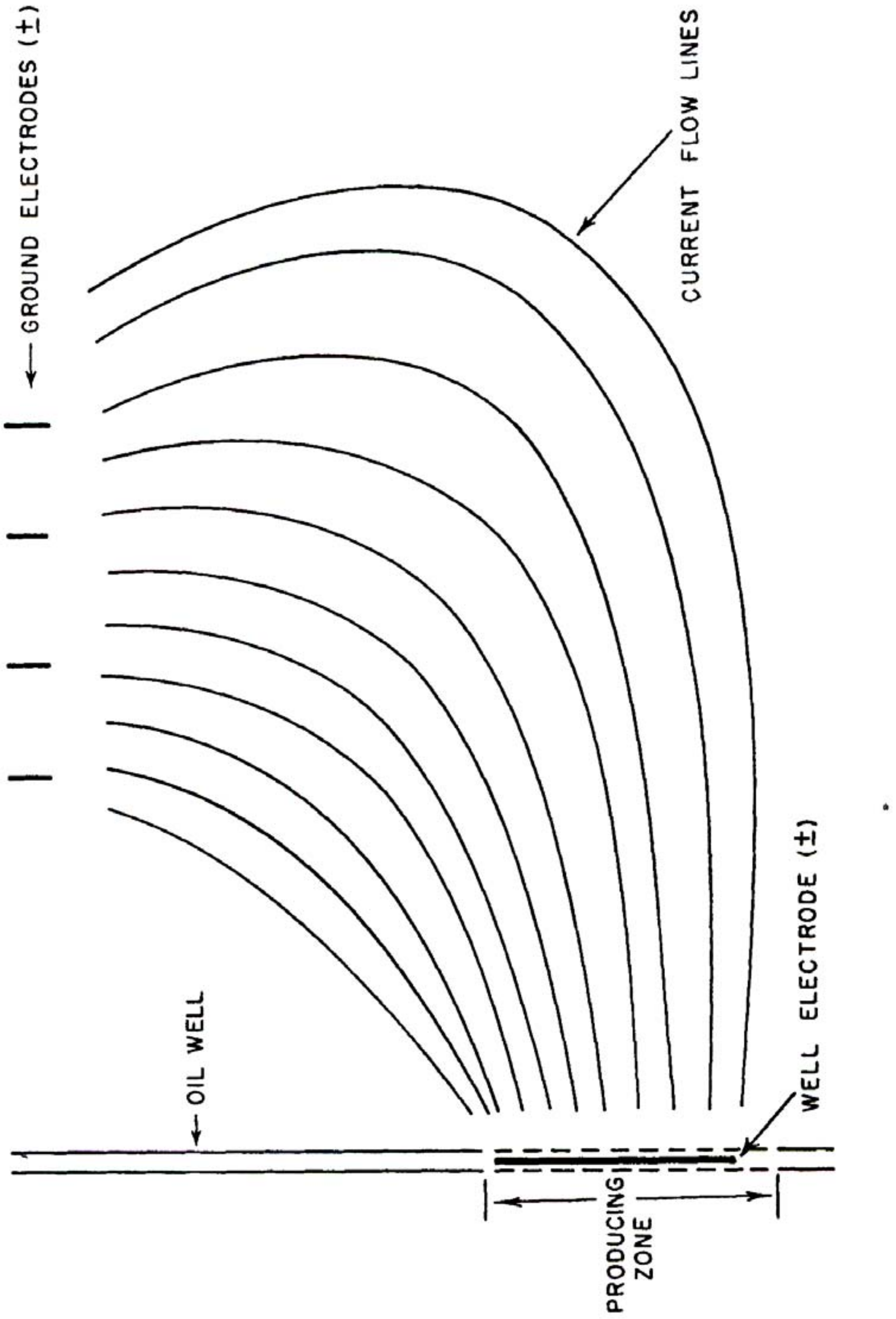

Figure 1-17: Electrode-arrangement for selective ion-drive. Conducting pipes driven into the wet ground are used as anodes or cathodes (Anbah et al. 1965).

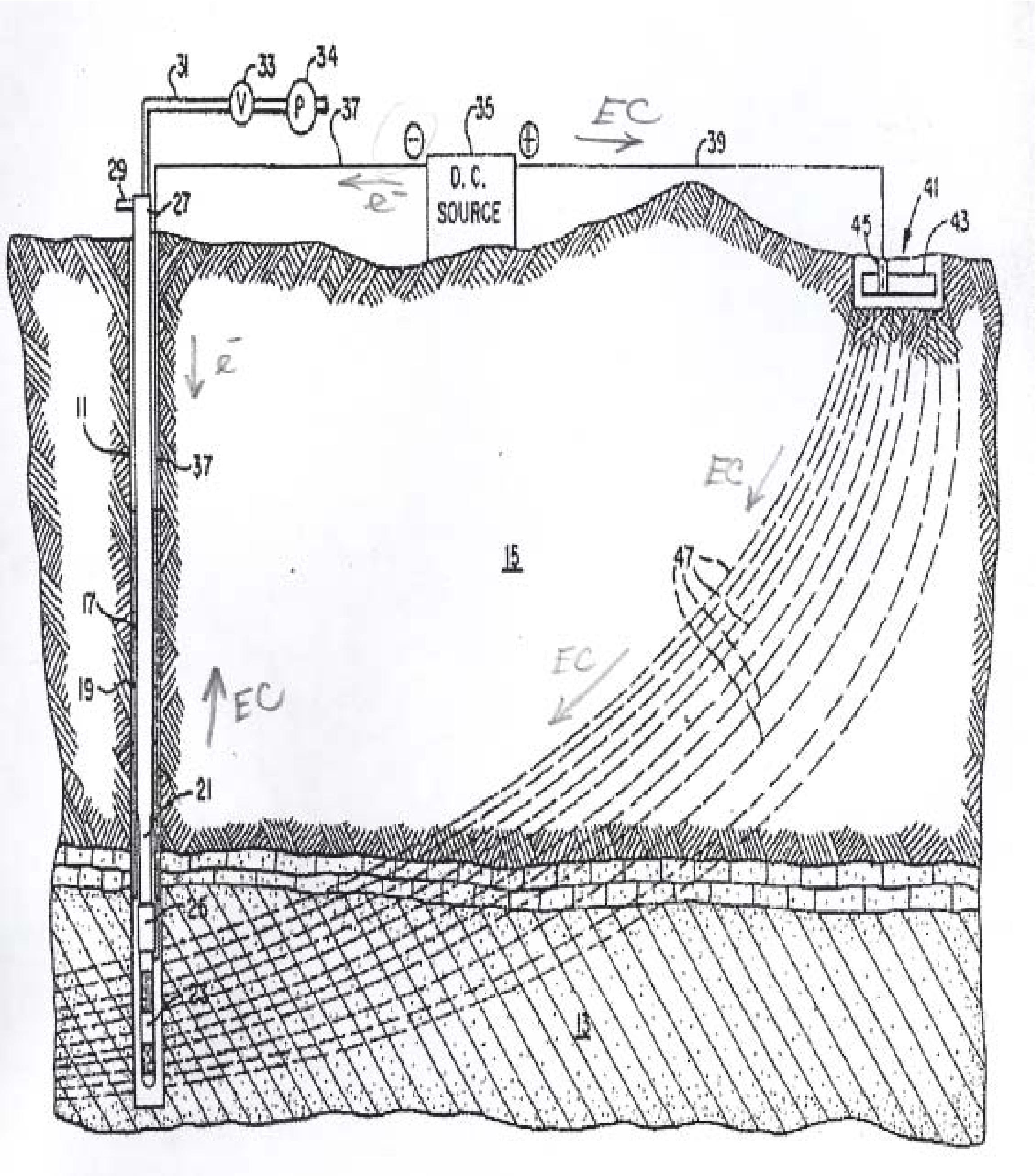

Figure 1-18: Schematic diagram of locations of cathode and anode in EEOR field operation. (Modified after Anbah et al., 1965; and Titus et al., 1985.)

Three-Dimensional Current Flow Ramifications

For one-dimensional linear circuit theory, Ohm's law is:

$$I = \Delta V/R \tag{1-60}$$

or $\Delta V = IR$ (1-61)

Joule heat loss across a given circuit element, with resistance R, as follows:

$$P = I\Delta V = I^2R \tag{1-62}$$

where: P = power loss, over the individual circuit element of resistance, R.

ΔV = voltage drop across the individual circuit element.

R = individual circuit element resistance.

I = current through the entire circuit, controlled by the total voltage drop across the entire circuit and the sum of all of the resistances in the circuit.

In three-dimensions, Ohm's law (Equation 1-60) becomes:

$$J = \sigma E = \sigma \nabla \Phi = \rho^{-1}\, \nabla \Phi \tag{1-63}$$

or

$$\nabla \Phi = \rho\, J \tag{1-64}$$

In three-dimensions, the local Joule heating power loss is given by:

$$p_{x,y,z} = J*E = J * \nabla \Phi = |J|^2 \rho \tag{1-65}$$

where: $p_{x,y,z}$ = local power loss at the point of interest

E = local electric field vector

$\nabla \Phi$ = local electrical potential field gradient

σ = local electrical conductivity tensor

ρ = the local electrical resistivity tensor (inverse of σ)

J = local current density vector

I is constant in equations 1-60 to 1-62, and is dependent only on the total voltage drop across the entire circuit element in the circuit, and the sum of the circuit element resistances in the circuit. All of the parameters in Eqs. 1-63 to 1-64 are functions of position for a heterogeneous earth model.

Electric current densities follow the paths of least resistance, so that the total Joule power loss:

$$P_T = \iiint P_{xyz}\, dxdydz \qquad (1\text{-}66)$$

For the entire (earth system is minimized, this means that regions of high resistivity, $|J|$ is much lower than in regions of low resistivity.

Figure 1-19 illustrate the Joule heating simulation results in the vicinity of the downhole electrode within a heavy oil reservoir (according to Wittle et al., 2008). Here it shows that even after 19.5 months of EEOR with DC application, the temperature beyond 14 ft of the electrode surface is essentially unchanged.

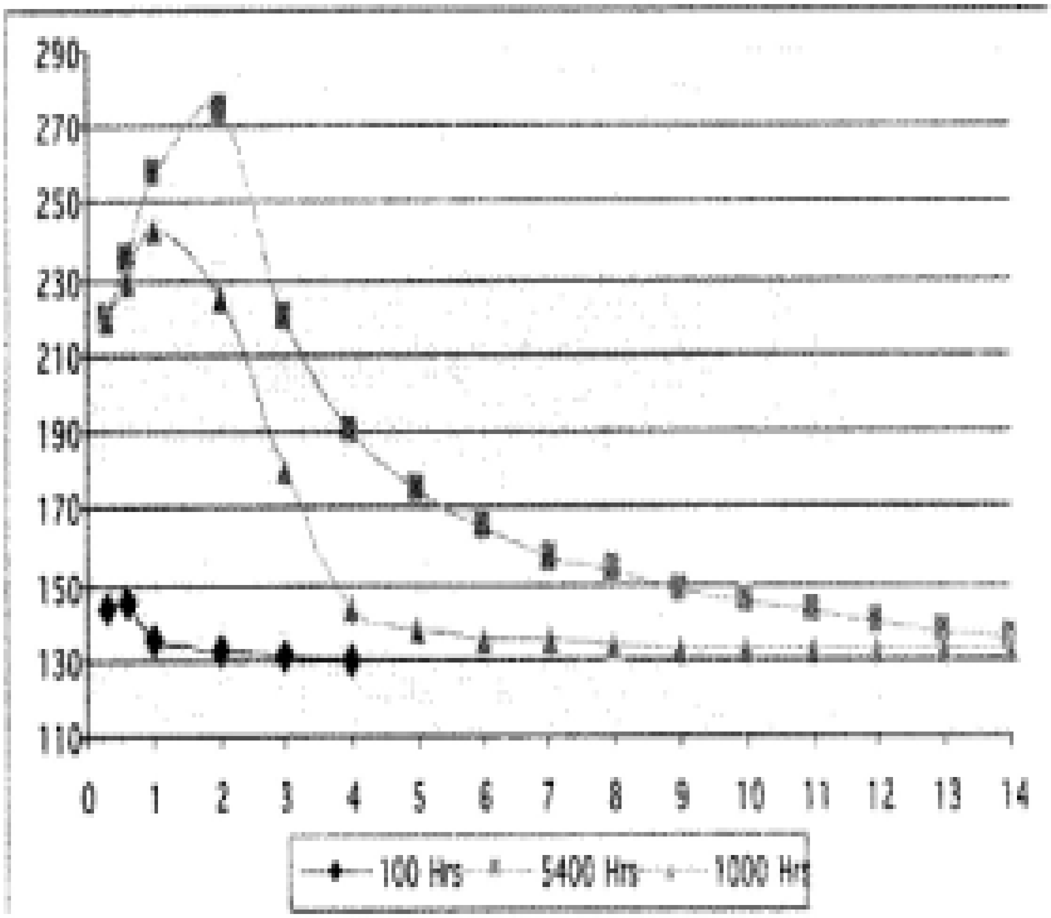

Figure 1-19: EEOR simulation results: reservoir temperatures after 100, 1000, and 5400 hours of stimulation. Temperatures in ^{o}F (ordinate) and distances are in feet (abscissa), from casing. (After Wittle et al., 2006.)

Figure 1-20 show a series of Gas Chromatography Mass Spectrograph (GCMS) spectras from polyaromatic Hydrocarbon (PAH) contaminated soils undergoing Electro-chemical Geo-Oxidation (ECGO) remediation. It demonstrates the spectra peak shift from complex hydrocarbons to simpler ones with time, as in in-situ cold-cracking.

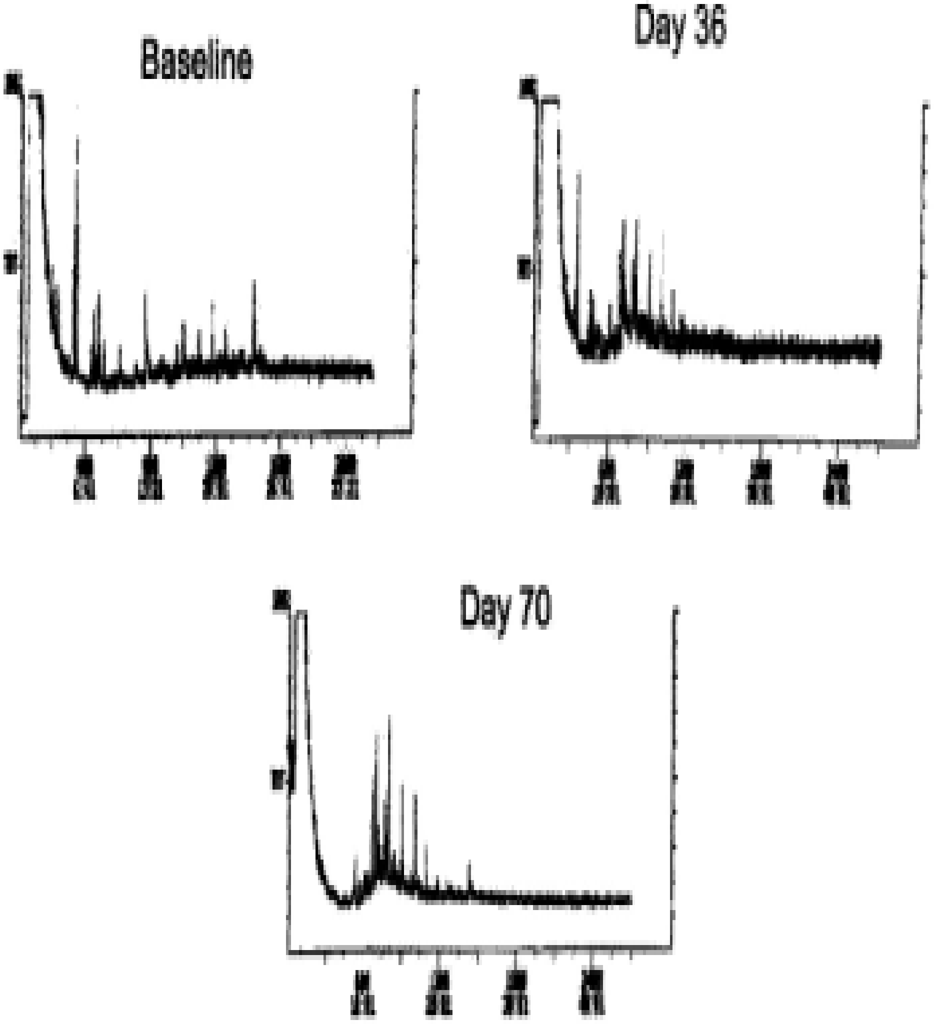

Figure 1-20: ECGO PAH destruction GCMS changes during treatment. (After Wittle et al., 2008.)

Wittle et al. (2008) did not explain why the water cut decreases on application of D.C. current. The writer believes that this is due to changing polarity of the oil upon application of D.C. current. As pointed out by Chilingar et al. (2005), with increasing polarity of oil, the relative permeability to oil increases, whereas the relative permeability to water decreases (Fig. 1-21).

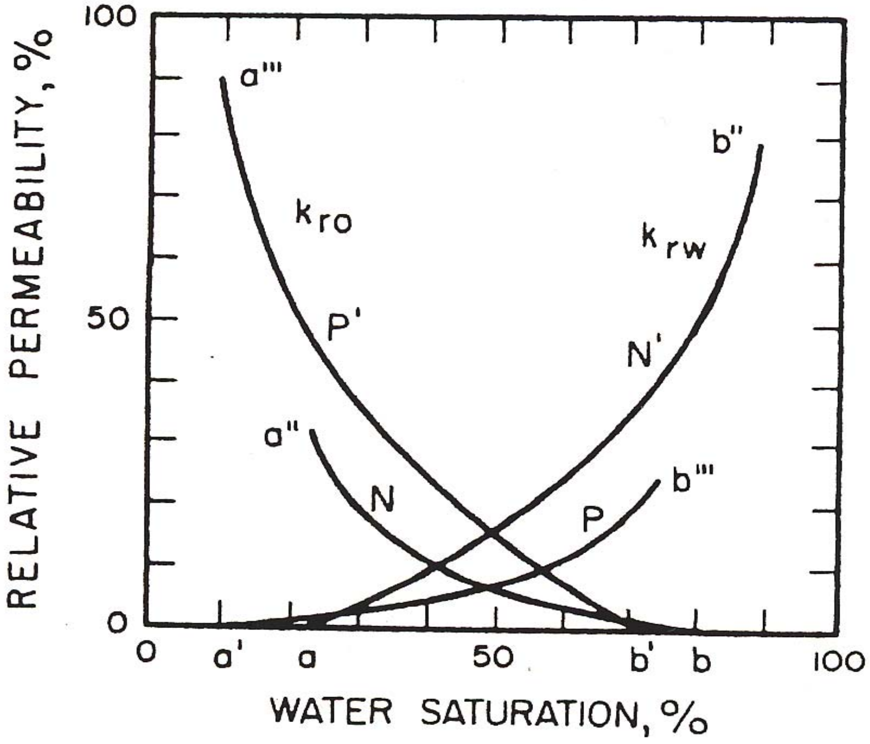

Figure 1-21: Relative permeability curves for polar and non-polar oil. Curves P and P' are for polar oil, whereas N and N' are for non-polar oil (modified after G.A. Babalyan, in: Langnes et al., 1972, p. 229).

Economic Feasibility

A very approximate estimation can be made for the economic feasibility of applying electrical current to enhance the flow of reservoir fluids during oil production.
Many assumptions should be made in order to make such rough calculation. The variables which will affect the economic considerations include: (1) thickness, depth, and resistivity of the pay zone, (2) arrangement of the electrodes, (3) duration of the electrical treatment, (4) labor cost, and (5) price of electricity at the site of application (Anbah et al., 1965).

In general, the rock resistivity is a function of the amount of interstitial water present. This, in turn, is determined by the rock porosity and the amount of pore space that is filled by interstitial water. The flow of electrical current in such a case in not a simple linear flow but follows an irregular path around the individual sand grains. This flow pattern will increase the length of the current flow lines and the resistivity of the rock. Inasmuch as the current is mainly transmitted through the rock in the form of electrolytic conduction, the resistivity of the interstitial formation water seems to be the deciding factor in the formation resistivity as a whole. The presence of clay, however, greatly affects the electrical resistivity of the formation, especially in the case of fresh formation water (Anbah et al., 1965).

Although the electroosmotic flow depends mainly on the imposed electrical potential gradient, the associated electrical current is conditioned by the type of formation under consideration and its electrolytic content. There is no simple relation between the amount of liquid transported by electroosmosis and the quantity of electricity consumed.

The presence of expandable colloidal matter in a microporous media further complicates the picture (Anbah et al., 1965).

In field application, the energy consumption will depend on the dimensions of the electrodes, the applied electrical potential, and the underground condition. If these factors are known, the amount of transmitted electrical current can be estimated. Upon switching the current on, it will drop gradually because the over-all resistance will increase after the oil starts flowing and the anode surface area will decrease as a result of corrosion and material selection (Anbah et al., 1965).

The total amount of current transmitted (I) for various electrode arrangement can be estimated (Rudenberg, 1945; Cassagrande, 1949) by using equations such as those presented below:

(a) For two cylindrical electrodes of equal length and crossectional area,

$$I = 2\pi LE/(\rho \ln d/r) \tag{1-67}$$

where ρ is the formation resistivity in ohm-meters; L and r are the length and radius of the electrode in meters, E is the imposed electrical potential in volts; and d is the distance between the anode and the cathode in meters.

(b) For two cylindrical electrodes with different radii,

$$I = (\pi LE/\rho)(1/\ln d/r_1 + 1/\ln d/r_2) \tag{1-68}$$

(c) For a row of alternate anodes and cathodes the amount of electrical current can be given approximately by

$$I = (N\pi LE/\rho)(1/\ln d/r_1 + 1/\ln d/r_2) \tag{1-69}$$

where N is the number of electrodes in each group.

(d) For spherical flow of current from a sphere with radius a to a distance x in the ground,

$$I = (2\pi LE/\rho)(1/a + 1x) \tag{1-70}$$

and when x approaches infinity, $1/x$ goes to zero and

$$I = 2\pi LE/\rho a$$

Before one can proceed with estimating the consumption of power, some assumptions have to be made. The following estimation of the current application, because it is very difficult to estimate the decrease in the current flow as a result of the increase in the overall resistance. On assuming that (1) the electrical current is available at the electrode; (2) the formation resistivity is constant and is equal to 10 ohm-meters; (3) the electrode-length and radius are equal to three and 0.1 meters, respectively; (4) the applied potential is equal to three and 0.1 meters, respectively; (4) the applied potential is equal to 100 volts, and (5) the distance between electrodes is equal to 40 meters (Anbah et al., 1965) and substituting the above values in Eq. 1-67:

$I = 2*3.14*3*100/(10*\ln 40/0.01) = 31.4$ amps

Thus, the power consumption is then equal to

31.4 *100/1000 = 3.14 Kw

The approximate cost of electricity (at $0.059/Kw.-hr.) = 3.14 x 24 x 0.059 = $ 4.45 per day per well. If the labor cost is assumed to be $50 per day per well, then the total cost becomes $230.76 per well per day. (See Handbook of Construction Cost, Halbert Powers Gillette, 2006.)

It is assumed that the equipment needed (electronic power supply, electrodes, power cables, etc.) will cost approximately \$55,000 per well. If the estimated life of the equipment is five years and its salvage value is 11,000, then by using straight-line depreciation at 6 per cent average interest, the annual depreciation plus interest is equal to \$10,494 per well. (Modified after Anbah et al. 1965)

According to laboratory experimental results and the application of electroosmosis in related engineering field, an average increase in the elctroosmotic flow rate of water (corresponding to 3.14 KW.-hr.) can be estimated as 0.75 cc./sec. or 41.7 B/D. If it is further assumed that a piston like displacement of water to oil (banking) takes places, an average increase in the oil produced is estimated to be 13.9 B/D per well. The annual gross dollar return (at \$70/Bbl) is equal to \$355,145.00, and after CMR tax (at \$6/Bbl) is equal to \$324,704.00. This value minus the annual labor and electricity cost will give the net annual profit of: \$324,704.00 - \$84,227.40 = \$240,476.60. The net profit is approximately equal to 240,476.60/10,494.00 ≈ \$22.92 dollar returned per dollar invested (modified after Anbah et al., 1965).

These sample calculations are presented here in order to indicate the possibility of such application in the field. It should be kept in mind, however, that for field application the current is best applied in an interruptive manner which will cause a considerable saving in power consumption. For the purpose of well stimulation, the application of current may not exceed a period of one to two weeks. It is believed that such short electrical treatment may lead to 50 or even 100 per cent increase in the average flow rate of oil and water. It is also believed that the electrochemical well stimulation method will prove in the future to be economically feasible, especially in specific cases where clay swelling is extremely active.

The economic feasibility of using this technique in oil production will be more apparent in a large-scale field application. In order to ensure optimum results, it is strongly recommended that such large-scale application should be preceded by a flood pot test followed by a pilot test (Anbah et al., 1965).

Summary

One can summarize the major features and advantages of electrokinetic technology as follows:

- The flow rate of oil and water can be increased by the application of direct current.
- Chemical additives may be used in conjunction with electrical treatment to augment the flow rate of transportable fluids in question.
- Electrochemical treatment may be used for well stimulation.
- Electrokinetics can be used as a selective ion-drive process.
- Electrokinetic flow rate increases with increasing potential gradient (or electrical current, *I*), first reaching a maximum, then decreasing with further increase in electrical current.
- Facilitates beneficial chemical changes in produced fluids.
- It is cost competitive with steam EOR, with no depth constraint.
- Thief zone problems (e.g., in the case of steam injection in EOR) do not exist.
- There is no water or working fluid requirement.
- Reduces water consumption and water cut when compared to steam EOR.
- No hazardous emissions or liquid problems.
- Facility installation can be incremental, allowing the spreading of capital over the lifetime of the desired projects.
- Brandon et al. (1993) showed the effectiveness of application of D.C. current in releasing the stuck drillpipe in aqueous drilling fluids. They quoted the earlier work of Chilingar et al. (1968).

Chapter 2: Electroremediation

Restoration of soils contaminated with hydrocarbons and metals is one of the most important problems of environmental protection. During the last 40 years, considerable progress has been made in the development of effective remediation technologies. Modem purging technologies are based on the chemical and biological degradation of contaminants and their conversion to safe forms or to intermediate substances convenient for transport in soils. To accelerate transport of contaminants or their intermediate substances in soils, electrical fields (direct current) are applied to zones being remediated. This allows the volumetric rate of transport to increase ≈ 50-60 times, and the substances to collect at convenient removal sites.

When a direct current electric field is applied to a wet porous medium polluted by hydrocarbons or by ionic species, the aqueous phase is displaced by electroosmosis in the pores and the ions migrate towards the electrodes. As a result, the value of the local pH at the interfaces between water, oil and solid is changed, as well as the electric conductivity of the medium: the ionic strength is increased towards each electrode and decreased between them.

These mechanisms result in release of the oil droplets which block the capillary tubes of the medium, either by mechanical action (movement of the water), or by chemical action (change of the surface tension at the interfaces). Additionally, the electromigration of ions through the medium can decrease the contamination level of aquifers by changed chemical species (Lancelot et al., 1987).

These mechanisms were identified on polluted chalk cores, sandstone blocks, and sand packs. The role of the various parameters was analyzed: the direction of the current is unsensitive, the adding of surfactants increases the flow and a sequence of currents plus water-drives with small gradient increases the oil recovery (Lancelot et al., 1987). The use of electric current for improving the remediation of aquifers polluted by hydrocarbons can be considered together with other commonly used techniques (e.g., gravitational pumping).

The electrokinetic method can also be used for remediation of aquifers polluted by ionic species (Lancelot et al., 1987). Electrokinetically-enhanced transport of contaminants is perhaps one of the most promising *in-situ* decontamination processes capable of removing heavy metals and organic contaminants from soils, sludges and lagoons.

The significance of this technology appears to be in its projected low operation cost and its potential applicability to a wide range of contamination situations. It is also viewed by researchers and industry as a potential "problem solver" when other remedial technologies appear non-workable or fail to remediate a site. Present day urgency to develop innovative technologies appears non-workable or fail to remediate a site. Present day urgency to develop innovative technologies to cleanup contaminated soils and ground water makes it necessary to look at the fundamental mechanisms associated with the electrokinetic technology and to develop it into a well-engineered and predictable process for field applications.

Fundamental experiments were performed by a group of researchers at the University of Southern California in the early sixties. The experiments involved application of direct electrical current for acceleration of the flow of solutions in soils (Chilingar et al., 1997).

This, together with the latest advances in biodegradation of the eighties and nineties, led to the development of sophisticated multicomponent remediation technologies.

Success of these technologies depends on the selection of appropriate combinations of microbiotic and chemicals degradation, and oriented electrokinetic transportation of contaminants to the collection site.

A proper combination of remediation techniques is determined by the biological, physical, chemical, and ecological conditions of the remediated zone.

The primary goal here is to:

(i) Review recent advances in electroremediation technologies and remediation science.

(ii) Evaluate the present state of the problem and the current trends in its development.

Another goal is to attract attention of the researchers to the key problems and bottlenecks of the theoretical foundations and mathematical modeling of remediation processes.

Many technological operations, such as oil and gas exploration, production, transportation, and usage of their derivatives lead to soil contamination by hydrocarbons. If leaks and spills occur at the sites of manufacturing plants, then the soils are usually contaminated with a mixture of hydrocarbons and metals. Contaminated areas cannot be reused for other purposes without careful cleanup of soils to guarantee compliance with the established environmental standards. Until recently, the only possible way to meet the strict Environmental Protection Agency (EPA) standards was excavation of contaminated soil, transportation, and burial at suitable places with all necessary precautions usually taken for waste disposal. This, however, is a very expensive procedure.

The first recorded use of electrokinetics applied to dewatering soils and sludges in the field was by Cassagrande (1949). Work and subsequent research in the electrokinetic decontamination of soils has accelerated in recent years following the detection of high concentrations of metals and organics in electroosmotically drained water of a dredged sludge by Segall et al. (1980). Other field work including that of Lageman et al. (1989) and Banarjee et al. (1988) has been conducted with reasonable success for heavy metal transport.

Many laboratory and field tests were very successful. The process, using both bacteria and D.C. current, was termed “electrobioremediation.” Huge volumes of offshore muds are contaminated with heavy metals. I believe that these muds can be cleaned by applying D.C. current to drive the heavy metals towards the cathode (well), where they can be disposed of.

Recently developed complex cleaning technologies combine several efficient methods of contaminant degradation with drastic acceleration of their transport in soils. There are many examples of their successful application in situ, so that in most cases of contamination with hydrocarbons and metals, it is possible to clean the sites to the established environmental standards in an acceptable length of time at reasonable cost without excavation of huge masses of soil.

Experiments on the application of direct electrical current for acceleration of the flow of solutions in soils and sandstones were performed by a group of researchers at the University of Southern California in the sixties under the direction of Professor George V. Chilingar (e.g., Chilingar, 1952; Adamson et al., 1963a, 1963b, 1966; Chilingar et al., 1964, 1965, 1966, 1968a, 1968b, 1968c, 1970; Amba et al., 1964, 1965).

These experiments, together with recent advances in biodegradation (Atlas, 1977, 1981; Wilson, 1985; Nelson et al., 1987; Roberts et al., 1989; Morgan & Watkinson, 1989; Leahy & Colwell, 1990; Sims, 1990; Hinchee et al., 1991; Huesemann, 1994), led to development of a set of sophisticated multicomponent technologies (e.g., Bumett & Loo, 1994; Loo, 1991, 1993, 1994; Loo et al., 1994).

These technologies use combinations of microbiotic and chemical degradation, appropriate for a particular site, and specific physical, chemical, geological, and biological conditions, together with an electrokinetic-accelerated controlled transport.

In spite of the fact that the spectrum of cleaning technologies is broad enough to meet any specific environmental and geological conditions, remediation technologies have not been widely applied in soil cleanup practice. One of the main reasons is a complicated science-intensive process of decision making on the choice of cleaning strategy for a site of interest.

Blacker and Goodman (1994) indicated that considerable improvement in this field could be achieved if policy judgments are separated from technical issues, and cleanup goals are translated into measurable performance criteria. After that, it is possible to apply well-developed optimization techniques to choose the "best" decision, which will include an optimal combination of remediation technologies, appropriate methods for waste ransport and removal, and methods for transformation of toxic waste into harmless substances.

The unfavorable factor is that in choosing the remediation process, multicriteria optimization may be the most appropriate because the state of the contaminated site and cleaning technologies is usually assessed with multiple criteria (concentrations of contaminants at many points of the site, for example).

At the final stage of optimization, inclusion of informal experts' opinions and informal schemes of compromise may be necessary that considerably complicate the decision—making process (Chilingar et al., 1997).

Electrokinetics essentially involves installing wells/drains, inserting electrodes, and applying a low electric potential across the electrodes. Nutrients may be added to the solution at the anode and/or cathode electrode, and, as a result of electromigration and/or electro-osmosis, the nutrients are transported from the electrodes into the soil.

Basically, electromigration refers to the transport of charged species toward the electrodes, whereas electro-osmosis refers to the bulk movement of liquid toward the electrodes (generally from the anode to the cathode; Eykholt, 1992; Acar and Alshawabkeh, 1993).

Statement of the Problem

A direct-current electric field applied to the electrolytic solution considerably accelerates the rate of its flow in porous media (Chilingar et al. 1968a, 1968b, 1968c; Shapiro &

Probstein, 1993). It permits control of the direction of purging underground currents and of the contaminants collection site. In combination with suitable amendments (nutrients, etc.), a direct-current electric field creates favorable conditions for chemical and biological degradation of hydrocarbon compounds (Cozzarelli et al., 1995; Morgan & Watkinson, 1989). Multiple laboratory experiments and mathematical modeling have proven the advantages of this technology. However, the application of bioremediation for in situ cleaning sometimes yields unexpected results. In situ, one can observe a situation when, after several days of successful cleaning, the species biodegradation and transport can be retarded or even interrupted. Among the possible causes of retardation, one can identify, for example, the soil cementation around the cathode or clogging of the purging system with the produced biomass (Chilingar et al., 1997).

Specially designed laboratory experiments and mathematical modeling can reveal the causes of these complications and suggest possible methods for their elimination. One needs to control the pH along the area between electrodes (Hicks & Tondorf, 1994). Also, it is necessary to calculate carefully the amount of amendments for biostimulation (Pollard et al., 1994).

Thus, as pointed by Chilingar et al. (1997), the understanding of the main features and control mechanisms of electrobioremediation is critical for successful application of this technology *in-situ*.To determine the necessary amount of amendments and to establish other control variables, one needs to solve some inverse mathematical problems for finding influences that cause desirable effects. For that purpose, one needs to use suitable mathematical models that reflect the main properties of underlying processes are needed. The example of such a model for the process of electrokinetic transport is given by Shapiro and Probstein (1993).

The reviewed publications show that good cleaning results *in situ* can be obtained by application of a suitable combination of several purging technologies. For the selection of an appropriate combination and its adjustment to the site's conditions, one needs a high level of understanding of the mechanisms of all underlying physical, chemical, and biological processes.

A review of the main technological aspects of the remediation procedure is presented here, including: methods of electrobioremediation of hydrocarbons and metals in soil, and transport and removal of the products of degradation using specially designed electrical fields.

Concepts and Methods of Biodegradation of Hydrocarbons

As stated by Pollard et al. (1994), the objective of bioremediation in situ is to stimulate the activity of the hydrocarbon-degrading microbiotic processes in the subsurface layer and zones saturated with water. This goal can-be achieved by adding oxygen and nutrients in a closed-loop control system (Hopper, 1989).

Amendments and solvents used to stimulate the biological activity of microorganisms are introduced to the contaminated zone using some natural or artificial channels such as a system of pores and fractures, wells, and infiltration galleries.

The process of biotreatment leads to the formation of soluble materials that are transported with controlled flow of underground fluids to the place of collection or the recovery system. If a recovery unit is used in the closed-loop remediation system, these solutions are treated at the surface and then reinjected to recharge the contaminated zone. Recharging of the purged zone prevents the possible ground subsidence caused by the soil dewatering. Careful control of the amount of oxygen, nutrients, and solvents used is necessary in order to accelerate the treatment process and prevent off-site migration of contaminants and potentially harmful metabolites. Specific problem associated with oil degradation in soil were considered by Raymond et al. (1976).

As Pollard et al. (1994) concluded, in most cases the main limiting factor for the rate of in situ remediation is the amount of amendments supplied to the subsurface microbial population (see also Lee et al., 1988). The sites with low horizontal hydraulic permeability are not considered amenable to biodegradation because of the retardation of transport flows that are necessary for the effective delivery of necessary amendments and removal of the products of biodegradation. Success of the treatment depends on the degree of hydraulic control that can be achieved in the "delivery-recovery system." Without continuous delivery of nutrients and removal of metabolites, the remediation system may become biologically inactive or clogged with biomass because of excessive microbial activity.

Both of these extreme situations mean failure of the process of bioremediation. A carefully dosed and controlled supply of amendments, therefore, is to be delivered to the contaminated soil to ensure optimal conditions for the growth of bacterial colonies. This condition leads to the formulation of the problem of optimal control of the delivery rate of various amendments.

In this process, only soluble by-products can be recovered from the contaminated site. Poorly soluble species, some of which may be harmful, may readsorb on the solid matrix. In such cases, Mahaffey et al. (1991) recommended intensive soil washing using surfactants. In turn, this demands precise identification of the components of contamination to select an appropriate surface detergent.

Under unfavorable environmental conditions, which can considerably restrain *in-situ* remediation, so-called enhanced land treatment procedures are being used. Enhanced land treatment technologies have been successfully used for the treatment of a wide variety of petroleum-contaminated soils (see references in Pollard et al., 1994). In these technologies the contaminated soil is excavated, mixed with necessary amendments, treated in special covered units to improve its characteristics, and then returned to the site. Actually, this is the process of production of a new soil with given desirable properties. Covered treatment facilities allow for organization of a highly effective process for controlling volatiles, temperature, and the water and air regime within the cleaning unit.

One should realize, however, that careful monitoring of remediation process performance must be conducted using a mass balance approach, physical and chemical measurements, and bioassay response data. This is the kind of complex, expensive, and scope-restricted technology that cannot be recommended for broad applications (Chilingar et al., 1997).

When time is critical for the process of restoration, slurry bioreactors are recommended. In this technology, soil is treated as a water slurry in a closed reactor

(Visscher et al., 1990). A well-characterized and carefully seeded microbial population is used for rapid biotransformation of even the most refractory contaminants.

Optimal process control allows for considerable reduction of the treatment time in comparison with in situ or enhanced land remediation. Reactors can operate under either aerobic or anaerobic conditions.

The anaerobic microbial population, however, is generally less flexible in adapting to changes in the substrate availability and is less tolerant of inhibitory toxic metals. The method can be recommended for the fast treatment of limited volumes of clayey soils (Pollard et al., 1994).

For the sandy soils, a combined technology can be used, consisting of soil washing, biological water-phase treatment, and slurry-phase bioreactor. One successful example of the application of this combined technology is described by Stinson et al., (1992). They reported that more than 87% removal efficiency was achieved for polynuclear aromatic hydrocarbons in this process. Bhandari et al., (1994) conducted a series of experiments on petroleum-contaminated soil washing and discovered that it was highly effective in combination with biotreatment.

European experience (Pheiffer, 1990; Nunno et al., 1988) has shown that soil washing can be conducted on a large scale and at low costs if the clayey fraction is low. Multiple studies in the United States, however. have demonstrated that each kind of soil requires a careful preliminary evaluation of its mineralogy, porosity, permeability. and contamination conditions because these factors considerably effect the final result of soil restoration (e.g., Nash & Traver, 1988).

For effective biodegradation, it is necessary to develop conditions for electron removal from the hydrocarbon compounds. The electron acceptance leads to faster degradation of complex-compound hydrocarbons. Ionization caused by electron acceptors allows for faster transport and removal of contaminants and their by-products from the remediation site under electromagnetic field.

Conditions favorable for electron acceptor development can be effectively reached under either aerobic or anaerobic conditions (Pollard et al., 1994).
Under aerobic conditions, oxygen serves as the terminal electron acceptor for the oxidation of organic compounds by microorganisms. Under anaerobic conditions, some other ions or compounds can serve as the terminal electron acceptors. Most of the biotreatability studies and applications are concentrated on aerobic conditions because these conditions provide the simplest and fastest means for oxidation and degradation of contaminants such as hydrocarbons. Various species of hydrocarbons undergo their own chain of transformations in soil and groundwater. Many researchers focused their investigations on the group of aromatic hydrocarbons because of their toxicity and high solubility in groundwater.

As Cozzarelli et al. (1995 and references therein) pointed out, these molecular-weight alkylbenzenes are frequently reported to be present in the groundwater. The hydrocarbons of this group are naturally degraded in the environment by aerobic and anaerobic microbial processes. Their degradation can be stimulated by adding certain substances, such as nitrates, as the electron acceptors to accelerate oxidation under anaerobic conditions (Chilingar et al., 1997).

In applying any bioremediation technology to the petroleum-contaminated site, it is necessary to be aware of considerable complications affecting the biodegradation process.

Pollard et al. (1994) and McCarty (1991) pointed out some of the typical factors that may lead to this type of complication:

(1) Multimedium nature of contamination process (soil, soil vapor, several soil layers, groundwater, distinct hydrocarbon phases);

(2) Existence of a complex and problematic matrix of organic and inorganic contaminants with a wide spectrum of environmental and toxicological properties;

(3) Heterogeneous subsurface conditions, which are difficult to characterize;

(4) Lack of optimal environmental conditions for the in situ treatment.

Methods of Continuous Control and Management of Biodegradation of Hydrocarbons *In-Situ*

Huesemann (1995) pointed out that the extent of hydrocarbon biodegradation in contaminated soils is critically dependent on four factors: "the presence of hydrocarbon degrading bacteria, the creation of optimal environmental conditions to stimulate biodegradative activity, the predominant petroleum hydrocarbon types in the contaminated matrix, and, finally, the bioavailability of the contaminants to degradative bacteria."

Biotreatment of contaminated soils in situ is difficult primarily because it involves many poorly defined situations and processes. Initially, it is necessary to conduct a pilot study to understand the geologic scenario of the site and to evaluate the types of hydrocarbons and degree of contamination. Sometimes this study can be time and budget consuming. It may even be difficult to define how to characterize the final goal of treatment: it can be characterized, for example, by the total petroleum hydrocarbon (TPH) feasible content in soil, or by the concentrations of separate hydrocarbon species. One also needs to evaluate an initial state of the site in quantitative terms to observe and monitor the remediation process. Then it is necessary to formulate a set of mathematical relations linking the site state variables with the modifiable control variables and parameters of the medium. These relations are often called the "governing equations" (in spite of the fact that they can include sets and inequalities as well) because they allow for defining quantitatively the studied process, and for choosing and controlling the direction and scope of desirable changes. (Chilingar et al., 1997.)

Finally, to realize the treatment process, one needs to choose some admissible values of the control variables and to apply them in situ. It is a typical control problem; however, it is a very difficult one. There are no readily applicable methods for its solution. In addition, all underlying processes occur underground, and the measurement tools are far from perfect. Solution and analysis of a remediation optimization problem must include uncertainty accepting approaches such as stochastic control, fuzzy sets, and sensitivity analysis.

The latter is especially important because it requires minimal additional information in comparison with deterministic models. An advanced version of the sensitivity analysis directly applicable to the considered problem was developed by Katz et al. (1996).

A pilot study is usually aimed at evaluation of the contaminated site. One of the main objectives of this study is to determine predominant petroleum hydrocarbon types in the contaminated matrix. To formulate the purpose of bioremediation cleanup correctly, one needs to estimate the possible extent of the degradation of the predominant petroleum hydrocarbon type in contaminated soils.

For that purpose, Huesemann (1995) developed a predictive model based on the correlation between the molecular structure of saturates and the extent of biodegradation. This model allows for estimation of the final gravimetric TPH concentration if the concentrations of the 86 compound classes in the initial gravimetric TPH are known.

There is considerable need for mathematical models describing the dynamics of hydrocarbon degradation and growth of bacterial colonies in the presence of various nutrients. This model can be formulated, for example, in terms of a system of differential equations describing general processes of growth. The current state of the hydrocarbon degradation study is favorable for the estimation of coefficients of such a model. Using this model, it will be much easier to choose the proper amounts of amendments that are necessary for optimal development of the process of biodegradation (Chilingar et al., 1997).

Concepts and Models of Electrokinetic Transport of Contaminants and Their Intermediate Substances

Methods of electrokinetic transport of solutions in soil attracted significant attention from many researchers in connection with in situ remediation (see, for example, a fundamental work of Shapiro and Probstein (1993) or Amba et al., (1964)). Biological ionization of contaminant solutions in soil allows electrokinetic methods to be applied for purging hazardous chemicals from a contaminated site. The most advanced variant of electrokinetic techniques for removing hazardous materials from soil is developed and described by Probstein et al. (1991).

Electrokinetic is described as the flow of an ionic liquid under interaction of an electric field with a charged surface formed in the pores and capillaries. One of the most important advantages of electrokinetic flow is that it is relatively insensitive to pore size. "That is, unlike pressure-driven flows in which channeling of the fluid through the largest pores is inevitable, electrokinetics permits a more uniform flow distribution and a high degree of control of the direction of flow" (Shapiro & Probstein, 1993; Chilingar et al., 1970).

On the basis of extensive research, the present authors believe that double—layer theory best explains the electrokinetic transport through porous media on application of direct current (Fig. 1-1). As the predominantly positively-charged mobile layer moves toward the cathode, the free solution in the center of the capillaries is dragged along owing to friction forces. Simple purging equipment for field reclamation includes a direct current power supply with a set of anode and cathode electrodes placed into wells drilled on the site. The direct current field causes an electrokinetic effect in which saturating liquid is driven by interaction of the electric field with the charged double layer.

The flow direction is from the anode to the cathode. After it accumulates in the cathode wells, highly contaminated effluent can be pumped, property treated, and disposed of. Or, possibly, the polarity can be changed temporarily to convert the cathode to the anode, where oxidation takes place.

Theory best explains the electrokinetic transport through porous media on application of direct current (Figure 1-1). Laboratory experiments and the results of application of electrokinetic reclamation in situ show that electrokinetic flow can successfully compete with hydraulic Darcy's flow in the soils with low hydraulic permeability.

Lageman et al.(1989) reported that the highest degree of removal of heavy metals (over 90% of the initial contaminants) had been achieved for clayey, low-permeability soils, whereas for porous, high-permeability soils, such as peat and river slush, the degree of removal was only *65%.* Laboratory results of Renaud and Probstein (1987), Shapiro et al. (1989), and Acar et al. (1990) on electrokinetic purging of acetate and phenol from saturated kaolinite clay had demonstrated more than 94% removal of the initial contaminants.

The process of transport of contaminants and their derivatives involves two major phenomena:

(1) the flow of contaminant solutions through a solid matrix due to Darcy's law and electrokinetics.

(2) spatial redistribution of dissolved substances with respect to moving liquid due to diffusion and migration of charged particles.

The total movement of the matter of the contaminant solution in the direct current electric field (DC field) can be expressed as the sum of four components: hydrodynamic flow of fluids driven by the pressure gradient, electrokinetic flow of fluids due to interaction of the double layer with the DC field, diffusion of components dissolved in the flowing solution, and migration of ions inside moving fluids due to attraction of charged particles to electrodes.

The obvious merits of electrorestoration are the high degree of contaminant removal, multifold acceleration of biochemical degradation, and directed rapid transport of contaminant solution to designated wells for removal. In spite of these merits, electrorestoration has not been widely applied as a purging technology in situ. Frequently, its application in the field yields unexpected results. The commercia1 application of this technology requires a careful pilot study for the contaminated site with the adjustment of the technology to the particular conditions of the site. In turn, the technology itself must be carefully studied to understand effective control influences for such an adjustment.

According to Hicks and Tondorf (1994), one might expect, for example, that removal of heavy metals in the DC field is effective because electromigration of ions is rapid and does not depend on the zeta potential. Laboratory experiments with single metals mostly demonstrate high removal efficiency.

The limited field trials, however, produced inconsistent results. (These results, by the way, can be reproduced in the laboratory.) Hicks and Tondorf arrived at the conclusion that poor performance in situ can be attributed to the interaction of metals with naturally occurring electrolytes, humic substances, and co-disposed wastes. "Immobilization of contaminants in the narrow band in the soil, analogous to isoelectric focusing, was reproduced experimentally and simulated with a mathematical model. It was shown that the focusing effect can be eliminated by controlling the pH at the cathode using a water rinse. Immobilization resulting from precipitation of carbonates and co-disposed wastes may additionally require chelating agents and control of the redox potential to achieve removal" (Hicks & Tondorf 1994).

As Shapiro and Probstein (1993) showed, the effect of electrode reactions on the process of electrokinetics can be significant. Their influence on pore fluid and surface charges of soil particles propagates at least several centimeters from electrodes. For the low-pH front that moves from the anode to the cathode, these reactions influence the whole area of medium involved in electrokinetic transport. At the cathode the area with high pH is generally localized at a radius of a few centimeters to around 20 cm. (Sometimes cathodes are converted into extremely hard, well-cemented pillars, owing to precipitation of carbonates and hydroxides.) This means that for understanding the electrokinetic transport in the field, one needs to conduct experiments covering the whole area between the two electrodes.

In addition, for successful application of electrokinetics in situ, one needs to provide continuous control of pH level in the vicinity of electrodes. One possible way to achieve this is the periodic rinsing of the cathode with fresh water.
These examples can explain some of the causes of failure of electrokinetic technology in situ. It is a complex technology that requires, for its successful application, understanding of the multiple features of interaction of an electric field with flowing charged fluid and a porous medium.

For widespread application *in situ*, one needs to carefully investigate the various possible conditions of contamination and soil and rock types. The results of such an investigation may indicate the cleaning policies to be recommended for in situ application.

Mathematical Modeling of Contaminant Transport in the Porous Medium

If the direction of the hydraulic pressure gradient coincides with the direction of the DC electric field current, i.e., Darcy's flow and the electrokinetic transport occur in the same direction, a one-dimensional mathematical model can be used to show the main mechanisms of species transport. In this case, redistribution of the species concentration in space can be described as a result of combined influence of three mechanisms: Darcy flow, electrokinetics, diffusion.

The first two relate to the contaminant solution flow with respect to the solid soil matrix, whereas the last redistributes the species inside the flowing fluids. (Chilingar et al., 1997.)

For the purpose of simplified analysis, it is reasonable to consider a one-dimensional fluid flow in the direction from anode to cathode. Denoting the distance from the anode by x and the distance between anode and cathode by *I ,* one can consider $0 < x < 1$.

The total fluid flow rate $q_t(x)$ at point x can be expressed for this case in the following form:

$$q_t(x) = q_h(x) + q_\theta(x) \tag{2-1}$$

where q_h is the hydraulic component of the flow and q_θ is the electrokinetic component of the total flow q_t.

To define $q_h(x)$, one can use Darcy's law (e.g., Bear, 1973):

$$q_h(x) = Ak_h\mu^{-1}dp/dx = Ak_h\mu^{-1}\nabla p \tag{2-2}$$

where A is the cross-sectional area perpendicular to the direction of fluid flow, k_h, is Darcy's permeability of a porous medium in the direction of flow, μ is the viscosity of fluid, and $dp/dx = \nabla p$ is the pressure derivative in the direction of flow at point x.

For the electrokinetic flow rate $q_\theta(x)$, one may use the Helmholtz—Smoluchowski

equation version of the following form (Smoluchowski, 1921):

$$q_\theta(x) = Ak_\theta\mu^{-1}d_\theta/dx = Ak_\theta\mu^{-1}\nabla_\theta \tag{2-3}$$

for which electrokinetic permeability k_θ, is defined by

$$k_\theta = (4\pi \mathrm{F})^{-1}\mathrm{D}\xi \tag{2-4}$$

where F is the formation factor, D is the dielectric constant, ξ is the zeta potential, Φ is the electric field potential, and $d\Phi/dx = \nabla \Phi$ is the potential derivative in the direction of flow at point x.

Chilingar et al. (1970) conducted a simple analysis of conditions that are responsible for the relationship between hydrodynamic and electrokinetic components of flow. Based on Eqs. (2-2) and (2-3), they presented the ratio:

$$(q_t - q_h) / q_h = k_\theta \nabla \Phi / k_h \nabla p \qquad (2\text{-}5)$$

This ratio shows that an increase in the electrokinetic flow rate is proportional to the zeta potential, dielectric constant, and potential gradient.

The direct conclusion from Eq. (2-5) is that the electrokinetic technique is especially effective in cases when hydraulic permeability K, is very small, which is valid, for example, for clays or clayey sands (Chilingar et al., 1997).

Electrokinetic flow rate increases with increasing clay content in sands. For sands, it is possible to raise the hydrodynamic component of the total flow by injection of special purging solutions (Shapiro & Probstein, 1993).

Electrical field application *in situ*, as a rule, leads to an increase in temperature. In turn, the temperature increase reduces the viscosity of hydrocarbon-containing fluids that, according to Eqs. (2-2) and (2-3), would result in an increase of the total flow rate (Chilingar et al., 1970).

Analyzing the results of "*in situ*" trials and verifying corresponding mathematical models, one should keep in mind this additional positive side effect to avoid possible misinterpretations of electrokinetic efficiency. This effect is insignificant for the dissolved gaseous hydrocarbons (e.g., butane and methane) (Chilingar et al., 1997).

For crude oils (e.g., California crude oils), however, the viscosity can be reduced more than 20 times upon heating from 50^{o} C to 100^{o} C (Ungerer et al., 1990), which (at least in theory) would increase the total fluid flow 20 times.

Discussing an electrical field application for the acceleration of fluid transport in situ, one needs to consider electrical properties of soils (electrical resistivity, for example) and ionization rate of the flowing fluids that can considerably affect the total flow rate. In addition, Chilingar et al. (1970) discovered that application of the DC field to some soils leads to an increase of their hydraulic permeability, which in turn, can considerably accelerate fluid transport. Some clays are destroyed (become amorphous) upon application of a direct electric current, possibly as a result of driving the interlayer water out (Harton et al., 1967).

Discussing the transport of contaminants in soil, one should remember that the final goal of this process is to collect wastes at some location of the site convenient for their final removal.

In terms of harmful species distribution, it means that initial uniform distribution of the contaminants must be changed in the process of transport to the "peak" form, with the sharp peak located at the place of removal.

The species concentrations at all other points of the site must be lowered considerably (below acceptable levels) in the process of cleaning. Desirable species distribution before and after purging is illustrated in Figures 2-1 and 2-2 (Chilingar et al., 1997).

Actually, in this situation one faces a control problem that can be formulated as follows. Starting from the distribution shown in Figure 2-1, one needs to achieve the distribution shown in Figure 2-2, for example. To achieve this, it is necessary to identify the control variables that affect the form of species distribution. For this purpose, it is necessary to use an appropriate mathematical model of the transport process.

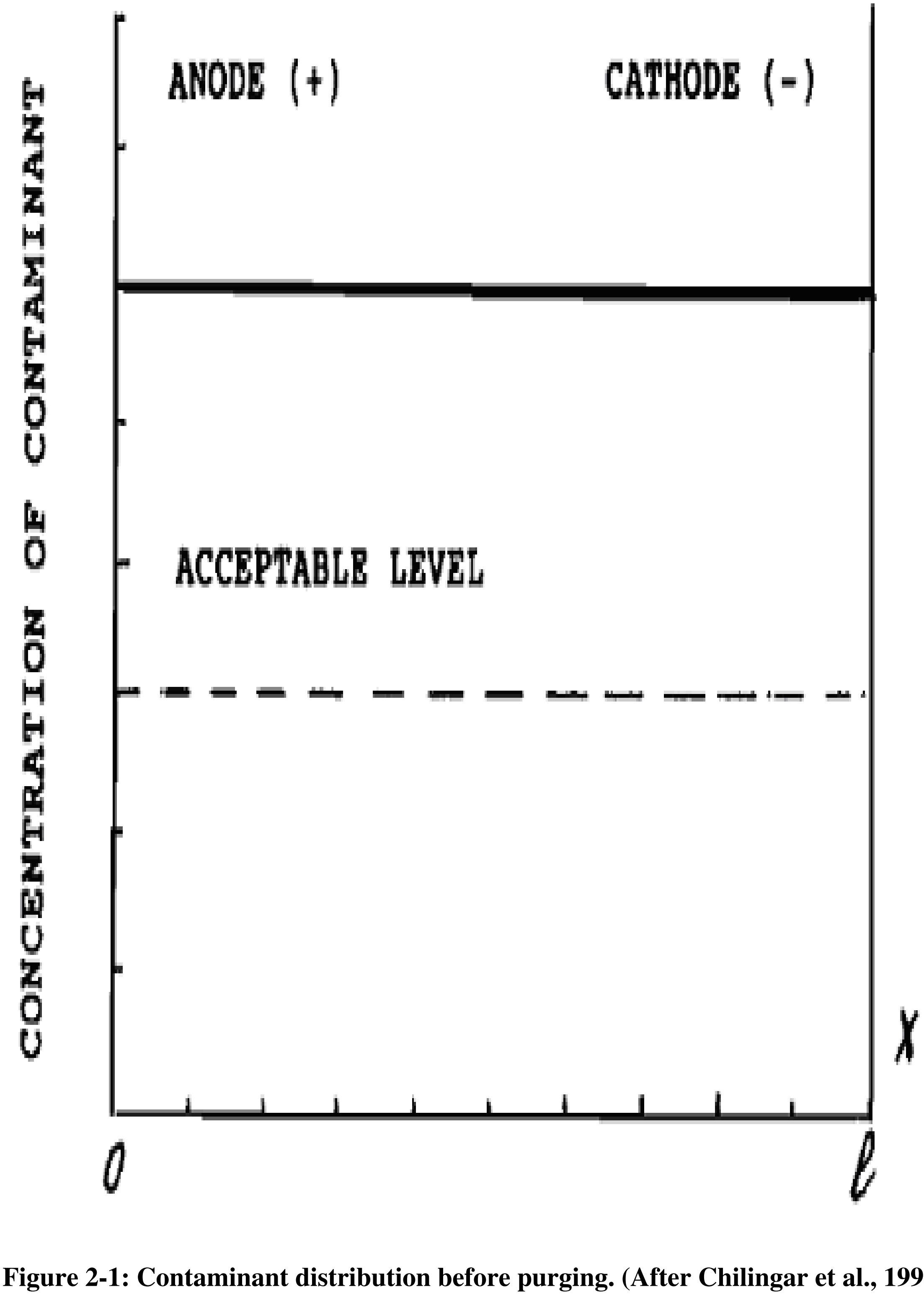

Figure 2-1: Contaminant distribution before purging. (After Chilingar et al., 1997.)

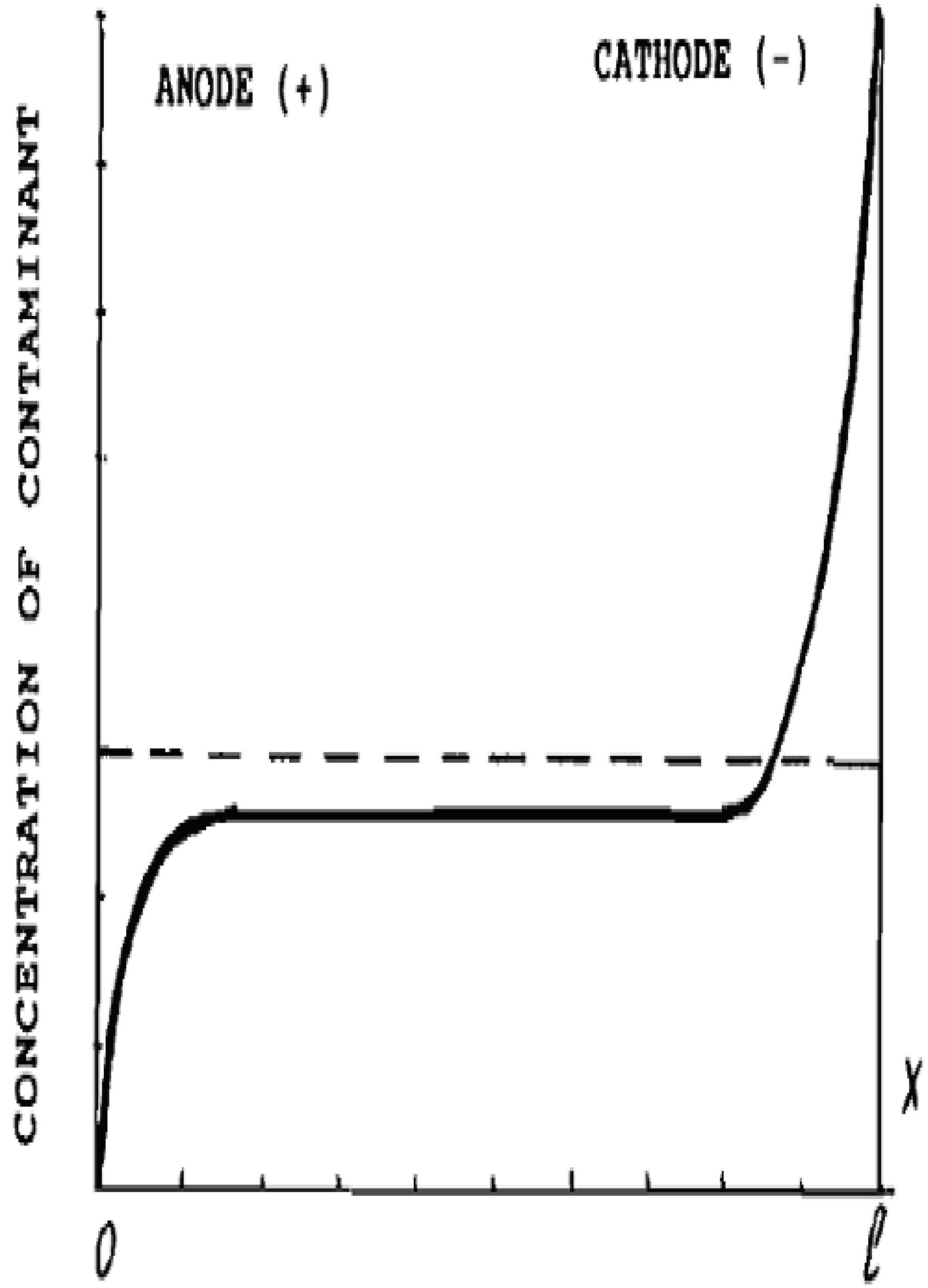

Figure 2-2: Contaminant distribution after purging. (After Chilingar et al., 1997.)

According to Shapiro and Probstein (1993), one can ascribe the redistribution of species in the flowing fluid to diffusion and electromigration. The process of redistribution can be described by equations for species concentration and electrical current density as follows:

$$\delta c_i/\delta t = - \nabla j_i + R_i \qquad (2\text{-}6)$$

$$I = - \sigma\nabla\Phi - F \sum_{i \in M} (z_i D_i \nabla c_i) + Fu \sum_{i \in M} (z_i c_i) \qquad (2\text{-}7)$$

where for each species i, $i \in M$, $M = (1,2,\ldots, m)$; c_i is the concentration in moles per unit volume of solution; $\delta c_i/\delta t$ is the partial derivative of c_i, with respect to time t; R_i is the molar rate of production of the ith species due to chemical reactions; j_i is the molar flux; I is the electric current density, Φ is the electric potential; D, is the diffusion coefficient; F is the Faraday constant; u is the mass average velocity of flow; z_i is the charge number; and σ is the scalar electrical conductivity of the solution:

$$\sigma = F^2 \sum (z_i^2 \upsilon_i c_i) \qquad (2\text{-}8)$$

Mobility υ_i, is related to the diffusion coefficient by the Nernst—Einstein equation:

$$\upsilon_i = D_i/RT \qquad (2\text{-}9)$$

The molar flux ji is given by the Nernst-Plank equation:

$$j_i = - \upsilon_i z_i F c_i \nabla\Phi - D_i \nabla c_i + c_i u \qquad (2\text{-}10)$$

Shapiro and Probstein (1993) applied these equations to a tortuous capillary model of a porous medium.

As a result, one can obtain a partial differential equation for the distribution of concentrations of species in the porous medium of the following form:

$$\delta C_i/\delta t = D_i/\tau^2\ \delta^2 C/\delta x^2 - \delta/\delta x[C_i(u_{\theta,i} + u_c + u_h)] + R_i \qquad (2\text{-}11)$$

with the parameter τ describing the tortuosity of the porous medium.

In Eq. (2-11), C_i is the average (through the cross section perpendicular to the direction of flow) concentration of the ith component; $u_{\theta,i}$, u_c, and u_h, are the average electromigration, electrokinetic, and hydraulic components of the flow velocity, respectively.

These components are changeable within some limits and can be considered as control variables.

Shapiro and Probstein (1993), computed several variants of the numerical solutions of Eq. (2-11) with realistic boundary conditions. The modeled distributions of concentrations for acetic acid in the saturated clay soil are in good agreement with the results of specially designed experiments. Their experiments showed that a very high degree of removal of contaminants can be achieved on application of a DC current when used under appropriate conditions. Thus for example, the phenol contaminant fraction removed from clay samples reached 95% of the initial phenol concentration after 1.5 pore volumes of effluent were collected and removed. These experimental results are in good agreement with the theoretical results predicted by the model. Applying Eq. (2-11) for the modeling of contaminant concentration distribution, one needs to be aware that a high degree of spatial and temporal resolution is required to integrate the differential equations used in the model (Chilingar et al., 1997).

Multicomponent Cleanup Technologies and Examples of Their Application

in-situ

Examples of successful application of cleanup technologies in situ show that the best final results are achieved when one uses some combination of several methods. There is a wide variety of mechanical, physical, chemical, and bioremediation cleaning methods that are applied in contemporary practices for the restoration of a contaminated site. It is even difficult to name and characterize all of them. (This can be the goal of a separate article. Good classification of the bioremediation methods with general recommendations of their applications was presented by Pollard et al. (1994).)

For any particular contaminated site, one should select the most appropriate cleanup technology (or the most appropriate combination of different technologies). The choice of a concrete technology (or technologies) depends on many factors, e.g., the site size, type of predominant contamination, the site's future use, and available resources (time and money). Examples of such an approach to the selection of cleanup strategy were presented by Blacker and Goodman (1994) and Fairless (1990).

They developed some reasonable selection methodology of cleaning technologies, based on the principles of system analysis: from the final goal, through the quantitative characterization of the problem to the choice of preferable alternatives.

Many good examples of successful application of the combined technologies were presented by W. Loo and associates. Loo (1994) used a combined system, including primarily passive co metabolic biotreatment and electrokinetic transport of amendments and contaminants in solution for degradation of gasoline and diesel in the soil and groundwater. In one case, leakage of g- gasoline and diesel from an underground storage tank caused soil and groundwater contamination in the clayey Bay Mud of Hayward, California. The soil contamination extended to a depth of about 10 ft (3 m) with a TPH concentration of 100-3900 ppm (Chilingar et al., 1997). The gasoline and diesel in the soil were degraded to less than 100 ppm of TPH and to less than 10 ppm in groundwater. The remediation process was completed in 4 weeks. A combination of biodegradation and electrokinetic transport with a hot air venting system and ultraviolet light biocontrol system was used by Loo et al. (1994) for degradation of gasoline in the clayey soil. The gasoline soil plume covered an area of about 2400 ft2 (223 m^2), to a depth of about 30 ft (9 m). The upper 15 ft (4.6 m) of sediments were composed of highly conductive marine clay, whereas the lower 15 ft consisted of well-cemented conglomeratic sandstone.

The gasoline concentration ranged from 100 td 2200 ppm. The process of remediation was completed after about 90 days of treatment. The concentration of gasoline in the soil after treatment was far below the proposed cleanup level of 100 ppm. The cost of treatment was about $50 per ton of soil for this advanced soil treatment process, which provided a cost-effective remediation with minimum disruption to business operations at the site (Chilingar et al., 1997).

A closed recovery system for soil and groundwater for a site contaminated with gasoline in Greenville, North Carolina, was developed by Burnett and Loo (1994). The dissolved contaminant plume covered an area of 18,000 ft2 (1672 m^2) and penetrated to a depth of about 15 ft. The total volume of spill was estimated at 300,000 gal (1,135,500 L). The initial concentration of gasoline in the plume averaged about 40 mg/L of total content of benzene + toluene + ethylene + xylene (BTEX).

A special enhanced bioremediation system was designed to clean this site. The system consisted of two groundwater recovery wells, a treatment unit, and an infiltration gallery.

The treatment unit consisted of transfer pumps, pressure filters, granulated activated carbon filters, air spargers, holding tanks, chemical feed system, water heater, and monitoring means. The bioenhancement process included heating, addition of nutrient amendments (monoammonium phosphate and trisodium phosphate), and oxygen addition (dilute hydrogen peroxide). In 6 months of operations, BTEX in the plume had been reduced to the level less than 6.5 mg/L with the passage of 11 pore volumes of displacement (Chilingar et al., 1997).

In the considered examples, the treatment was successful owing to specially developed and designed combined systems of remediation. These systems were developed on the basis of information about the scale of contamination, concentrations of contaminants, soil type, and final goal of remediation. For the widespread application of cleanup technologies *in situ,* one needs to achieve a high degree of formalization and unification in the development of cleanup projects.

Electroremediation of Soils

The methodology can be imagined as a set of decision-making matrices (tables), which lists the characteristics of contaminants, soils, and groundwater, the scope of contamination, and the corresponding combinations of cleanup technologies. Performance of all technological units must be carefully controlled to avoid possible complications in situ. To understand and control the remediation processes, one needs mathematical models that can be easily tuned for specific site conditions. As an example, one can consider the model of electrokinetic transport discussed by Shapiro and Probstein (1993). Such models can be used to formulate control problems for various performance criteria and a variety of realistic constraints for in situ cleanup.

It was shown in recent publications (Hicks & Tondorf, 1994; Shapiro & Probstein, 1993) that for successful electrorestoration of hydrocarbon- and metal contaminated soils, it is necessary to control redox potential and pH along the path of electrokinetic transport to prevent cementation and stabilization.

These parameters can considerably affect the results of restoration. Understanding- their influences on electrokinetics for various combinations of contaminants, purging fluids, soils. and characteristics of the applied electrical field allows for the design of effective techniques to achieve a high degree of decontamination.

Chapter 3: Apparatus and Experimental Procedure

Laboratory Equipment

In figures 3-1 and 3-2, an illustration diagram shows the first apparatus and connections used in D.C. technology at the laboratory at the University of Southern California by Professor George V. Chilingar. (After Adamson et al., 1962-1963.)

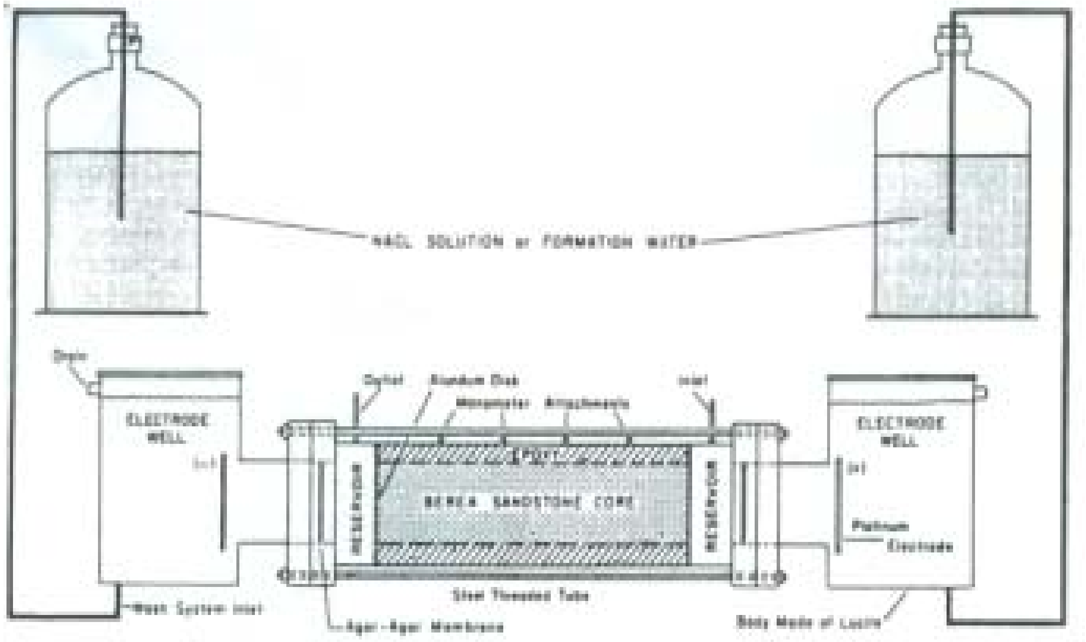

Fig 3-1: A schematic diagram showing the first apparatus and connections used in Petroleum Engineering Laboratories at the University of Southern California. (After Chilingar et al., 1962.)

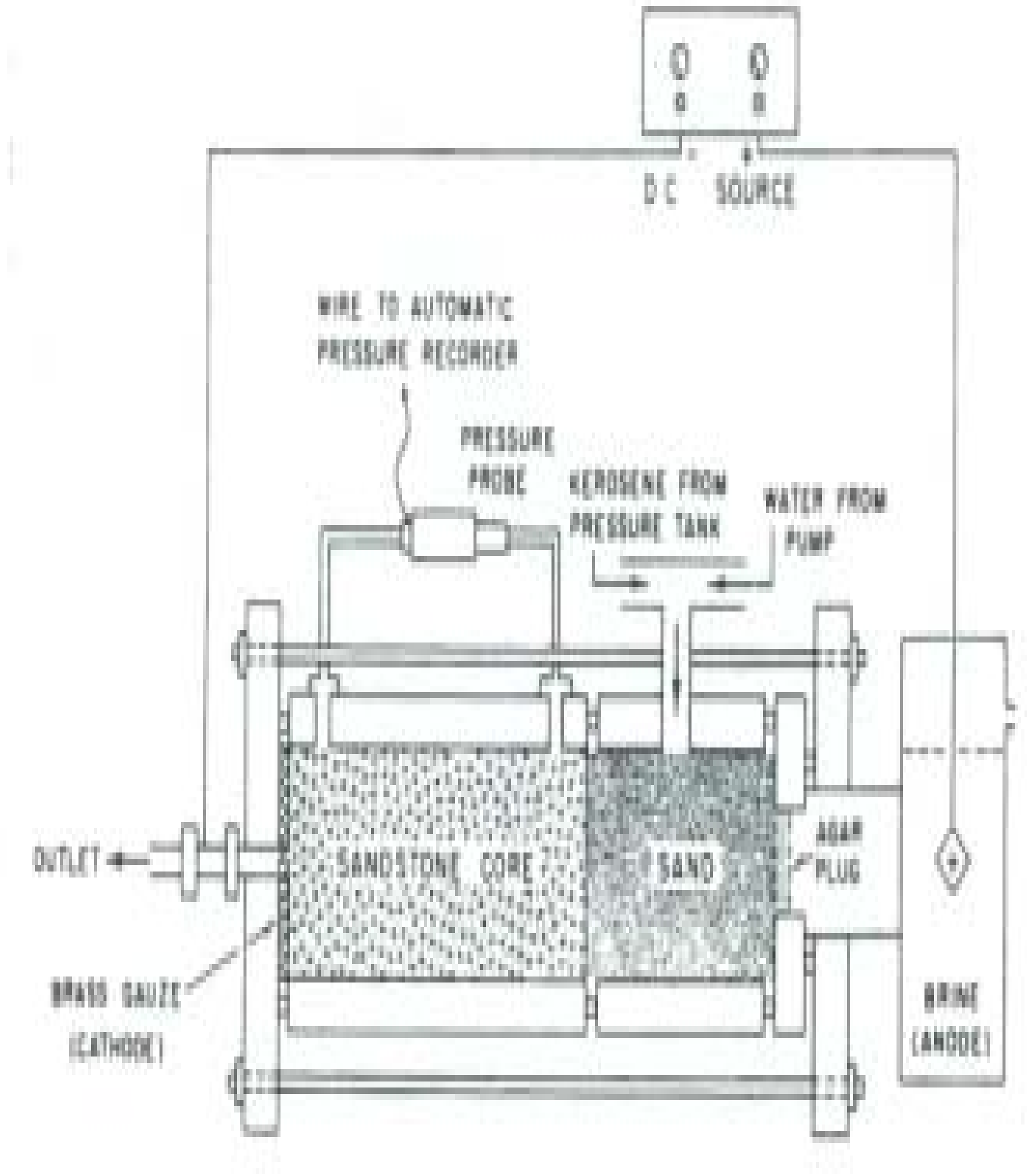

Fig 3-2: Schematic diagram of second apparatus and connections used in Petroleum Engineering Laboratories at the University of Southern California. (After Chilingar et al., 1962.)

In figures 3-3, 3-4, 3-5 and 3-6, an illustration diagram shows the glass core electrokinetic apparatus and connections used at the Fritz Engineering laboratory of the Lehigh University by Professor Sibel Pamukcu. (After Pamukcu et al., 1993.)

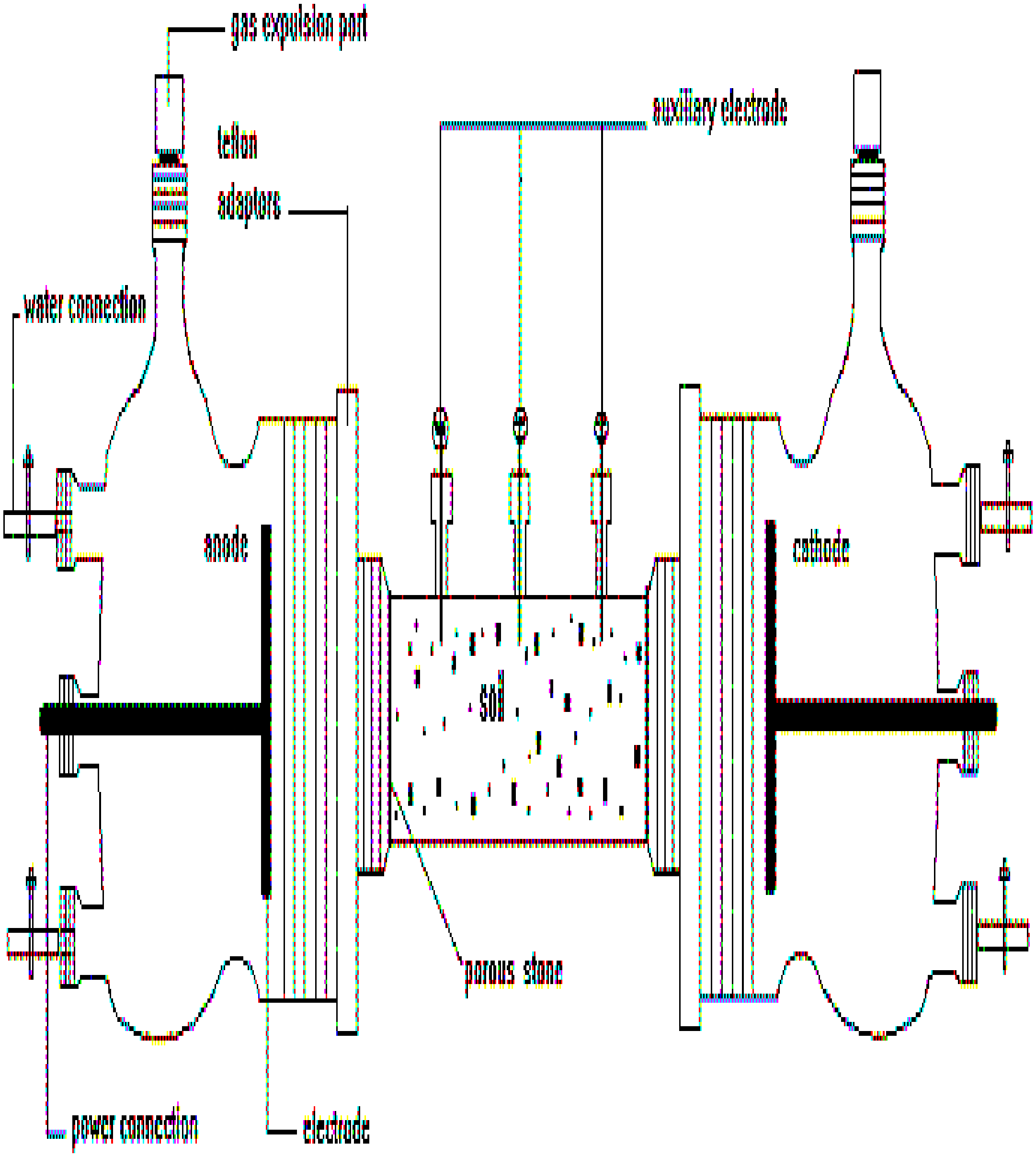

Fig 3-3: Schematic diagram of glass elektrokinetic cell (After Pamukcu et al., 1993)

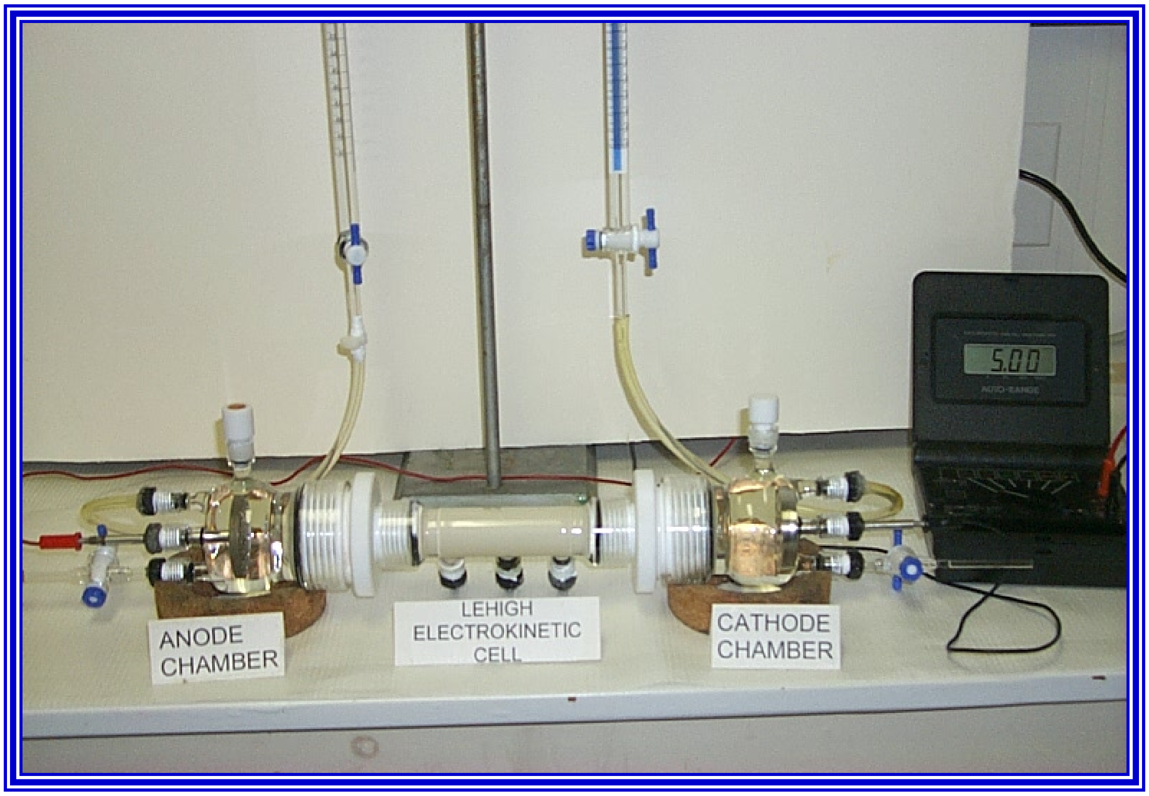

Fig 3-4: Photograph of electrokinetic apparatus and multimeter for measuring voltage, current and resistance. (See Fig. 1-8.)

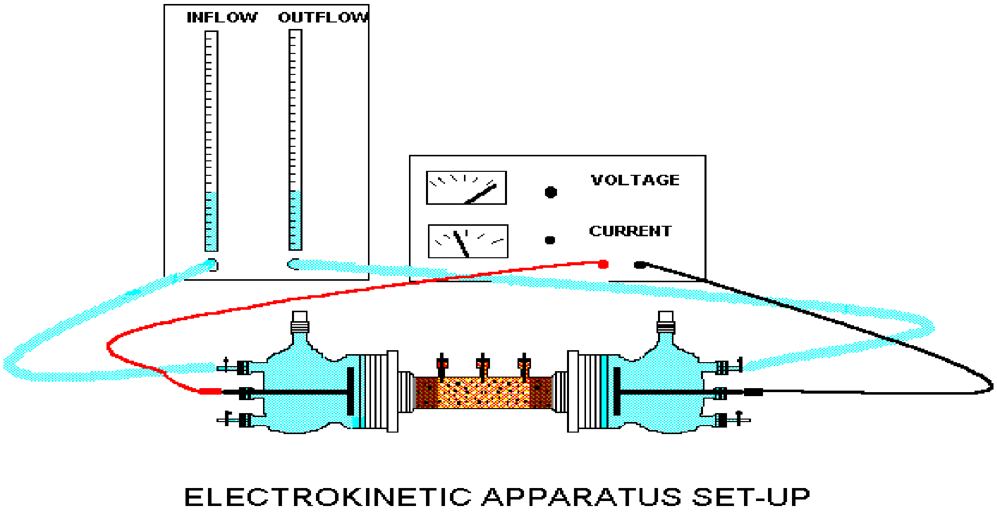

Fig 3-5a: Electrokinetic apparatus, DC power source and graduated glass burettes to measure both inflow and outflow at each of the two electrode ends (anode and cathode). (See Fig. 3-3.)

Fig 3-5b: Electrokinetic apparatus, DC power source and graduated glass burettes to measure both inflow and outflow at each of the two electrode ends (anode and cathode). (See Fig. 1-8.)

Fig 3-6a: Photograph of electrokinetic apparatus for measuring large cores (1 meter x 1 meter x 15 cm). (Designed by Dr. Sibel Pamukcu.)

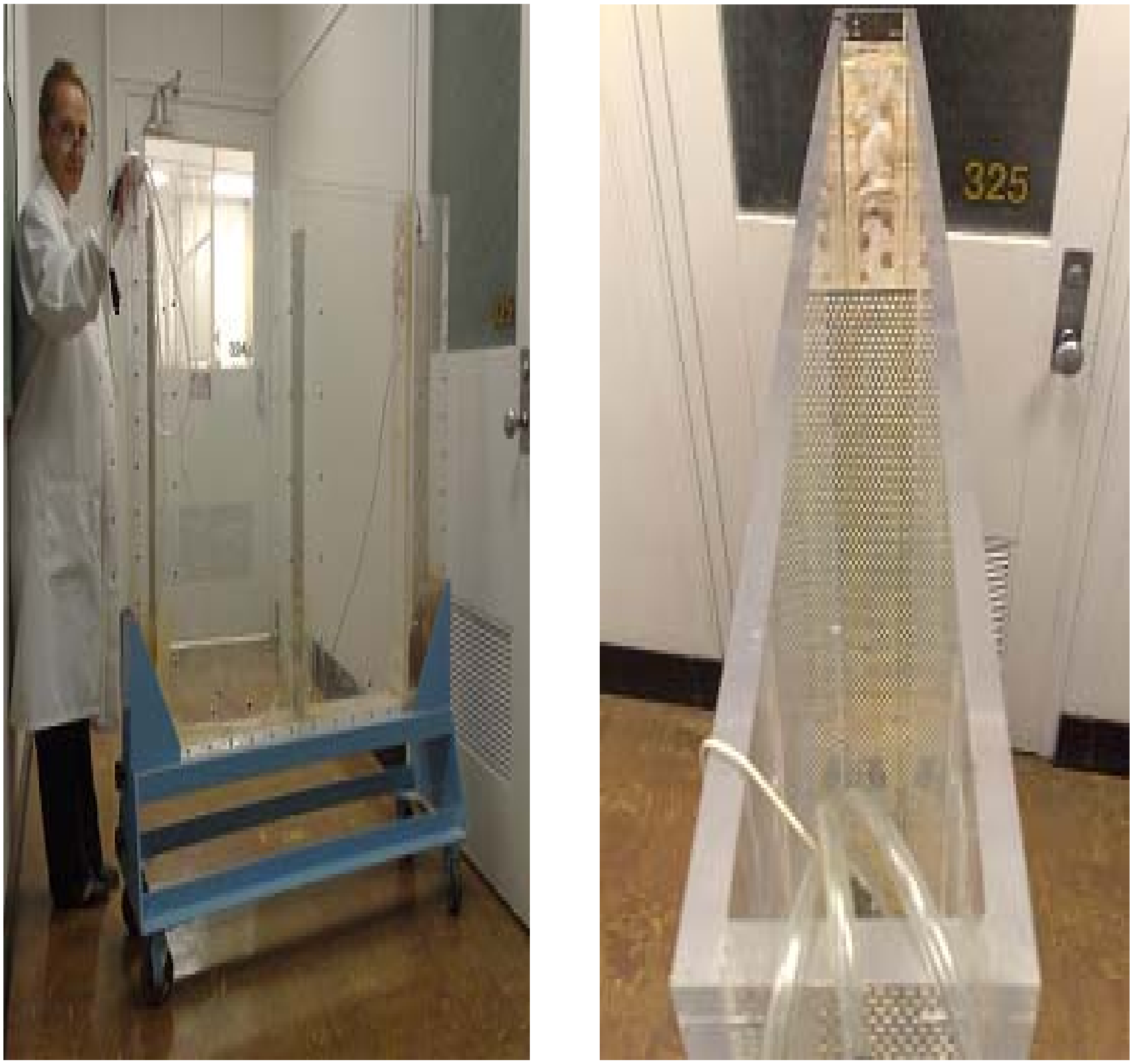

Fig 3-6b: Photographs of electrokinetic apparatus for measuring large cores (1 meter x 1 meter x 15 cm). (Designed by Dr. Sibel Pamukcu.)

Experimental procedure and preliminary results of electroremediation by the writer

The following heavy metals were tested in the laboratory for part (I) of this study using kaolinite clay in:

(1) Distilled water.
(2) Ground water.
(3) Water with humic substances of 900 ppm.

- Arsenic
- Cadmium
- Chromium
- Lead

Slurry samples of kaolinite clay were prepared each containing one of the heavy metals. The slurry was compacted into an EK sample tube and tested for 24 hours. The initial concentration of the contaminant was recorded at three positions along the sample tube: anode, center and cathode. After the 24-hour test, samples were extracted using the 3050B EPA method for acid digestion. The AAS and ICP-MS methods were used for chemical analysis of lead. All other heavy metal concentrations were determined using the ICP-MS equipment.

The initial and final sample water content and pH were determined for each test.

Facilities and Equipment

The apparatus consisted of two parts: an electrokinetic (E-K) cell and a flow control panel. A schematic diagram of the electrokinetic apparatus assembly is given in Figures

3-3 – 3-5. The electrokinetic test apparatus used in this project was developed based in the following considerations (Pamukcu et al., 1993):

i) electrode reactions will take place and hence electrodes should be isolated from the soil;

ii) electrode reactions will produce gas at the electrode surfaces due to electrolysis, and a convenient method for gas ventilation has to be provided to accurately measure the water transport;

iii) electrode surface has to be larger than the soil cross sectional area so the a low current density at the electrodes will produce a relatively large current density in the soil;

iv) ports for extracting inflow and outflow fluid samples have to provided for the analysis and monitoring process.

Based on these considerations, the electrode surface area was selected to be six times larger than the sample cross-sectional area. Clear acrylic plastic was used for all cell parts to provide visibility and also defect gas generation at the electrode sites, the soil-water interface and possibly in the soil. The electrodes are made of high grade graphite rods to minimize electrode deterioration.

The electrokinetic cell has the following components (Pamukcu et al., 1993):

Sample tube: The sample tube has an ID of 3.55 cm and a length of 7.62 cm and is made of clear acrylic tube. The tube accommodates three auxiliary graphite electrodes (1 mm diameter), separated at equal distance along one side, through which voltage can be measured during experiments. The tube is assembled to the electrode chambers with O-rings placed inside the housings cut on the inner walls (facing the sample tube) of the chambers.

Porous stones: Carborandum porous stones are placed at each end of the sample tube to hold the soil sample in place during the experiment. The porous stones have a permeability of 10^{-3} cm/sec, which is highly porous compared to the clay soils tested which have hydraulic permeabilities ranging from 10^{-6} to 10^{-8} cm/sec. Therefore, they do not influence the rate of flow through soil. The stones are washed with dilute nitric acid to ensure removal of metal impurities and particles which might clog the stone or influence the results of the chemical analyses. They are then boiled in distilled water before each usage.

Electrode chambers: These chambers are approximately 130 cm^3 in volume. They house the electrodes at each end of the soil sample tube. The end plates are removable for filling and emptying these chambers of fluid. This feature also facilitates cleaning of the chambers and electrodes after each test run. Teflon membrane gaskets situated at these ends provide a water tight seal.

Electrodes: Electrode assemblies with a surface area of 22.6 cm^2 facing the soil specimen were constructed of graphite rods with a 0.635 cm diameter held together with graphite conductive adhesive. The assembly’s connecting rod is flush with the outer surface of the back wall. An electrode socket is placed through the center of the exposed rod and fixed in place with carbon conductive epoxy glue. These connections are wired to a variable DC power source.

Fluid connections: Teflon or stainless steel quick-connections are provided on the bottom of the back wall of the electrode chambers. These outlet or inlets are then connected to volume measuring tubes and pumped via Teflon tubing. The advantage of the quick connections is that they close the connection upon detachment, which allows the electrokinetic (E-K) cell to be detached from the control panel while the electrode chambers are still charged with fluid.

Gas expulsion or sample extraction/injection ports: These ports are pressure valves provided on the cover plate over each electrode chamber. These valves have metal surfaces which are coated to control any deterioration by electrochemical reactions or metal ion deposition on them. Sample extractions or fluid injections are accomplished using a volumetric syringe which allows for accurate control of quantities of fluids.

Burettes: Glass burettes with a capacity of 25 cc are used to measure inflow, normally at the anode (positive electrode) chamber, and outflow, normally at the cathode (negative electrode) chamber to an accuracy of 0.1 cc.

Vent-pressure valves: Vented pressure valves exist at the top of each burette to provide gas expulsion.

Power supply: Dedicated electrical units for each E-K cell consist of variable direct current (DC) power supply capable of applying either constant voltage (0 to 30.6 volt), or constant current (0 to 2500 mA). These units also contain analog meters for measuring voltage and current.

Compaction Apparatus: A schematic diagram of the compaction apparatus used is shown in Figure 2-3. The apparatus consist of a PVC sample cell (guide tube) measuring 45.72 cm length by 2.67 cm diameter, in which the slurry sample is injected. The weight base with compacting column causes a piston like displacement based on choice of several weights that allow for a varied pressure range of 5 psi to 30 psi. This is then placed on top of the injected slurry that's contained within the PVC sample cell with the porous stone placed at the bottom end. The weights are placed in the tray at the top of the compacting column in progressive increments, throughout a period of 24 hours amounting to a final pressure of 30 psi to be exerted for final compaction to reach a compacted sample having uniform density, porosity and contaminant concentration distribution. During compaction, fluid is drained at the top and bottom of the sample via porous stones resting on both ends of the core.

Soil slurries are prepared by mixing an aqueous solution of the desired contaminant with the soil, and the type of water chosen with a prepared water content of 55%. After the 24 hour period of compaction, all the samples had a water content of 40% recorded as the initial water content before the E-K test.

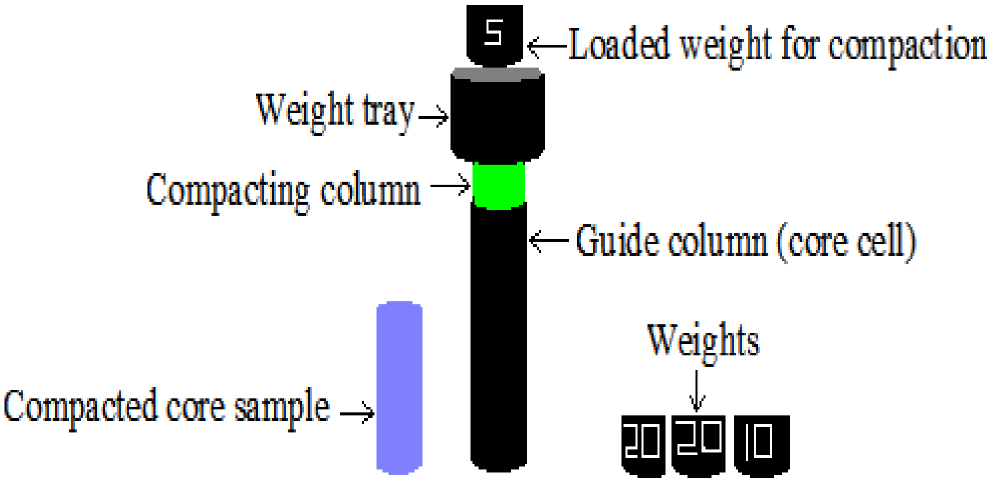

Figure 3-7: Compaction apparatus used to prepare samples for E-K tests.
Electrokinetic Testing

In all experiments, a constant 20-volts DC potential was applied across the core samples.

<u>During the E-K test</u>: Volumetric electroosmotic inflow and outflow readings are take n from the graduated burettes. The system is checked to insure the delivery of the 20 V applied, recording the current density as well. This is done using a multi-meter to read voltage across the E-K apparatus via power connections to each of the primary electrodes and on the secondary electrodes along the sample tube. Readings were taken at 0, 15 and 30 minutes and one and two hours after the start of the test (Pamukcu et al., 1993).

<u>After the E-K test</u>: During cell disassembly, the pH of the anode and cathode fluid is recorded and a sample is taken for analysis. Since the cathode fluid is generally basic (high pH), it may contain some precipitates of certain metals, it is acidifed with HCl to ensure a more accurate chemical analysis of the chemical content. The colors of both water and soils are noted. Finally the soil is extruded from the sample tube and measured at the center of the soil cross-section at 5 evenly spaced points along its length for pH, water content and redox-potential in millivolts (Pamukcu et al., 1993).

Chapter 4: Experimental Results

Here, we will demonstrate the feasibility of using electrokinetics to decontaminate heavy metals from clay formations. In the first part of this chapter, experimental testing confirmed the efficiency of using electroremediation to treat moderately and highly artificially contaminated clays in labs at both Lehigh University as well as at the University of Southern California. In the final part, the world's first conducted test on field collected data of contaminated offshore muds was performed at the Petroleum Institute in Abu Dhabi, U.A.E. to prove the efficacy of using electrokinetics in such a high salinity environment as a suitable option for *in-situ* treatment

The results will be split into two sections:

1. a) Artificially polluted clay specimens of low concentration heavy metals performed at Lehigh University by Dr. Sibel Pamukcu.

   b) Artificially polluted clay specimens of high concentration heavy metals performed at USC by the writer.
2. Field collected data from the coastline of two geographic locations in Abu Dhabi, U.A.E. by the writer.

Part I

	Laboratory Simulation
pH	7.90 ppm
Ca	47.06
Mg	14
Bicarbonate	90.51
Chloride	83.43
Sodium	32.04
Potassium	3.51
Sulfate	55.34
Fluoride	--
Silica	--
Nitrogen, Nitrite	--
Nitrogen, NO_2 + NO_3	--
Arsenic	2.01 ppb
Barium	54.95
Beryllium	--
Cadmium	0.098
Strontium	171.61
Zinc	173.66

Table 4-1: Ground water composition of Jefferson County water, Id (USGS 1989)

The following results were obtained after 24-hour EK tests:

The following results of part I, are split into two categories, low concentration (L) and high concentration (H) samples. The low concentration tests were performed by Dr. Pamukcu at Lehigh University, while the high concentration tests were performed by the writer at the University of Southern California.

(i) Arsenic: Arsenic was in anionic ($HAsO_4^{2-}$) form in the initial mixing state into the slurry. Fig. 2-4 through 2-6, show the fraction of arsenic found at three different locations in the core: the anode, the center, and the cathode end. Arsenic content was reduced (from its initial concentration) at both the cathode and anode regions of cores. Highest concentration of arsenic was present at the center of the cores by the end of treatment. Arsenic speciation and solubility is greatly affected by the pH and redox potential of the soil. The availability of arsenic, in the form of aresnite (As(III)) increase at low redox potential and alkaline conditions. The average pH of the center section was 2.9 ranging from 1.8 to 3.0. Subsequent analysis of redox potential variation of kaolinite clay during electrokinetics showed that, in general, the anode end of the soil remains in oxidizing state, while the cathode end is in reducing state. At high redox levels (oxidizing state) the majority of As is found in arsenate form (As(IV)) which is not as soluble as As(III), and tend to be retained on the oxide surfaces of the clay minerals (Masscheleyn et al., 1991). Accumulation of arsenic at the center of the soil specimens can be explained by the low pH and the oxidizing state of the soil at that location. Accumulation was evident at the center of the soil samples for most of the specimens except for the low concentration case in which the metal appeared not to migrate substantially (Pamukcu et al., 1993).

Distilled water:

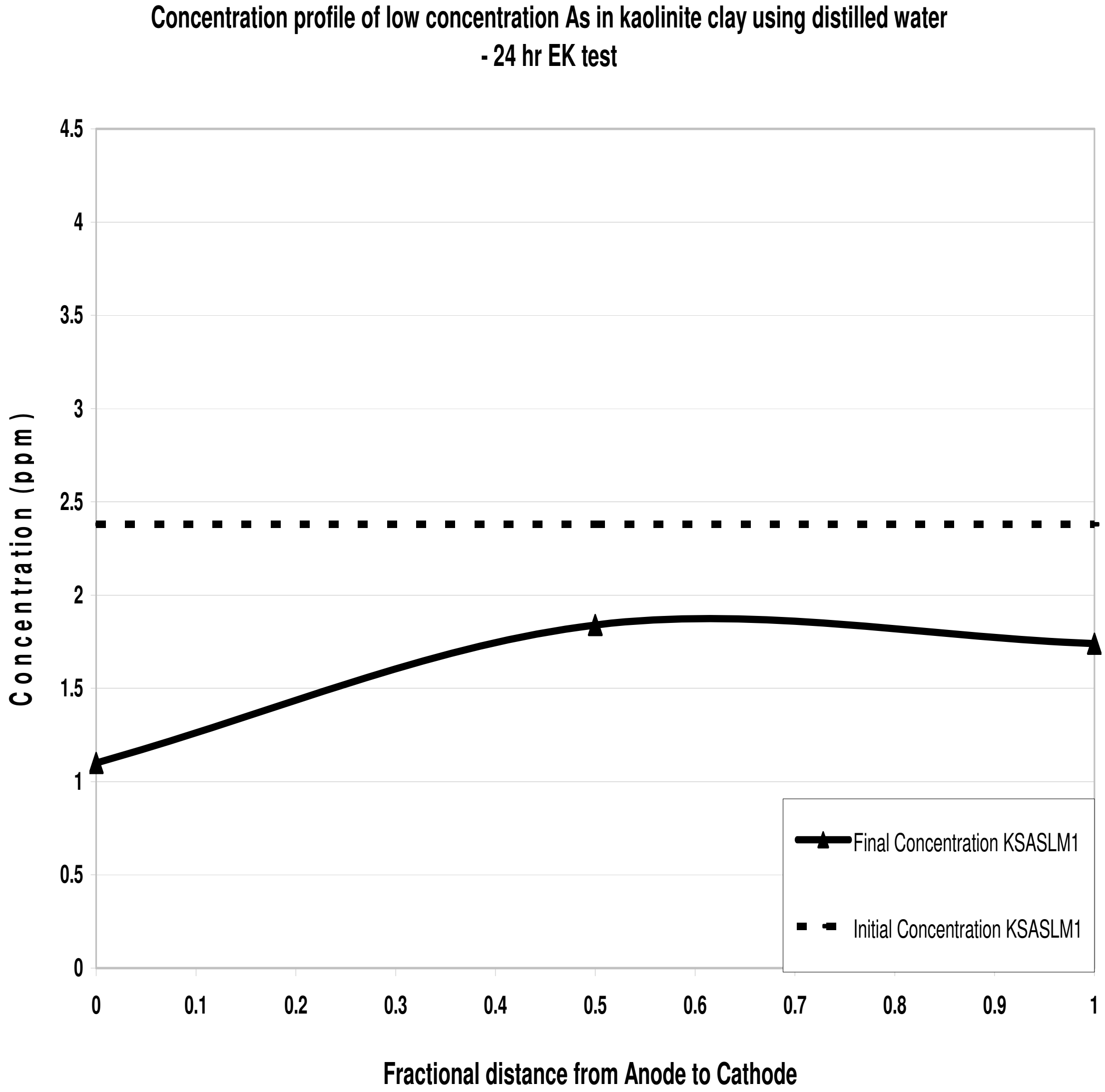

Figure 4-1-L-a: Results of EK test for electroremediation of arsenic using distilled water (Pamukcu et al., 1993).

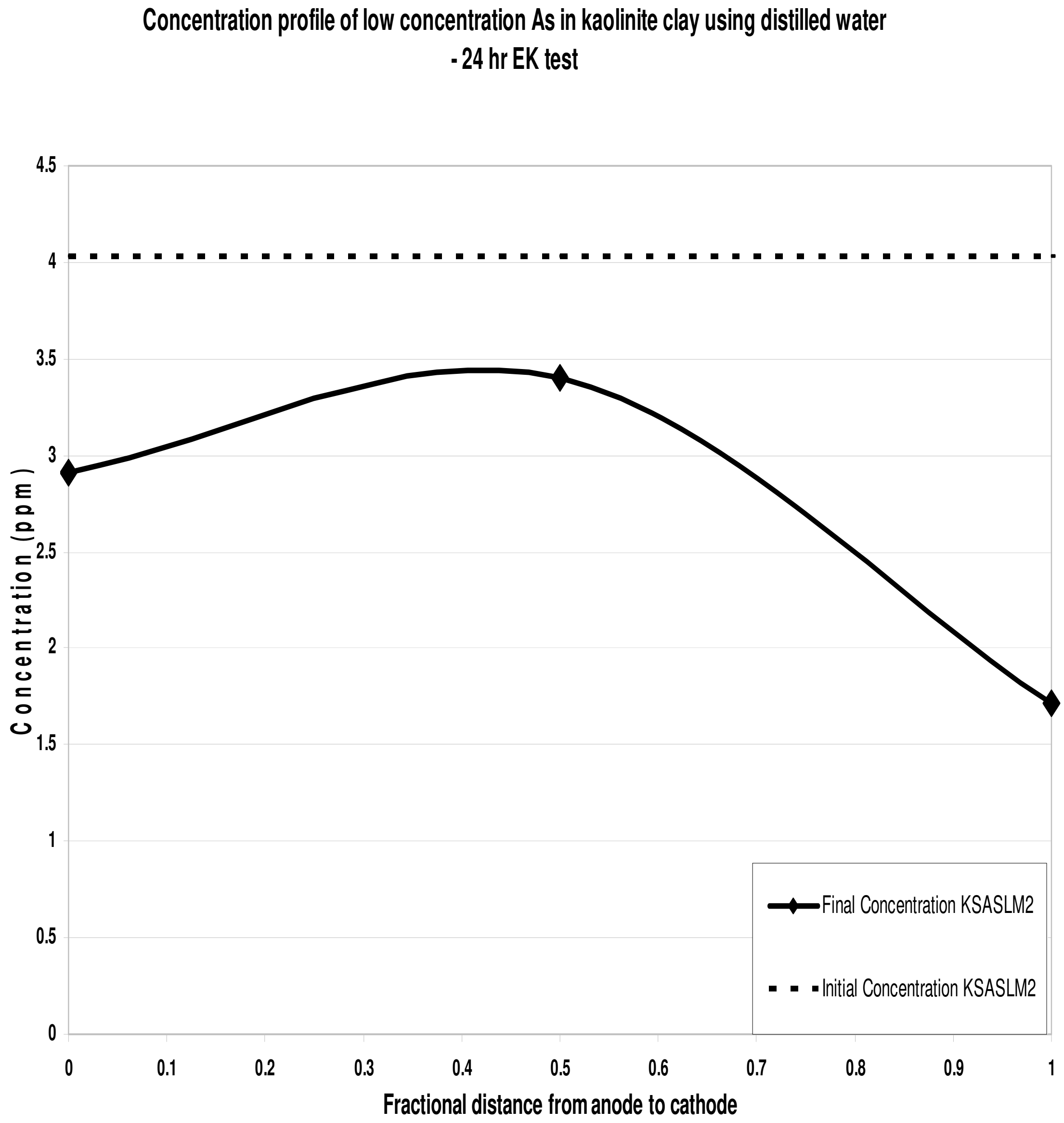

Figure 4-1-L-b: Results of EK test for electroremediation of arsenic using distilled water (Pamukcu et al., 1993).

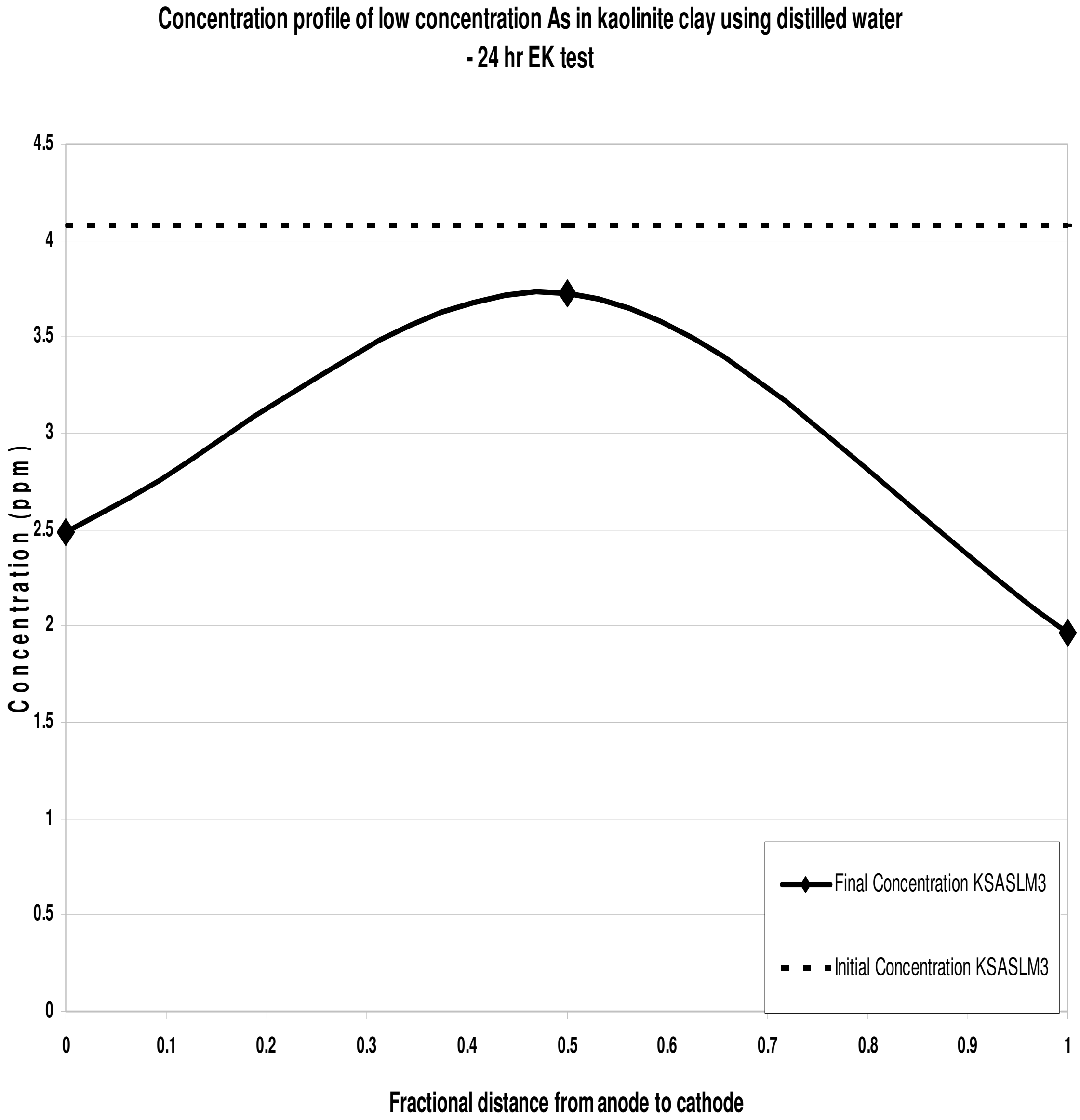

Figure 4-1-L-c: Results of EK test for electroremediation of arsenic using distilled water (Pamukcu et al., 1993).

Ground water:

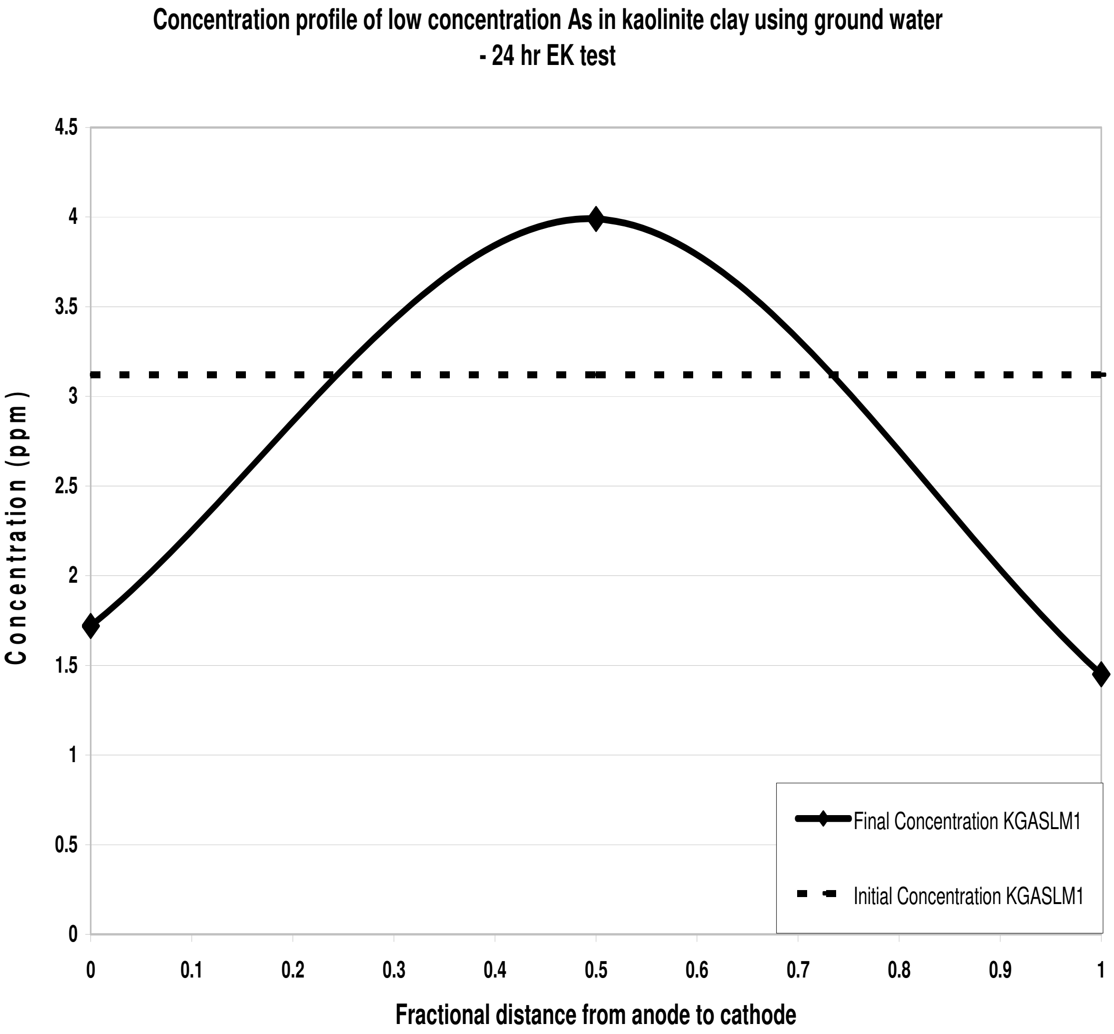

Figure 4-2-L-a: Results of EK test for electroremediation of arsenic using ground water (Pamukcu et al., 1993). (See Table 4-1 for composition)

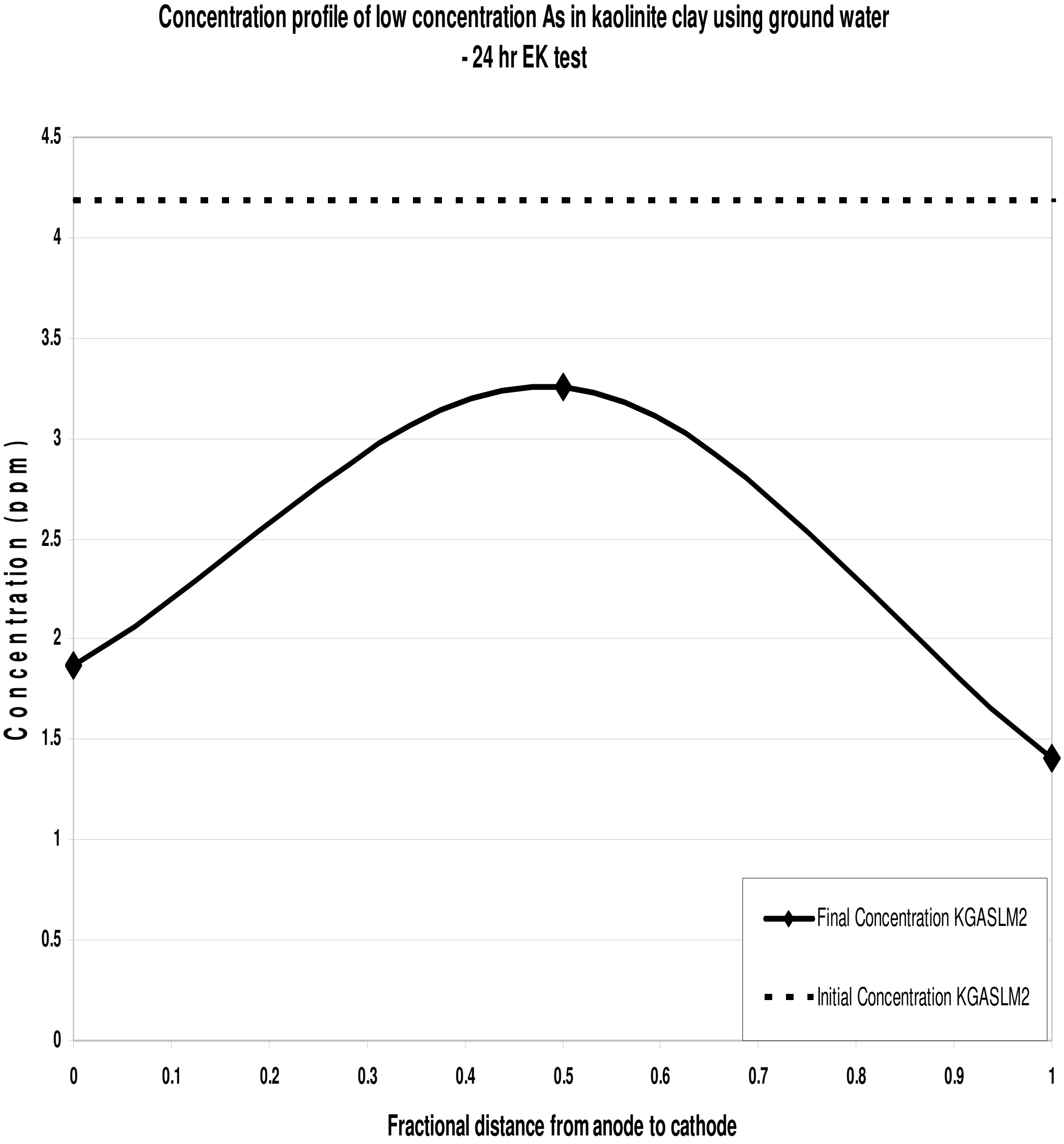

Figure 4-2-L-b: Results of EK test for electroremediation of arsenic using ground water (Pamukcu et al., 1993). (see Table 4-1 for composition)

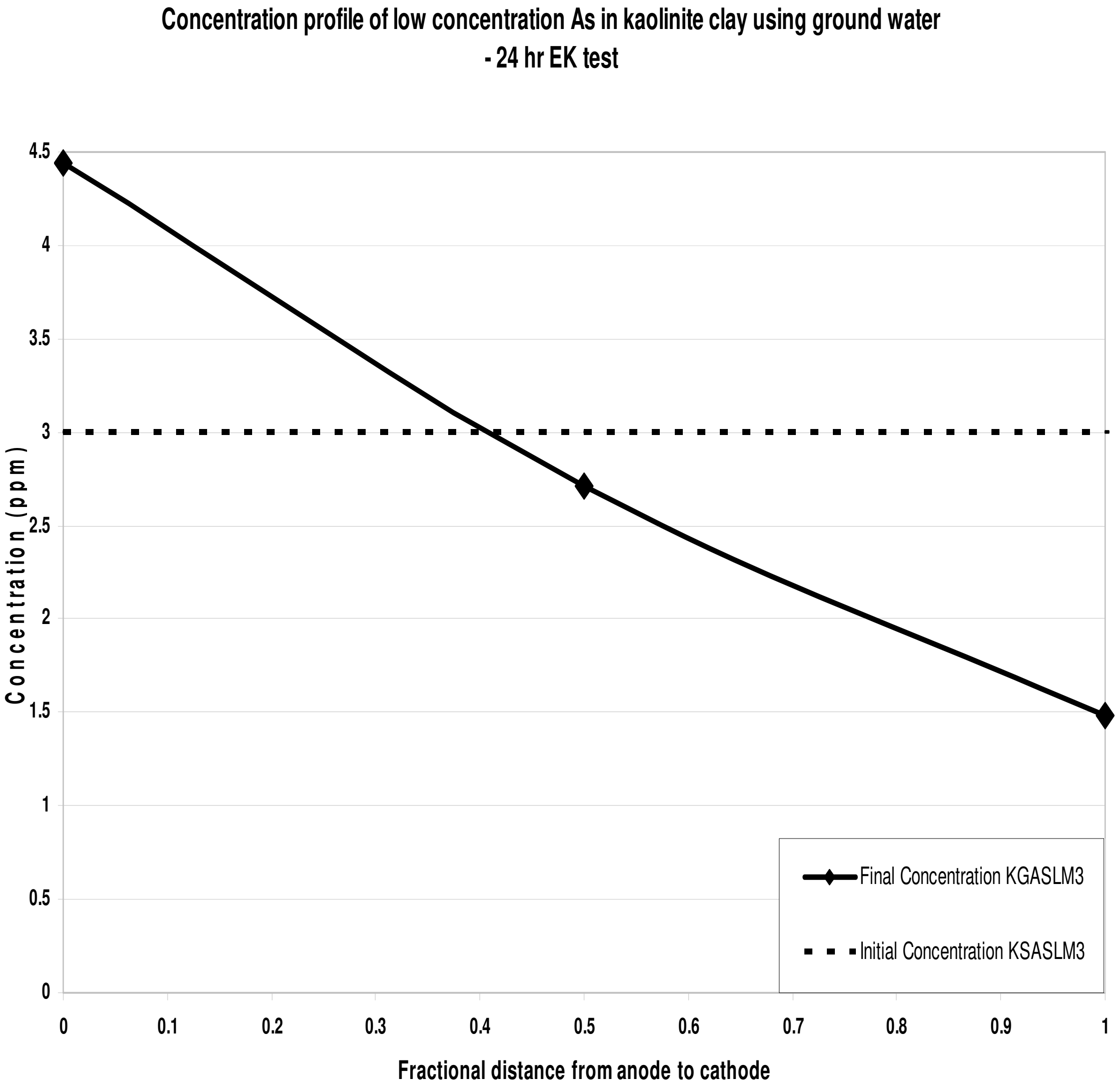

Figure 4-2-L-c: Results of EK test for electroremediation of arsenic using ground water (Pamukcu et al., 1993). (see Table 4-1 for composition)

Water with humic substances (900ppm):

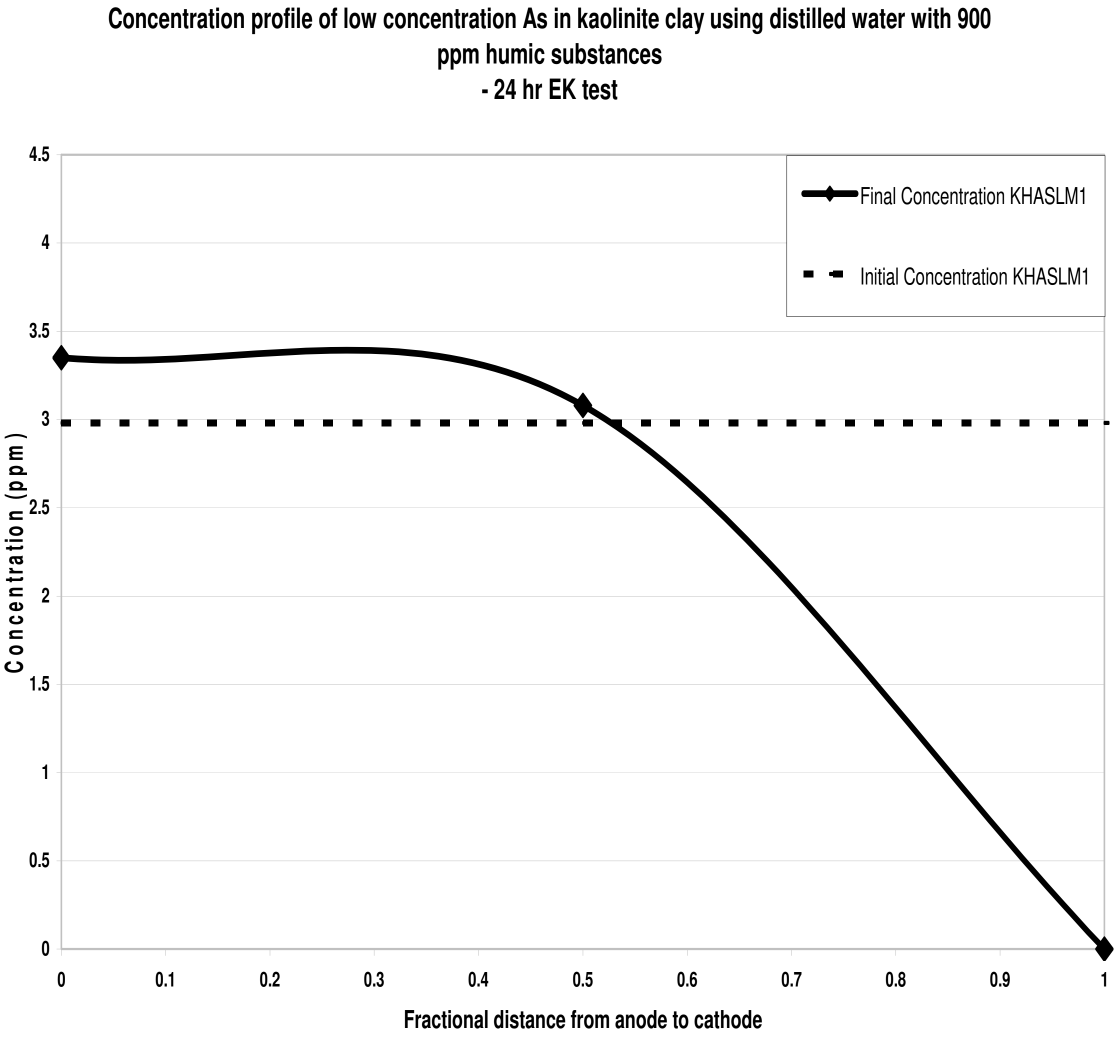

Figure 4-3-L-a: Results of EK test for electroremediation of arsenic using water with humic substances (900ppm) (Pamukcu et al., 1993).

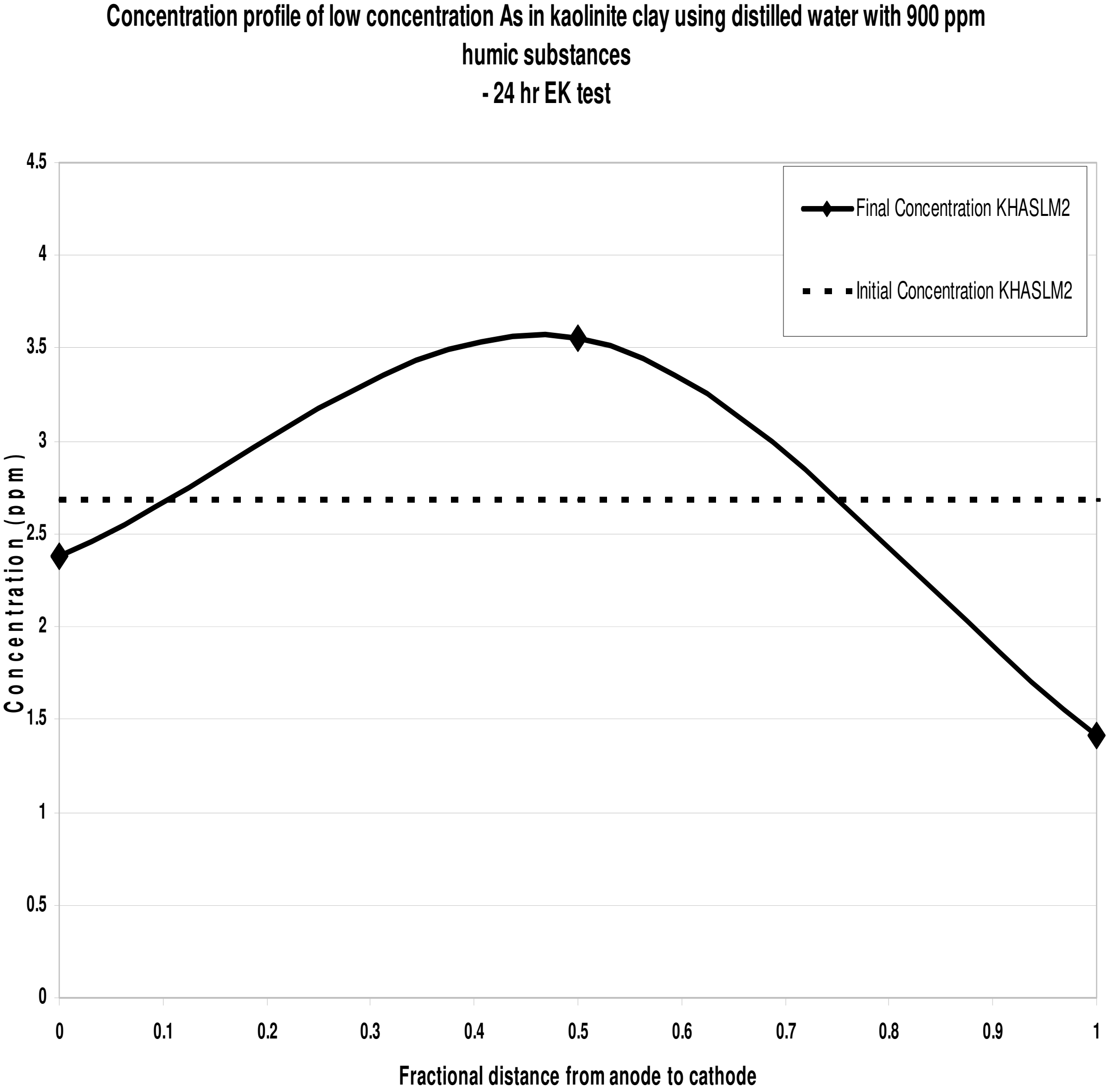

Figure 4-3-L-b: Results of EK test for electroremediation of arsenic using water with humic substances (900ppm) (Pamukcu et al., 1993).

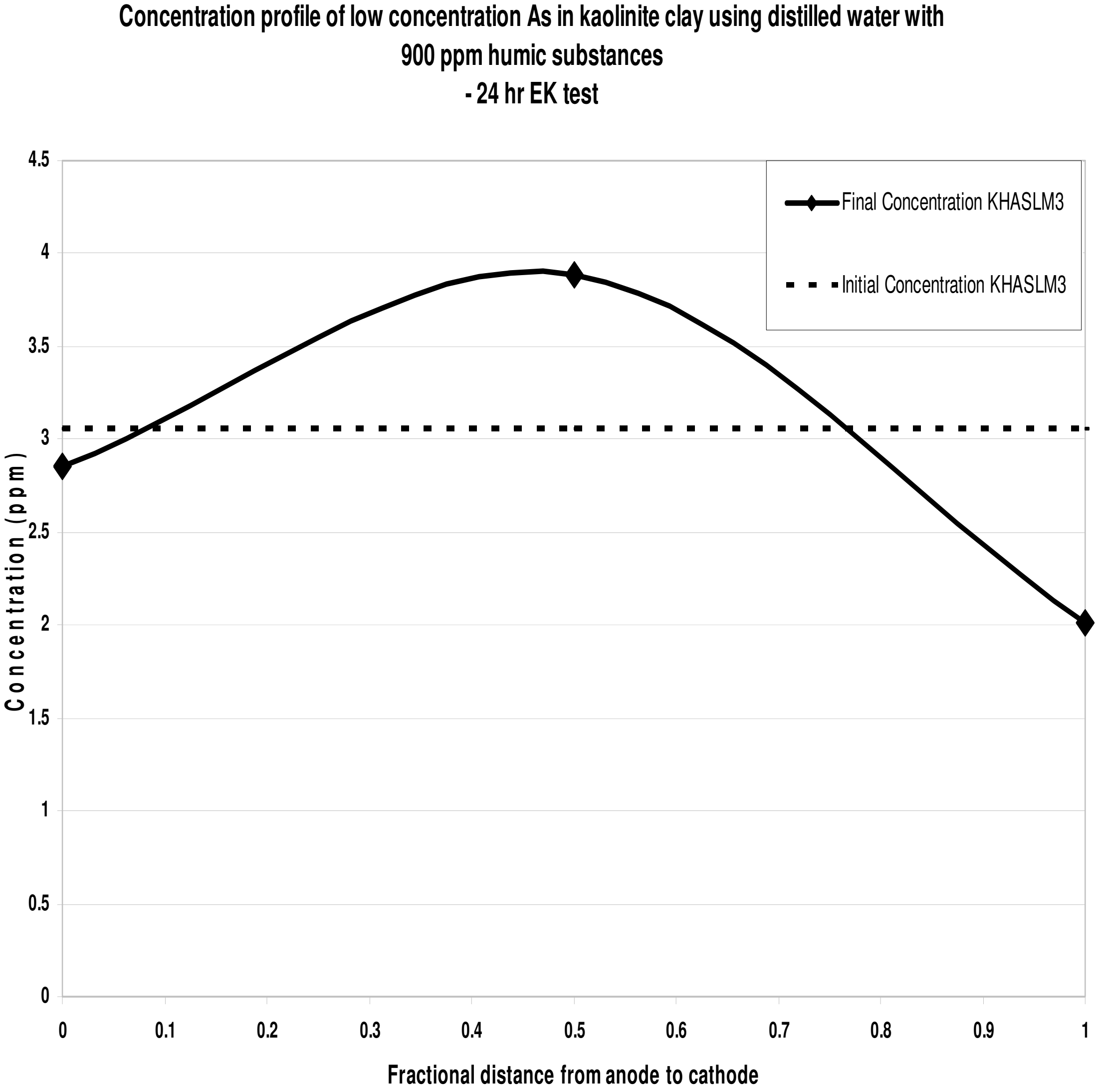

Figure 4-3-L-c: Results of EK test for electroremediation of arsenic using water with humic substances (900ppm) (Pamukcu et al., 1993).

(ii) Cadmium: Figs. 4-4 – 4-6, show the fraction of cadmium found at three different locations in the soil after the 24 hours of electrokinetic treatment of soil specimens containing high cadmium concentration. Cadmium is a divalent cation which showed a migration path toward the cathode. Cadmium exhibited a maximum concentration at the cathode end of the soil sample. This is attributed to the increase in the hydrolysis with an increase in pH at the cathode end. The average pHs measured at the cathode ends were 5.3, 8.1 and 9.0 for distilled water, groundwater and humic solution specimens of kaolinite clay, respectively. Until around pH 8, Cd remains in its divalent cationic form. Beyond this value it starts forming complex species which are either charged positively or negatively or neutral. The tendency and the abundance of these products control the removal rate until the acid front reaches the cathode region in the soil. However, with high pH prevailing at the soil—water interface of the cathode end of the soil, a thin layer of precipitate would form at the interface making it difficult for cadmium to be removed into the cathode electrode water chamber (Pamukcu et al., 1993). There is also an increase in soil adsorption capacity with increasing pH which would contribute to the accumulation of the metal at this region (Sposito, 1984; Basta and Tabatabai, 1992).

Distilled water:

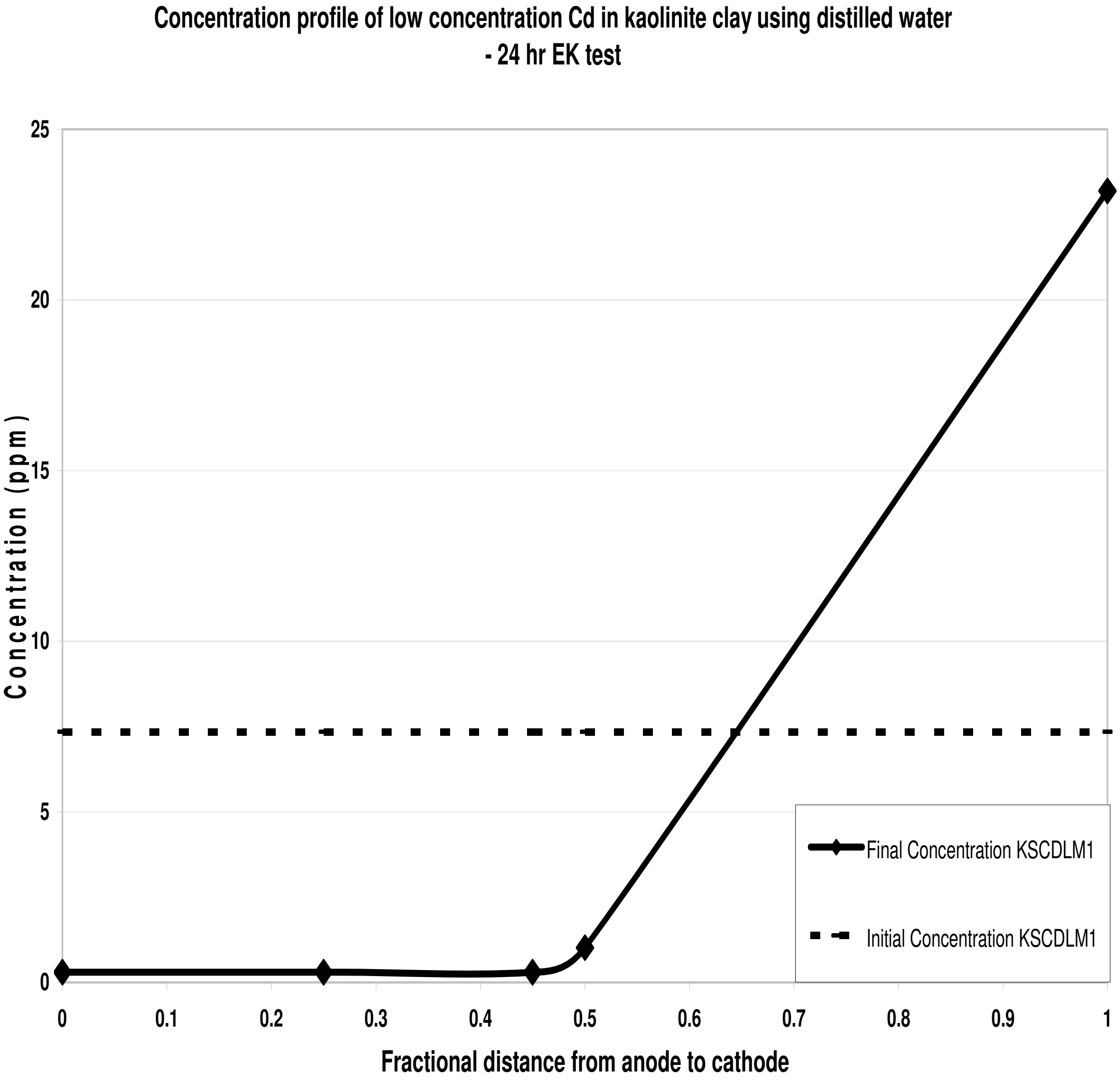

Figure 4-4-L-a: Results of EK test for electroremediation of cadmium using distilled water (Pamukcu et al., 1993).

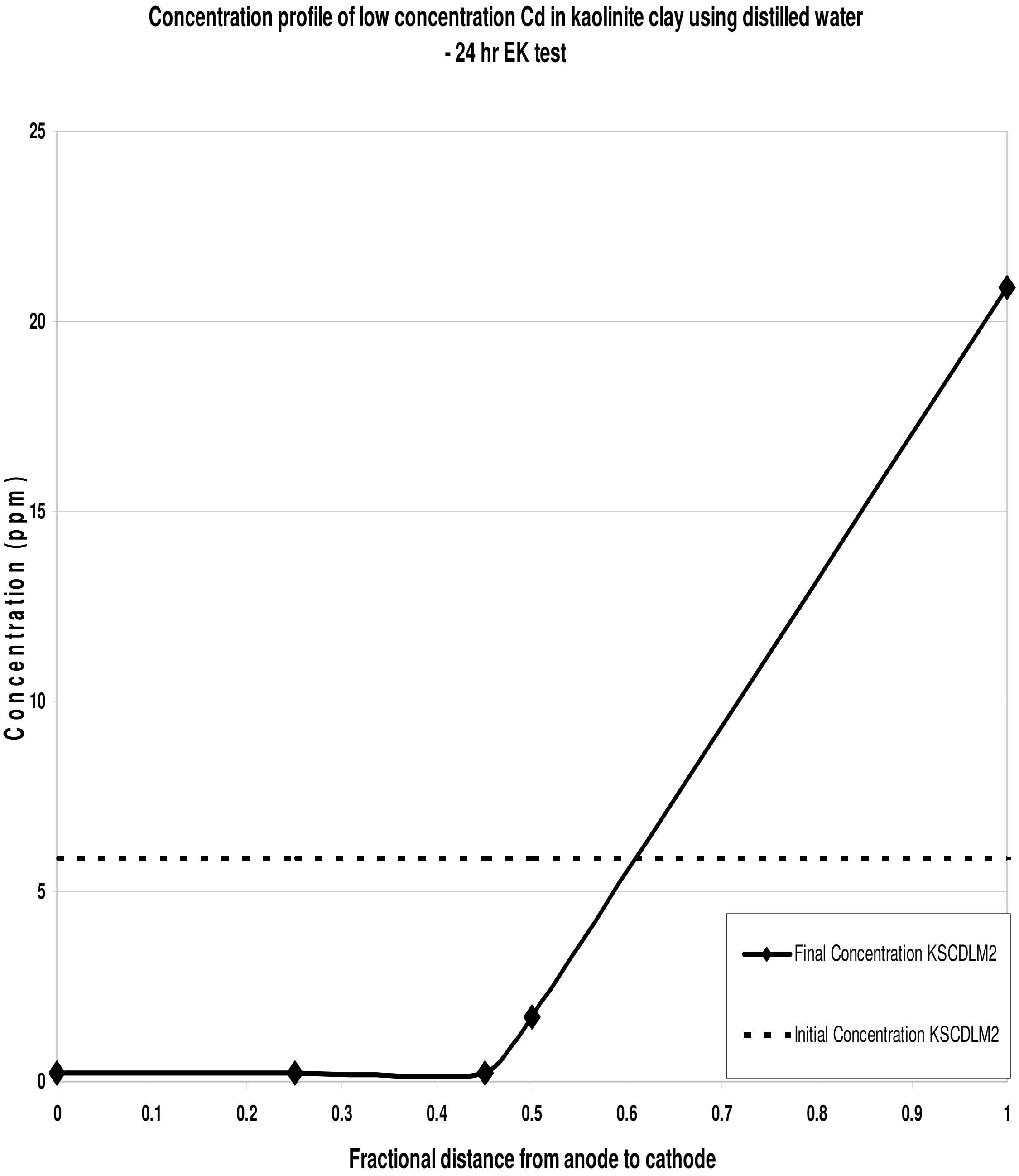

Figure 4-4-L-b: Results of EK test for electroremediation of cadmium using distilled water (Pamukcu et al., 1993).

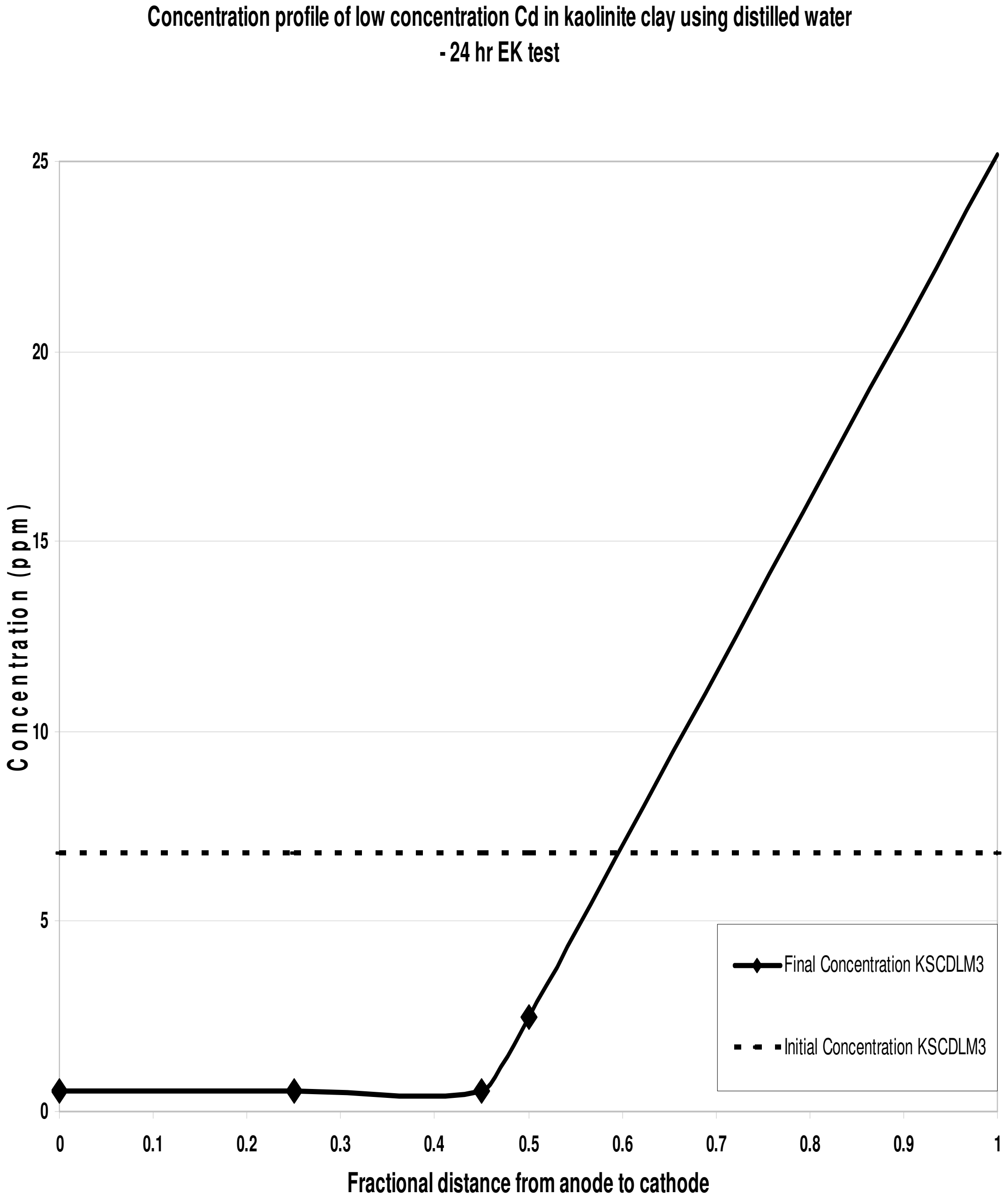

Figure 4-4-L-c: Results of EK test for electroremediation of cadmium using distilled water (Pamukcu et al., 1993).

Ground water:

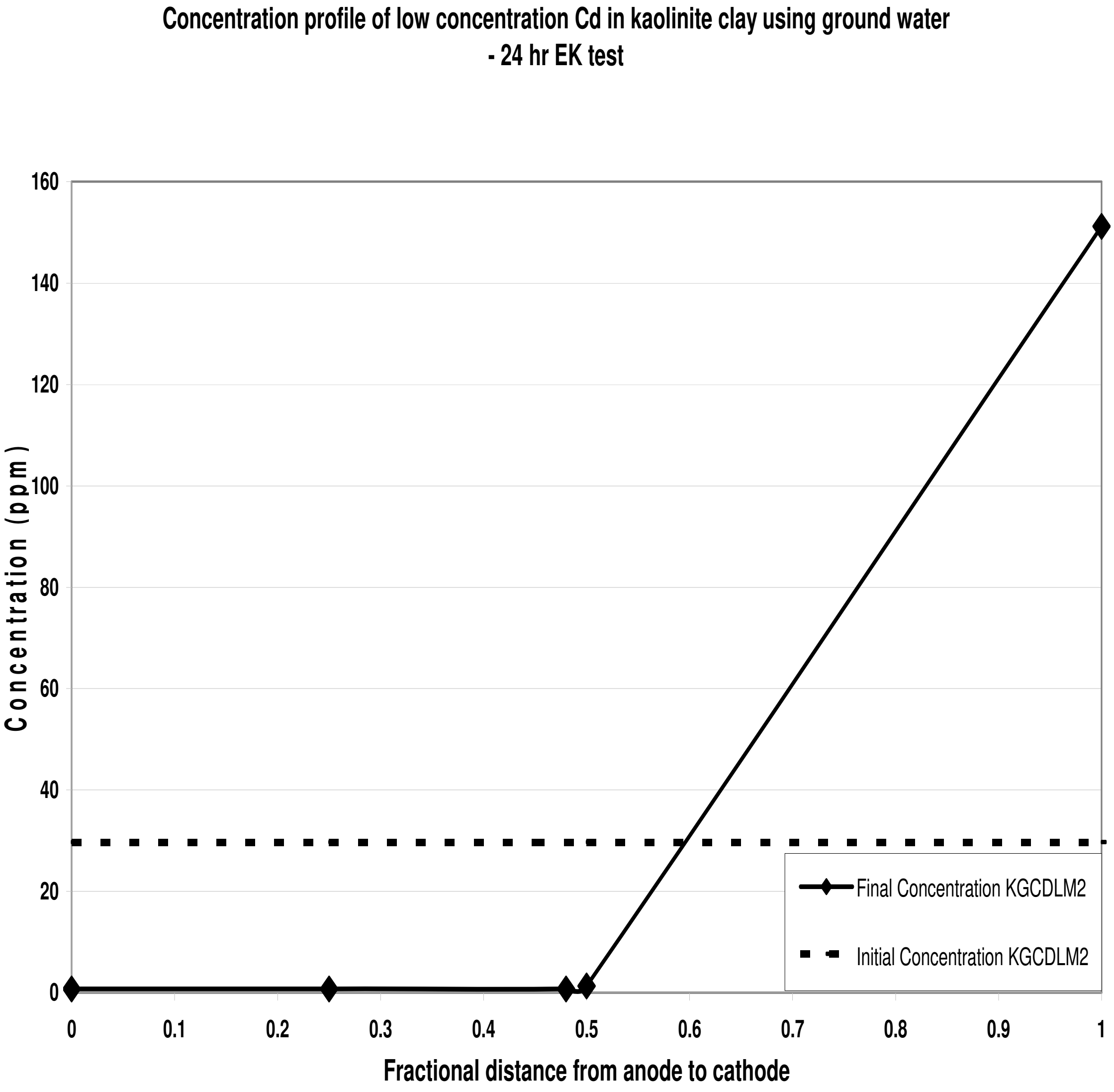

Figure 4-5-L-a: Results of EK test for electroremediation of cadmium using ground water (Pamukcu et al., 1993). (See Table 4-1 for composition)

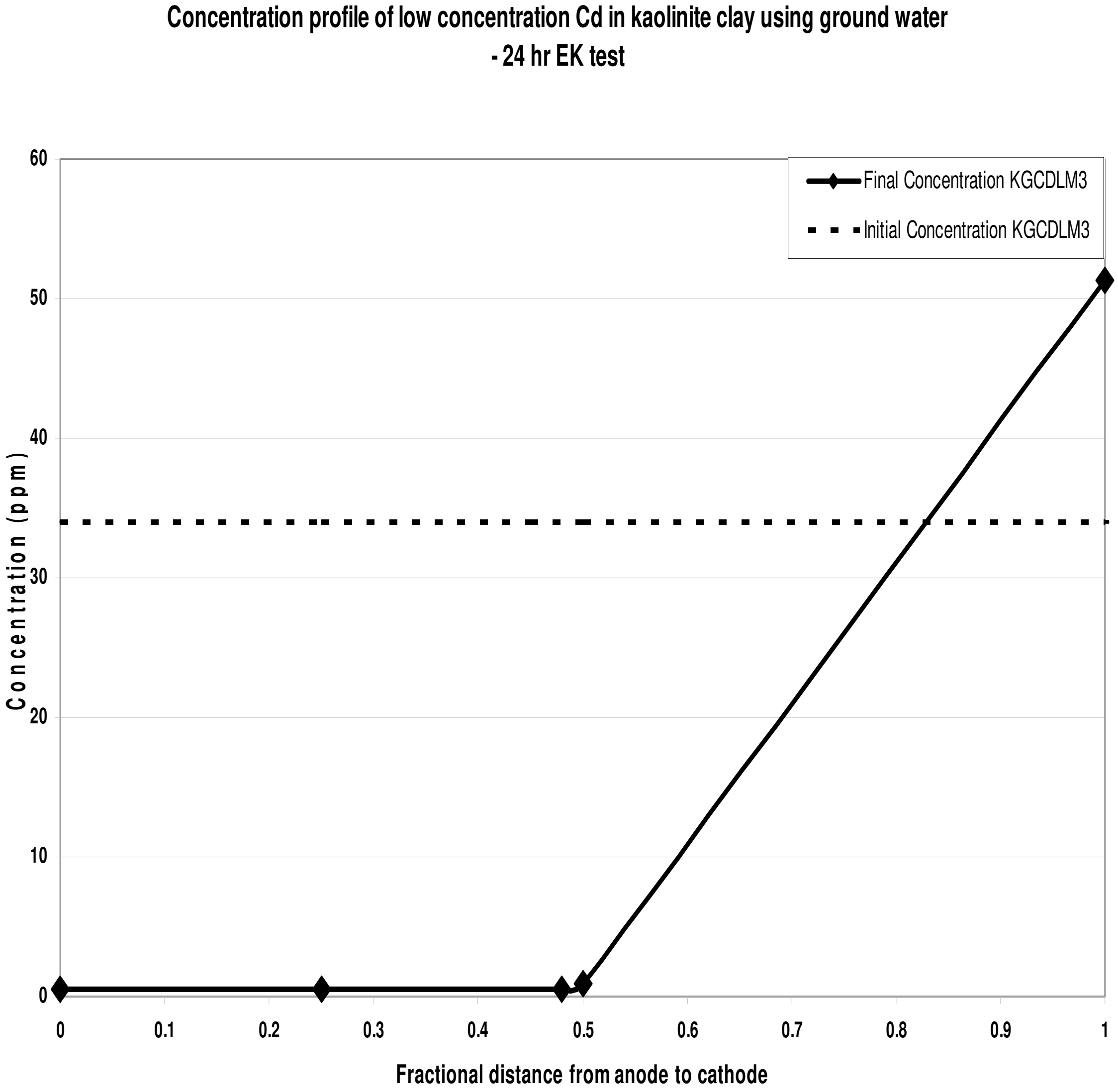

Figure 4-5-L-b: Results of EK test for electroremediation of cadmium using ground water (Pamukcu et al., 1993). (See Table 4-1 for composition)

Water with humic substances (900ppm):

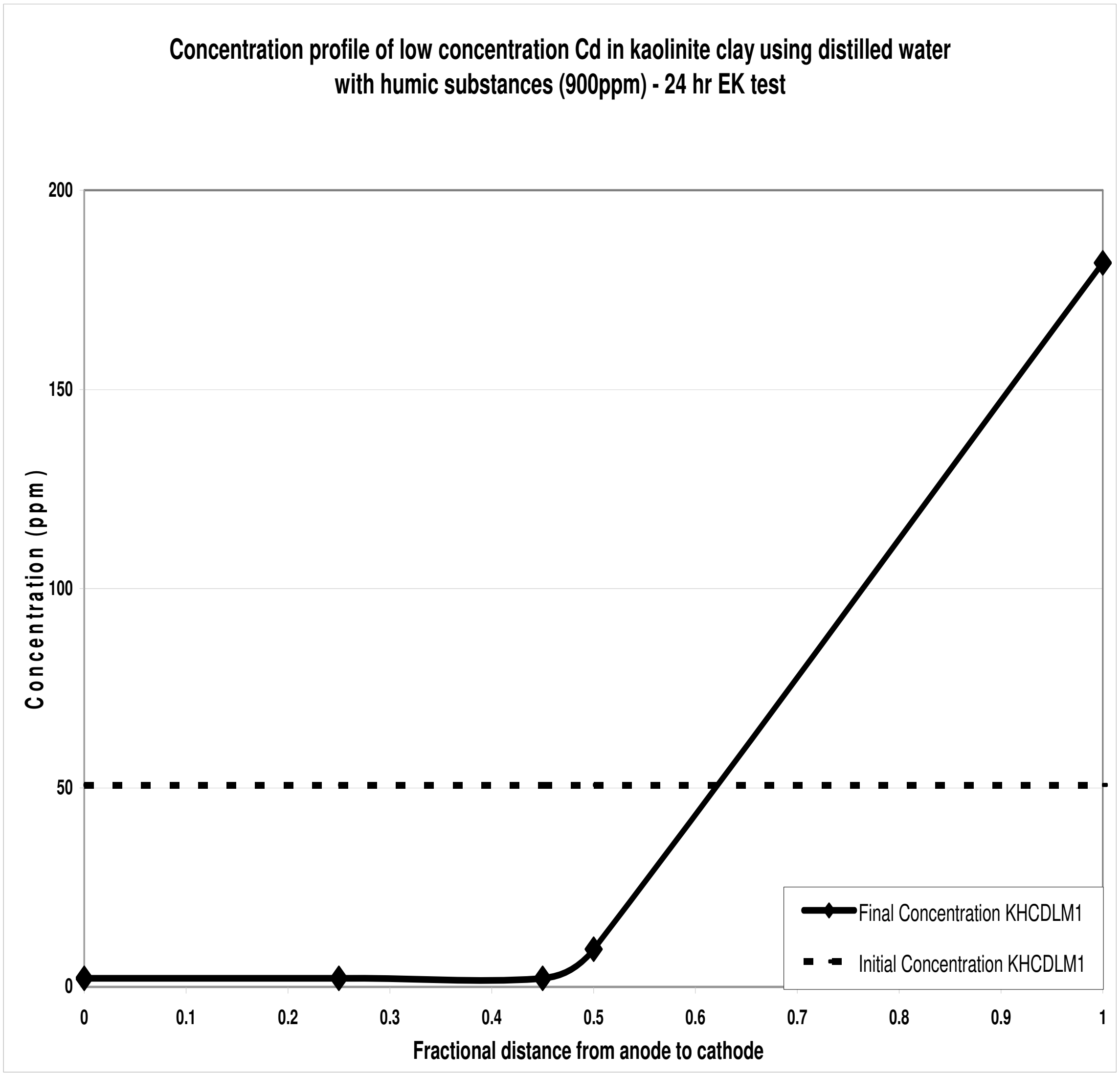

Figure 4-6-L-a: Results of EK test for electroremediation of cadmium using water with humic substances (900ppm) (Pamukcu et al., 1993).

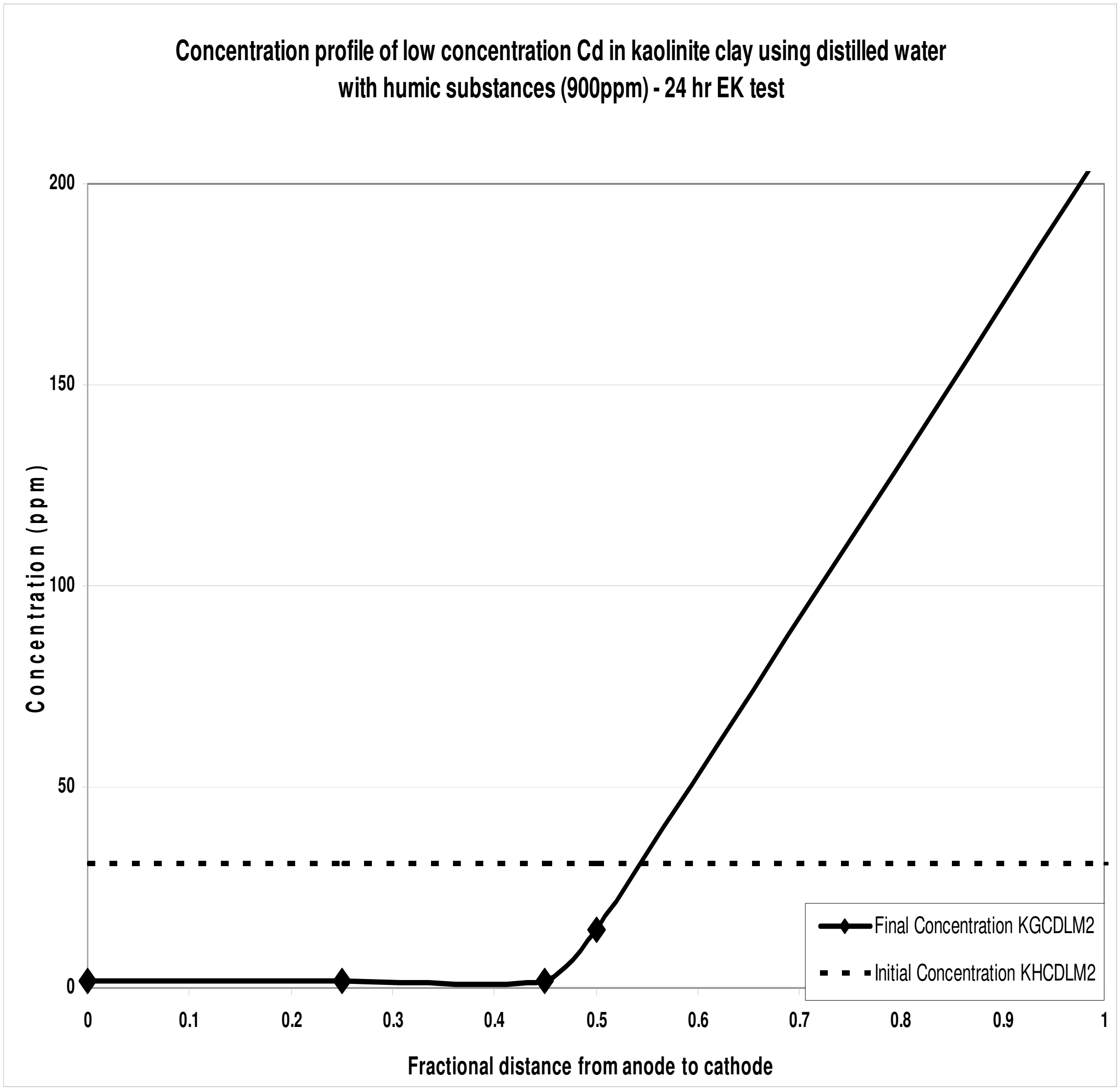

Figure 4-6-L-b: Results of EK test for electroremediation of cadmium using water with humic substances (900ppm) (Pamukcu et al., 1993).

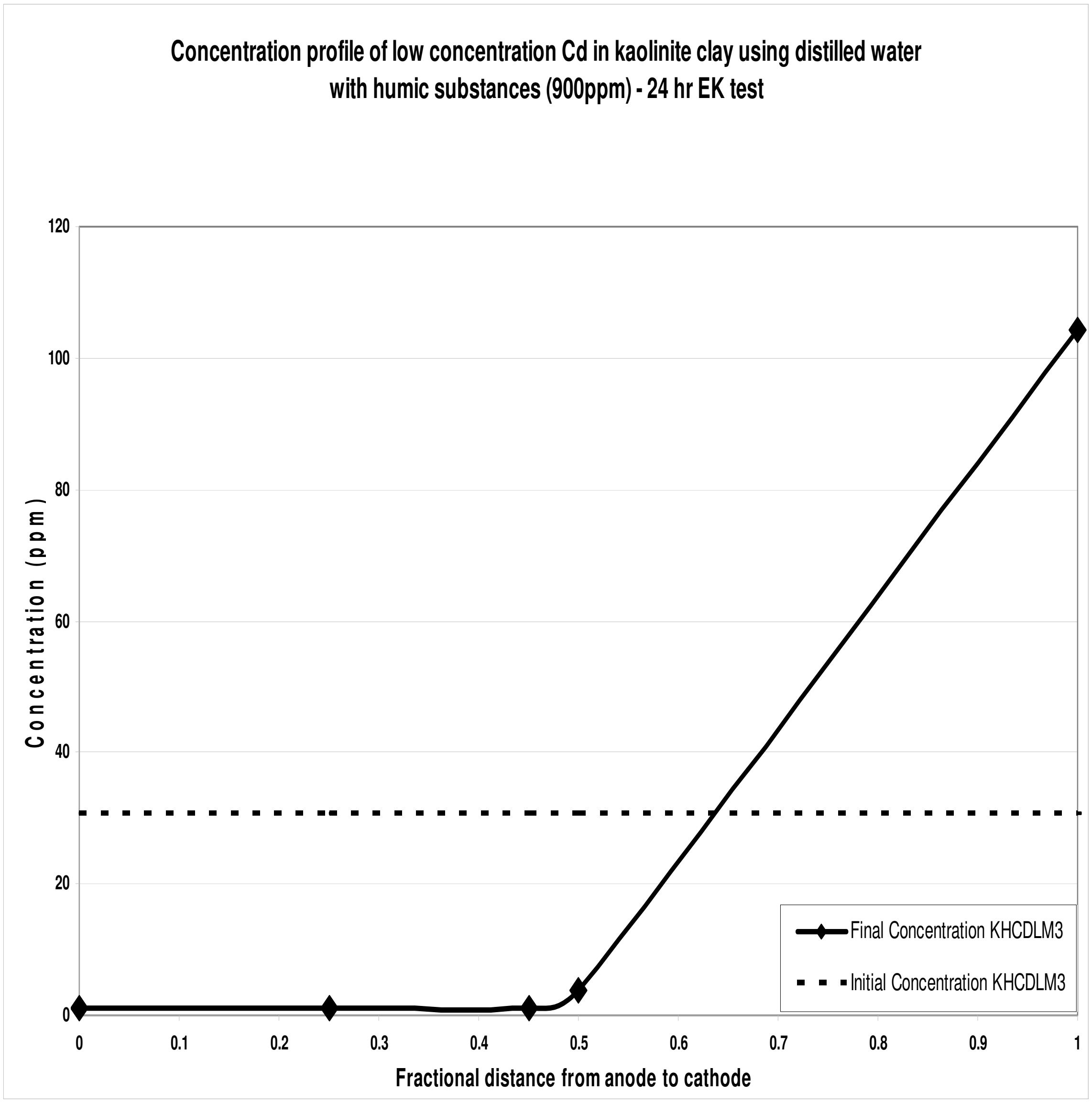

Figure 4-6-L-c: Results of EK test for electroremediation of cadmium using water with humic substances (900ppm) (Pamukcu et al., 1993).

(iii) Chromium: Chromium was introduced to the soil in anionic form—($Cr_2O_7^{2-}$). Chromate (chromium in the hexavalent oxidation state) is an anion which carries two negative charges. Approximately, 30% of the Cr was extracted at the anode chamber by the end of the 24 to 48 hours of treatments (see Fig. 4-7 – 4-9). In this case, the electromigration of the ion took place in the opposite direction of the electrokinetic water flow. There was accumulation of metal at the discharge end (anode end of the soil) (Pamukcu et al., 1993).

Distilled water:

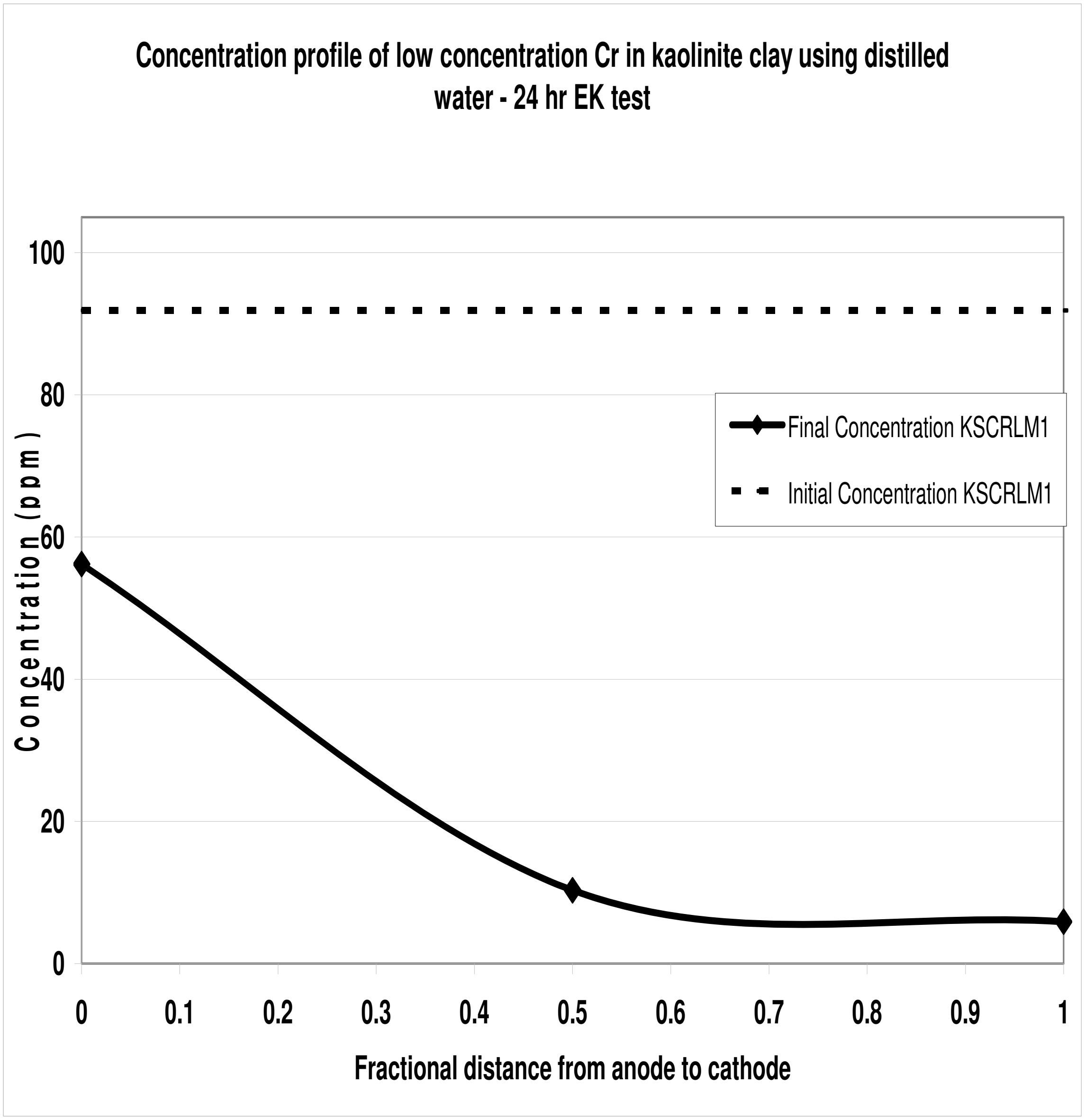

Figure 4-7-L-a: Results of EK test for electroremediation of chromium using distilled water (Pamukcu et al., 1993).

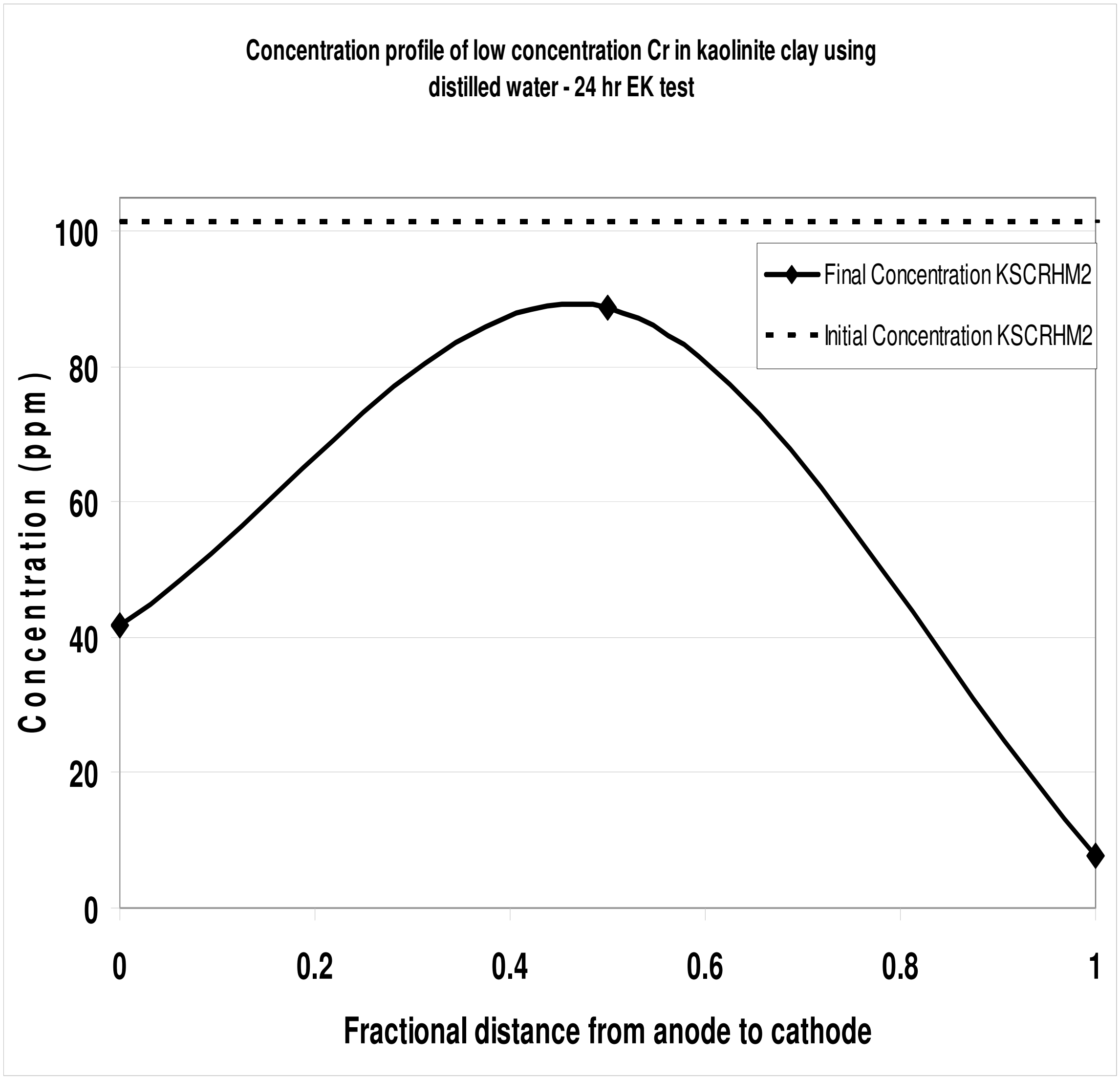

Figure 4-7-L-b: Results of EK test for electroremediation of chromium using distilled water (Pamukcu et al., 1993).

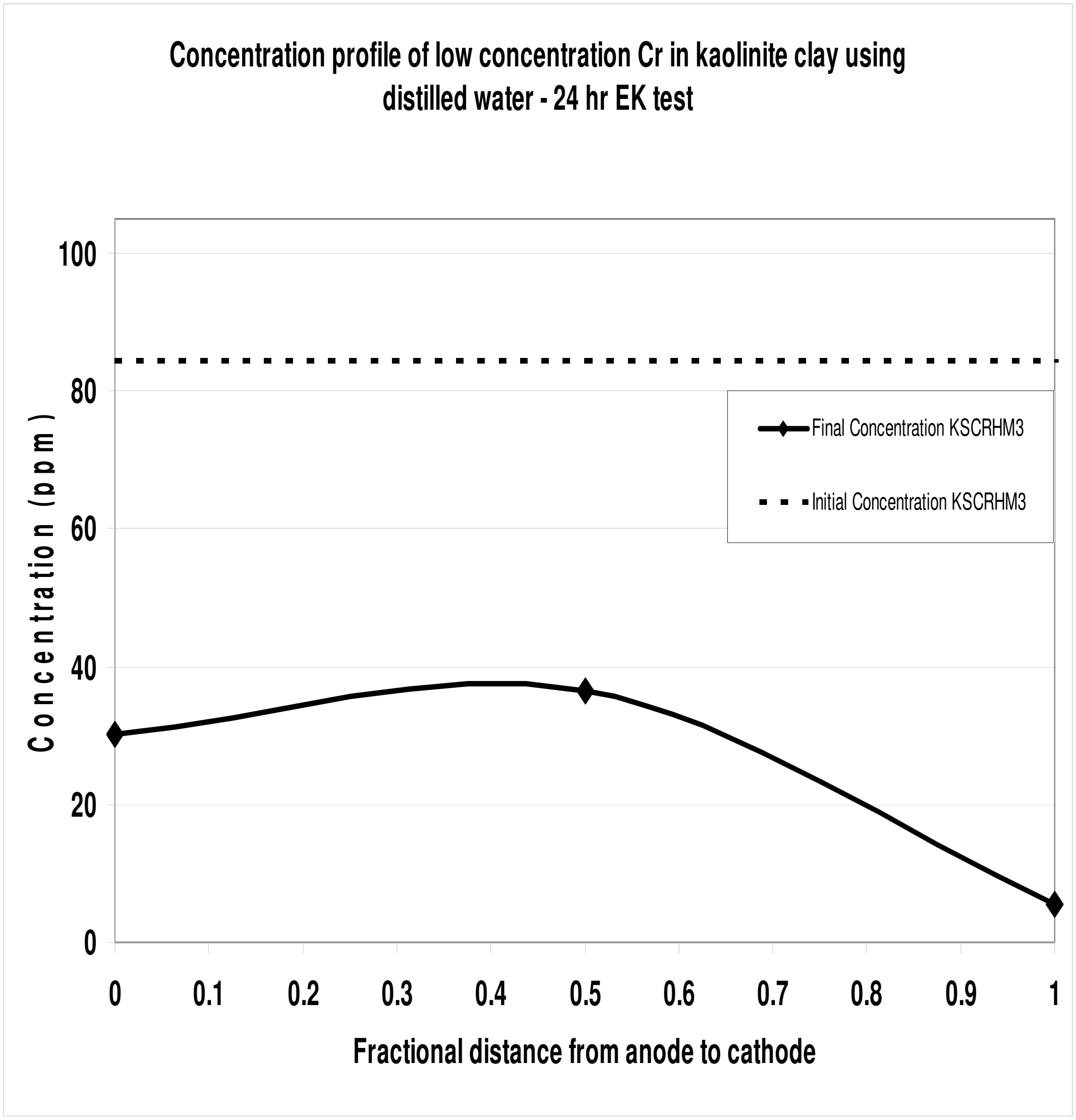

Figure 4-7-L-c: Results of EK test for electroremediation of chromium using distilled water (Pamukcu et al., 1993).

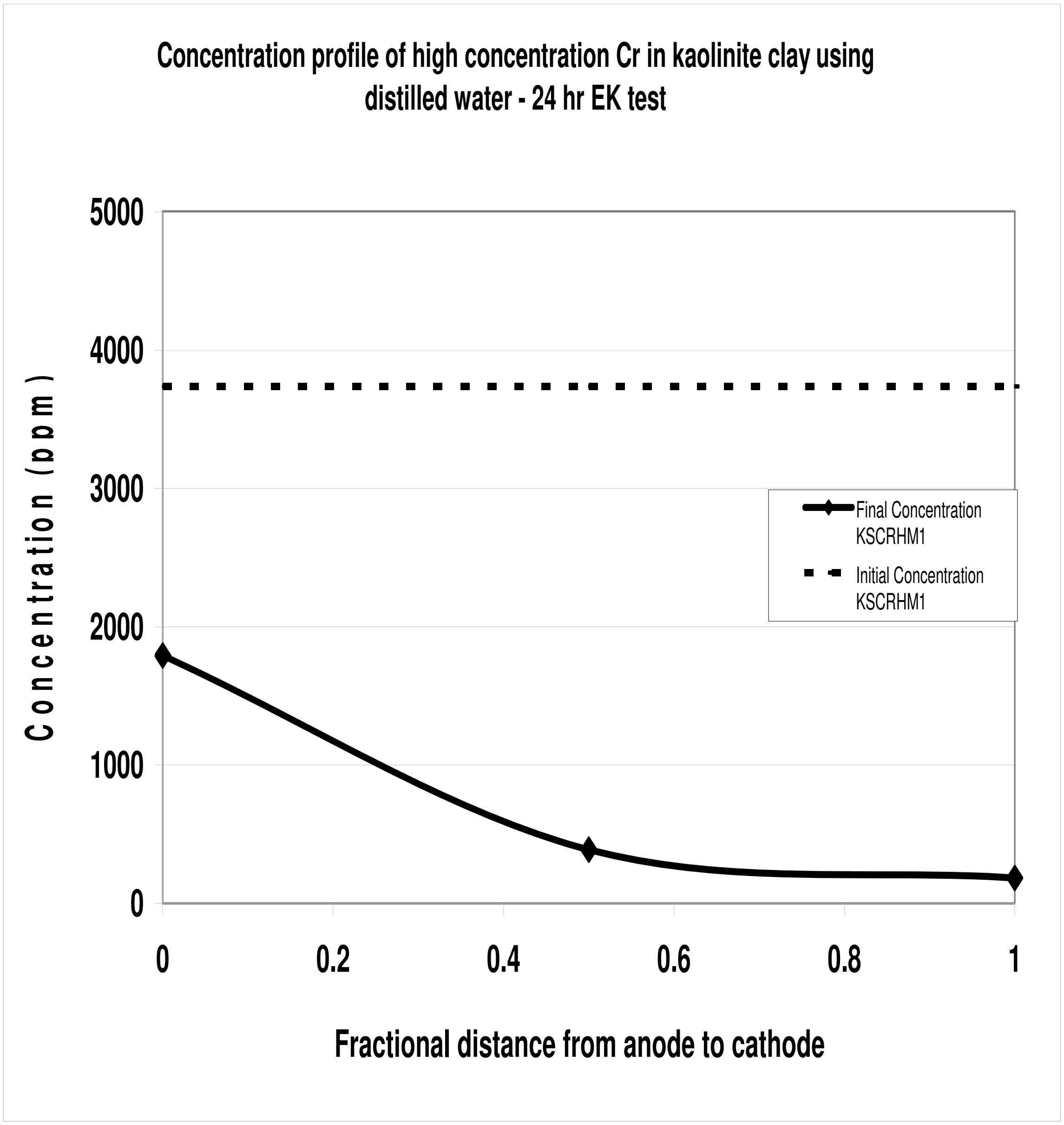

Figure 4-7-H-a: Results of EK test for electroremediation of chromium using distilled water.

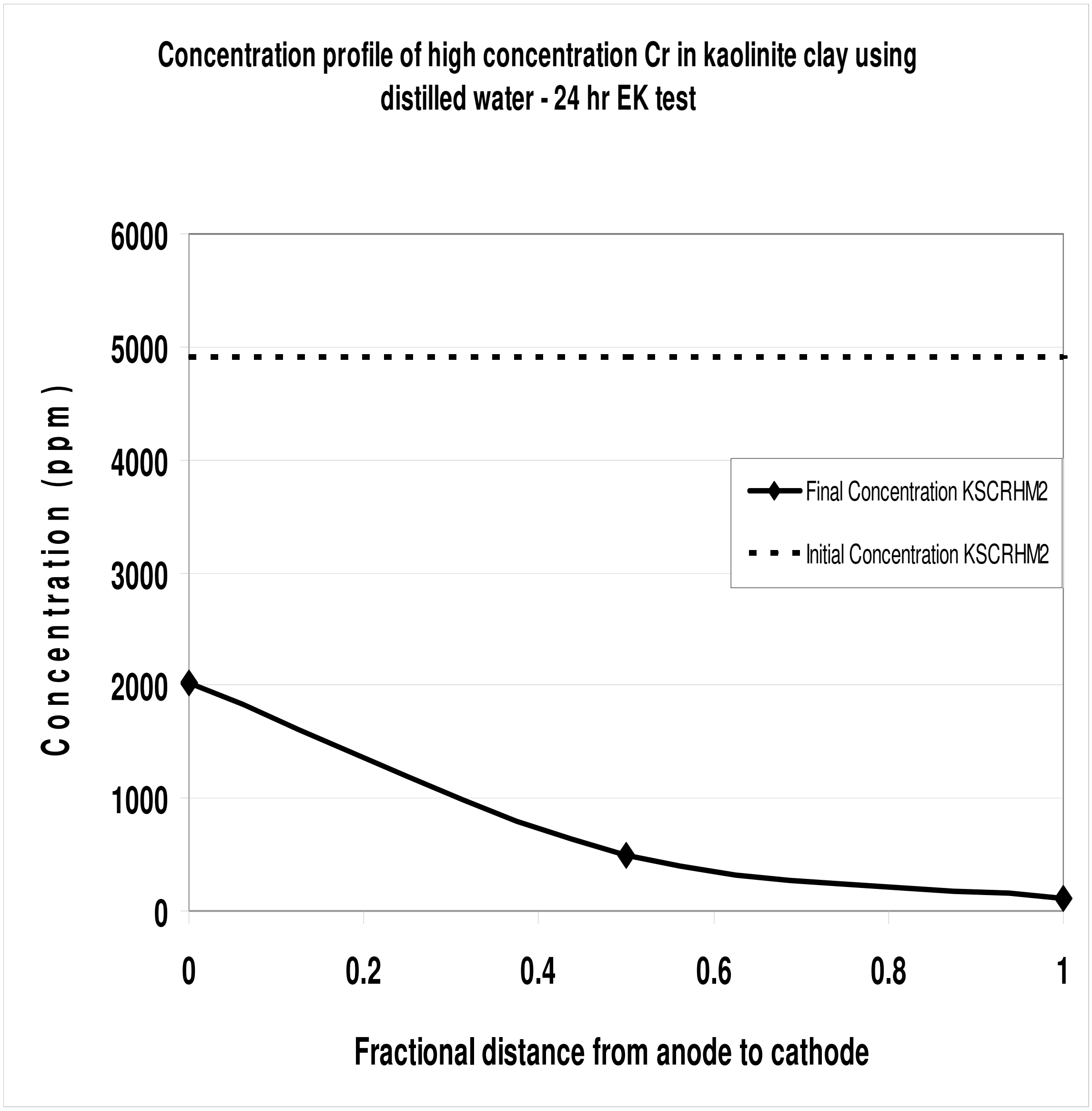

Figure 4-7-H-b: Results of EK test for electroremediation of chromium using distilled water.

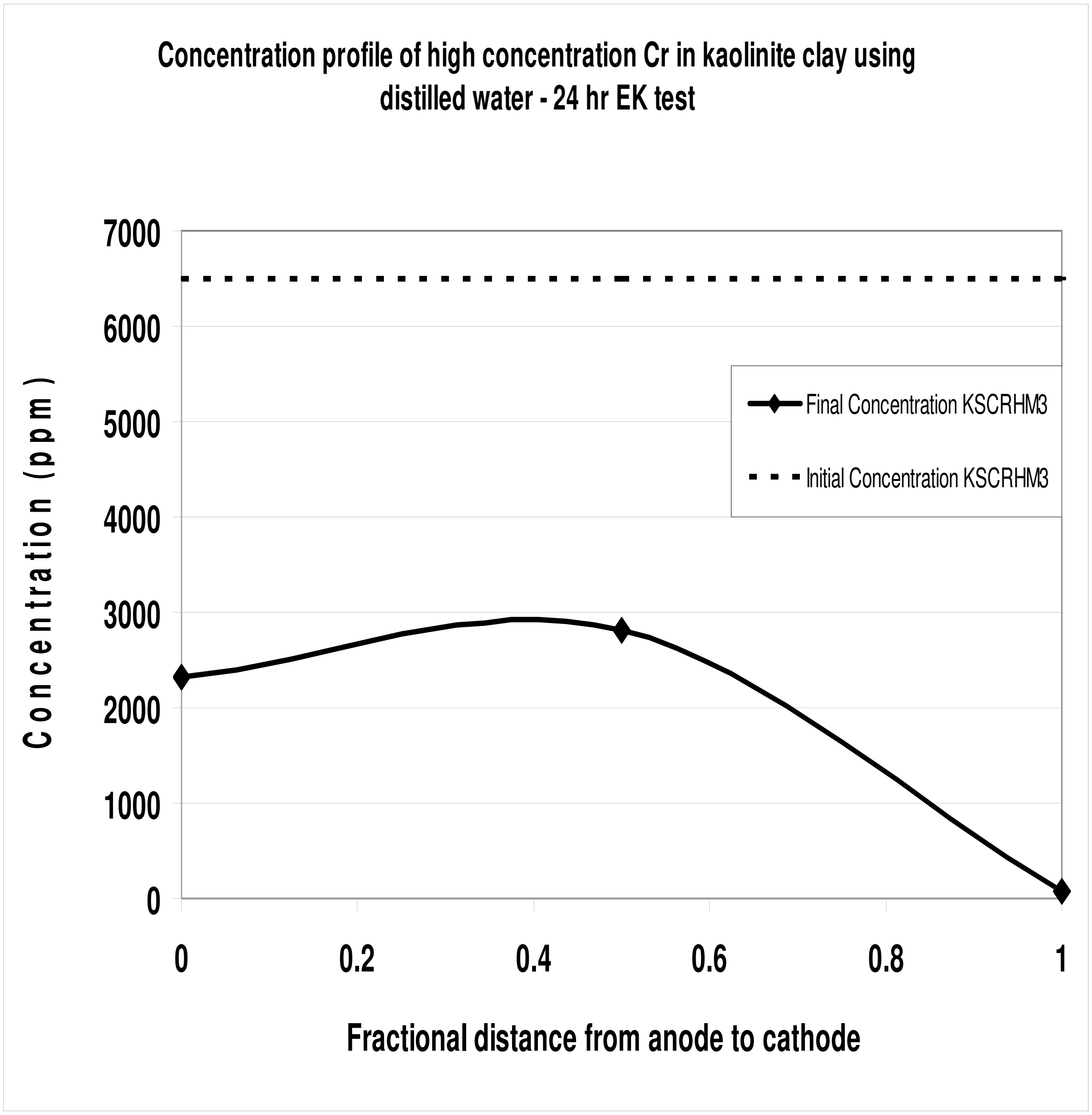

Figure 4-7-H-c: Results of EK test for electroremediation of chromium using distilled water.

Ground water:

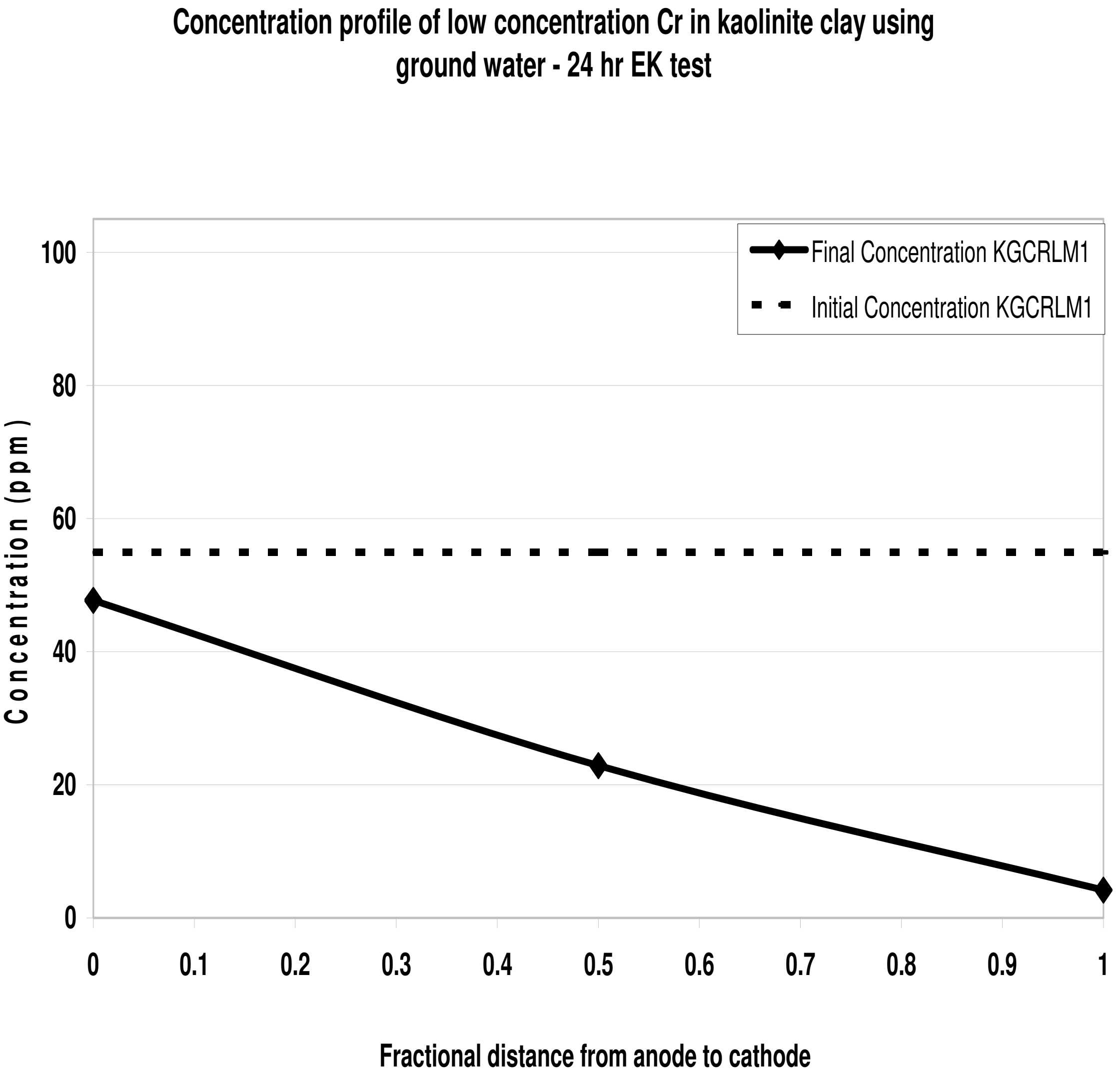

Figure 4-8-L-a: Results of EK test for electroremediation of chromium using ground water (Pamukcu et al., 1993). (See Table 4-1 for composition)

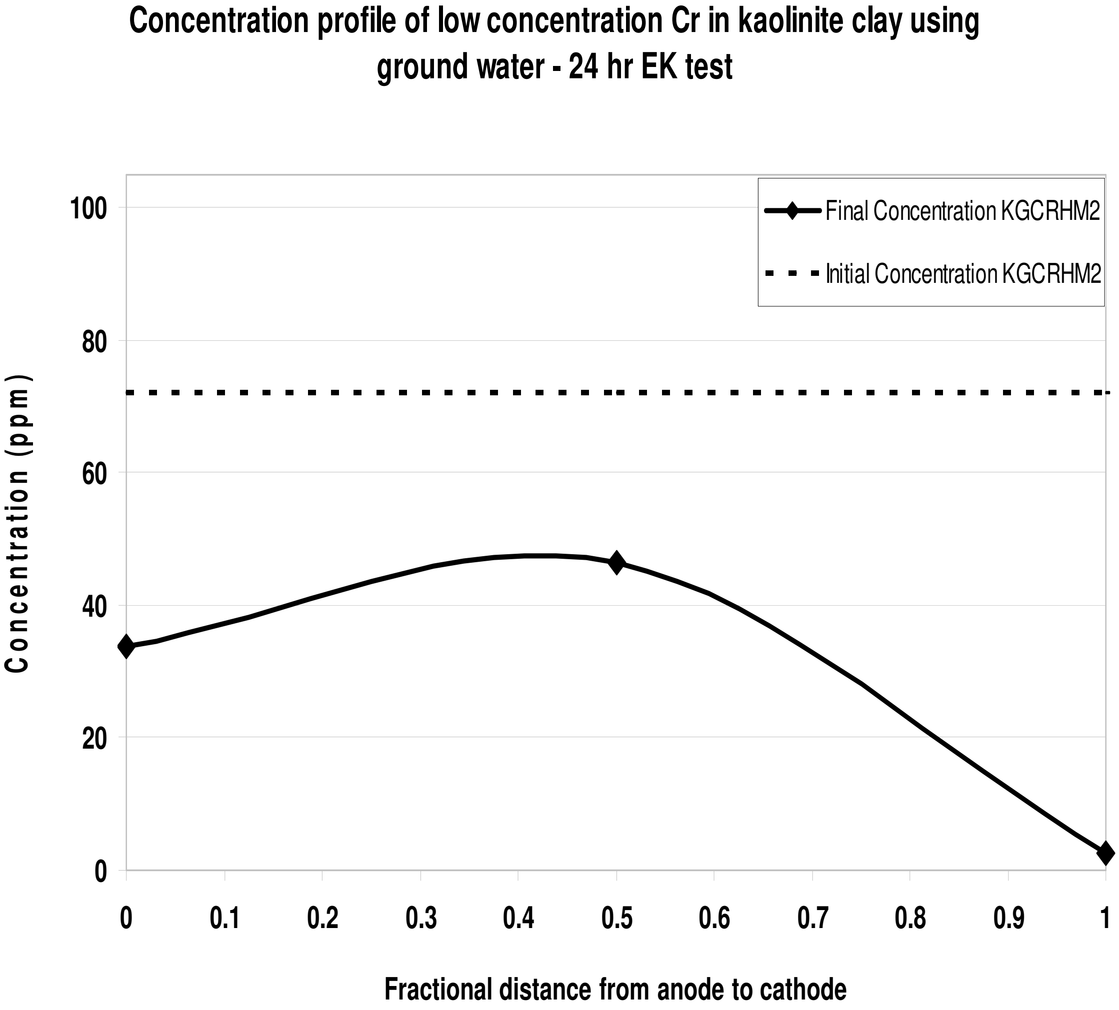

Figure 4-8-L-b: Results of EK test for electroremediation of chromium using ground water (Pamukcu et al., 1993). (See Table 4-1 for composition)

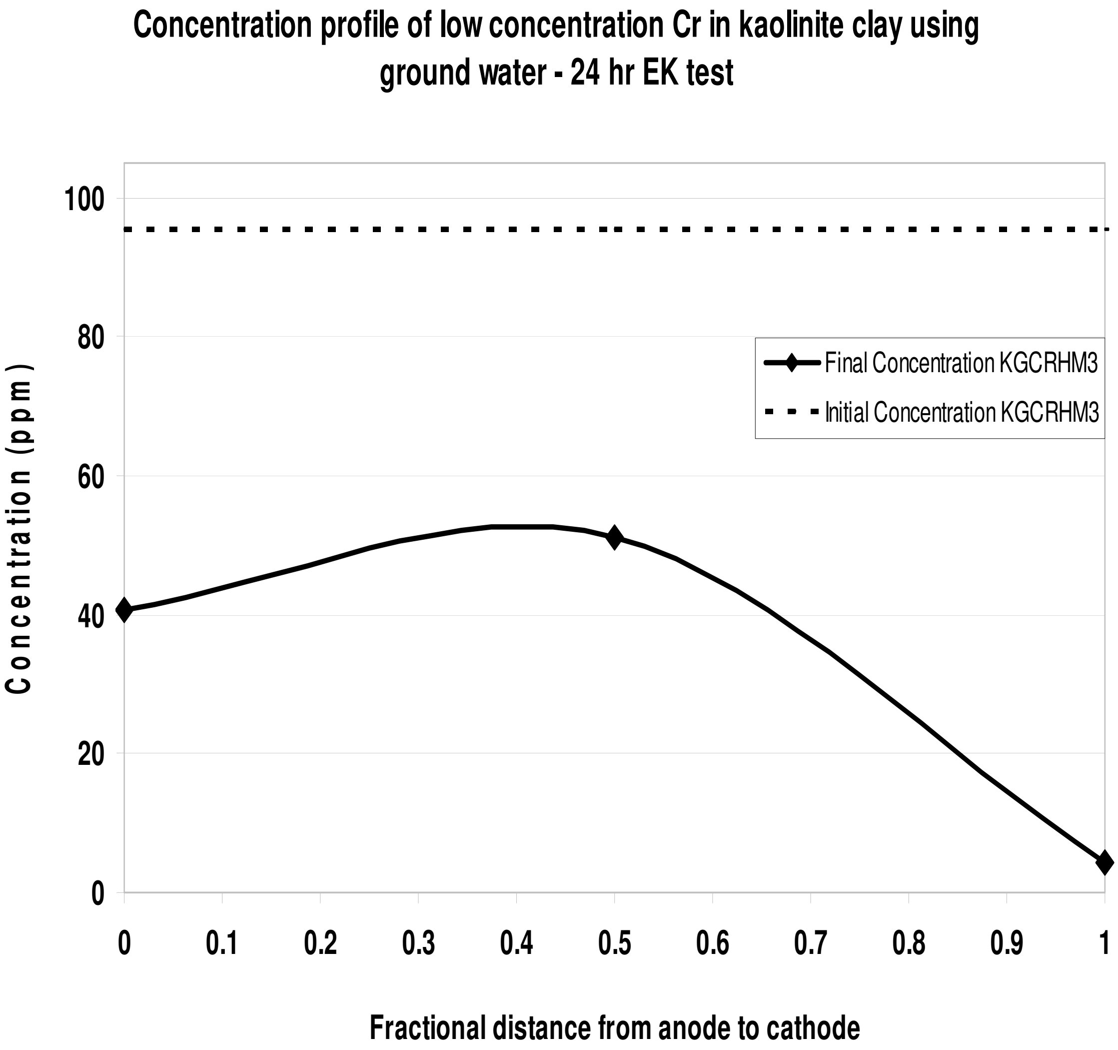

Figure 4-8-L-c: Results of EK test for electroremediation of chromium using ground water (Pamukcu et al., 1993). (See Table 4-1 for composition)

Water with humic substances (900ppm):

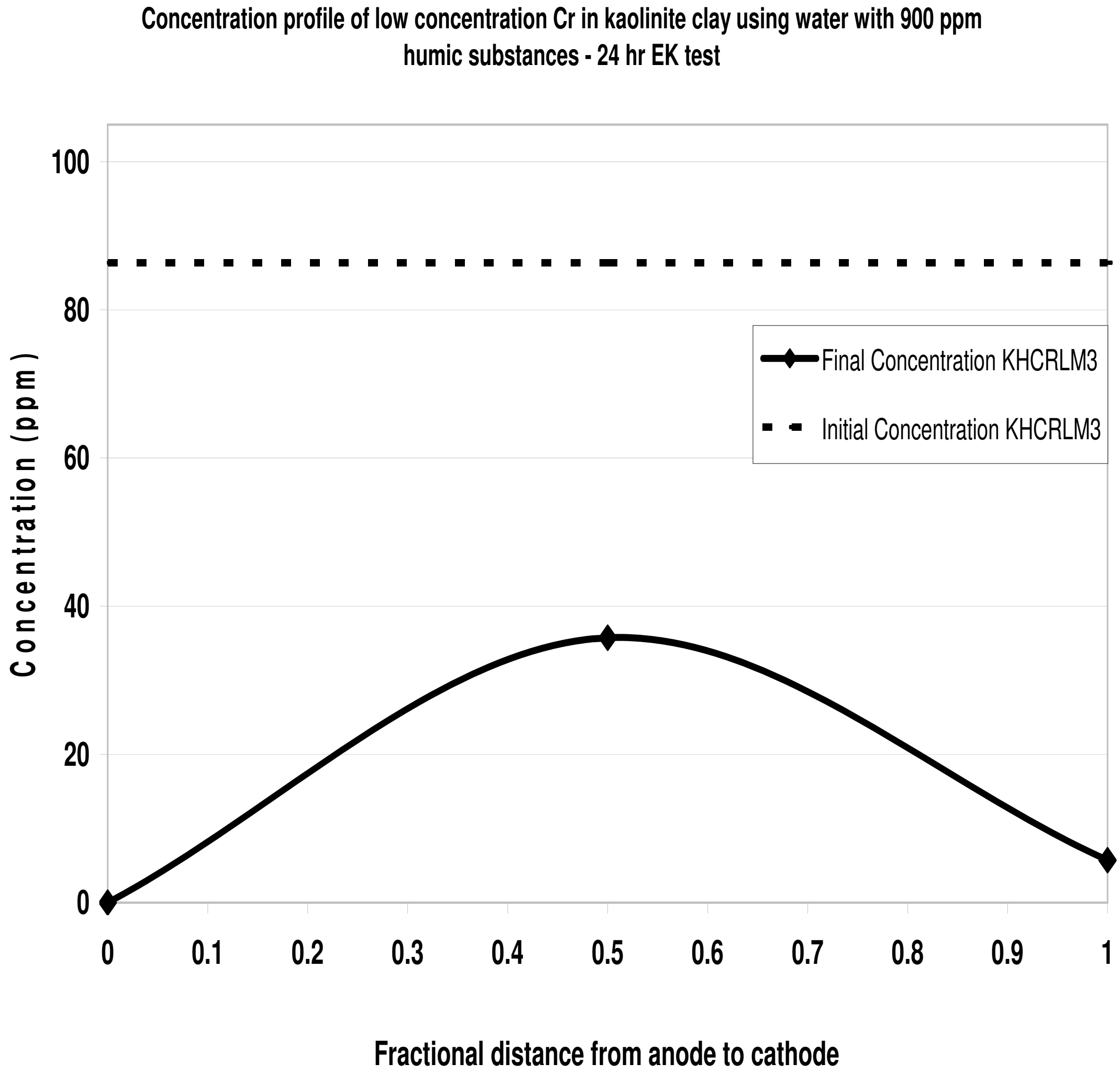

Figure 4-9-L: Results of EK test for electroremediation of chromium using water with humic substances (900ppm) (Pamukcu et al., 1993).

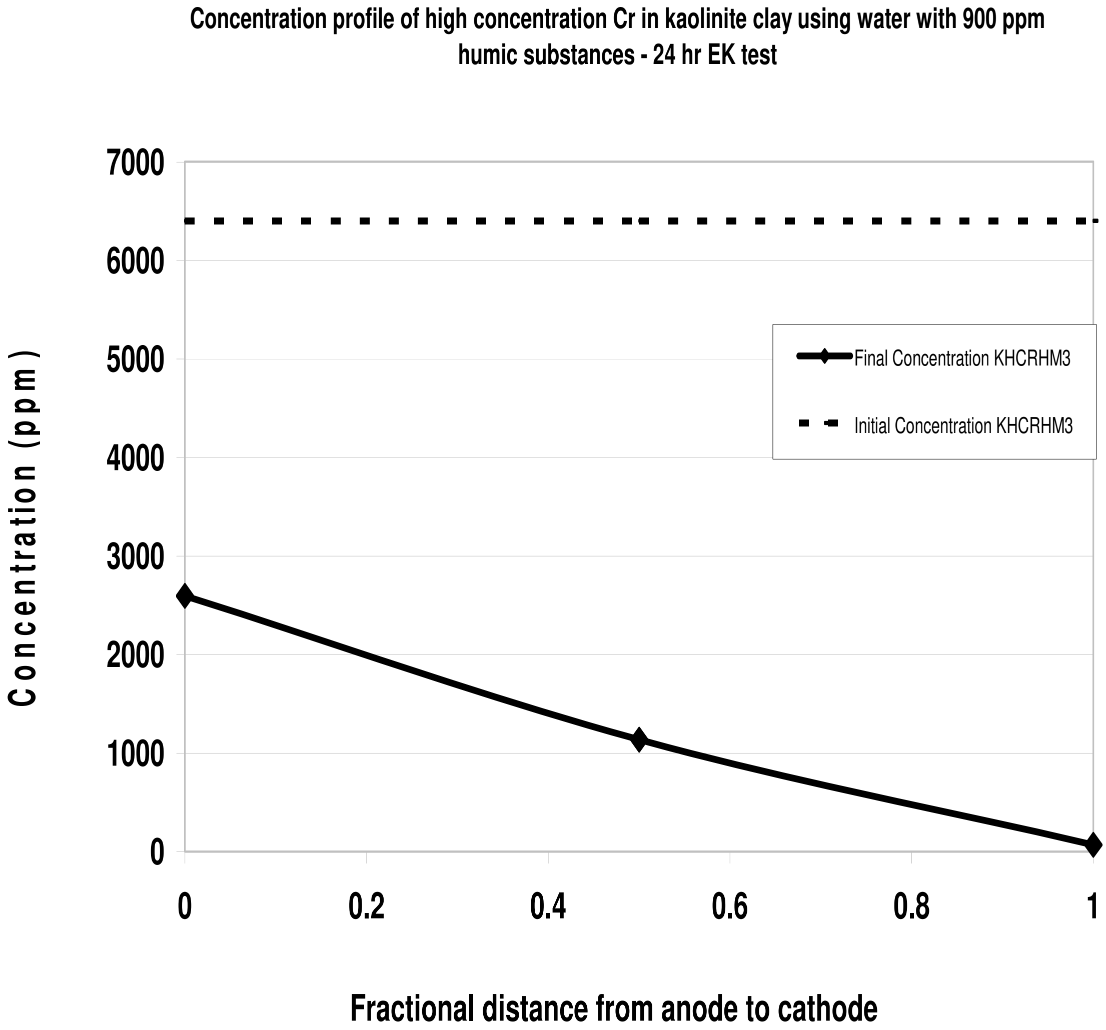

Figure 4-9-H-a: Results of EK test for electroremediation of chromium using water with humic substances (900ppm).

(iv) Lead: Results are shown in Figure 4-10 – 4-12. Lead is one of the preferentially adsorbed metals by clay minerals (Basta and Tabatabal, 1992). It is mostly in the form of a divalent cation below pH of 9. Above pH 9, the Pbo is the stable species (Dragun, 1988). At sufficiently high pH (>11) it forms an anionic species of hydrolysis product, $Pb(OH)_6^{-2}$, which is expected to migrate in the opposite direction of electrokinetic flow. Other hydrolysis products of lead which occur at pH levels greater than 6 are: $Pb_2(OH)_4^{+3}$, $Pb_4(OH)_4^{+4}$, $Pb_6(OH)_8^{+4}$. These species would exhibit increased ionic velocities due to their higher valances. The effect of high pH on the clay adsorption of metal becomes more significant at high concentrations of the metal, as shown in Fig. 4-10. This accumulation is attributed to: (i) precipitation and anion species formation, (ii) increased concentration of lead at the discharge end (cathode region of soil), (iii) increased adsorption and retention of lead on clay due to high pH and increased concentration at the cathode region of the soil (Pamukcu et al., 1993).

Distilled water:

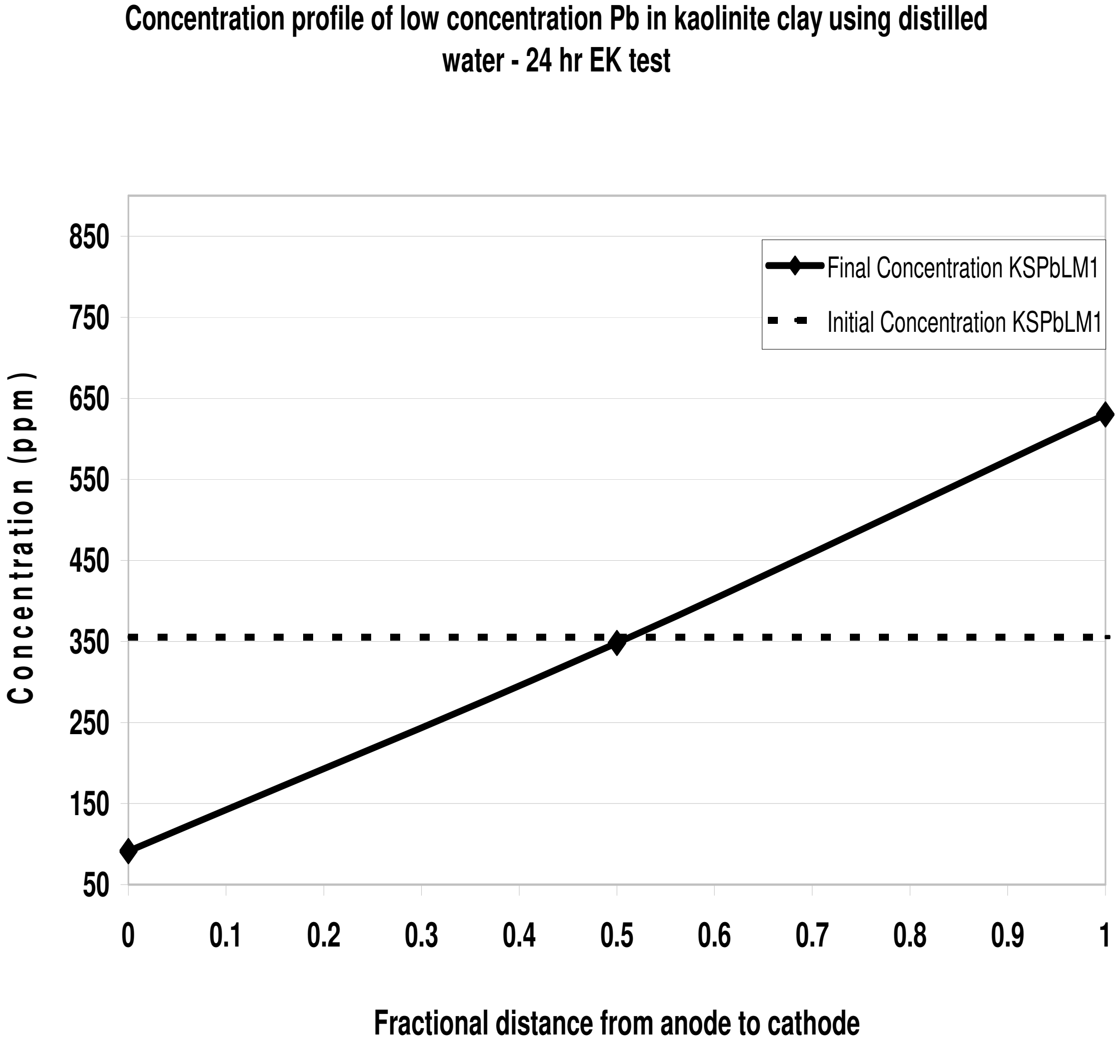

Figure 4-10-L-a: Results of EK test for electroremediation of lead using distilled water (Pamukcu et al., 1993).

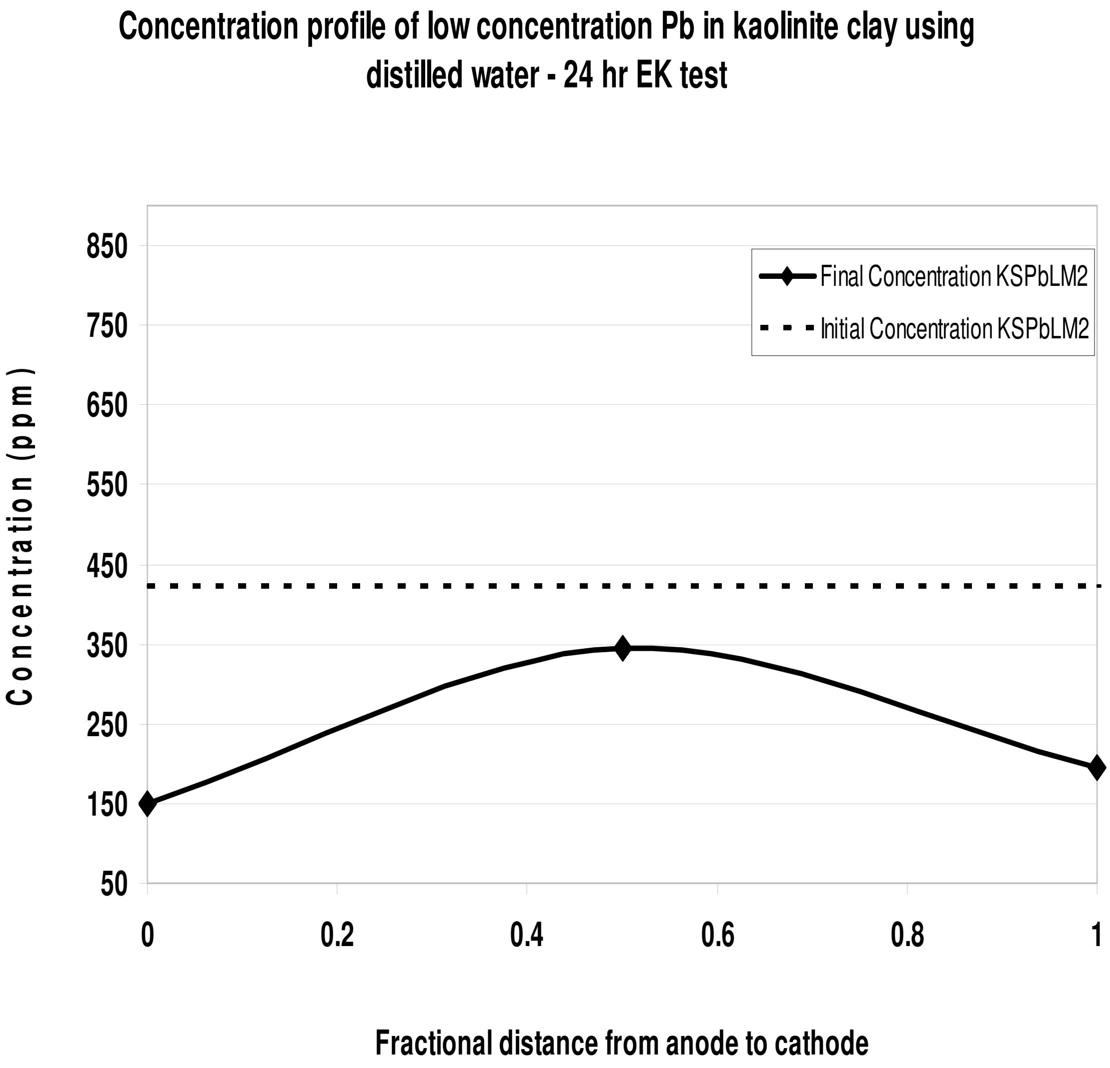

Figure 4-10-L-b: Results of EK test for electroremediation of lead using distilled water (Pamukcu et al., 1993).

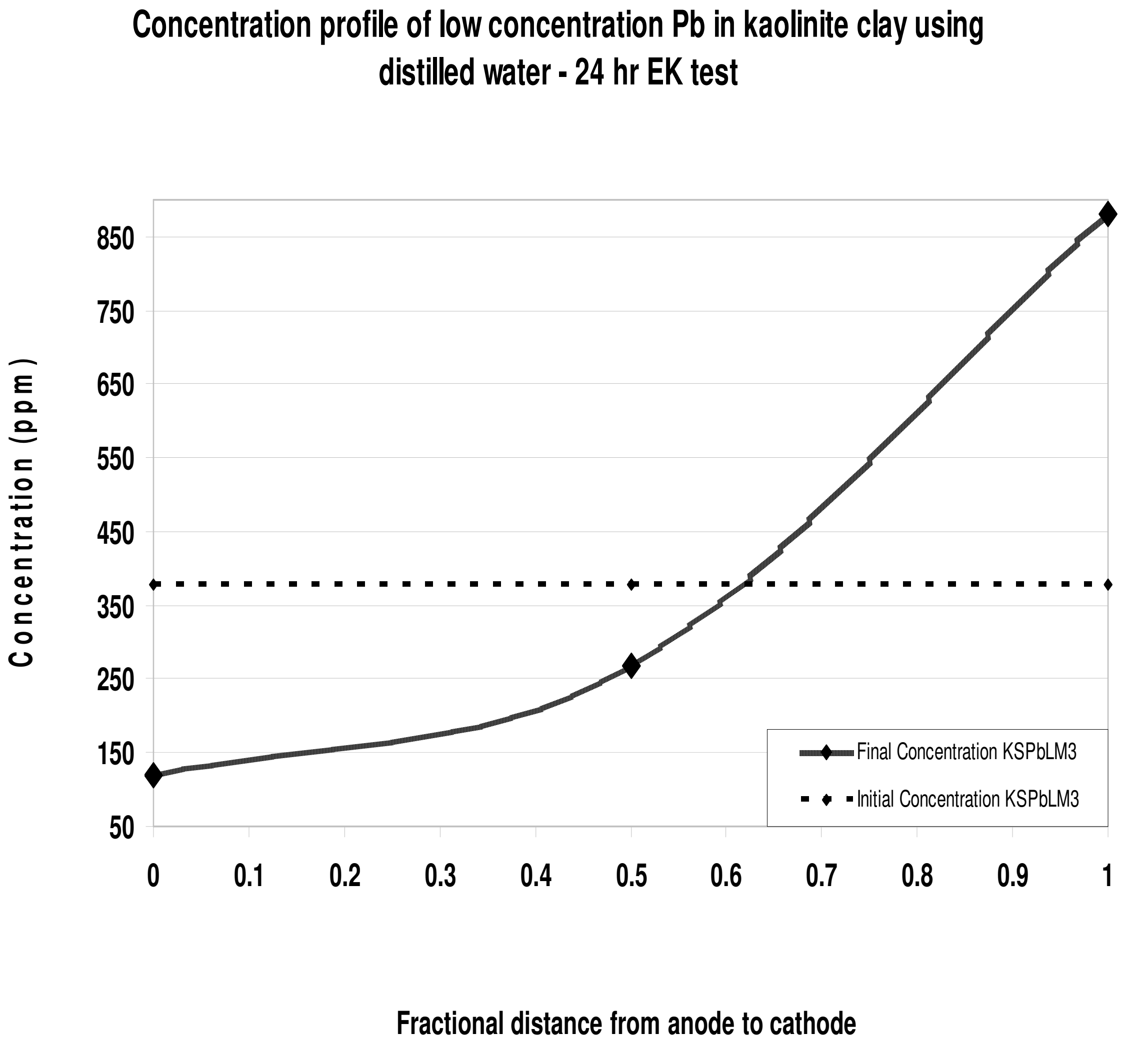

Figure 4-10-L-c: Results of EK test for electroremediation of lead using distilled water (Pamukcu et al., 1993).

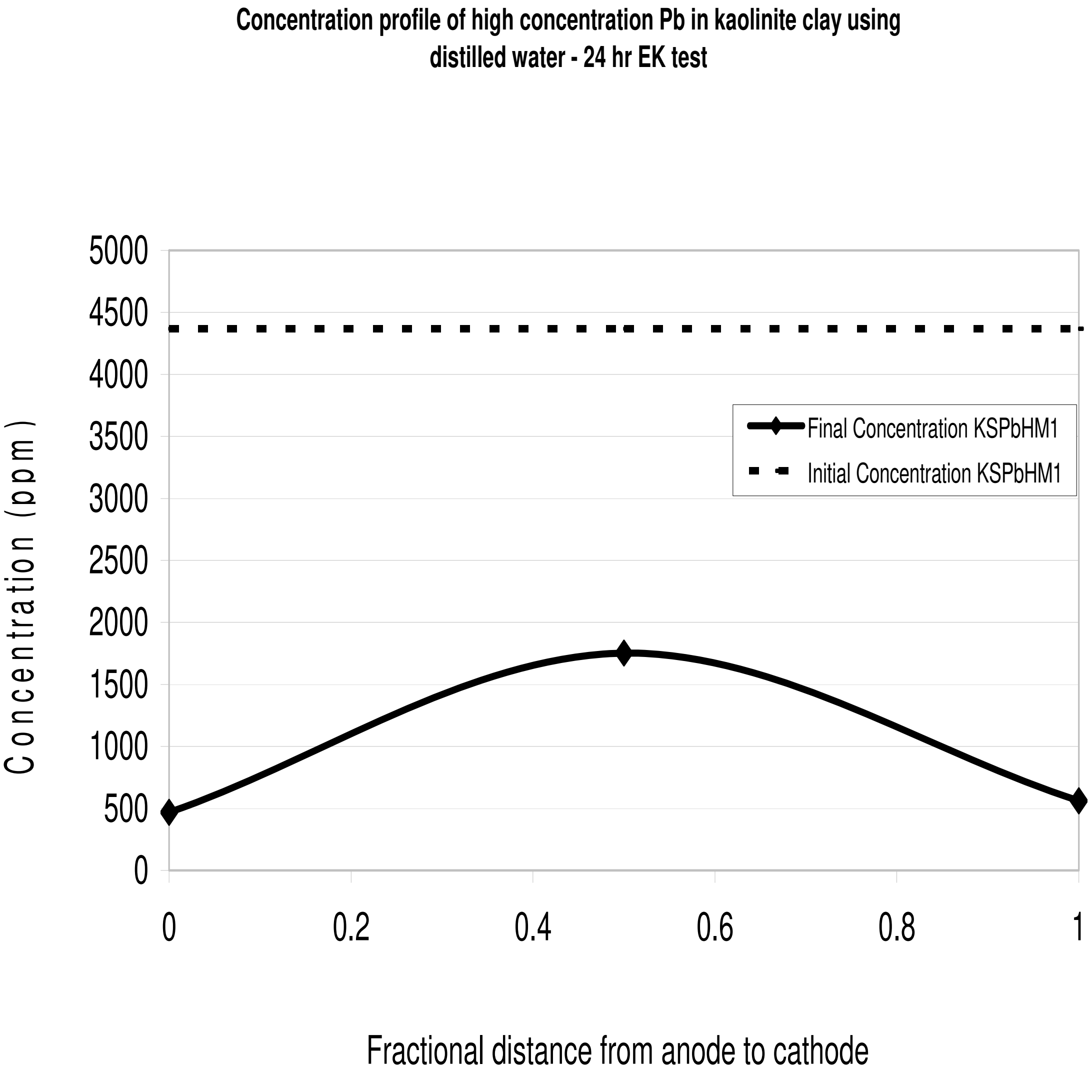

Figure 4-10-H-a: Results of EK test for electroremediation of lead using distilled water.

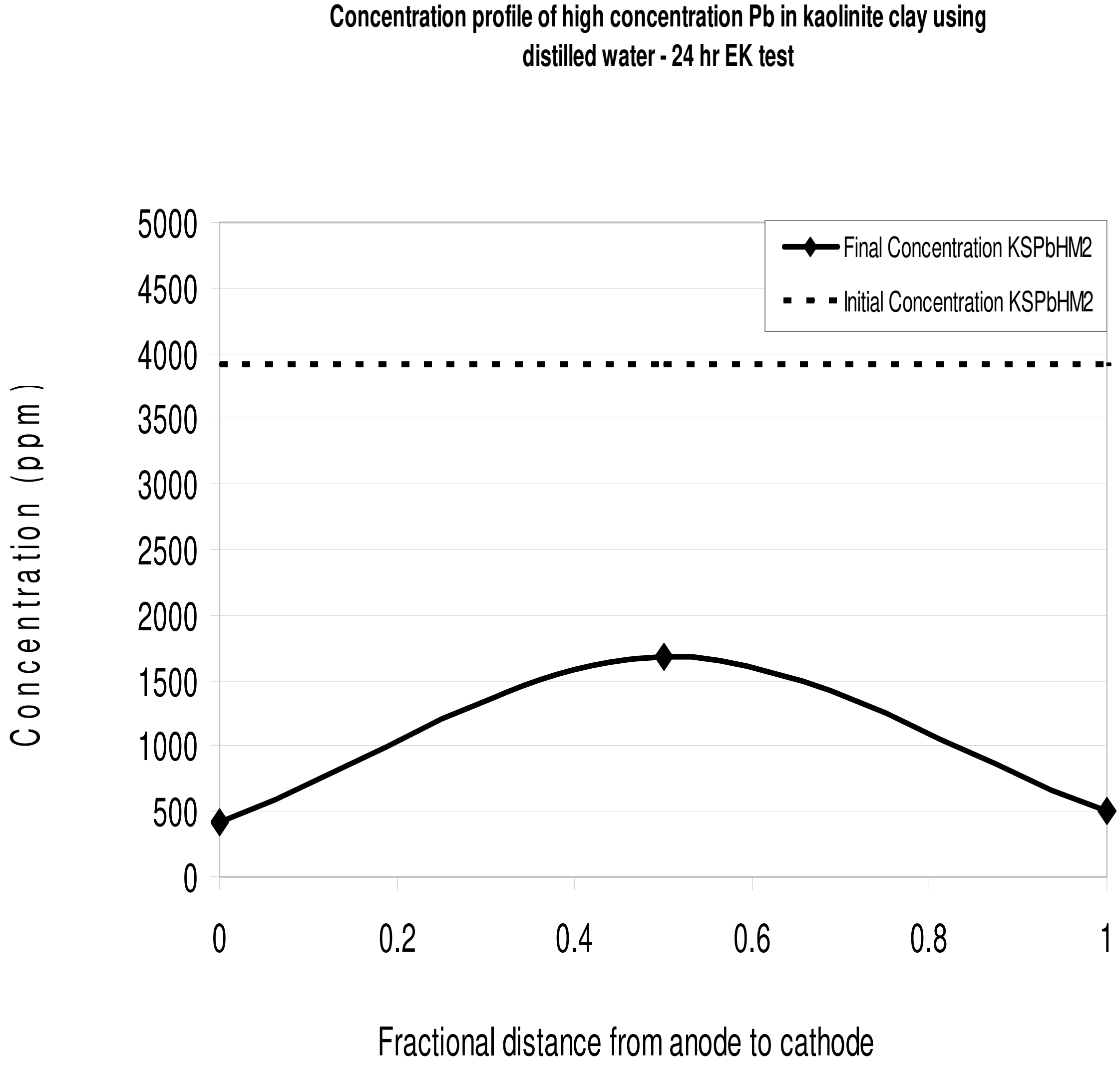

Figure 4-10-H-b: Results of EK test for electroremediation of lead using distilled water.

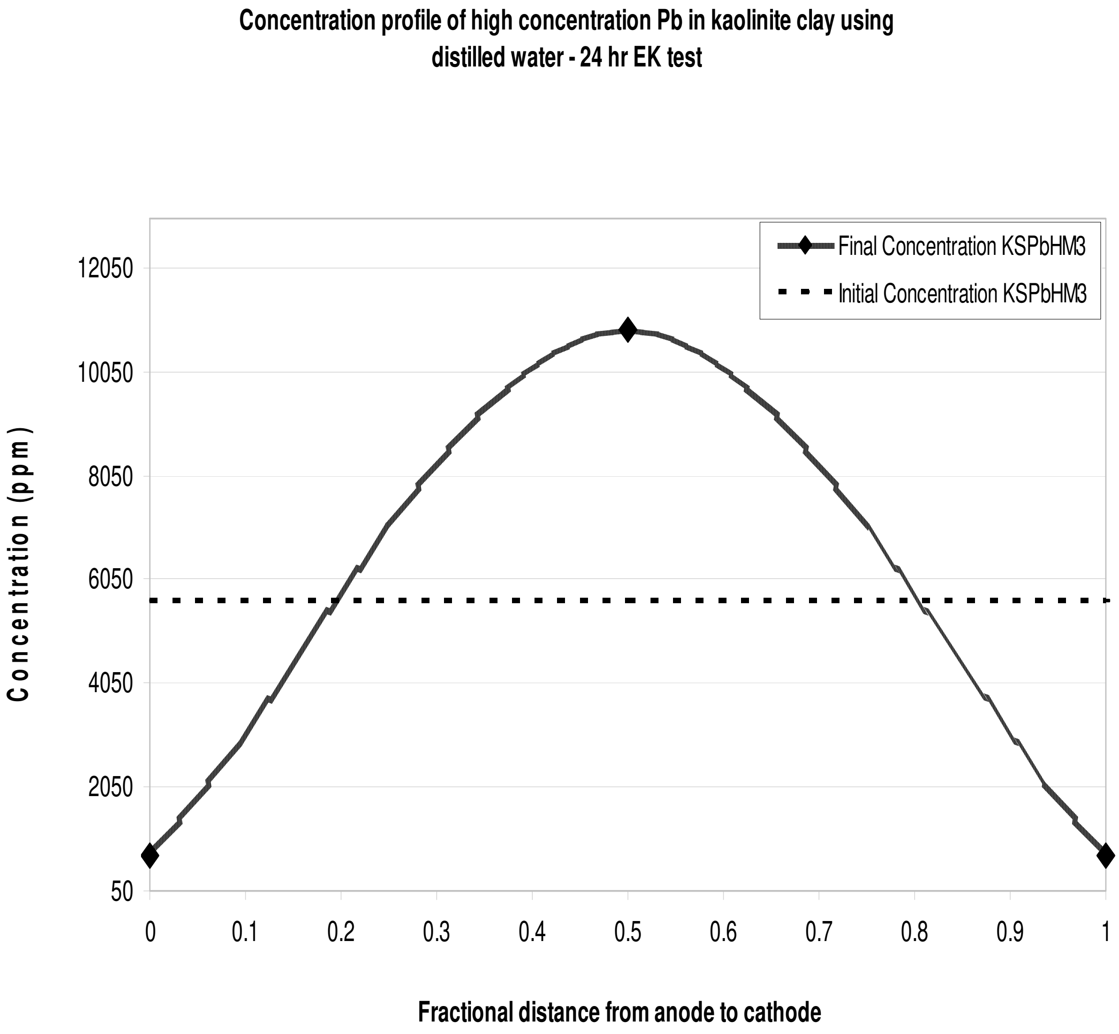

Figure 4-10-H-c: Results of EK test for electroremediation of lead using distilled water.

Ground water:

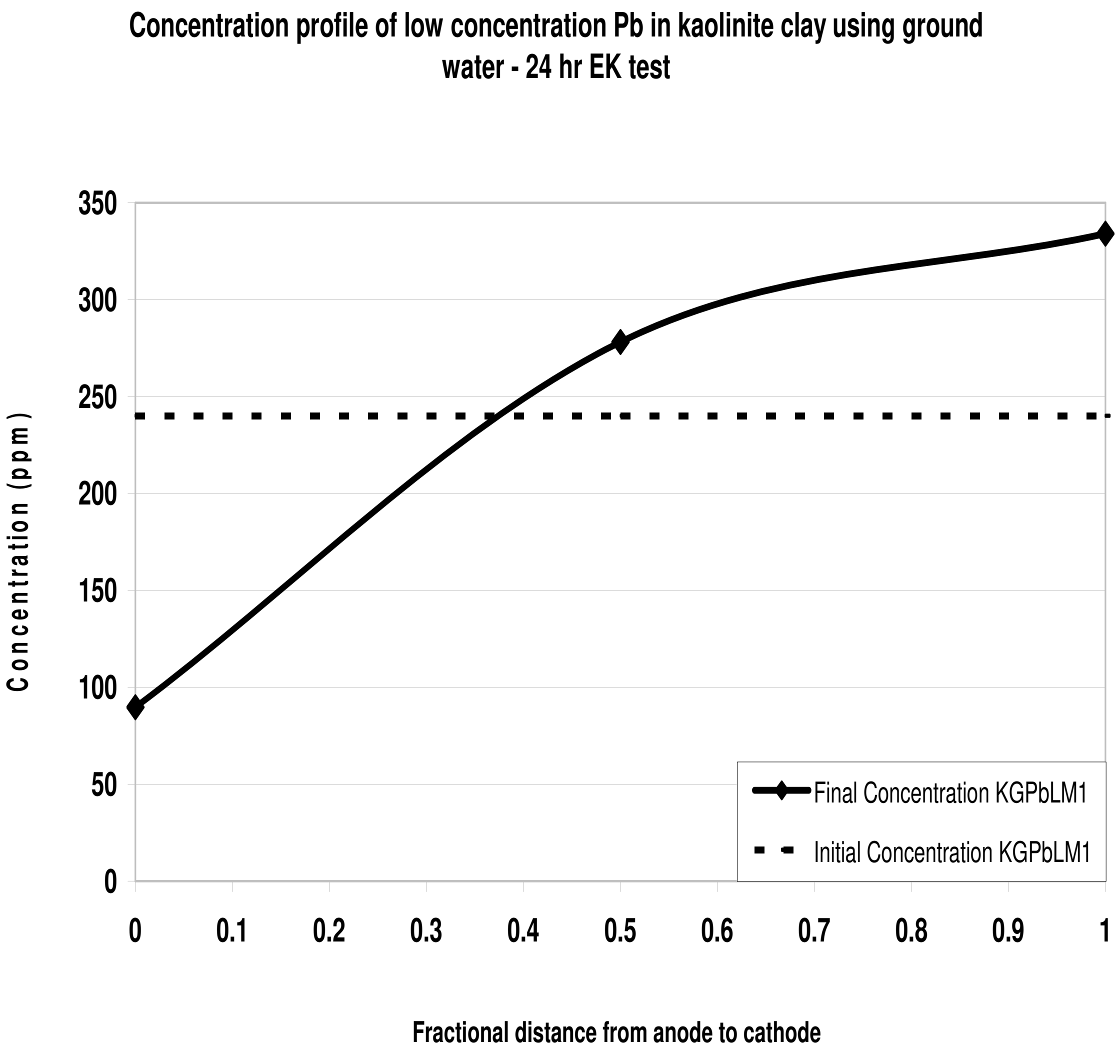

Figure 4-11-L-a: Results of EK test for electroremediation of lead using ground water (Pamukcu et al., 1993). (See Table 4-1 for composition)

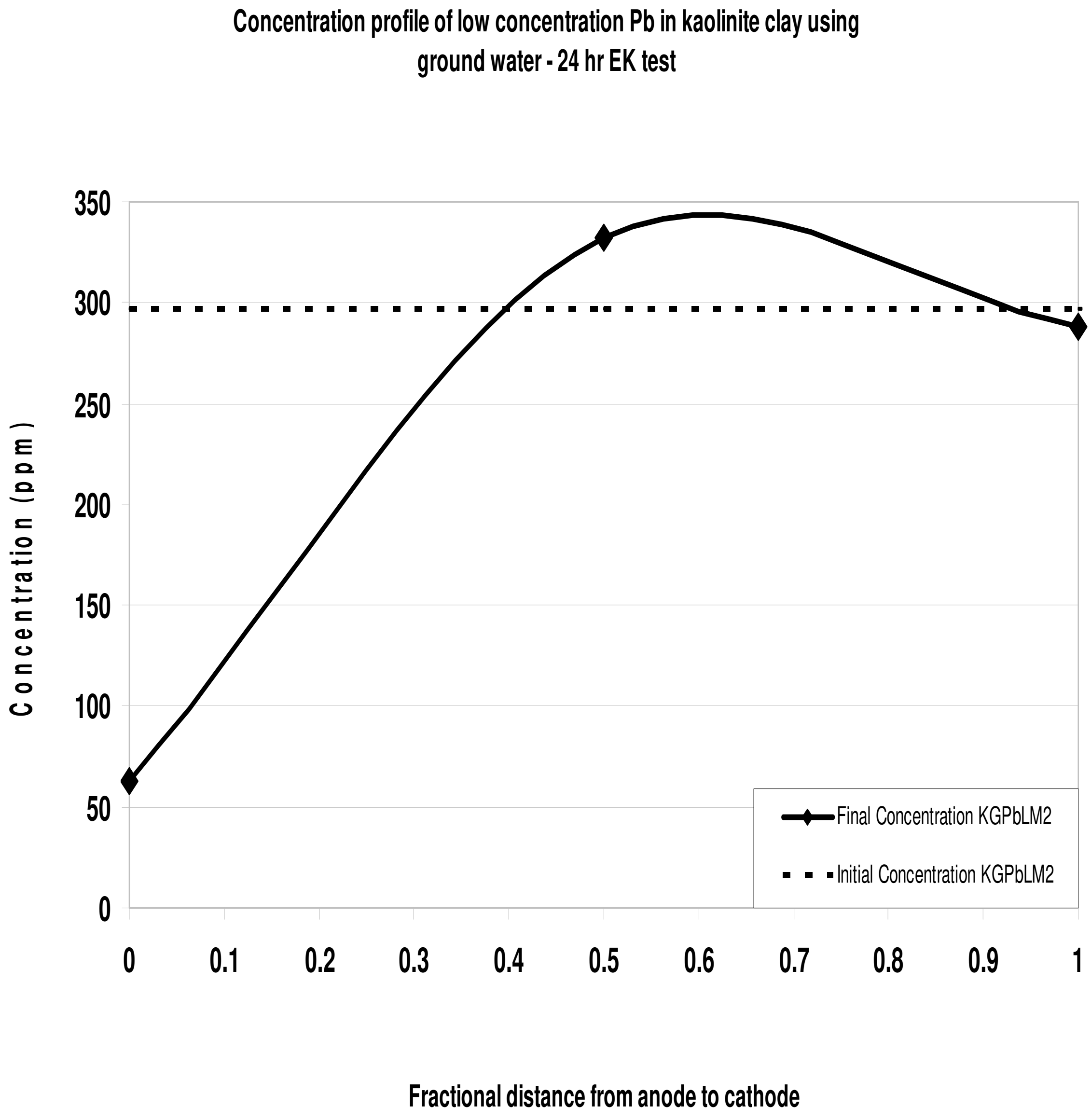

Figure 4-11-L-b: Results of EK test for electroremediation of lead using ground water (Pamukcu et al., 1993). (See Table 4-1 for composition)

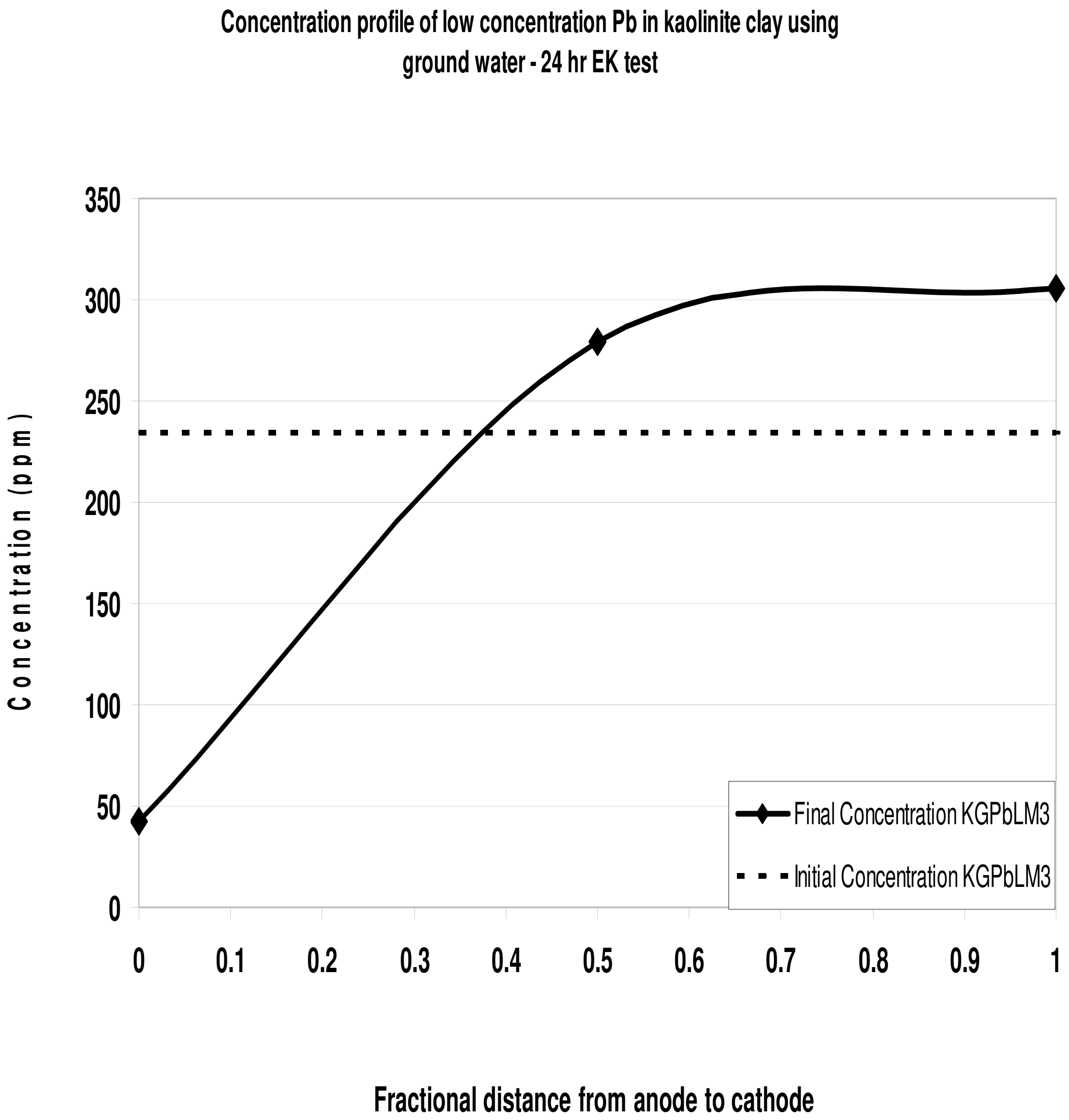

Figure 4-11-L-c: Results of EK test for electroremediation of lead using ground water (Pamukcu et al., 1993). (See Table 4-1 for composition)

<u>Water with humic substances (900ppm):</u>

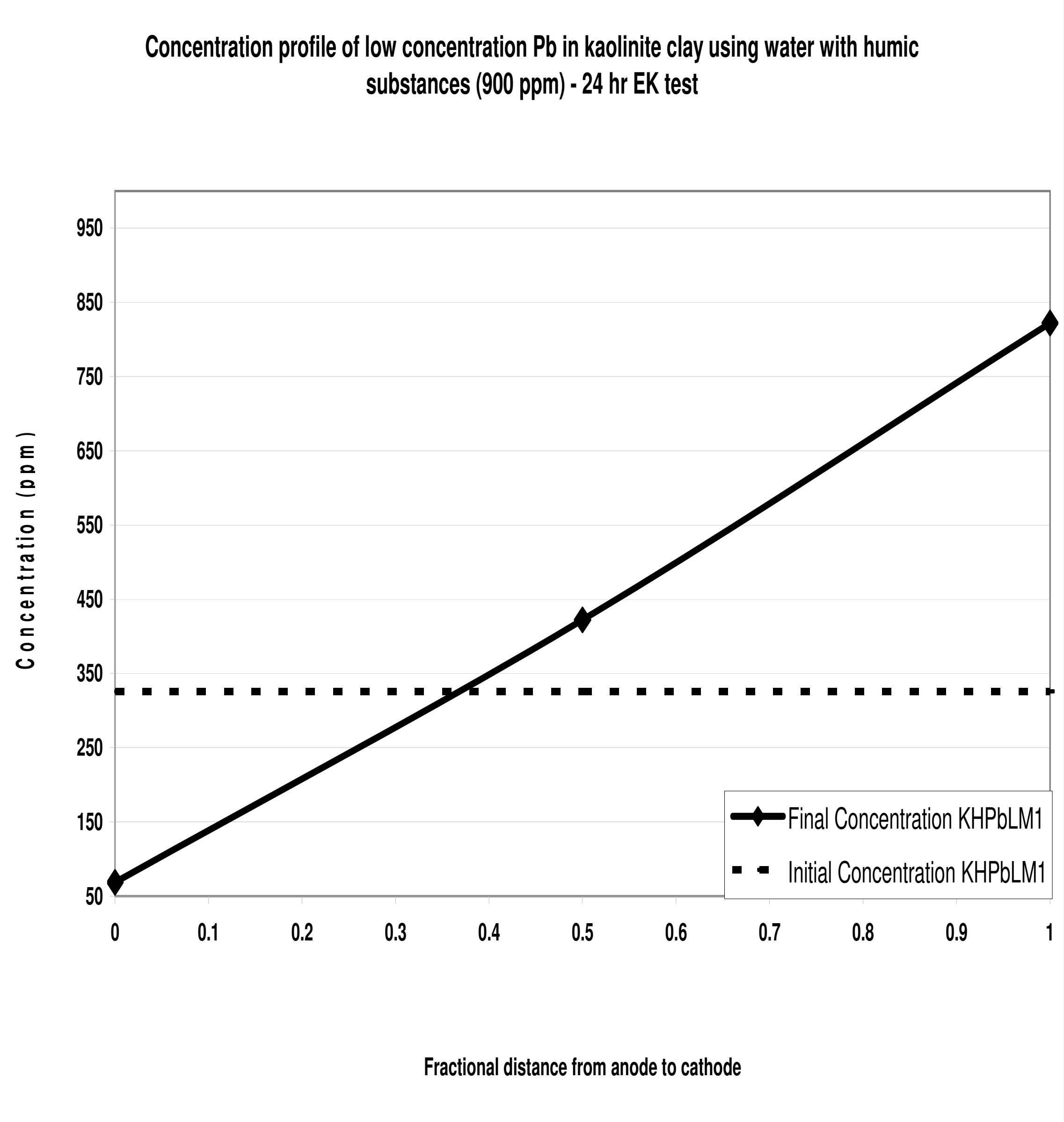

Figure 4-12-L-a: Results of EK test for electroremediation of lead using water with humic substances (900ppm) (Pamukcu et al., 1993).

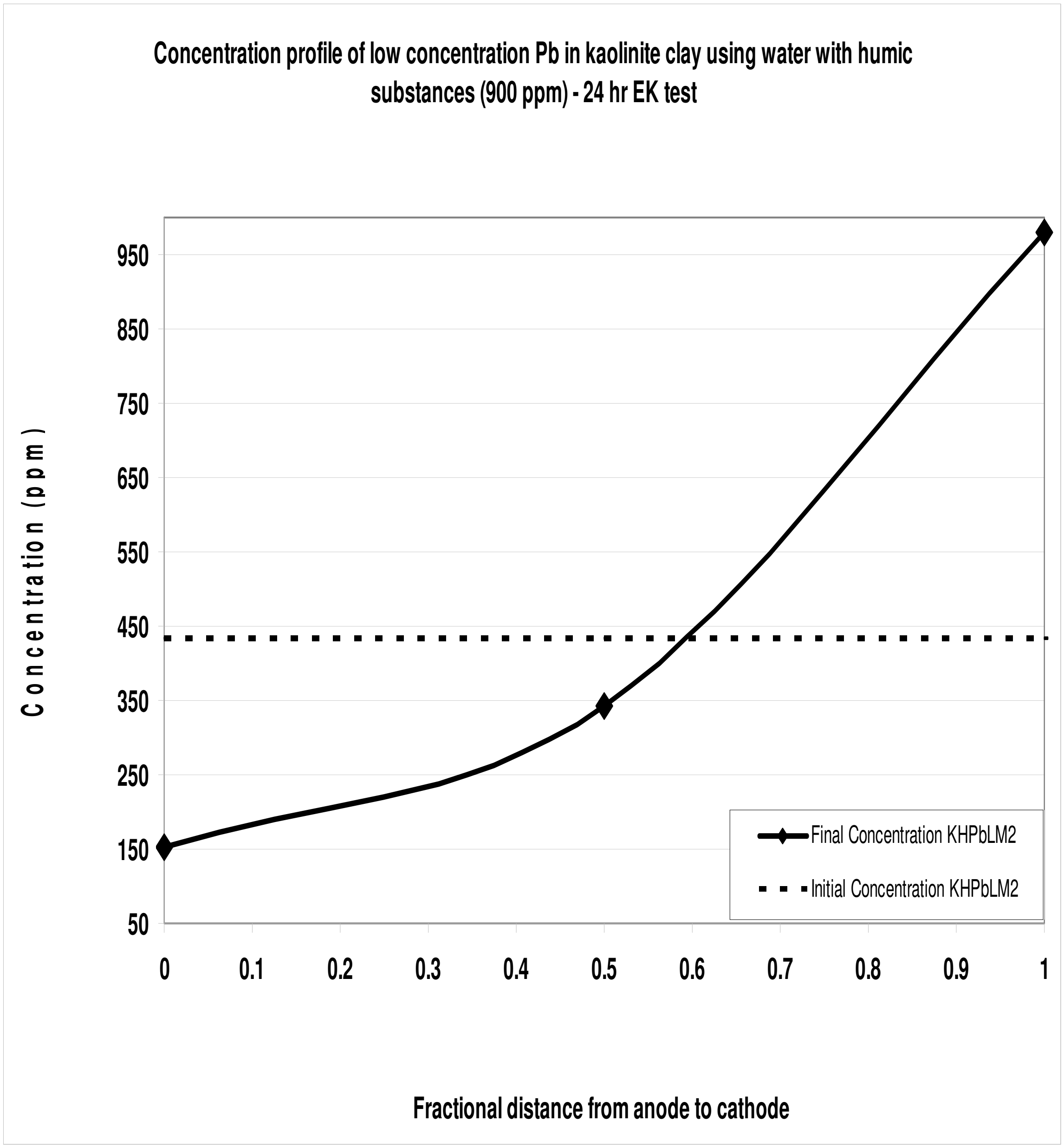

Figure 4-12-L-b: Results of EK test for electroremediation of lead using water with humic substances (900ppm) (Pamukcu et al., 1993).

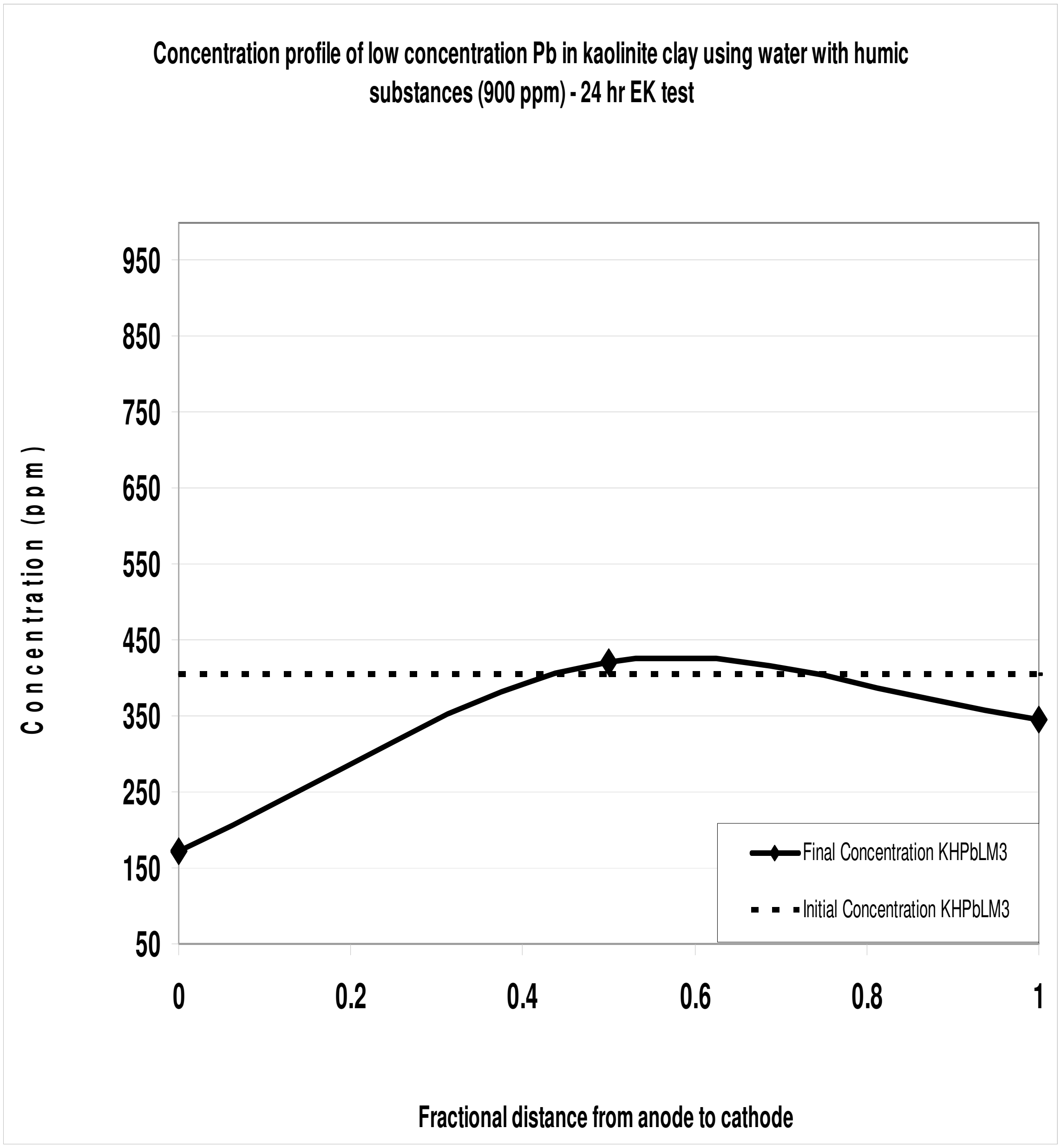

Figure 4-12-L-c: Results of EK test for electroremediation of lead using water with humic substances (900ppm) (Pamukcu et al., 1993).

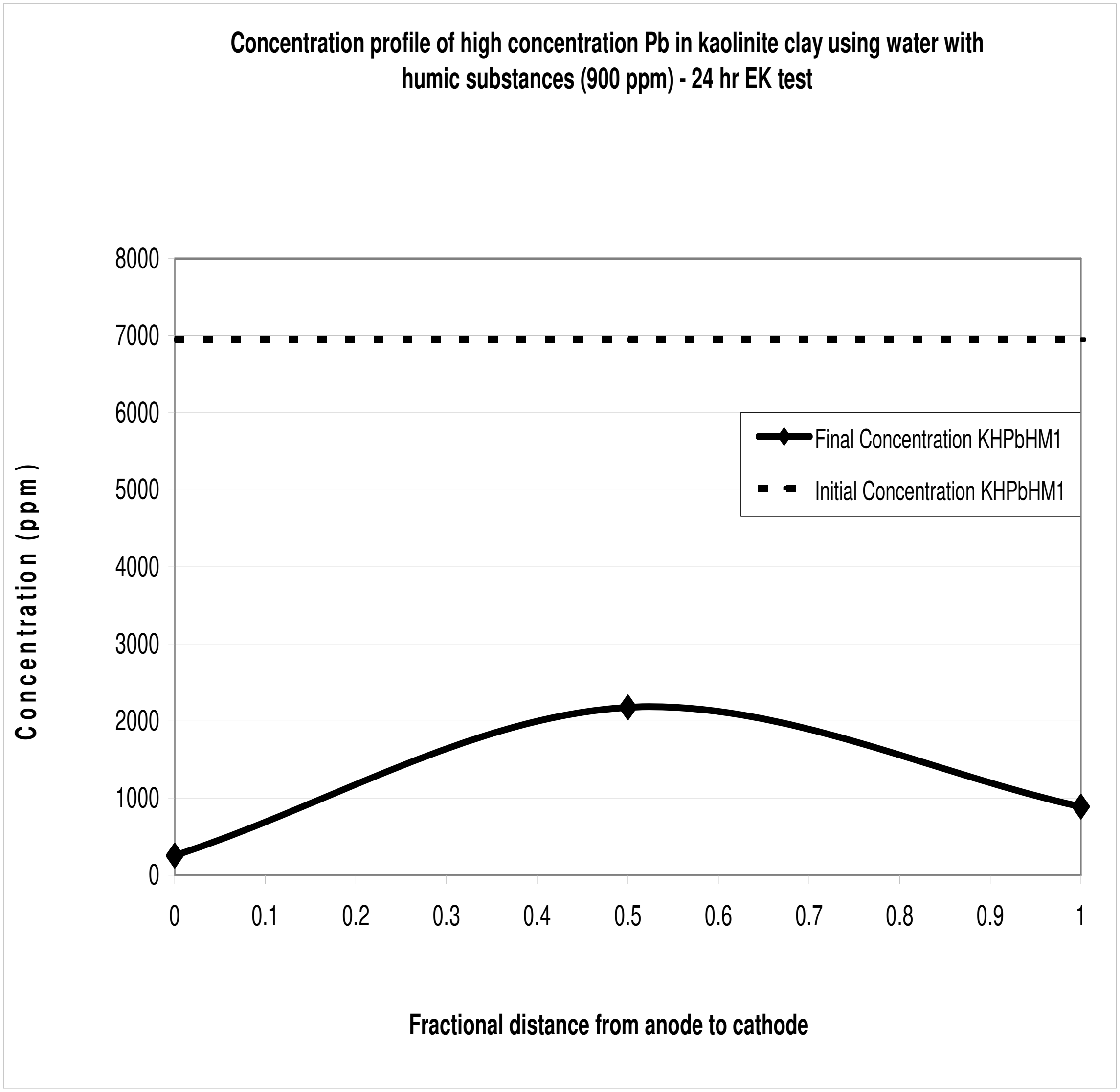

Figure 4-12-H-a: Results of EK test for electroremediation of lead using water with humic substances (900ppm).

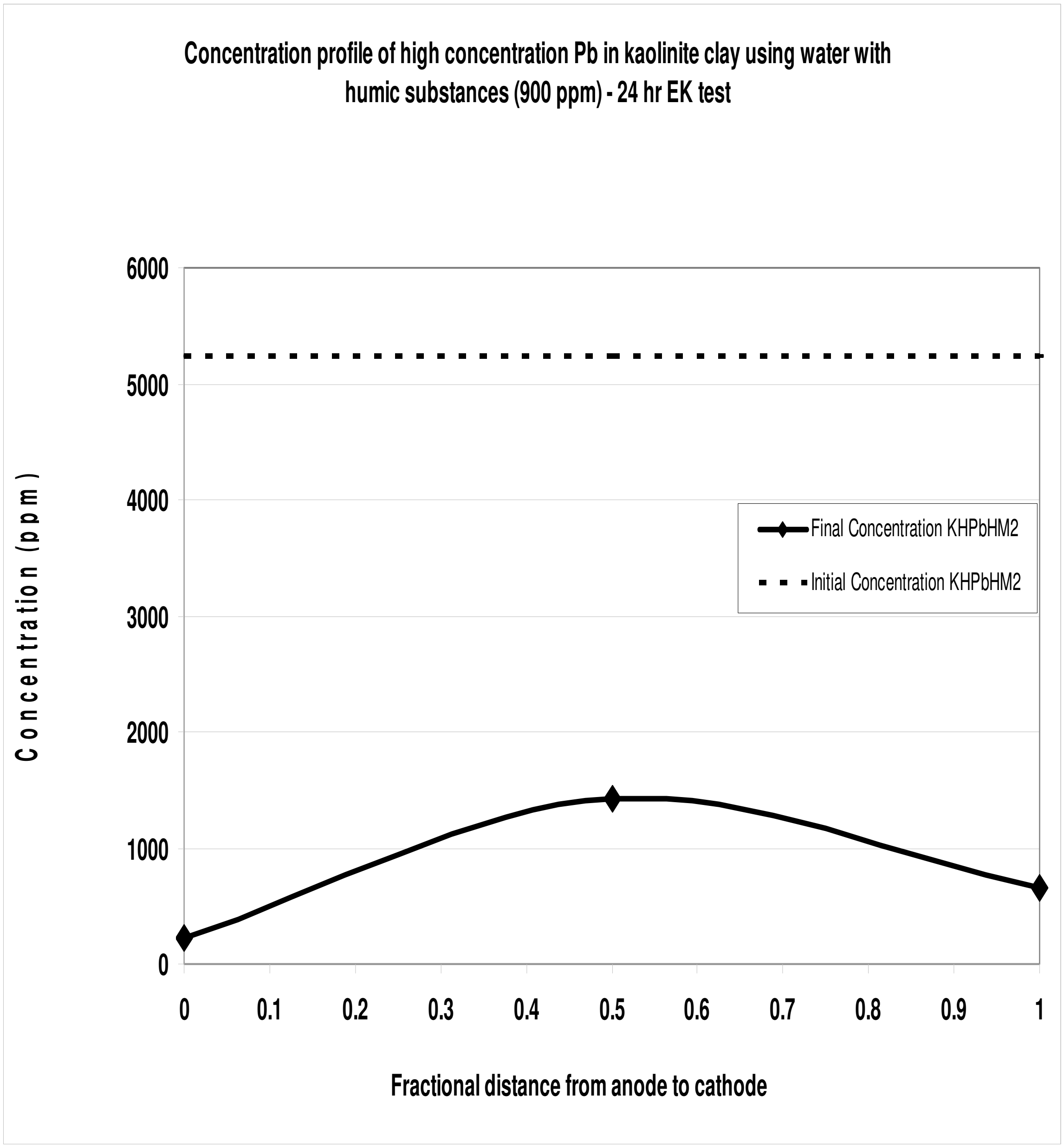

Figure 4-12-H-b: Results of EK test for electroremediation of lead using water with humic substances (900ppm).

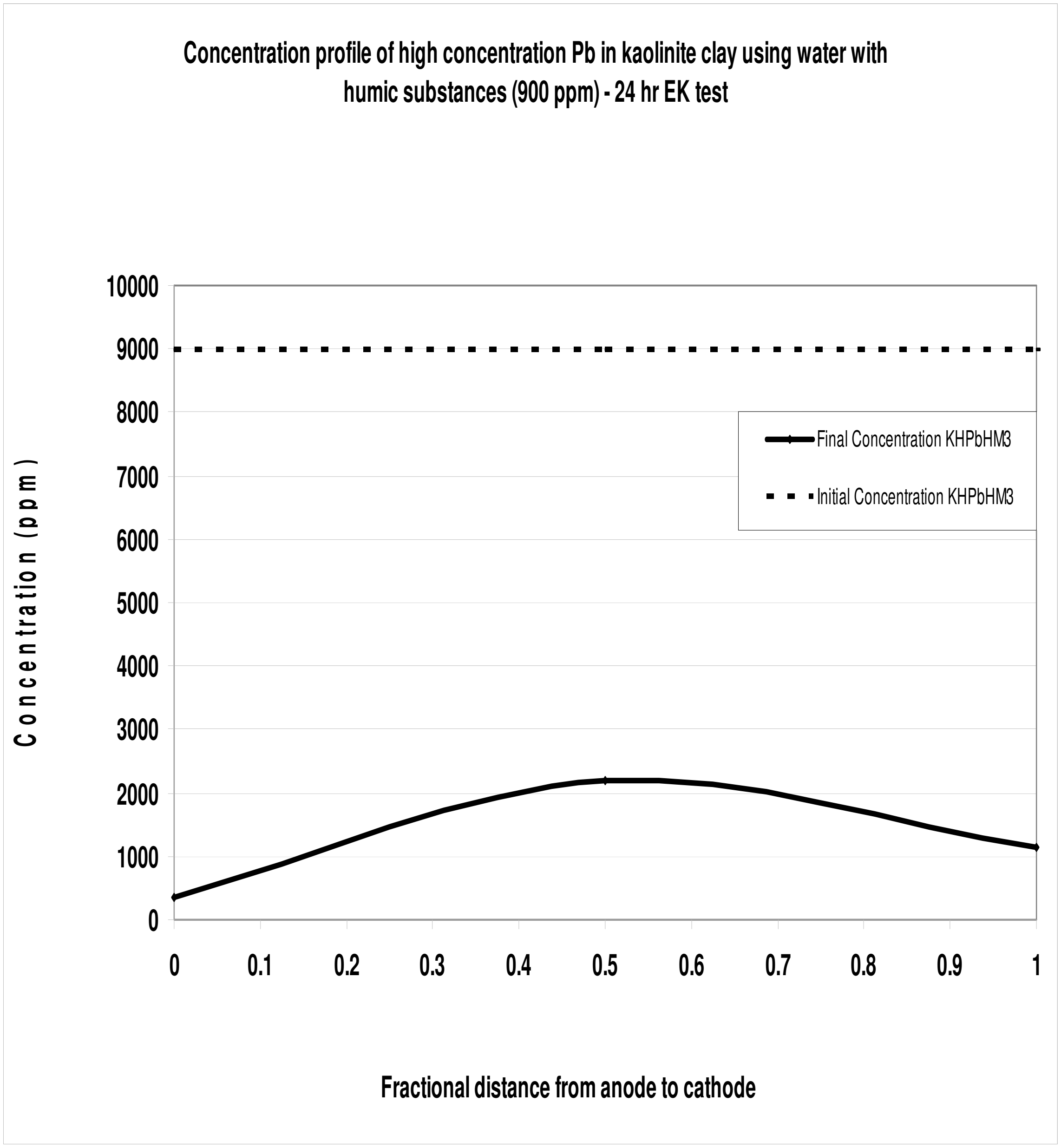

Figure 4-15-H-c: Results of EK test for electroremediation of lead using water with humic substances (900ppm).

pH Values before and after the E-K 24 hour test:

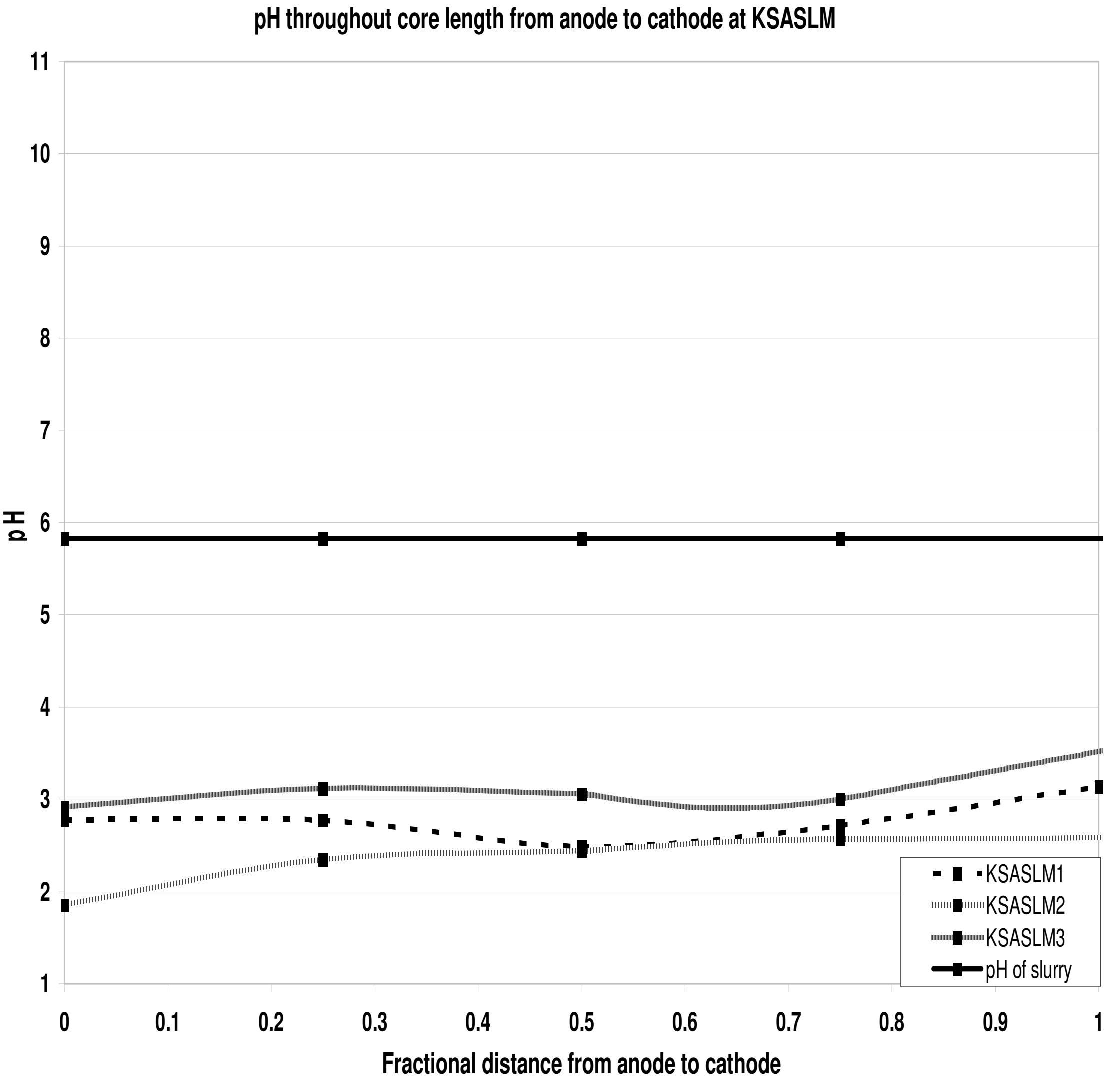

Figure 4-16-L: pH values before and after EK test for electroremediation of arsenic using distilled water (Pamukcu et al., 1993).

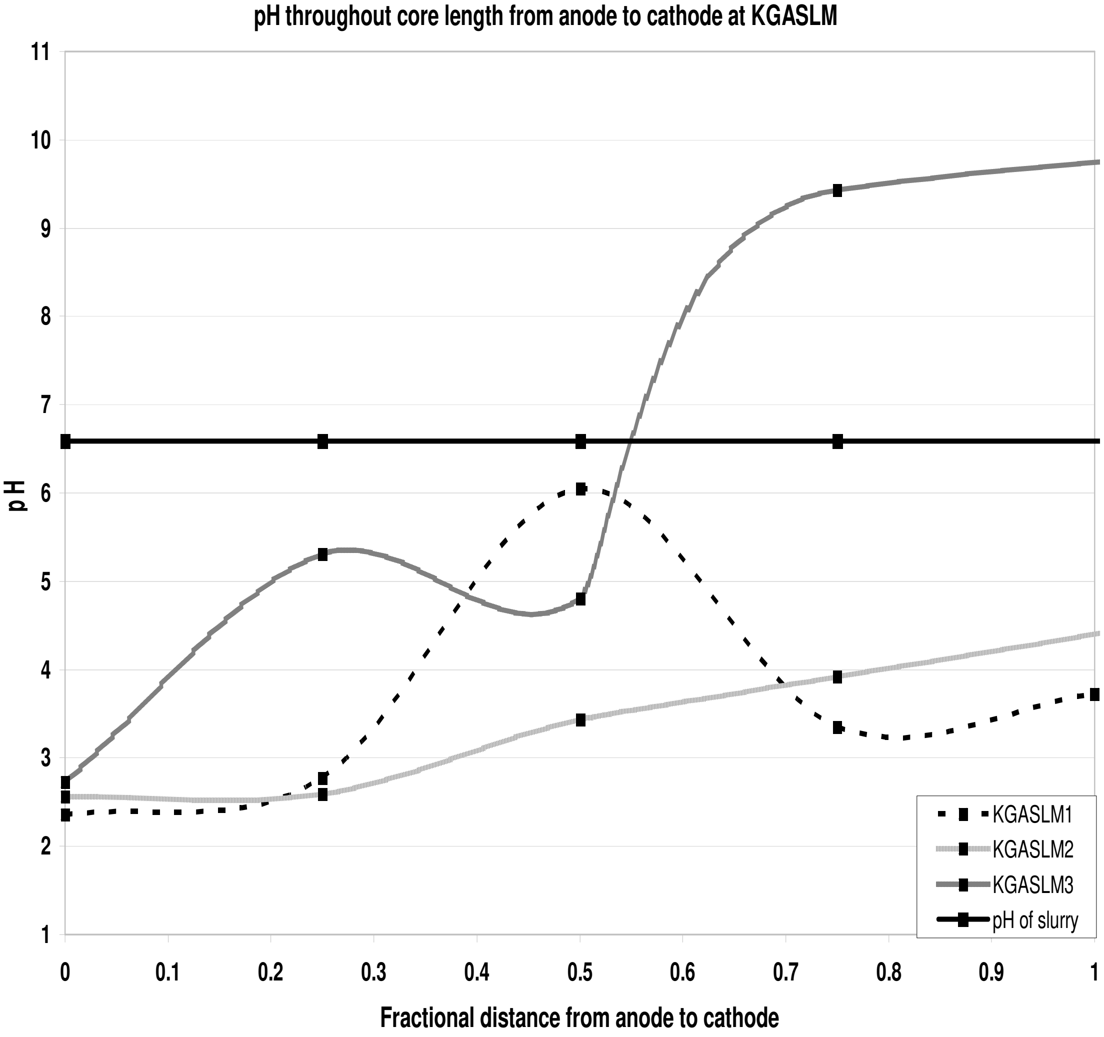

Figure 4-17-L: pH values before and after EK test for electroremediation of arsenic using ground water (Pamukcu et al., 1993). (See Table 4-1 for composition).

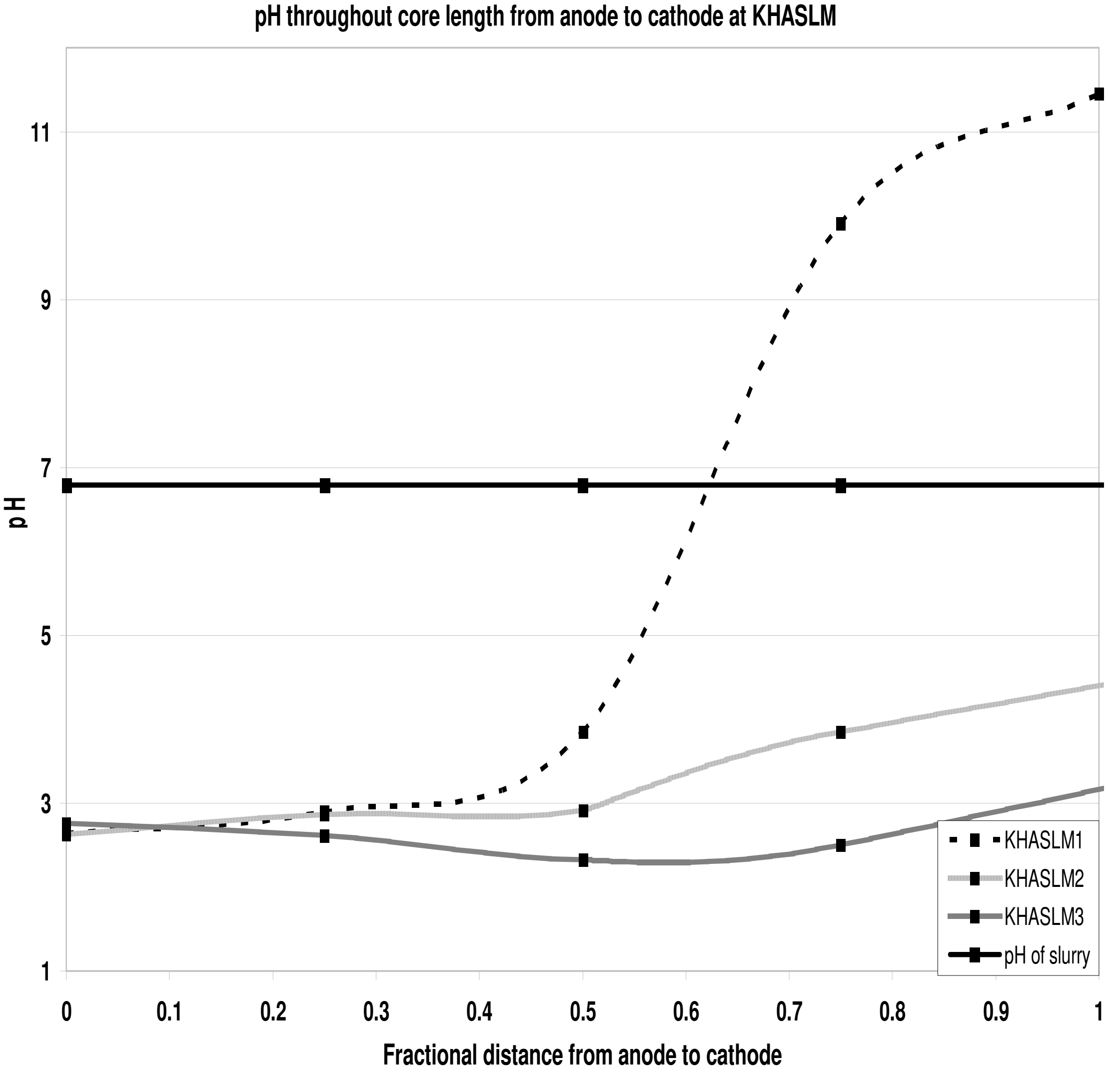

Figure 4-18-L: pH values before and after EK test for electroremediation of arsenic using water with humic substances (900ppm) (Pamukcu et al., 1993).

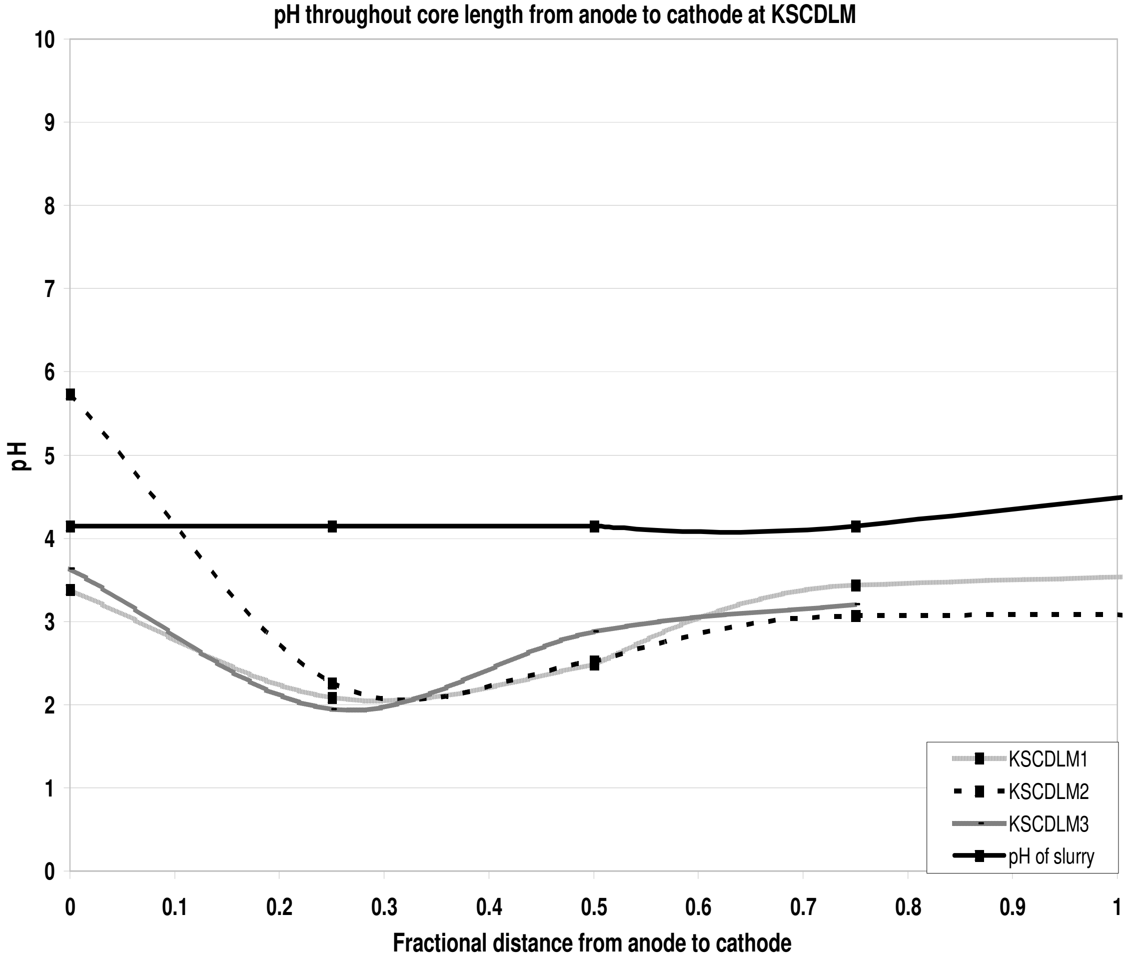

Figure 4-19-L: pH values before and after EK test for electroremediation of cadmium using distilled water (Pamukcu et al., 1993).

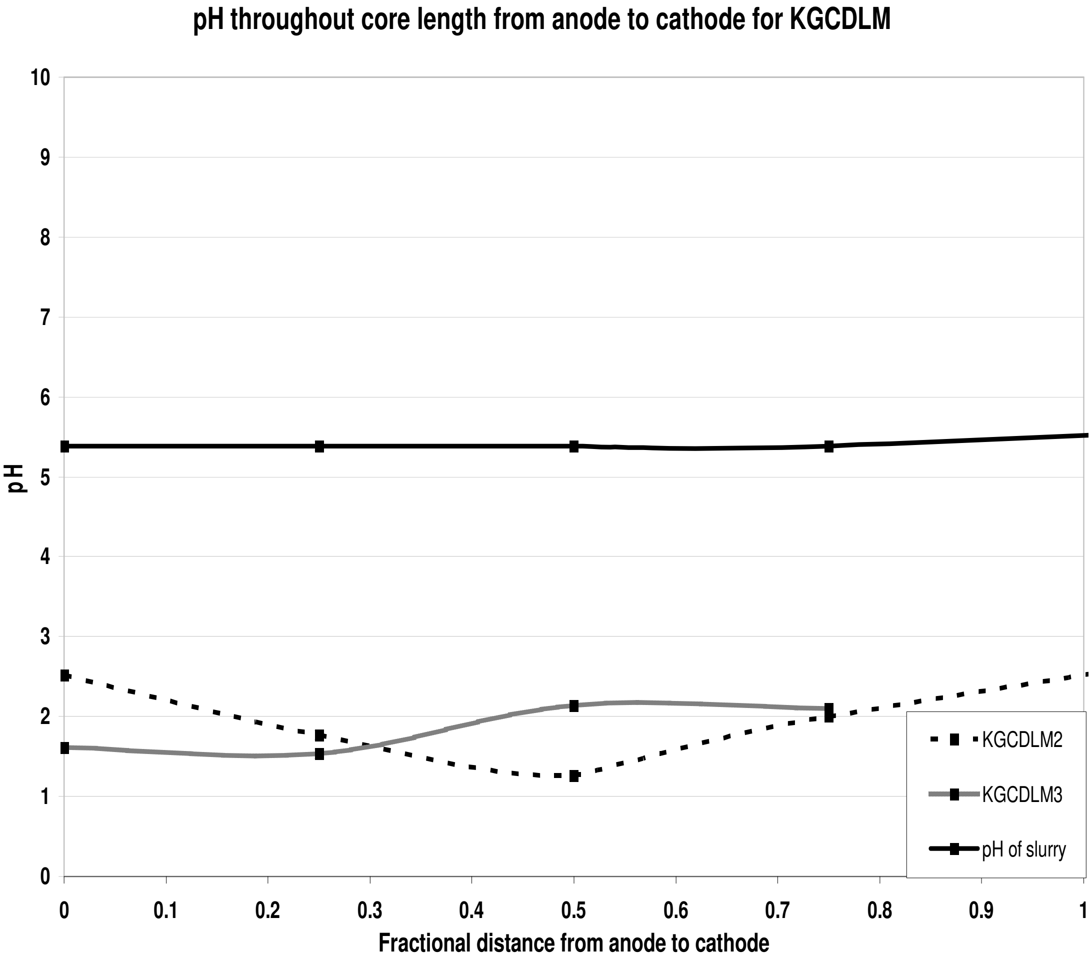

Figure 4-20-L: Results of pH before and after EK test for electroremediation of cadmium using ground water (Pamukcu et al., 1993). (See Table 2-1 for composition).

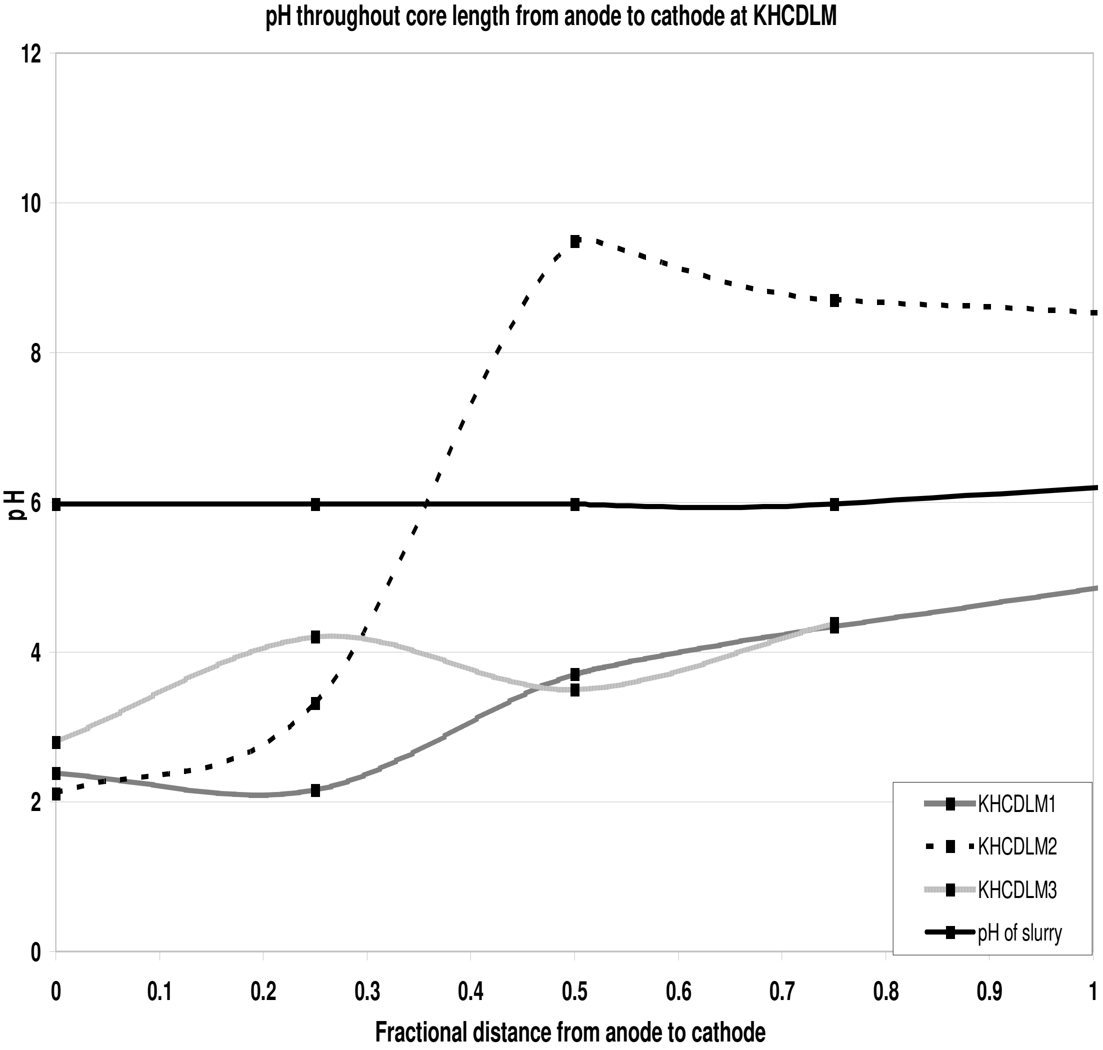

Figure 4-21-L: pH values before and after EK test for electroremediation of cadmium using water with humic substances (900ppm) (Pamukcu et al., 1993).

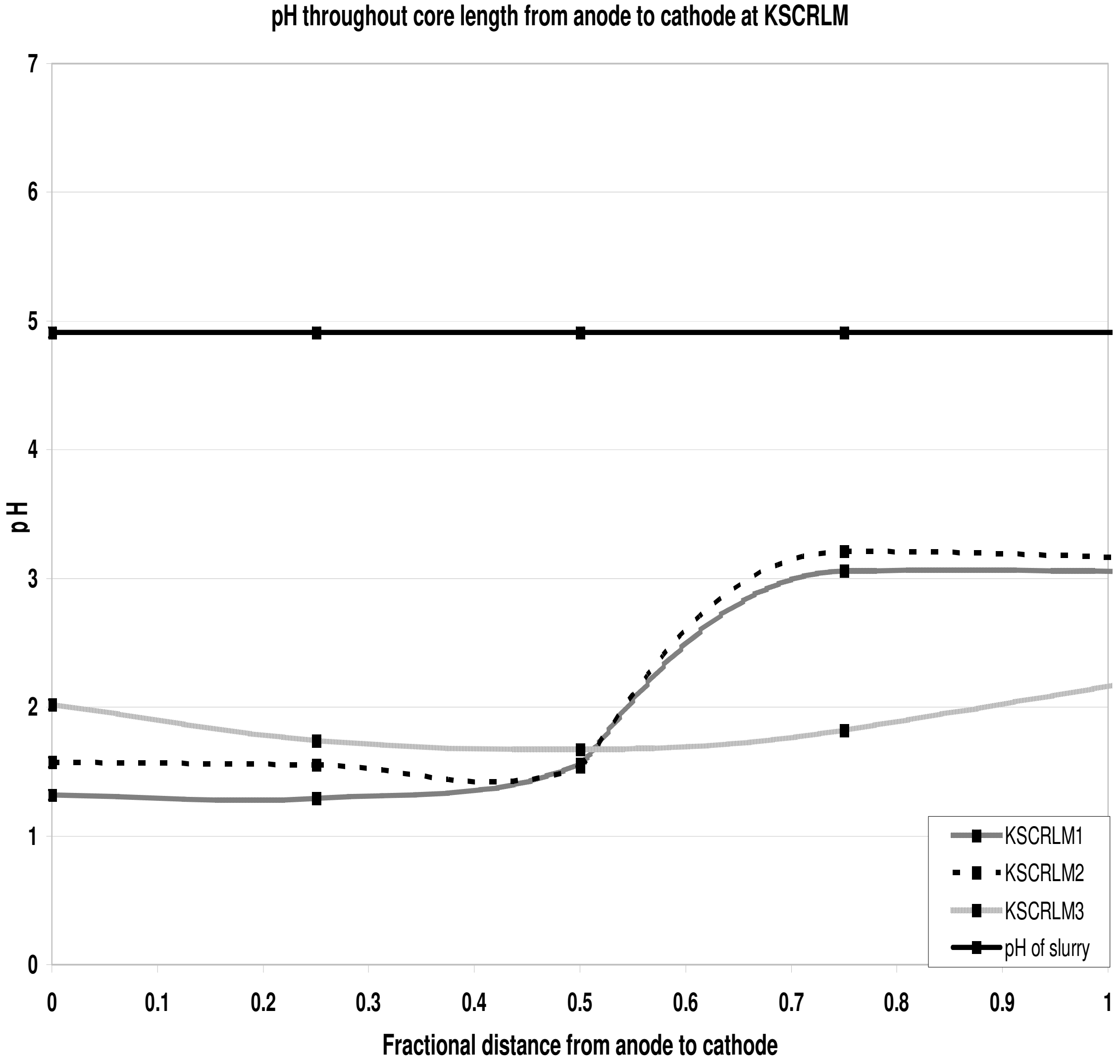

Figure 4-22-L: pH values before and after EK test for electroremediation of chromium using distilled water (Pamukcu et al., 1993).

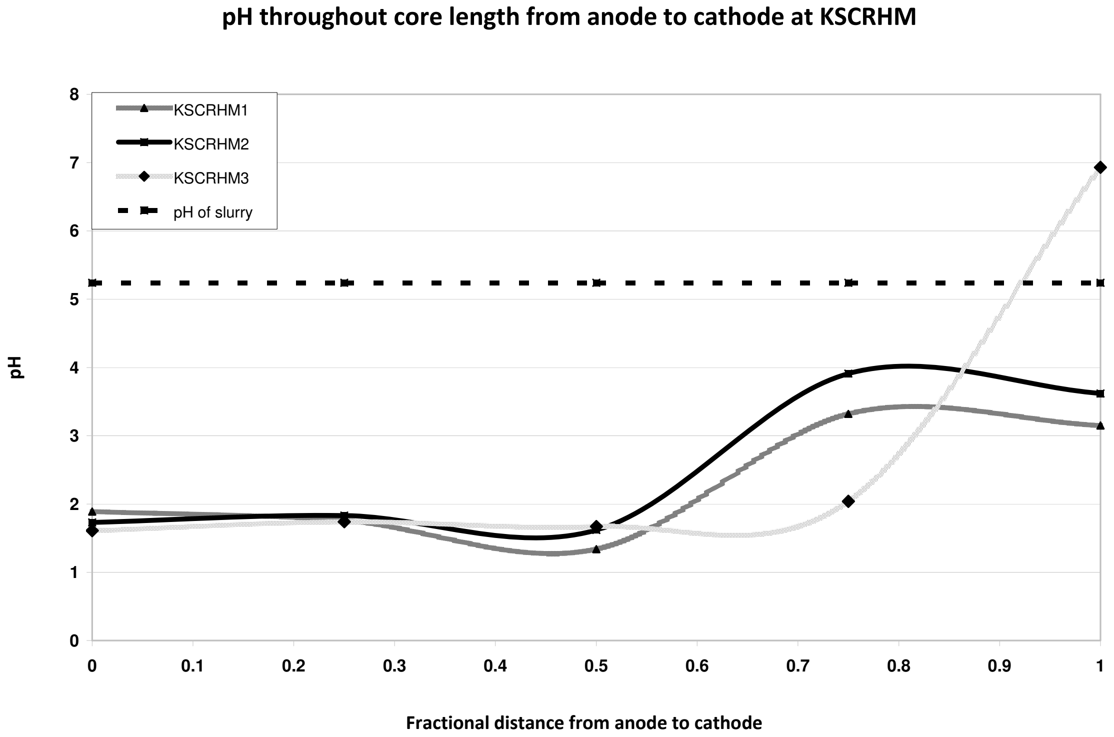

Figure 4-22-H: pH values before and after EK test for electroremediation of chromium using distilled water.

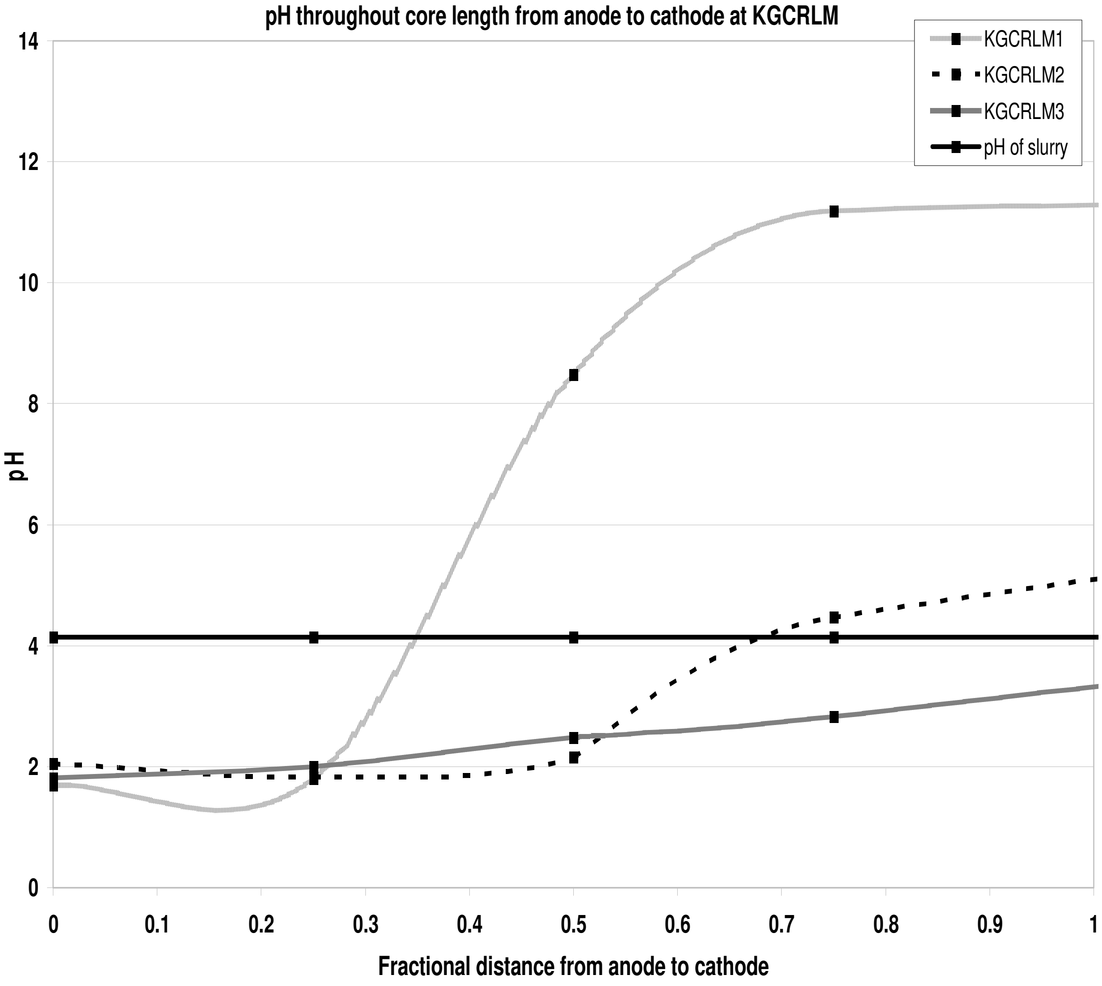

Figure 4-23-L: pH values before and after EK test for electroremediation of chromium using ground water (Pamukcu et al., 1993). (See Table 2-1 for composition)

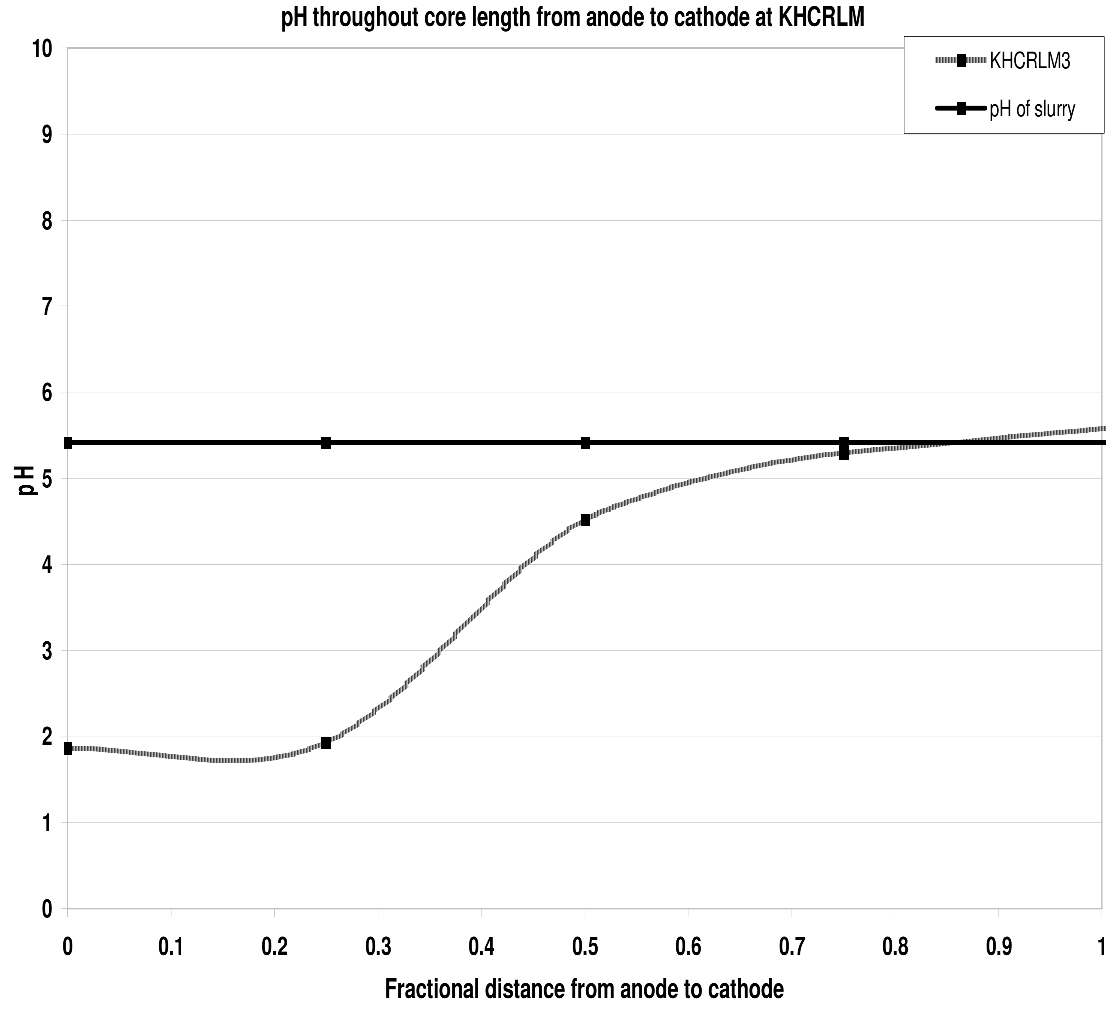

Figure 4-24-L: pH values before and after EK test for electroremediation of chromium using water with humic substances (900ppm) (Pamukcu et al., 1993).

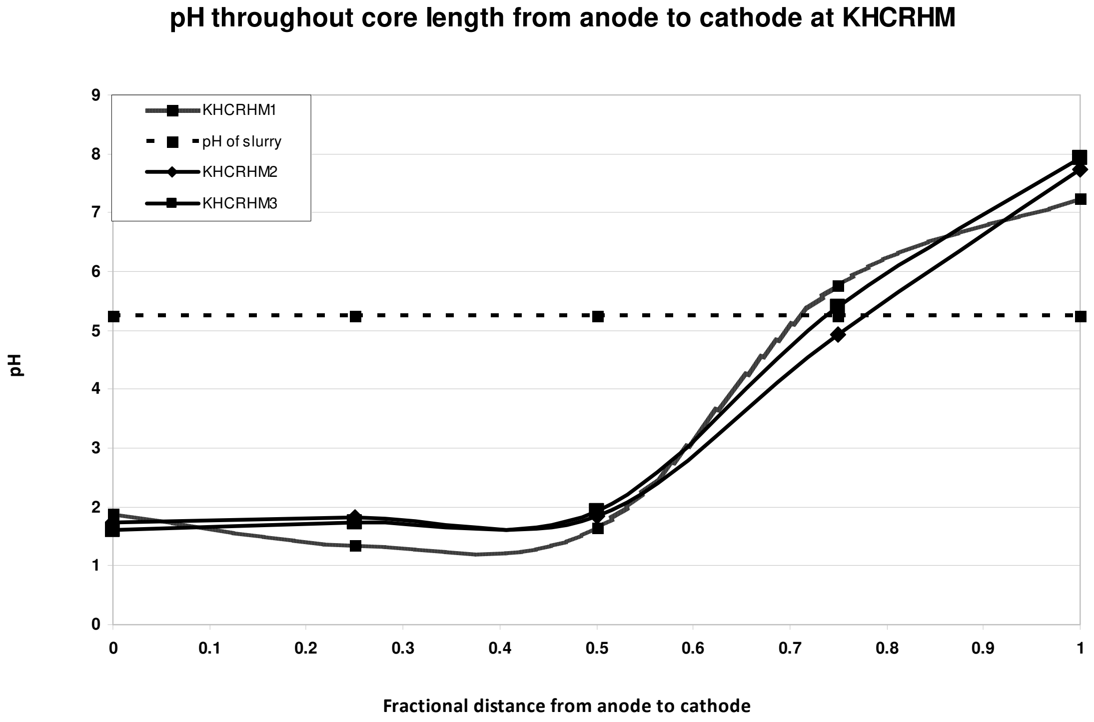

Figure 4-24-H: pH values before and after EK test for electroremediation of chromium using water with humic substances (900ppm).

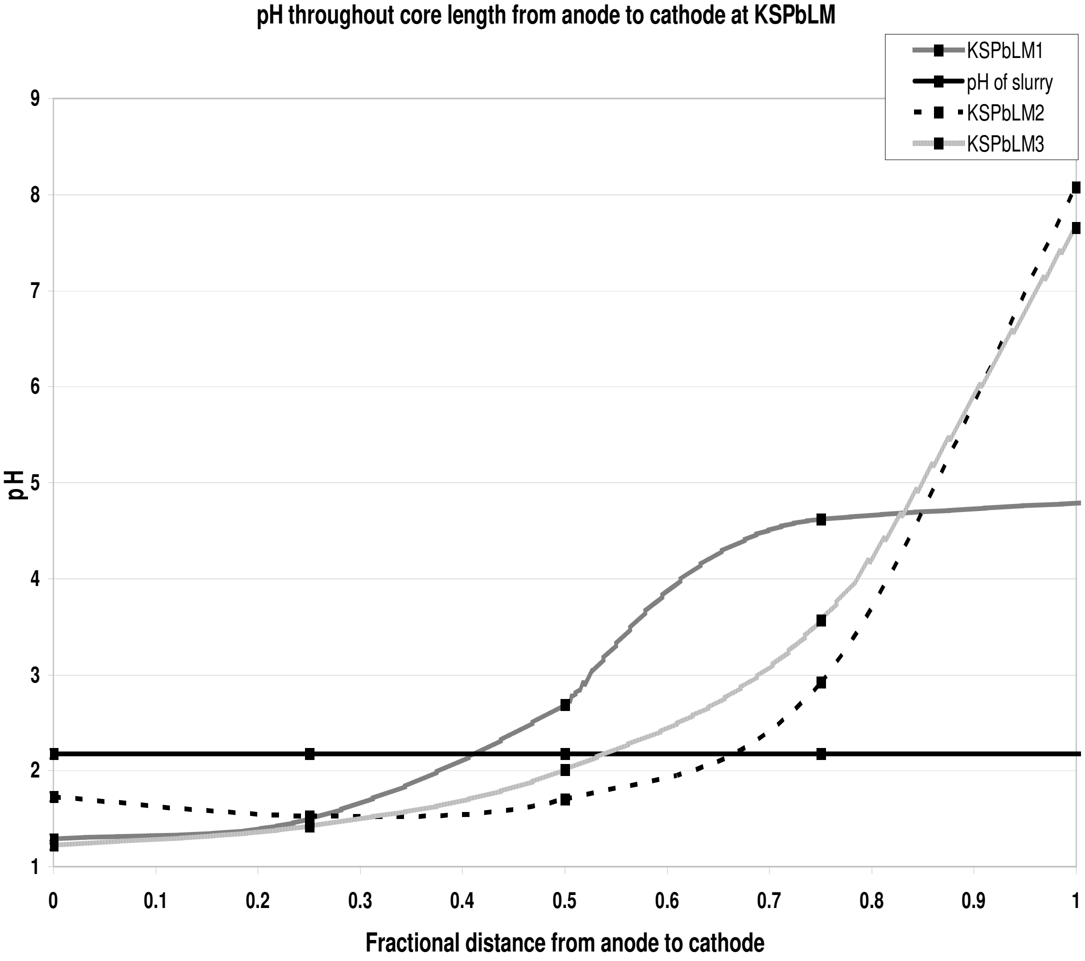

Figure 4-25-L: pH values before and after EK test for electroremediation of lead using distilled water (Pamukcu et al., 1993).

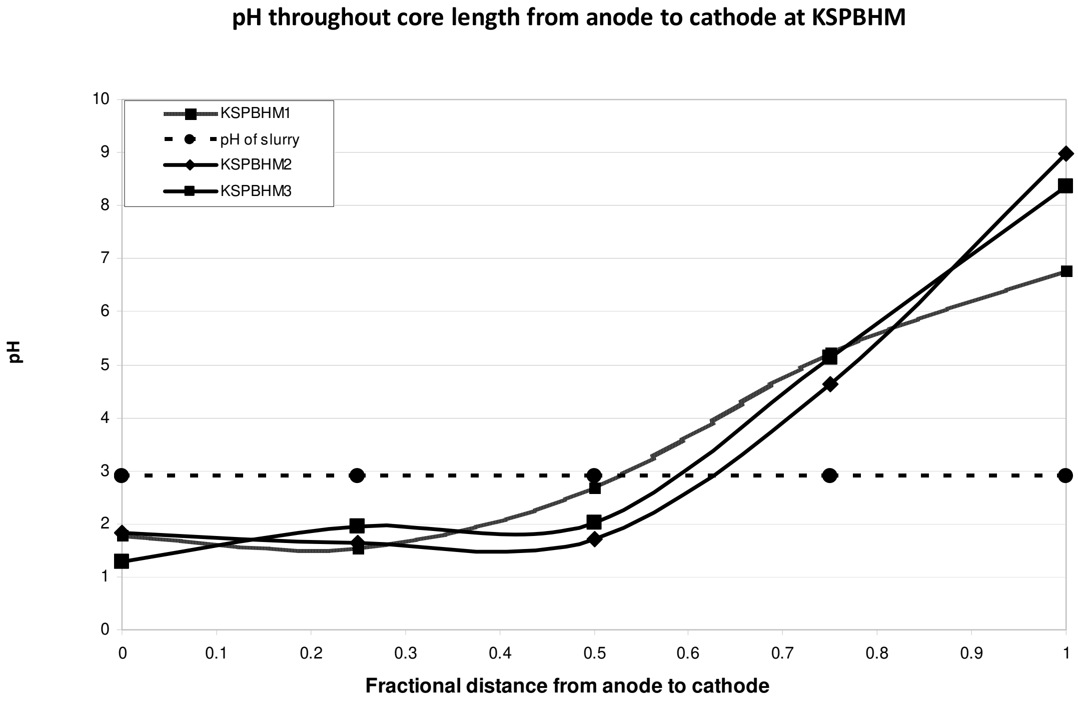

Figure 4-25-H: pH values before and after EK test for electroremediation of lead using distilled water.

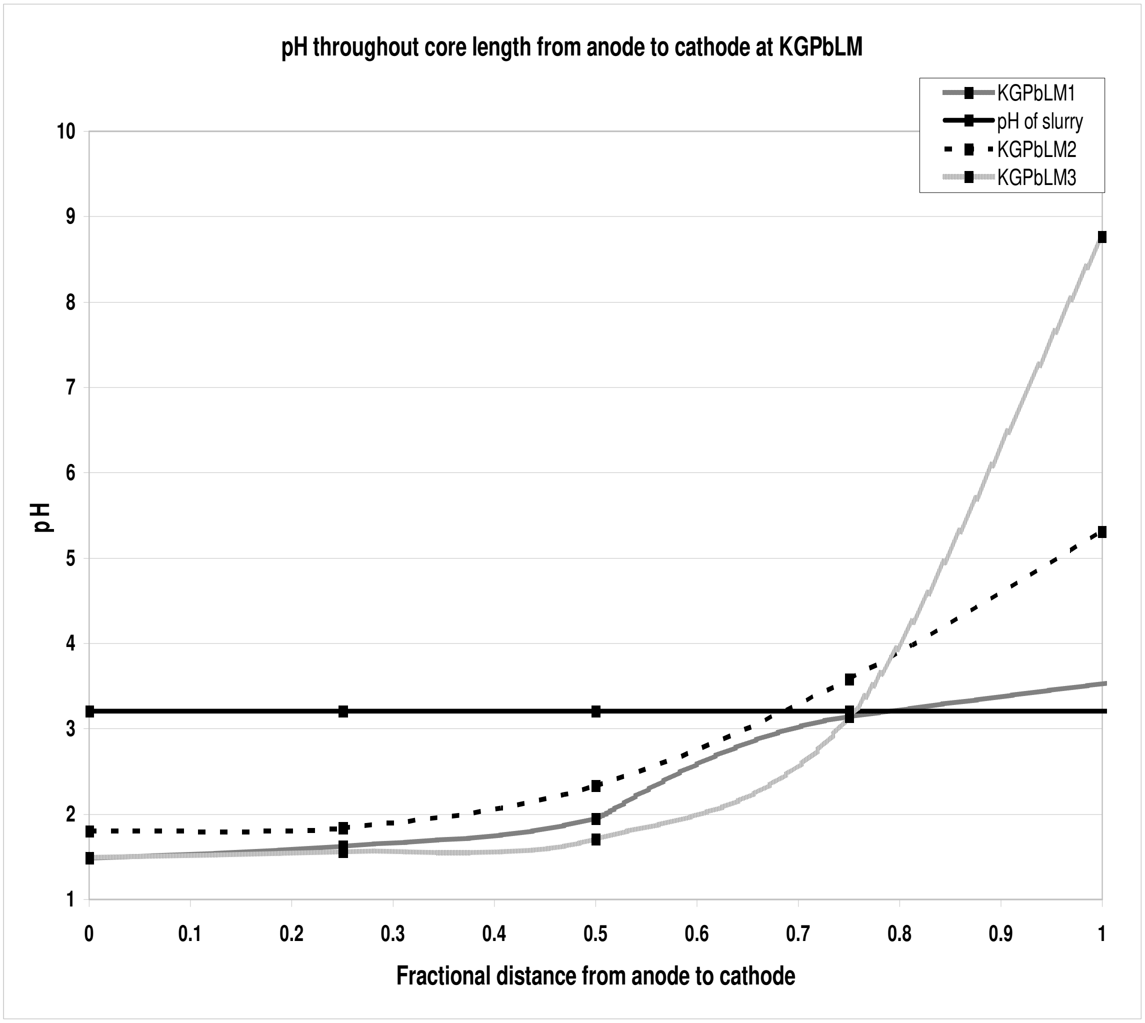

Figure 4-26-L: pH values before and after EK test for electroremediation of lead using ground water (Pamukcu et al., 1993). (See Table 2-1 for composition).

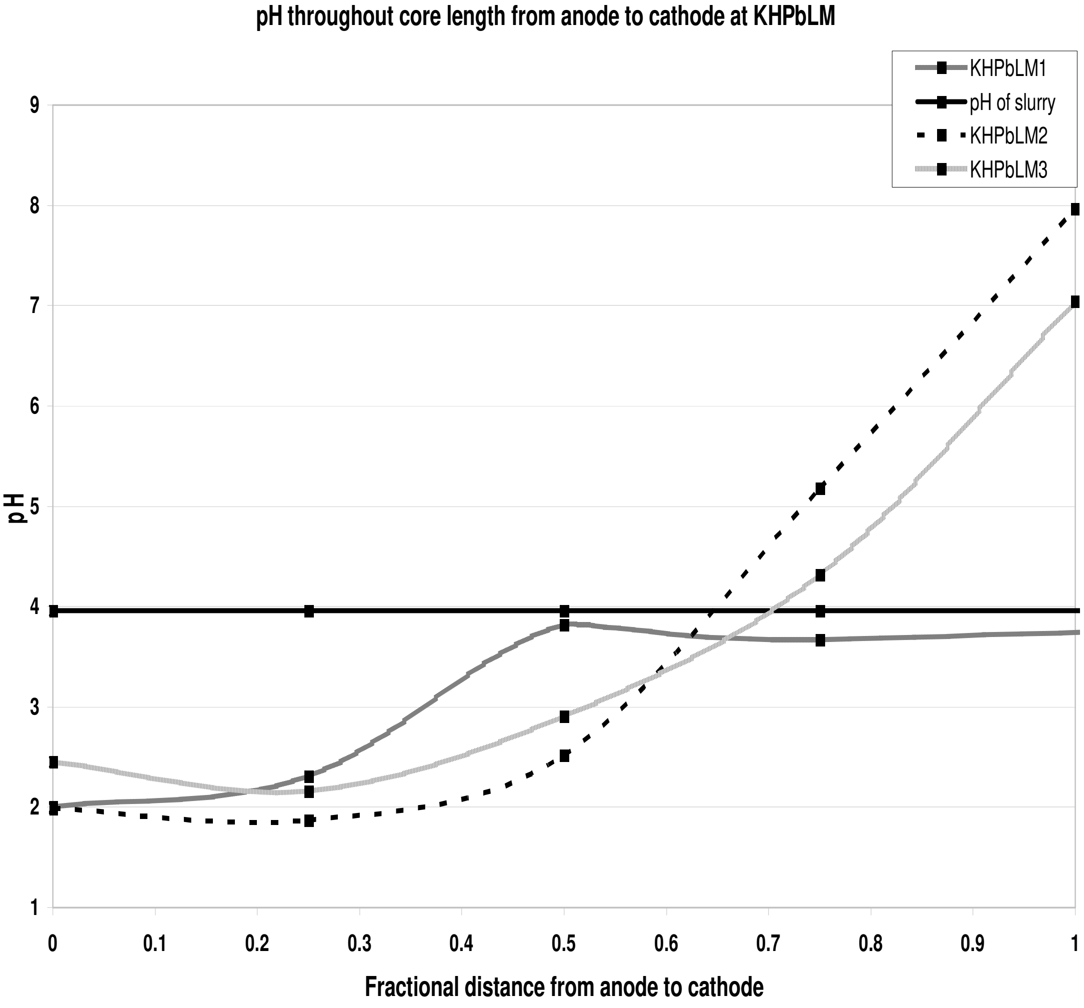

Figure 4-27-L: pH values before and after EK test for electroremediation of lead using water with humic substances (900ppm). (Pamukcu et al., 1993).

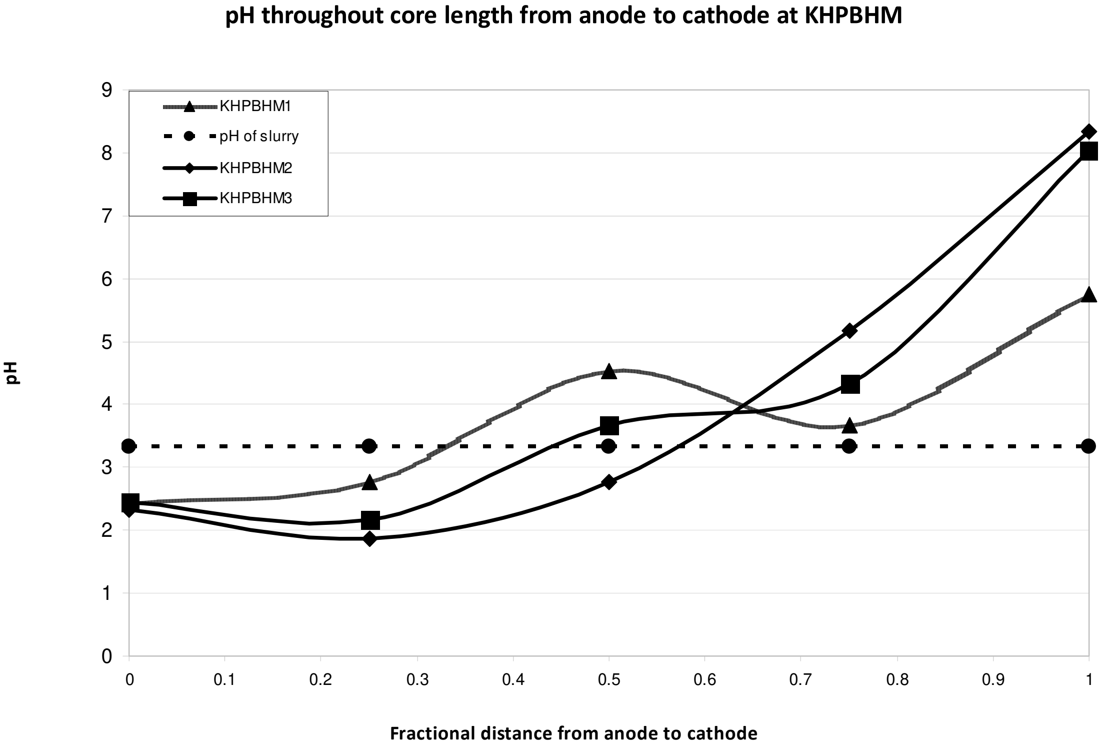

Figure 4-27-H: pH values before and after EK test for electroremediation of lead using water with humic substances (900ppm).

Table 4-2-L: Removal efficiency for low concentration tests recorded at fractional ends of core (Pamukcu et al., 1993).

Removal Efficiency (%) at:

Heavy Metal	Sample	Anode	Center	Cathode
Arsenic	KSASHM1	53.78	22.69	26.89
	KSASHM2	27.79	15.51	57.44
	KSASHM3	38.82	8.35	51.84
	KGASHM1	44.87	-27.88	53.53
	KGASHM2	55.26	22.01	66.27
	KGASHM3	-48.00	9.67	50.67
	KHASHM1	-12.42	-3.36	0.00
	KHASHM2	11.19	-32.46	47.39
	KHASHM3	6.56	-27.54	34.10
Cadmium	KSCDHM1	95.91	86.10	-216.08
	KSCDHM2	96.25	71.38	-256.22
	KSCDHM3	91.73	63.37	-272.23
	KGCDHM2	97.44	95.59	-409.09
	KGCDHM3	98.58	97.17	-51.33
	KHCDHM1	95.72	81.28	-258.58
	KHCDHM2	94.85	53.40	-576.70
	KHCDHM3	96.73	87.61	-241.18
Chromium	KSCRHM1	38.83	88.78	93.59
	KSCRHM2	58.70	12.54	92.35
	KSCRHM3	64.25	56.83	93.50
	KGCRHM1	13.11	58.29	92.42
	KGCRHM2	52.92	35.42	96.47
	KGCRHM3	57.23	46.54	95.59
	KHCRHM3	N/A	58.58	93.37
Lead	KSPBHM1	74.24	1.94	-77.36
	KSPBHM2	64.25	18.09	53.94
	KSPBHM3	68.52	29.17	-133.17
	KGPBHM1	62.63	-15.88	-39.17
	KGPBHM2	78.77	-11.90	2.93
	KGPBHM3	82.05	-19.23	-30.77
	KHPBHM1	78.89	-29.65	-152.53
	KHPBHM2	64.44	20.83	-126.85
	KHPBHM3	57.38	-4.46	14.36

Heavy Metal	Sample	Anode	Center	Cathode
Chromium	**KSCRHM1**	**52.00**	**89.61**	**95.08**
	KSCRHM2	**58.70**	**89.97**	**97.85**
	KSCRHM3	**64.25**	**56.83**	**98.81**
	KHCRHM1	**51.78**	**91.12**	**98.06**
	KHCRHM2	**55.18**	**85.13**	**99.14**
	KHCRHM3	**59.45**	**82.24**	**98.93**
Lead	**KSPBHM1**	**89.29**	**59.90**	**87.18**
	KSPBHM2	**89.26**	**56.97**	**87.18**
	KSPBHM3	**87.04**	**-92.63**	**87.18**
	KHPBHM1	**96.36**	**68.68**	**87.18**
	KHPBHM2	**95.72**	**72.74**	**87.471**
	KHPBHM3	**95.93**	**75.53**	**87.18**

Table 4-2-H: Removal efficiency for high concentration tests recorded at fractional ends of core.

Part II

Study Area A in Abu Dhabi city, U. A. E.

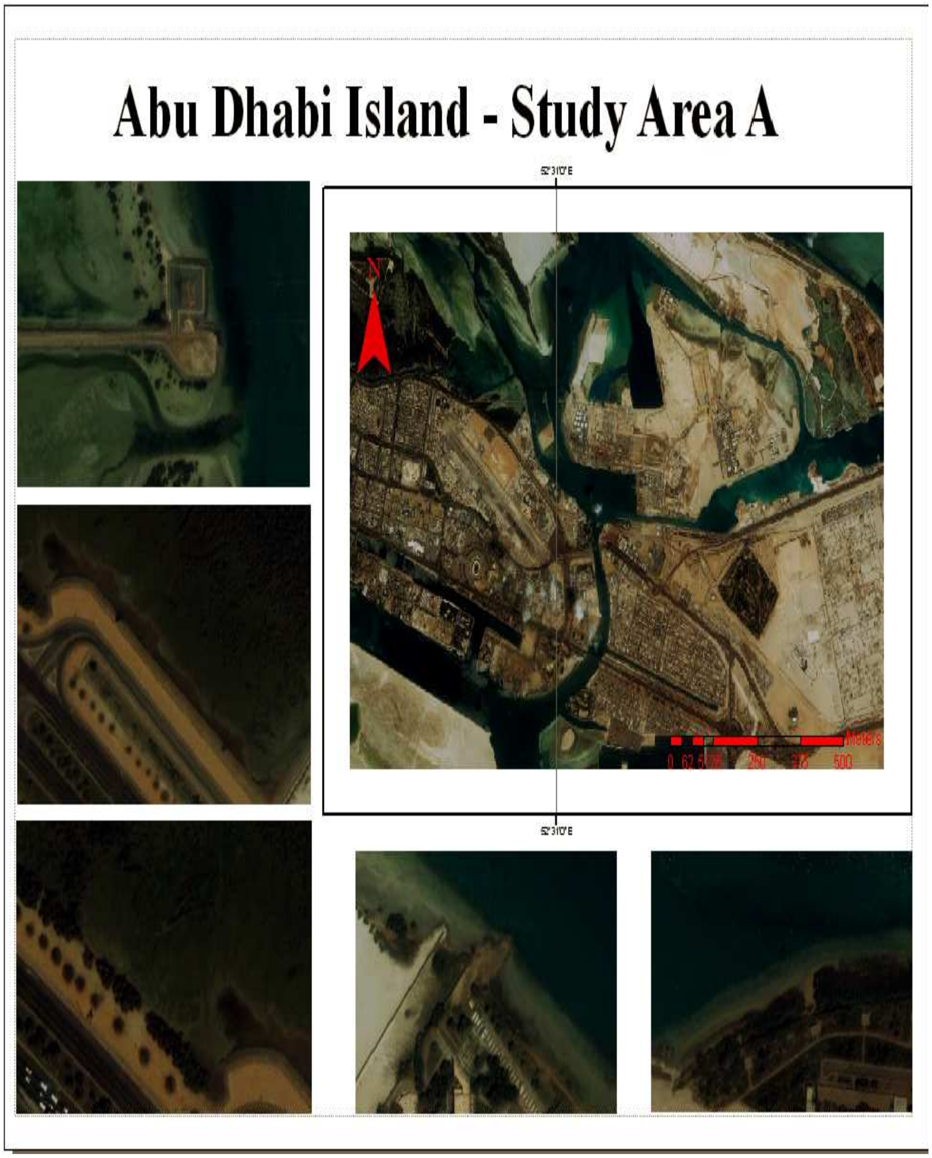

Figure 4-28-a: Abu Dhabi Island – Study Area A

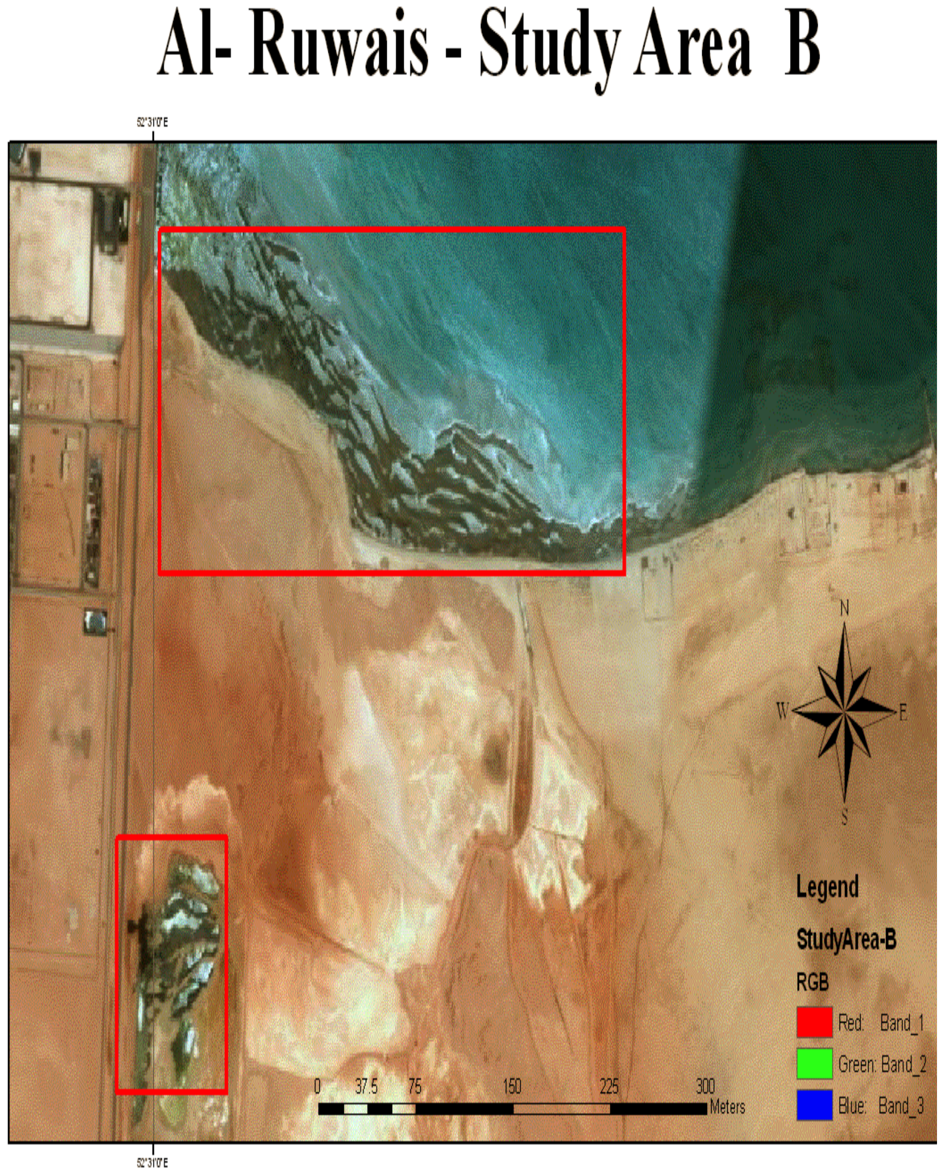

Figure 4-28-b: Al-Ruwais (Ruwais Industrial Complex) – Study Area B

Geological and Sedimentlogical Setting

The Holocene sediment province of the Arabian Gulf coast is dominated with shallow water carbonate/evaporite facies of the Permian subsurface and consists of seaward reefs, islands and tidal deltas protecting sheltered saline lagoons and supertidal evaporate/carbonate flats. Holocene sediments of the United Arab Emirates (UAE) coast accumulate on rocks of Miocene and Pleistocene age. The Miocene substrate consists of a sequence of marls, sandstone limestone and evaporates which slope gently southward *(Al-Sharhan, A.S. and A.A.El-Sammak, 2004).*

The barrier island-lagoon subsystem runs along a wide stretch of the UAE coast from Jebel Dhana to Ras Ghanada. The physiography of the eastern part of this subsystem is strongly affected by the presence of the Great Pearl Bank and associated islands. The western section of this subsystem is composed of a complex of islands and lagoons. Eastward, in the protected lagoons, carbonate muds and pellets are accumulating, whereas to the west of Al Dhabaiya Island, only carbonate muds accumulate in a narrow belt south of the offshore bank. Grapestones and skeletal debris are the dominant components of the deposits *(El Gawad, E. A., et al.*, 2008).

Occasional mangrove colonization of small areas of sand and mud flats occur. Seaward of the algal flats and hardground is an undulating surface of carbonate sands and muds. Locally, in the lower lying areas tidal creeks dissect this surface and incise it into carbonate muds. Also, along tidal channels mud-cracks are common *(Alsharhan, A.S., Kendall, C.G.St.C., 2002).*

Abu-Dhabi Island

This area is dominated by intertidal flats, lagoons, tidal deltas, barrier islands and coastal terraces except where local hills of Tertiary and Quaternary rocks jut out as peninsulas. In places, the sabkha surface lies flush with eroded Quaternary rocks. The seaward margins of the "T" shaped islands parallel the coast while their stems lie at right angles to the dominant wind direction and separate the protected lagoons to the south associated with narrow tidal channel and deltas.

The sediments of the sabkha area around Abu Dhabi consist of a mixture of sand sized carbonate-evaporite minerals. Algal mats and mangroves (*Avicennia marina*) dominate the intertidal zone. Flanking these salt flats are remnants of the intertidal zone characterized by the presence of algal mats, mangroves or both of them *(El Gawad, E. A., et al.*, 2008).

Study area A is dominated by carbonate mud that accumulates around mangroves, this muddy facies is commonly densely burrowed by crabs. In addition, tidal channels and mud-cracks are common around mangrove areas. In the lower lying areas tidal creeks dissect this surface and incise them into narrow strips of carbonate muds parallel to the shore at the top of the intertidal flats *(Kendall, C. G., Alsharhan, A.S. and Whittle, G.L., 1995).*

Al-Ruwais Area:

The Ruwais area is situated on the Gulf coast 250 km west of the capital Abu Dhabi. The port's cargo consists primarily of fuel, crude oils and petrochemical products. Study area B is dominated by beach rock and old shoreline. Intertidal and shallow subtidal areas (0-2m) with exposed surfaces are dominated by micro and macro algal species. Significant seasonal variation occurs with macroalgal die-off and loss off biomass during the summer period with re-growth occurring during the cooler winter season. This biological assemblage traps the wave action suspended fine sediments present in the water column and results in an accumulation of deposited fine sediment within this area *(Kendall, C. G., Alsharhan, A.S. and Whittle, G.L., 1995).*

Here, sandy shoals and coral banks are cut by tidal channels. The lagoon south of the barrier is a continuous open body of water connected to the Arabian Gulf with circulation that is less restricted than the lagoons to the northeast and the west *(El Gawad, E. A., et al.*, 2008).

Results

Twenty two different samples of offshore muds were collected along the coastline from both study areas A and B. Out of the 35 heavy metals, 29 were present with varying concentrations depending on the proximity to refineries, aluminum plants, petrochemical plants, desalinization plants, and other industries. The salinity of those samples was in the order of 20,000 ppm allowing a significantly high current to pass through with just 20 V applied by a DC power supply. The voltage may be optimized in the future to improve the removal efficiencies, while reducing both the operating cost as well as the electrode reactions that produces the O_2 gas at anode and H_2 gas at cathode. In-as-much as basic conditions are established at the cathode, there is precipitation of hydroxides and carbonates, which causes cementation at the cathode region. The reactions at the electrodes are as follows:

Anode: $2H_20 - 4e^- => O_2 + 4H^+$

Cathode: $1/2O_2 + H_20 + 2e^- => 2OH^-$ (neutral & alkaline solution)

$2e^- + 2H^+ => H_2$ (acidic solution)

Thus, there is a need to control the acidity, during the application of DC current.

In our tested samples, the current ranged from 10 mA to 85 mA depending on the salinity of water in each specimen. The first 75 runs were performed using distilled water with 10 ppm salinity without pH control. The final 30 runs were performed using the actual Gulf sea water (26,000 ppm) salinity containing 450 ppm of maleic acid for pH control.

Heavy Metals:

Arsenic: Figures 4-28-c through 4-30 show the fraction of the arsenic found at three locations: anode side, center and cathode end of tested core after 24 hours of electrokinetic treatment. The initial concentrations were predetermined at the anode end of the contaminated offshore mud sample. The removal efficiency was calculated at the anode using equation 4-1 for all results obtained. After 24 hours, substantial reduction of arsenic from its initial concentration at the anode region at the anode region using distilled water with 10 ppm salinity, was found to be 34.25, 17.67, and 10.07% as shown in Figures 4-28-c through 4-30 respectively. Electrokinetics was the main driving force of the As ion in the direction of the water flow. There was accumulation of metal at the discharge end (cathode end of the mud sample as can be seen in Figure 4-28-c through 4-30, where Figure 4-30 displayed a significant level of accumulation at the cathode region. The shape of the curve in Figure 4-30 can be explained by the lack of pH control. (Pamukcu et al., 1993).

Arsenic: ADOMAS4, ADOMAS5, RICOMASR3 samples in Figure 4-28-c through 4-30 using Distilled water with 10 ppm salinity

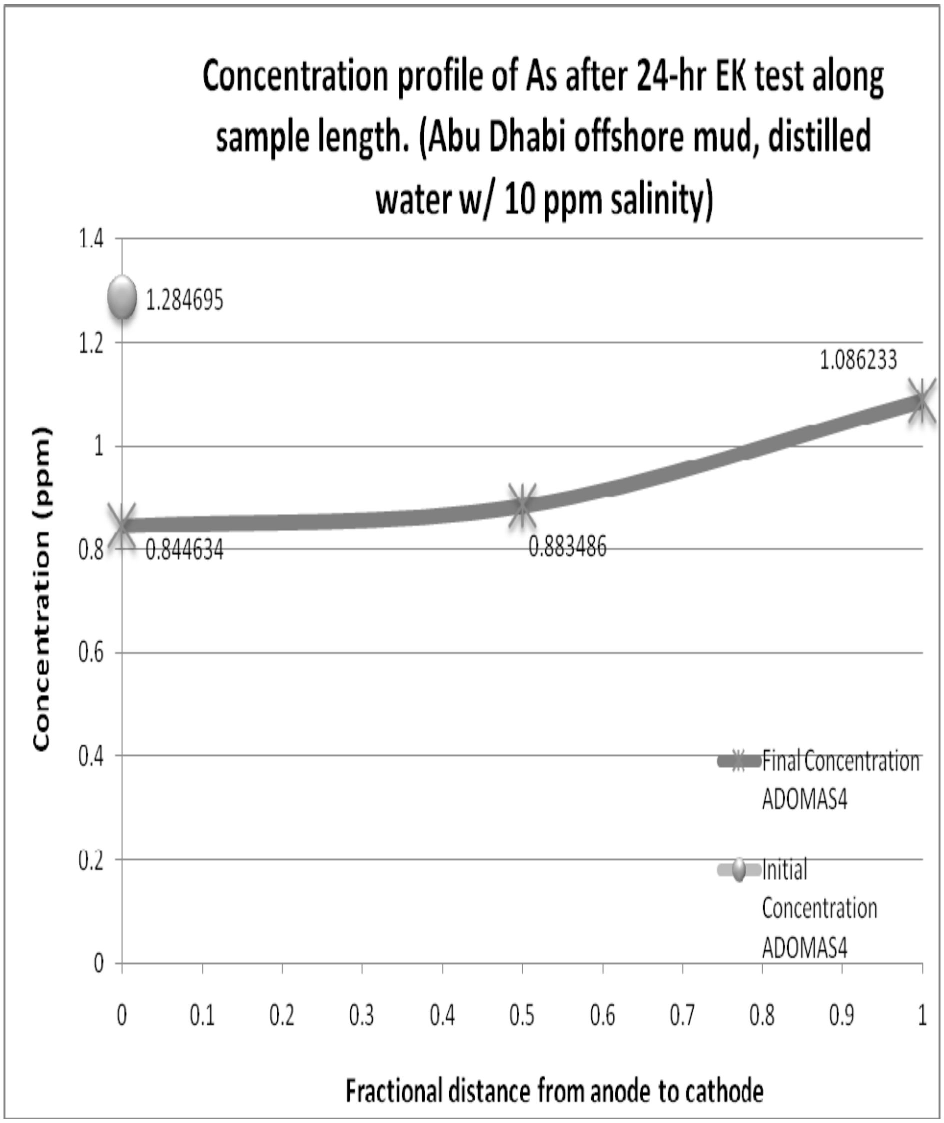

Figure 4-28-c: Concentration profile of As after 24-hr EK test a long sample length (Abu Dhabi offshore mud, distilled water 10 ppm salinity).

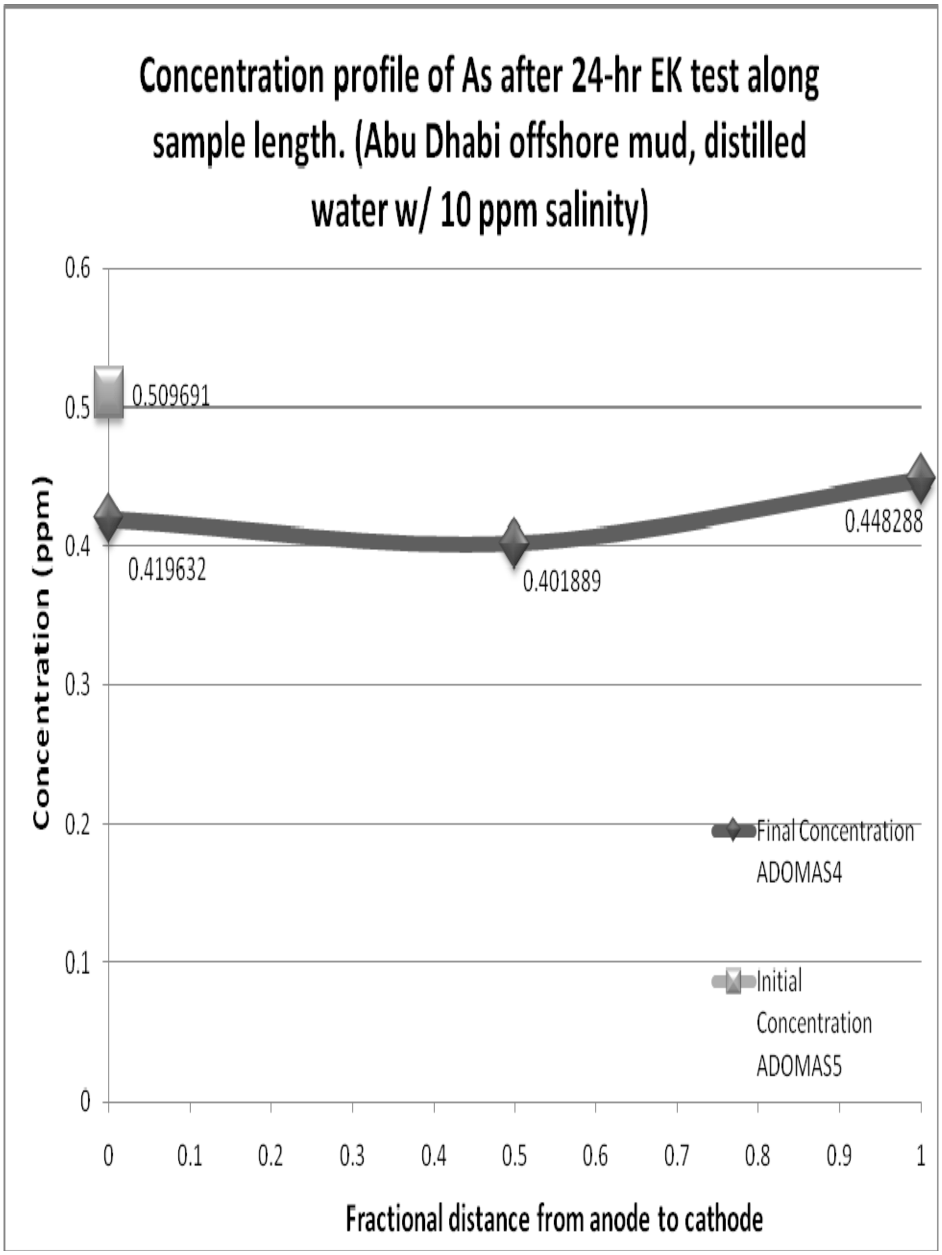

Figure 4-29: Concentration profile of As after 24-hr EK test a long sample length (Abu Dhabi offshore mud, distilled water 10 ppm salinity).

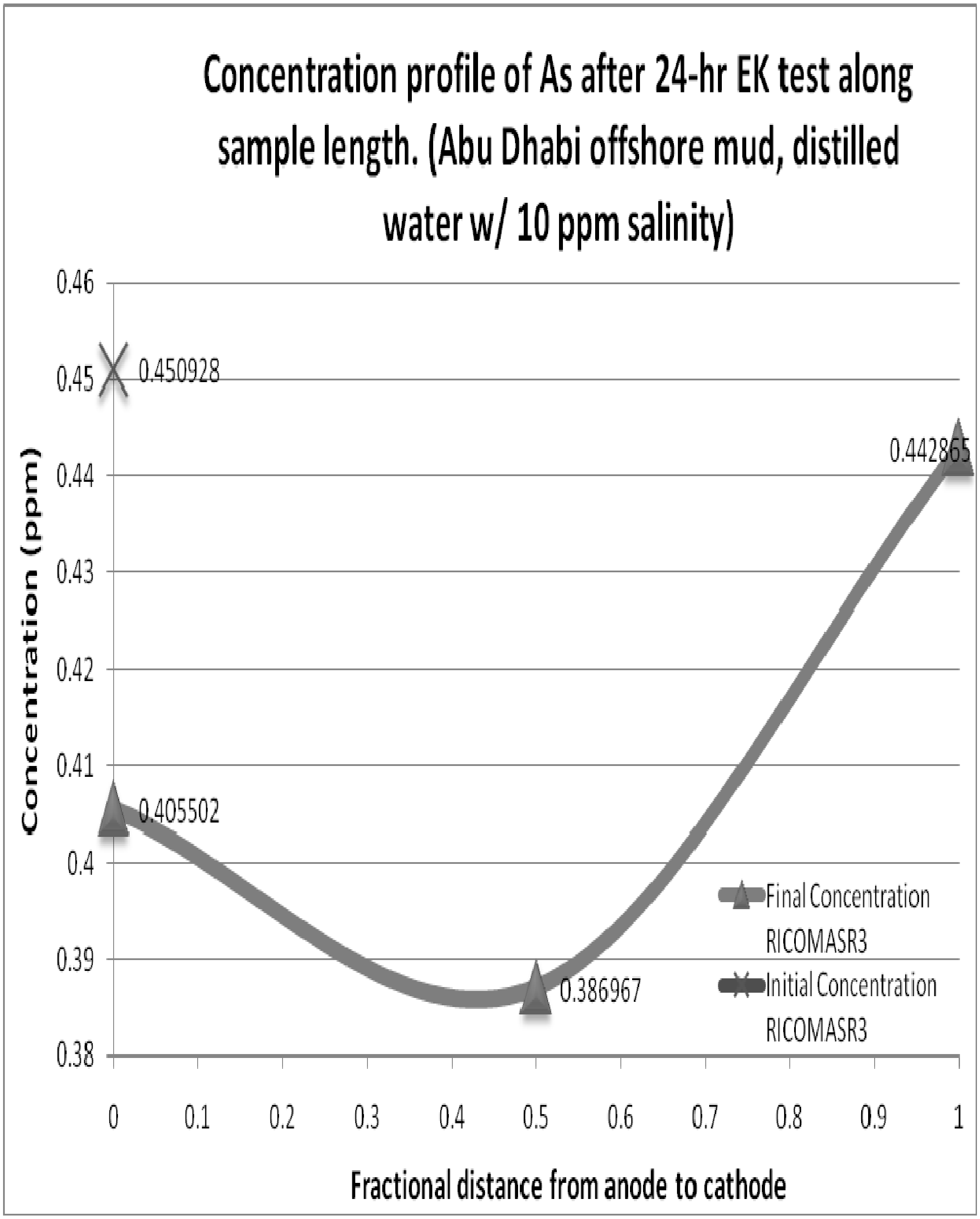

Figure 4-30: Concentration profile of As after 24-hr EK test a long sample length (Abu Dhabi offshore mud, distilled water 10 ppm salinity).

Barium: Figures 4-31, 4-32 and 4-33 show the fraction of the barium found at three locations: anode side, center and cathode end of tested core after 24 hours of electrokinetic treatment. The initial concentrations were predetermined at the anode end of the contaminated offshore mud sample. The removal efficiency was calculated at the anode using equation 4-1 for all results obtained. After 24 hours, substantial reduction of barium from its initial concentration at the anode region using distilled water with 10 ppm salinity, was found to be 11.04 and 13.81% as shown in Figures 4-31 and 4-32 respectively. The migration pattern after the 24-hour period accumulated at the cathode region. Electrokinetics was the main driving force of the Ba ion in the direction of the water flow. There was accumulation of metal at the discharge end (cathode end of the mud sample) as can be seen in Figure 4-35 and 4-36. The shape of the curve in Figure 4-34 can be explained by the lack of pH control.

Figure 4-33 shows the results conducted with Abu Dhabi seawater having 26,000 ppm salinity, as well as 450 ppm of maleic acid added for pH control. The migration pattern was similar to that of Figure 4-31, through 4-32, however, the maximum removal efficiency of barium after 24 hours at the anode region here 36.68% as opposed to the 13.81%. This finding was interesting as it confirmed that the presense of both high salinity and pH control mechanism influenced all the samples tested here to consistently show higher removal efiiciencies at all the three locations analyzed. As you can see the bell shaped curve of figure 4-32, was eliminated here due to the pH control. The high salinity caused a higher conductivity in the bulk solution, where both the current and electrokinetic flow increased several fold. One explanation for this is that the

electromigration force is now a dominat force allowing the ionic mobility to travel at 2-3 times faster than in the case of dominant electroosmosis, while another theory is the abundance of large volumes of cations in this high salinity carrying their waters of hydration further promoting ionic species velocity. This needs to be investigated further.

Barium: ADOMBA2, ADOMBA4 samples in Figure 4-31 through 4-32 using Distilled water with 10 ppm salinity

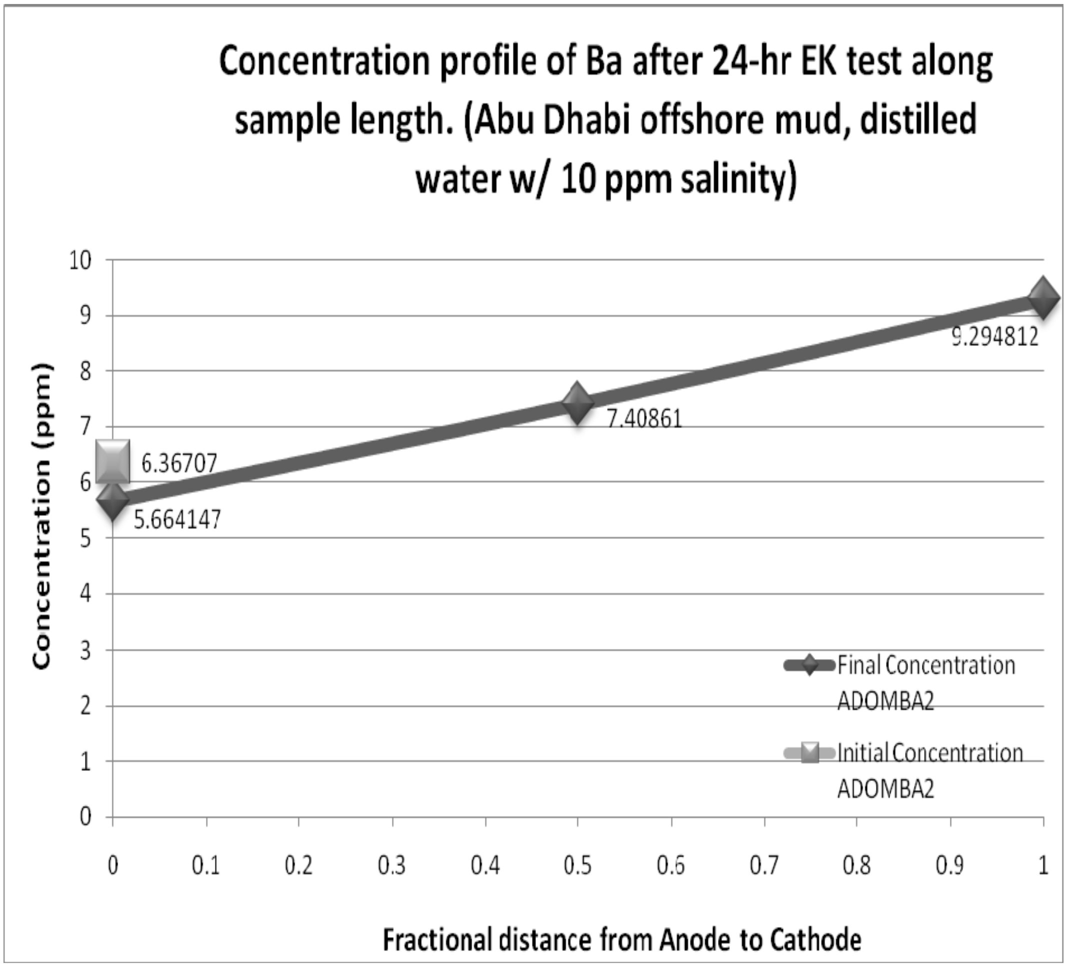

Figure 4-31: Concentration profile of Ba after 24-hr EK test a long sample length (Abu Dhabi offshore mud, distilled water 10 ppm salinity).

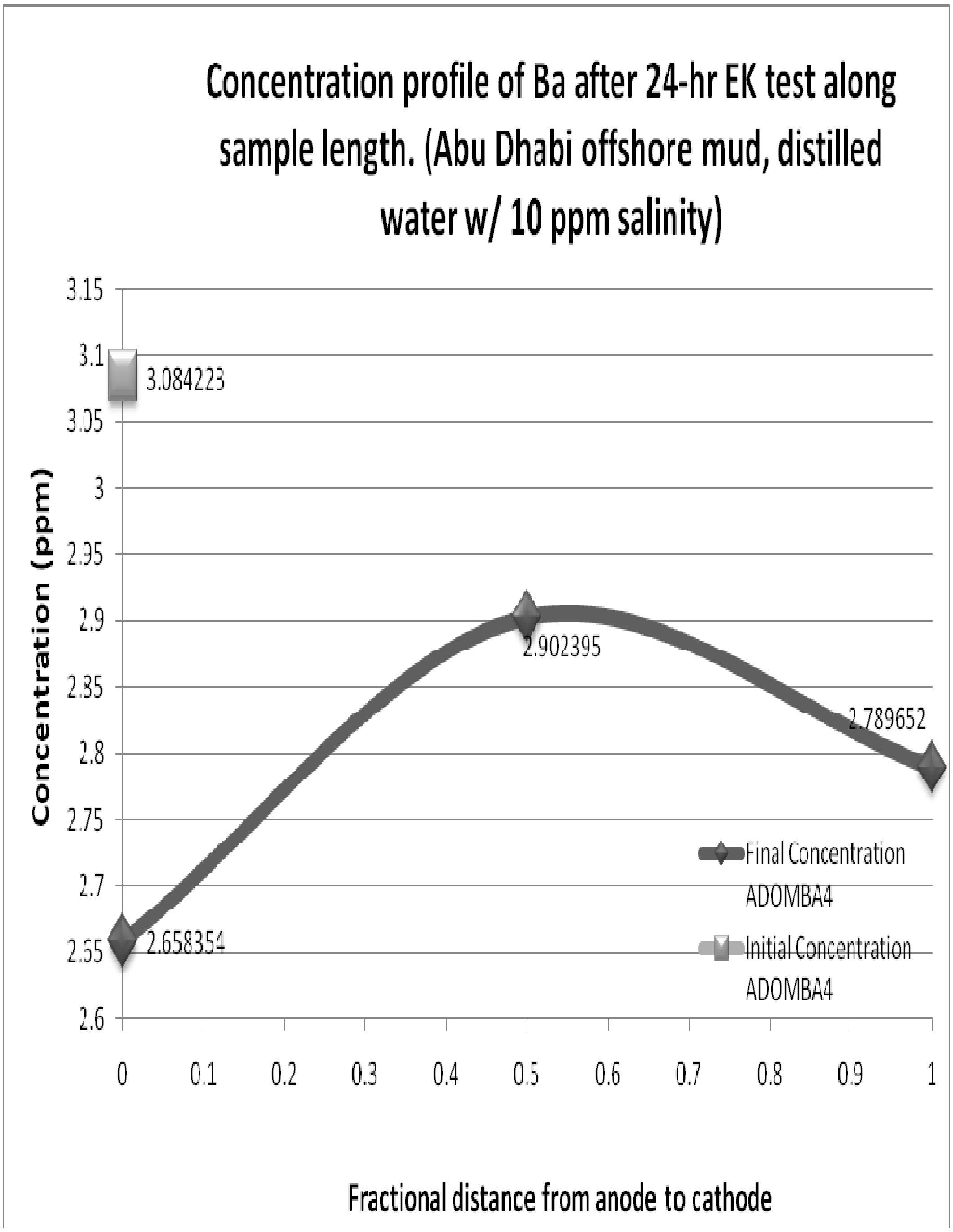

Figure 4-32: Concentration profile of Ba after 24-hr EK test a long sample length (Abu Dhabi offshore mud, distilled water 10 ppm salinity).

Barium: Sample RICOMSWPHBA3 in Figure 4-33 using Abu Dhabi seawater with 26,000 ppm salinity and 450 ppm maleic acid

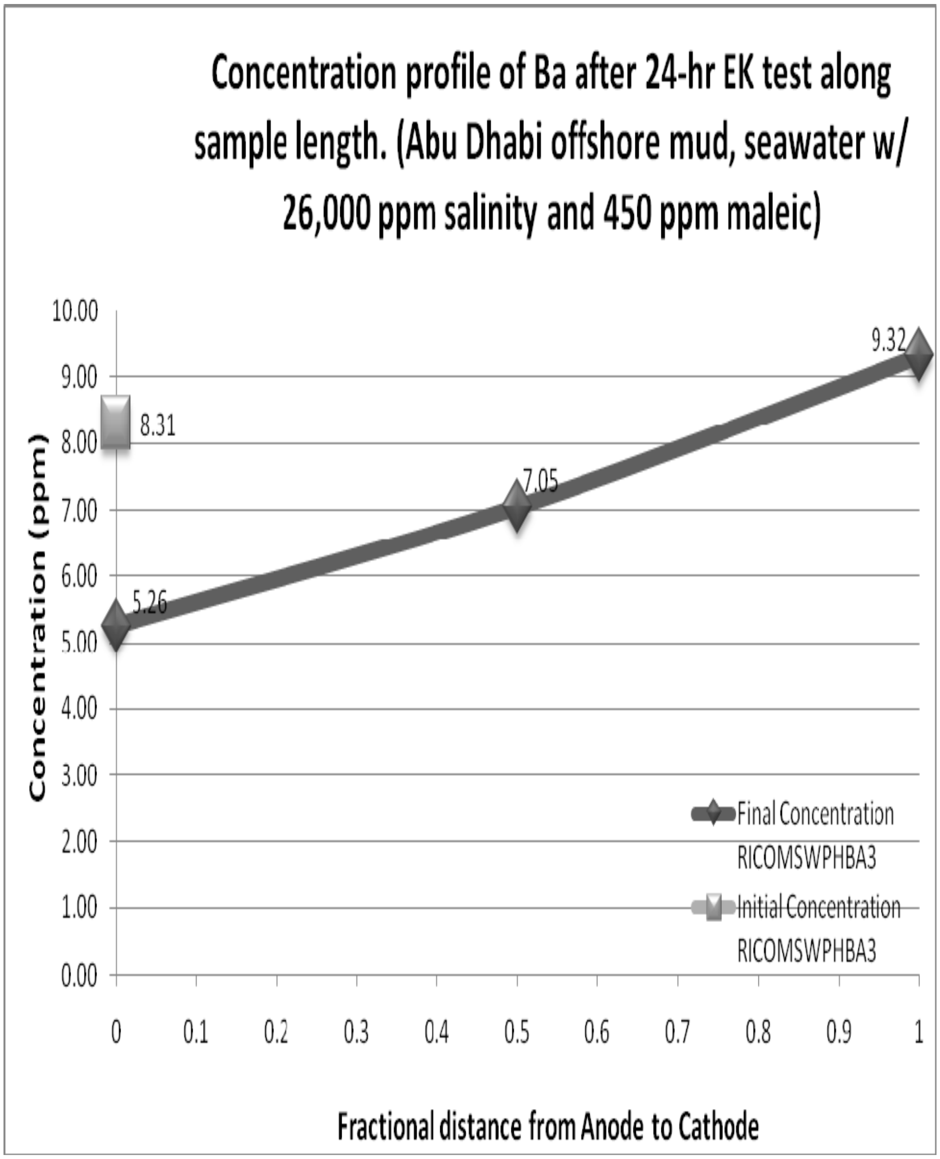

Figure 4-33: Concentration profile of Ba after 24-hr EK test a long sample length. (Abu Dhabi offshore mud, 26,000 ppm salinity & 450 ppm maleic acid)

Beryllium.

Figures 4-34 through 4-37 show the fraction of the beryllium found at three locations: anode side, center and cathode end of tested core after 24 hours of electrokinetic treatment. The initial concentrations were predetermined at the anode end of the contaminated offshore mud sample. The removal efficiency was calculated at the anode using equation 4-1 for all results obtained. After 24 hours, substantial reduction of beryllium from its initial concentration at the anode region using distilled water with 10 ppm salinity, was found to be 8.66, 22.16 and 23.77% as shown in Figures 4-34 through 4-36 respectively. Beryllium is a cation which carries three positive charges.

Electrokinetics was the main driving force of the Be ion in the direction of the water flow. There was accumulation of metal at the discharge end (cathode end of the mud sample) as can be seen in Figure 4-35 and 4-36. The shape of the curve in Figure 4-34 can be explained by the lack of pH control.

Figure 4-37 shows the results conducted with Abu Dhabi seawater having 26,000 ppm salinity, as well as 450 ppm of maleic acid added for pH control. The migration pattern was similar to that of Figure 4-34, through 4-36, however, the maximum removal efficiency of beryllium after 24 hours at the anode region here 27.82% as opposed to the 23.77%. This finding was interesting as it confirmed that the presense of both high salinity and pH control mechanism influenced all the samples tested here to consistently show higher removal efiiciencies at all the three locations analyzed. As you can see the bell shaped curve of figure 4-34, was eliminated here due to the pH control. The high salinity caused a higher conductivity in the bulk solution, where both the current and electrokinetic flow increased several fold. One explanation for this is that the

electromigration force is now a dominat force allowing the ionic mobility to travel at 2-3 times faster than in the case of dominant electroosmosis, while another theory is the abundance of large volumes of cations in this high salinity carrying their waters of hydration further promoting ionic species velocity. This needs to be investigated further.

Beryllium: 4, 5, R3 samples in Figure 4-34 through 4-36 using Distilled water with 10 ppm salinity

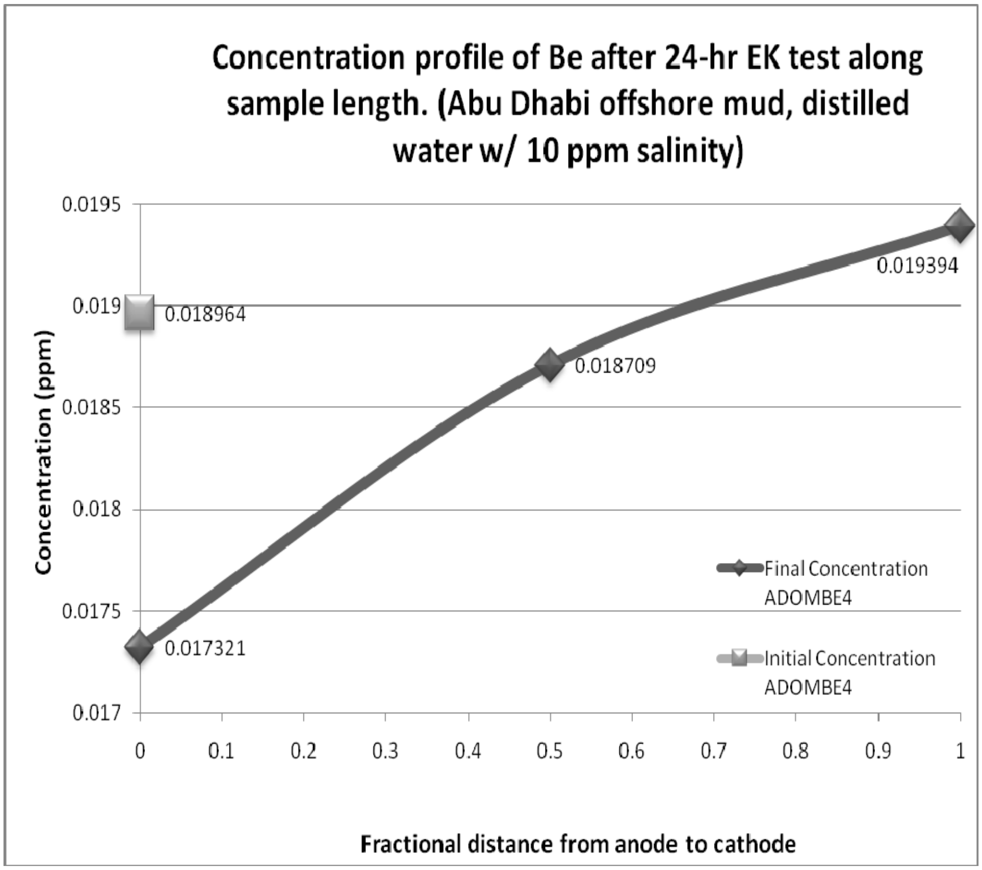

Figure 4-34: Concentration profile of Be after 24-hr EK test a long sample length (Abu Dhabi offshore mud, distilled water 10 ppm salinity).

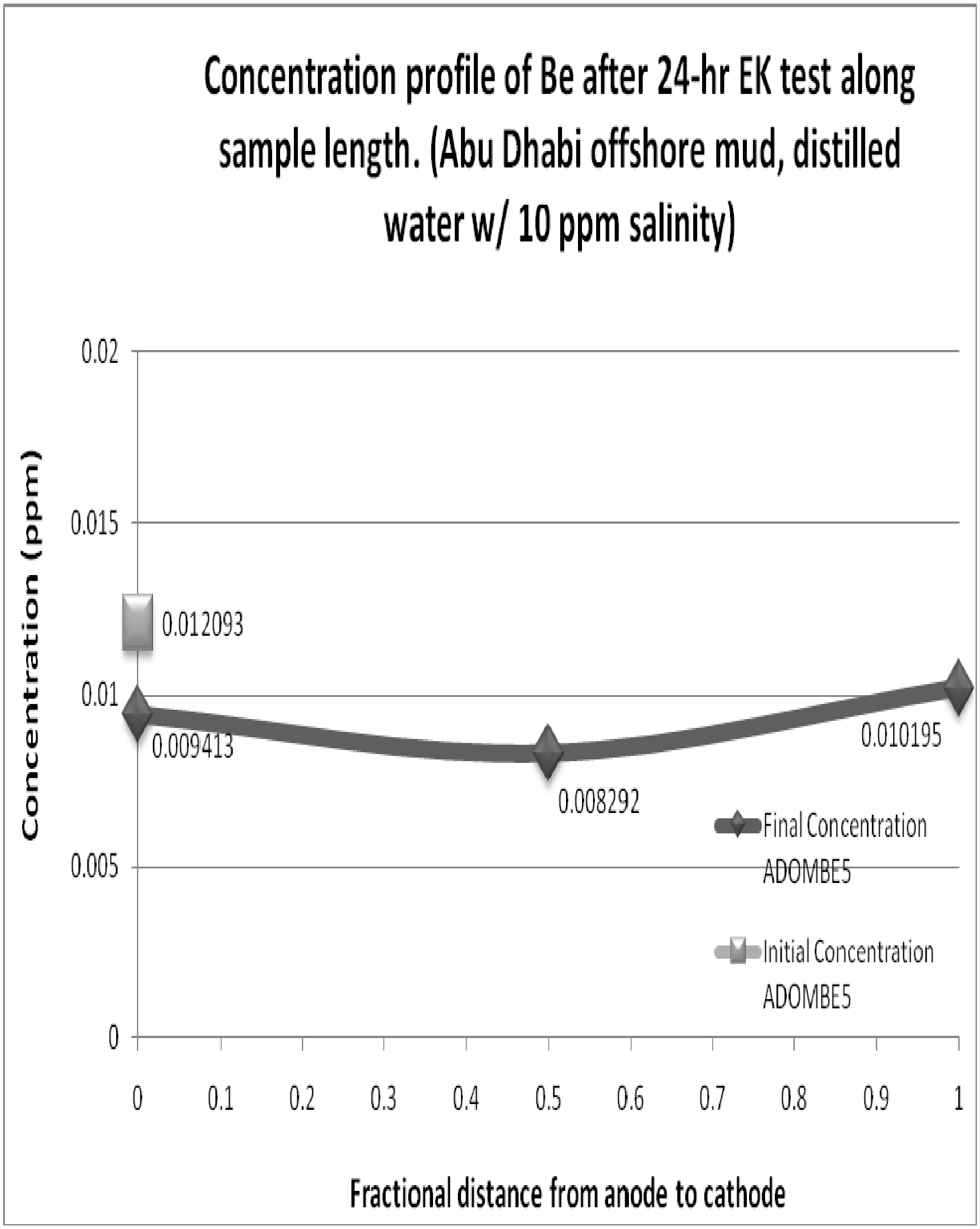

Figure 4-35: Concentration profile of Be after 24-hr EK test a long sample length (Abu Dhabi offshore mud, distilled water 10 ppm salinity).

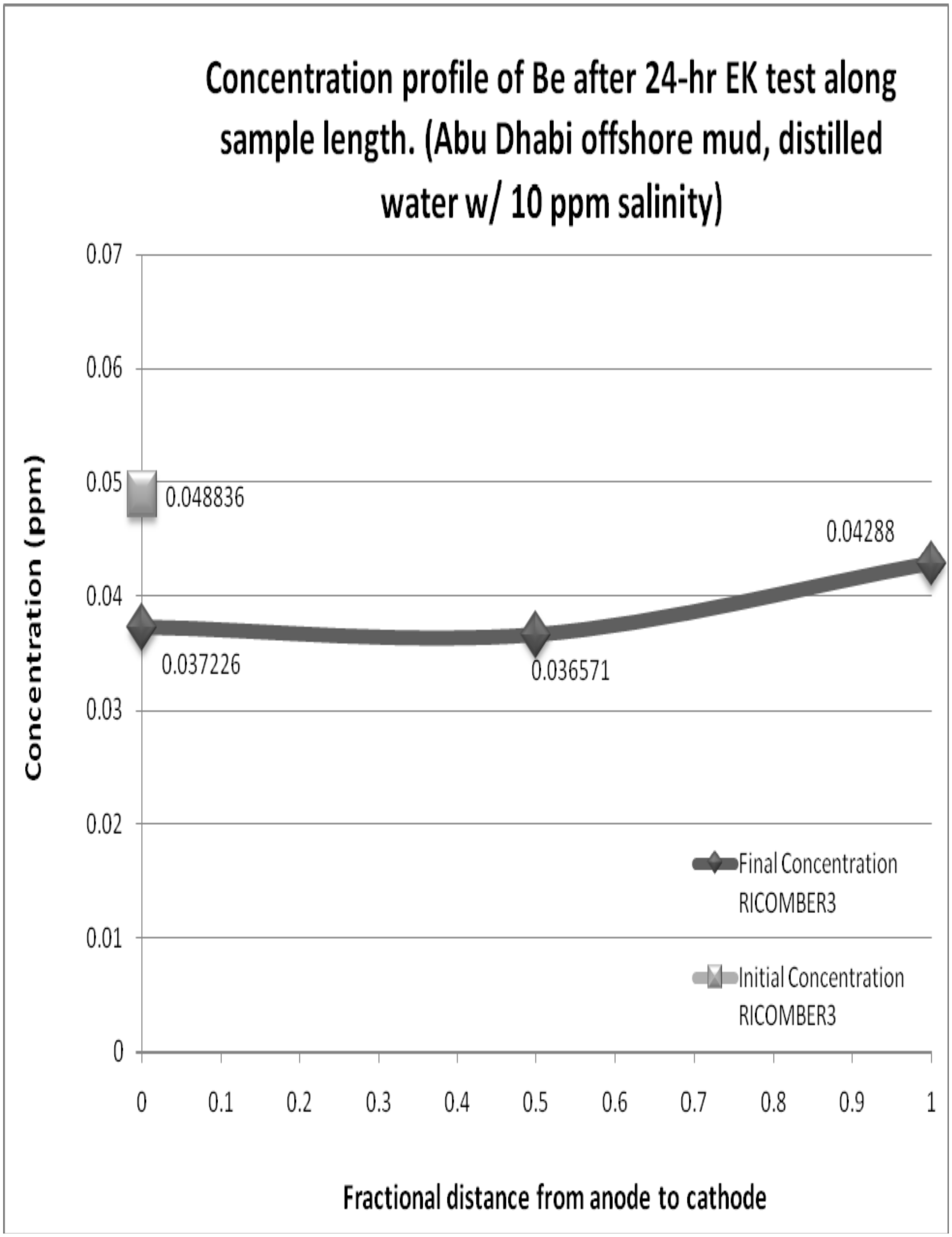

Figure 4-36: Concentration profile of Be after 24-hr EK test a long sample length (Abu Dhabi offshore mud, distilled water 10 ppm salinity).

Berellium: Sample RICOMSWPHBE2 in Figure 4-37 using Abu Dhabi seawater with 26,000 ppm salinity and 450 ppm maleic acid

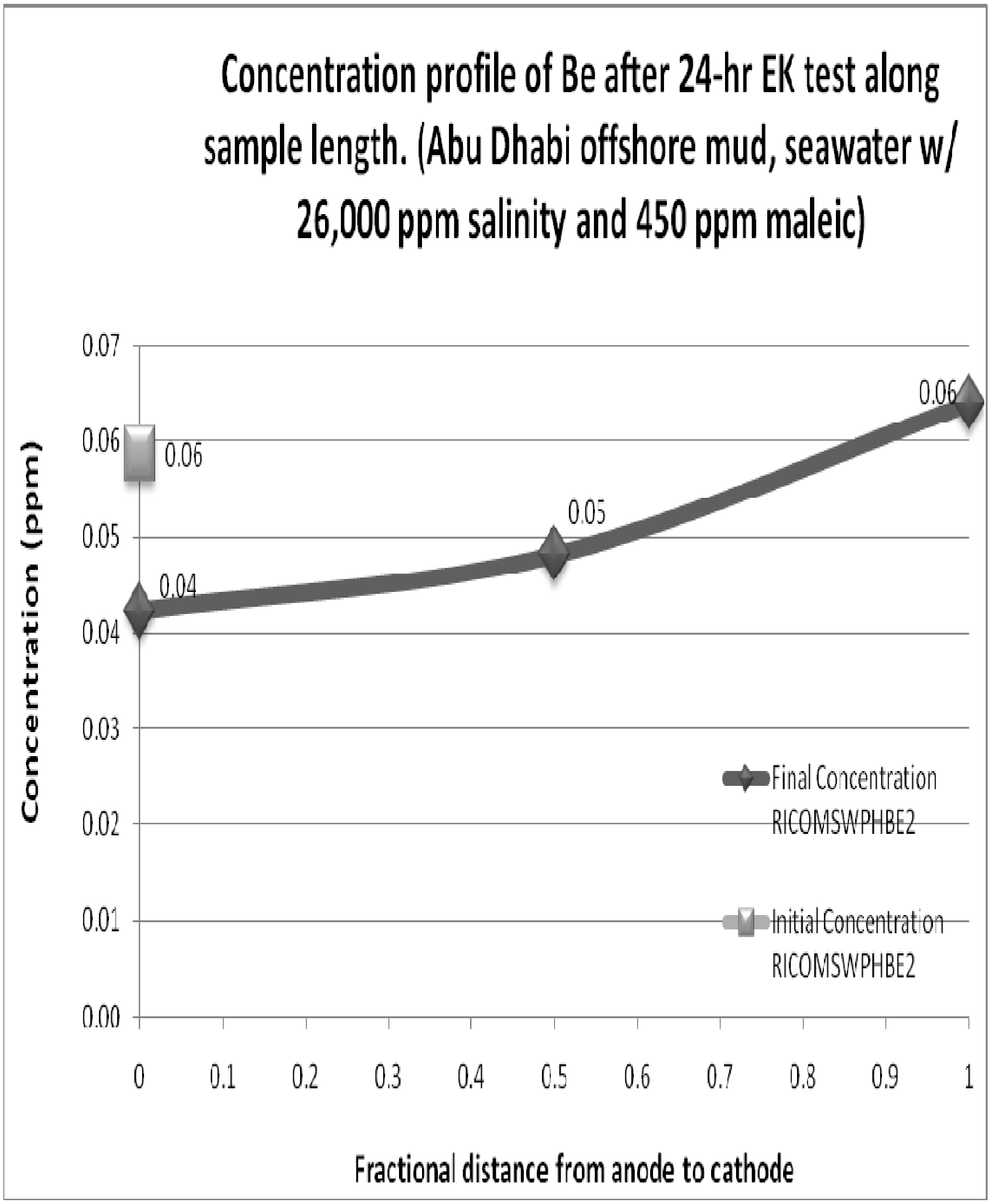

Figure 4-37: Concentration profile of Be after 24-hr EK test a long sample length. (Abu Dhabi offshore mud, 26,000 ppm salinity & 450 ppm maleic acid)

Bismuth: Figures 4-38 through 4-40 show the fraction of the bismuth found at three locations: anode side, center and cathode end of tested core after 24 hours of electrokinetic treatment. The initial concentrations were predetermined at the anode end of the contaminated offshore mud sample. The removal efficiency was calculated at the anode using equation 4-1 for all results obtained. After 24 hours, substantial reduction of bismuth from its initial concentration at the anode region using distilled water with 10 ppm salinity, was found to be 12.75 and 40.06% as shown in Figures 4-38 through 4-39 respectively. after 24 hours. Electrokinetics was the main driving force of the Bi ion in the direction of the water flow. There was accumulation of metal at the discharge end as shown in both figure 4-35 and 4-36 (cathode end of the mud sample) as can be seen in Figure 4-38 and 4-39.

Figure 4-40 shows the results conducted with Abu Dhabi seawater having 26,000 ppm salinity, as well as 450 ppm of maleic acid added for pH control. The migration pattern was similar to that of Figure 4-38, through 4-39, however, the maximum removal efficiency of bismuth after 24 hours at the anode region here 28.94% as opposed to the 40.06%, however consistency was achieved using the seawater and pH control, where the lowest removal efficiency recored at the anode here was 21.93 as opposed to 12.75% as shown in Figure 4-39. This finding was interesting as it confirmed that the presense of both high salinity and pH control mechanism influenced all the samples tested here to consistently show higher removal efiiciencies at all the three locations analyzed. The high salinity caused a higher conductivity in the bulk solution, where both the current and electrokinetic flow increased several fold. One explanation for this is that the

electromigration force is now a dominat force allowing the ionic mobility to travel at 2-3 times faster than in the case of dominant electroosmosis, while another theory is the abundance of large volumes of cations in this high salinity carrying their waters of hydration further promoting ionic species velocity. This needs to be investigated further.

Bismuth: 3, R3 samples in Figure 4-38 through 4-40 using Distilled water with 10 ppm salinity

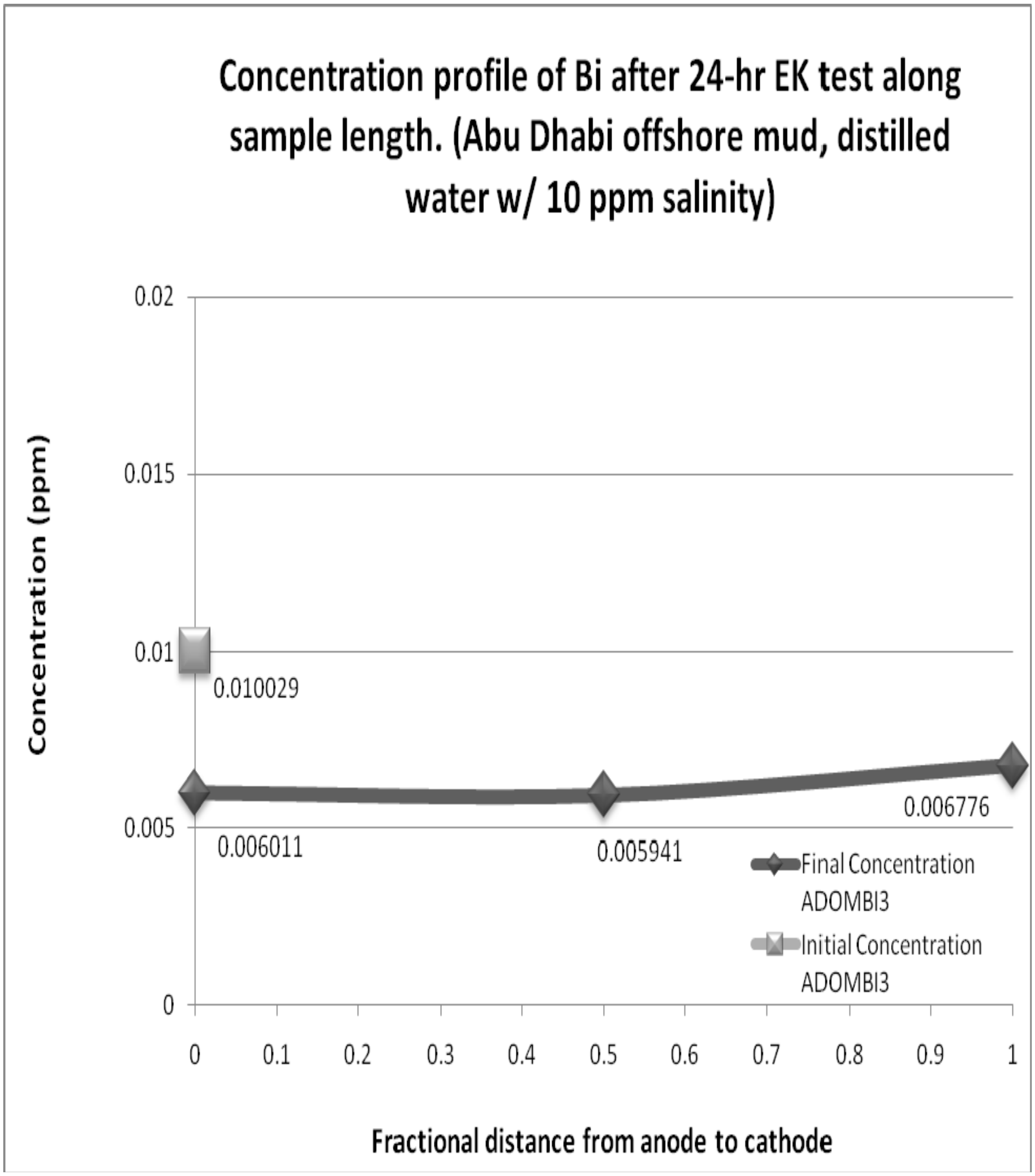

Figure 4-38: Concentration profile of Bi after 24-hr EK test a long sample length (Abu Dhabi offshore mud, distilled water 10 ppm salinity).

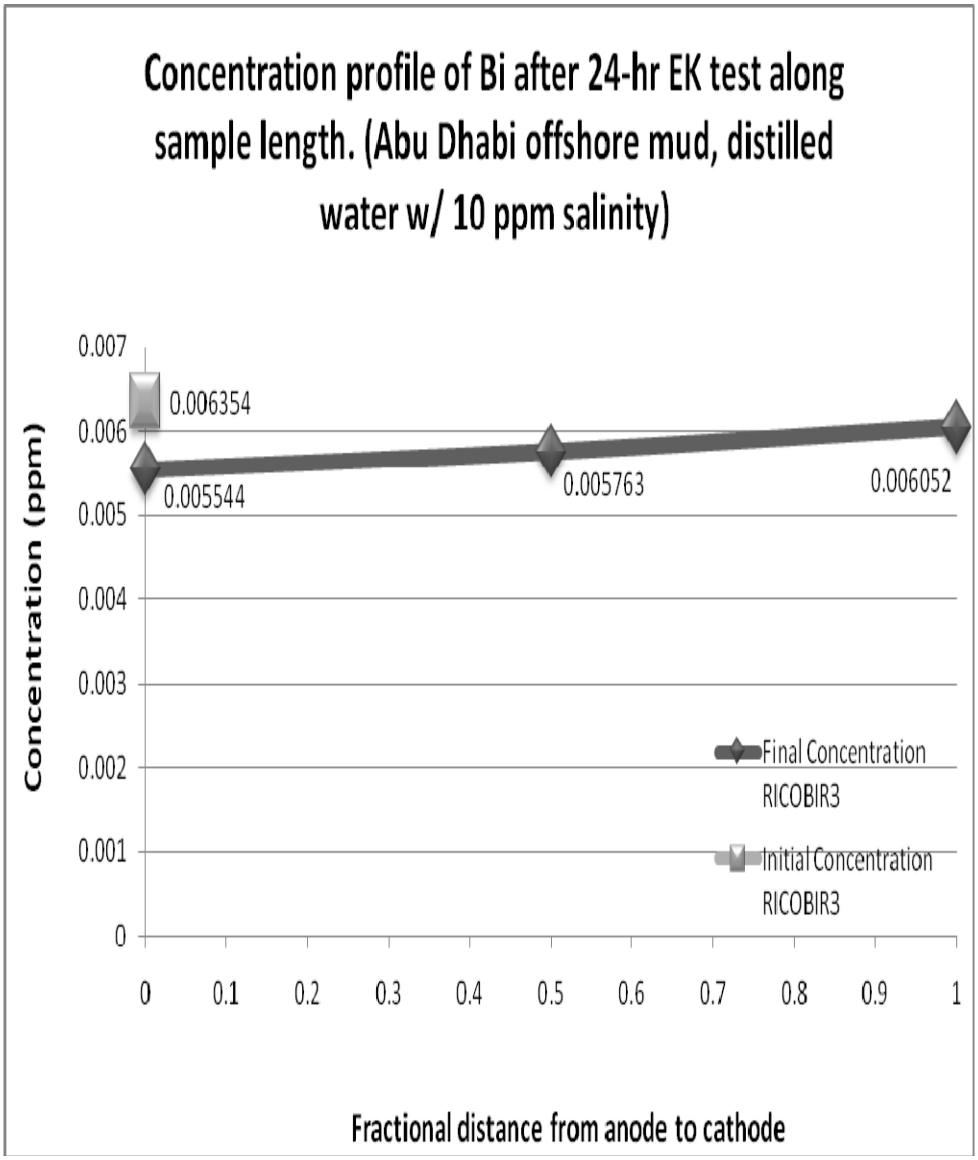

Figure 4-39: Concentration profile of Bi after 24-hr EK test a long sample length (Abu Dhabi offshore mud, distilled water 10 ppm salinity).

Bismuth: Samples RICOMSWPHBI1 in Figure 4-40 using Abu Dhabi seawater with 26,000 ppm salinity and 450 ppm maleic acid

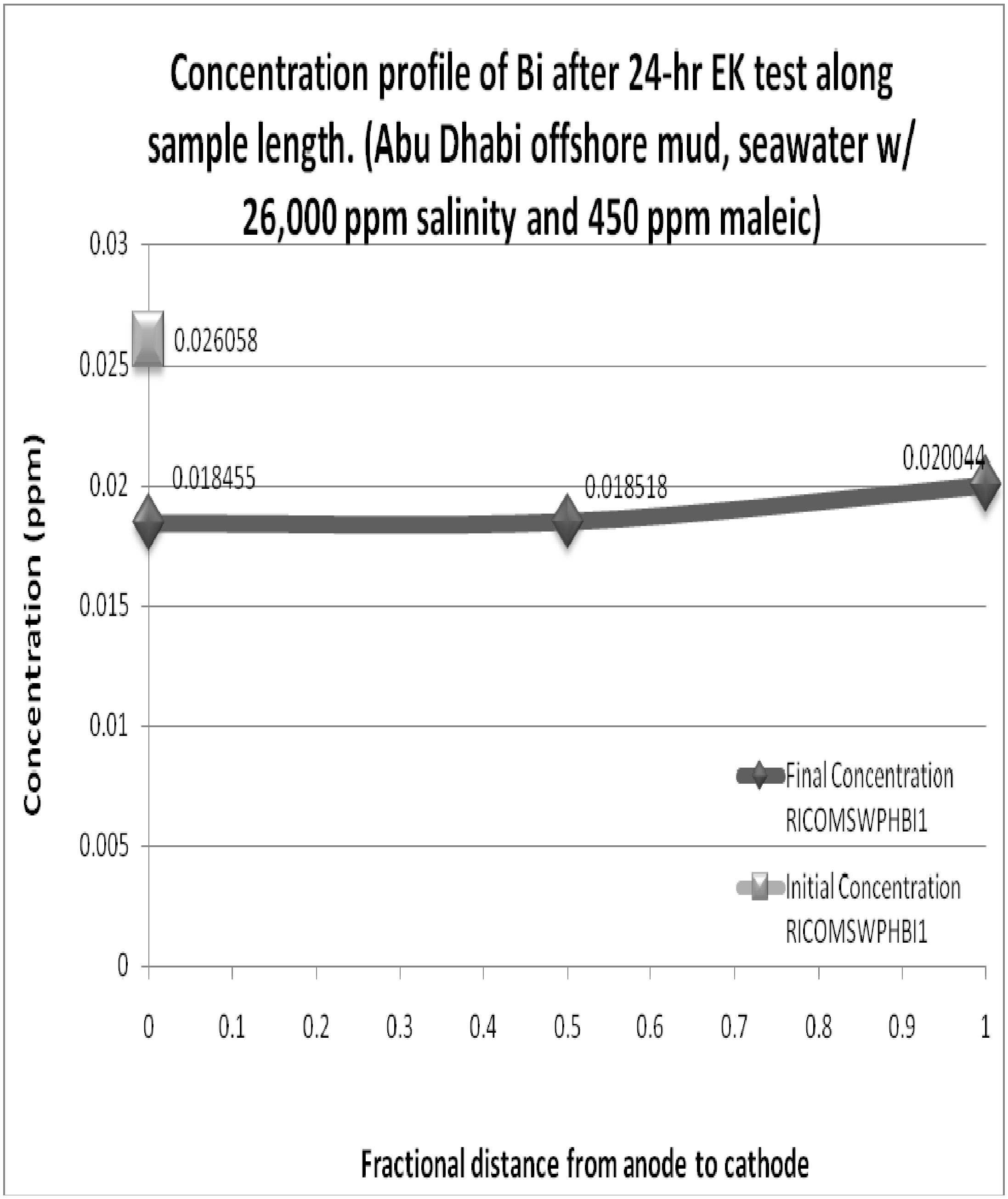

Figure 4-40: Concentration profile of Bi after 24-hr EK test a long sample length. (Abu Dhabi offshore mud, 26,000 ppm salinity & 450 ppm maleic acid)

Cadmium: Figures 4-41 through 4-44 show the fraction of cadmium found at three locations in the tested offshore mud specimens after the 24 hours of electrokinetic treatment. Being a divalent cationic species, cadmium exhibited a migration path toward the cathode. The maximum cadmium accumulation was recorded at the cathode region. This is attributed to the increase in the hydrolysis with an increased pH at the cathode end due to the electrode reactions triggered. Until around Ph 8, Cd remains in its divalent cationic form. Beyond this value it starts forming complex species which are either positively, negatively charged or neutral. The tendency and the abundance of these products control the removal rate until the acid front reaches the cathode region in the mud. However, the with the high pH prevailing at the clay-water interface of the cathode end of the mud, a thin layer of precipitate would form at the interface making it difficult for cadmium to be removed out of the cathode end of the mud. There is also an increase in mud adsorption capacity with increasing pH which would contribute to the accumulation of the metal in this region (Sposito, 1984; Basta and Tabatai, 1992; Pamukcu 1993). The initial concentrations were predetermined at the anode end of the contaminated offshore mud sample. The removal efficiency was calculated at the anode using equation 4-1 for all results obtained. After 24 hours, substantial reduction of Cd from its initial concentration at the anode region using distilled water with 10 ppm salinity, was found to be 31.7, 24.91, 8.74 and 12.40% as shown in Figures 4-41 through 4-44 respectively. Electrokinetics was the main driving force of the Cd ion in the direction of the water flow. There was accumulation of metal at the discharge end (cathode end of the mud sample) as can be seen in Figure 4-42 through 4-44. The shape of the curve in Figures 4-42 through 4-44 can be explained by the lack of pH control.

Cadmium: 2, 3, 5, R3 samples in Figure 4-41 through 4-44 using Distilled water with 10 ppm salinity

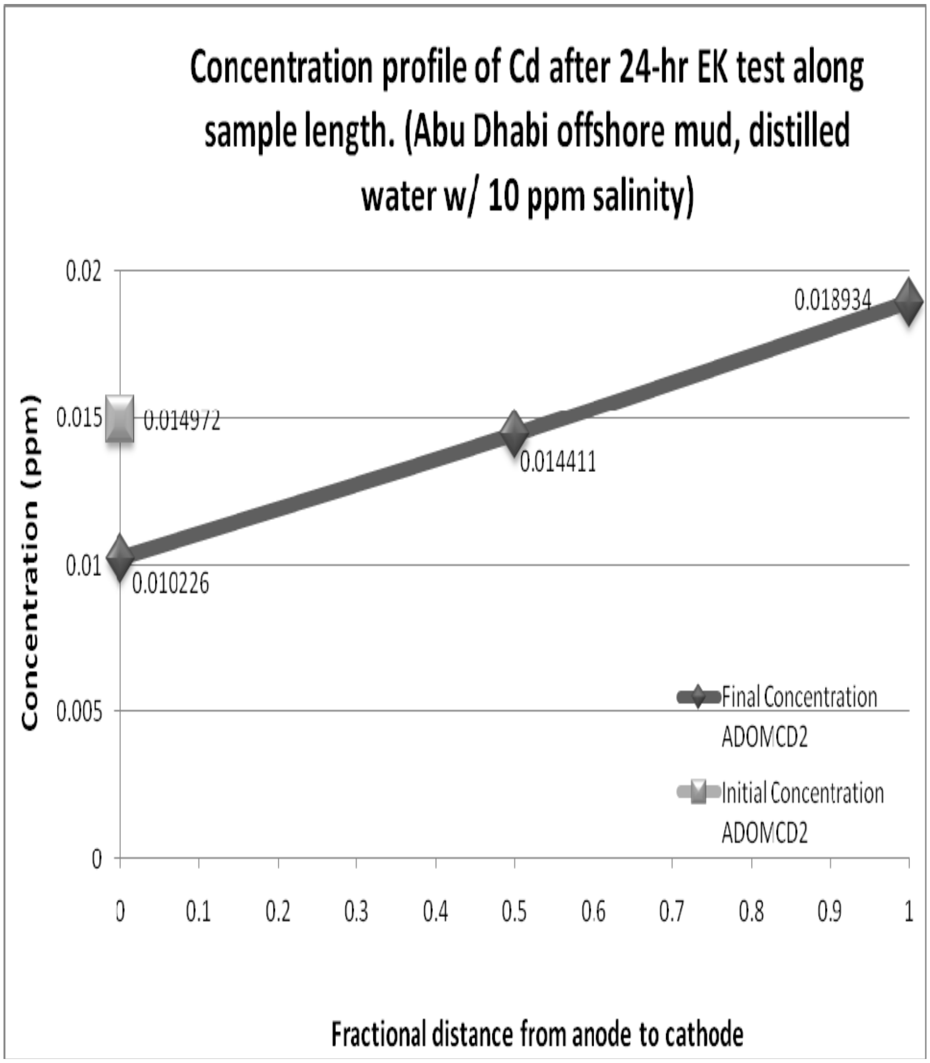

Figure 4-41: Concentration profile of Cd after 24-hr EK test a long sample length (Abu Dhabi offshore mud, distilled water 10 ppm salinity).

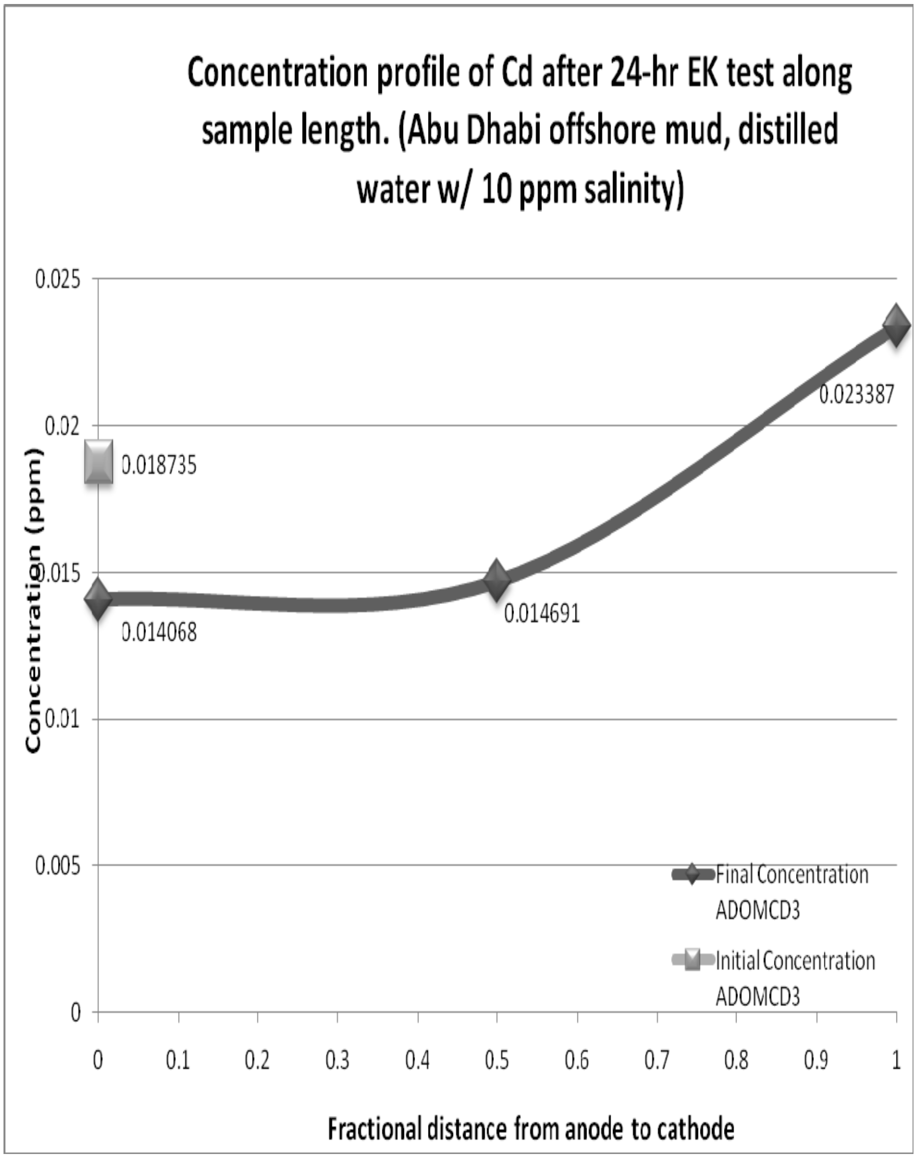

Figure 4-42: Concentration profile of Cd after 24-hr EK test a long sample length (Abu Dhabi offshore mud, distilled water 10 ppm salinity).

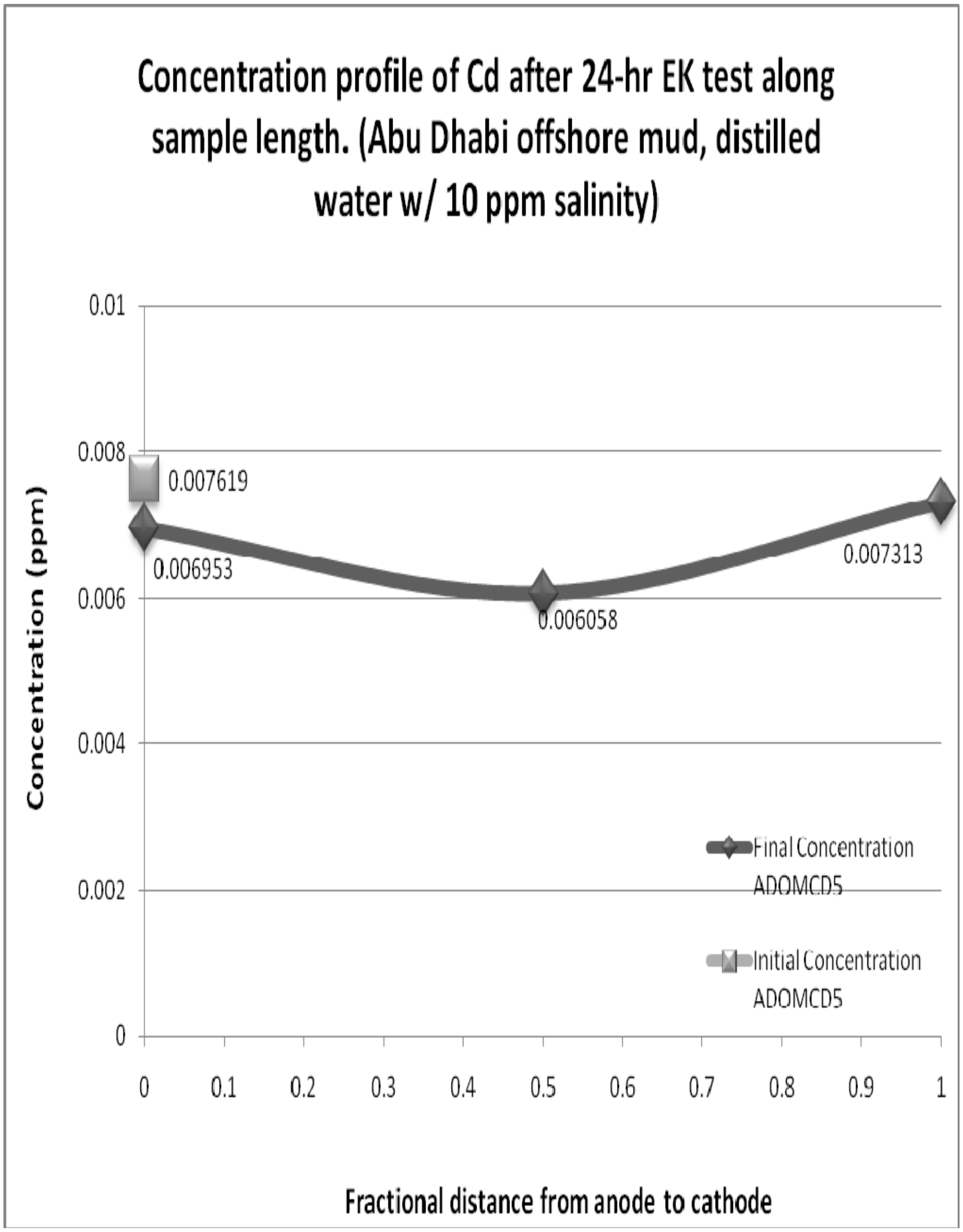

Figure 4-43: Concentration profile of Cd after 24-hr EK test a long sample length (Abu Dhabi offshore mud, distilled water 10 ppm salinity).

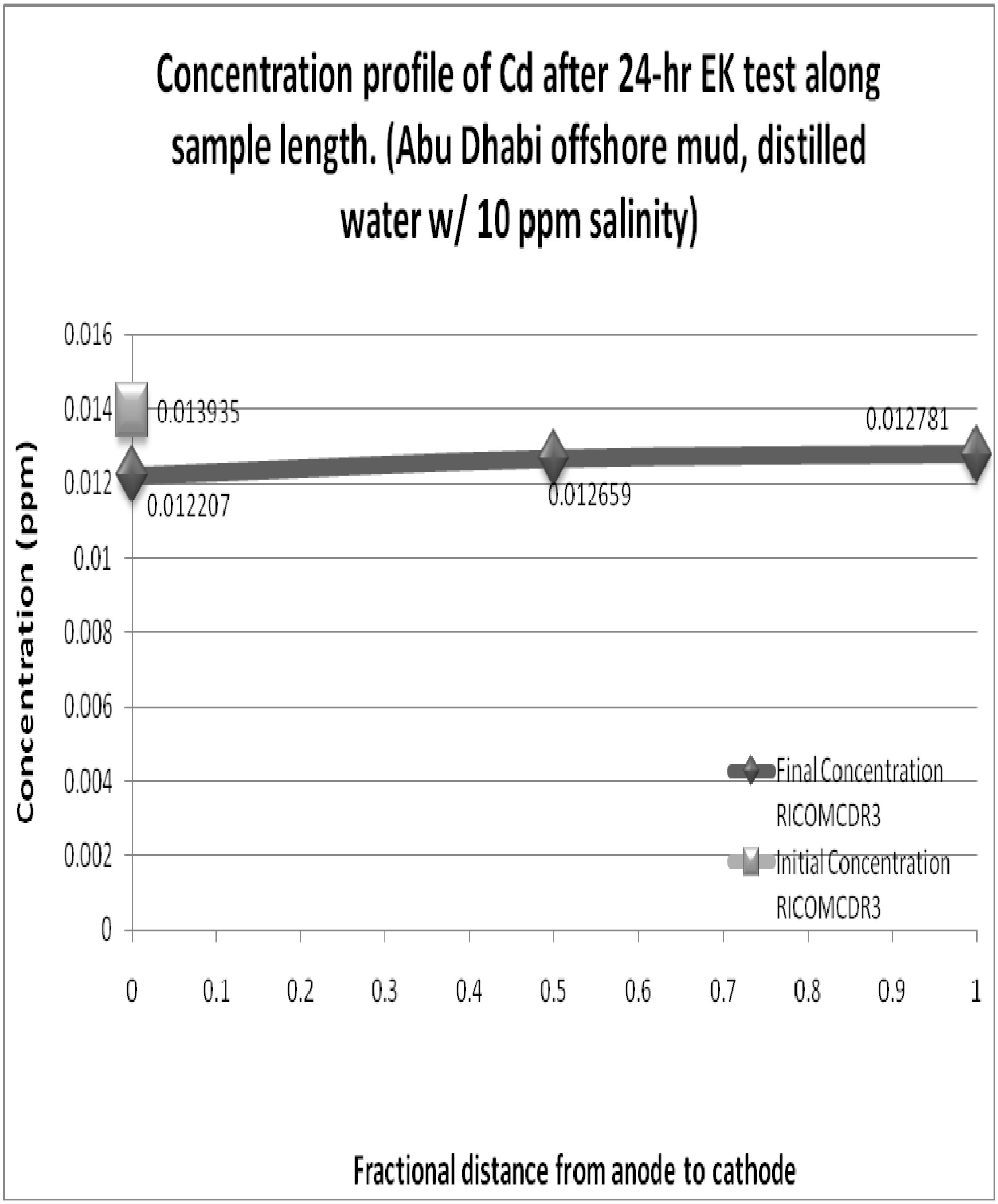

Figure 4-44: Concentration profile of Cd after 24-hr EK test a long sample length (Abu Dhabi offshore mud, distilled water 10 ppm salinity).

Cesium: Cesium is a monovalent cation which strongly exchanges with most clays. During the short term test, more than 16.17% was transported out of the anode region towards the cathode chamber of the offshore mud cores after 24 hours of electrokinetic treatment. This is illustrated in figures 4-45 similar results observed with cesium as with strontium. The initial concentrations were predetermined at the anode end of the contaminated offshore mud sample. The removal efficiency was calculated at the anode using equation 4-1 for all results obtained. In the Cs case, the migration rate of the metal appeared to be slower, perhaps due to the larger ionic atmosphere of Cs which would promote lower electromigration velocity. Also, the affinity of the clay to Cs may have contributed to the delayed response. Electrokinetics was the main driving force of the Cs ion in the direction of the water flow. There was accumulation of metal at the discharge end as shown in both figure 4-45 (cathode end of the mud sample).

A significant fraction of the cesium was removed to the cathode water chamber in the offshore mud sample by use of the electroosmotically permeated water that included the 26,000 ppm salinity seawater with pH control mechanism consisting of 450 ppm of maleic acid through the anode chamber. Here a maximum removal efficiency of 31.45% as opposed to 16.18% was achieved. This result demonstrates the high affinity of the acid solution to cesium and its potential as an effective chelating agent to mobilize the cesium from the offshore muds. Electrokinetics was the main driving force of the Cs ion in the direction of the water flow. There was accumulation of metal at the discharge end (cathode end of the mud sample). The shape of the curve can be explained by the lack of pH control. (Pamukcu et al., 1993).

This finding was interesting as it confirmed that the presense of both high salinity and pH control mechanism influenced all the samples tested here to consistently show higher removal efiiciencies at all the three locations analyzed. The high salinity caused a higher conductivity in the bulk solution, where both the current and electrokinetic flow increased several fold. One explanation for this is that the electromigration force is now a dominat force allowing the ionic mobility to travel at 2-3 times faster than in the case of dominant electroosmosis, while another theory is the abundance of large volumes of cations in this high salinity carrying their waters of hydration further promoting ionic species velocity. This needs to be investigated further.

Cesium: R3 samples in Figure 4-45 using Distilled water with 10 ppm salinity

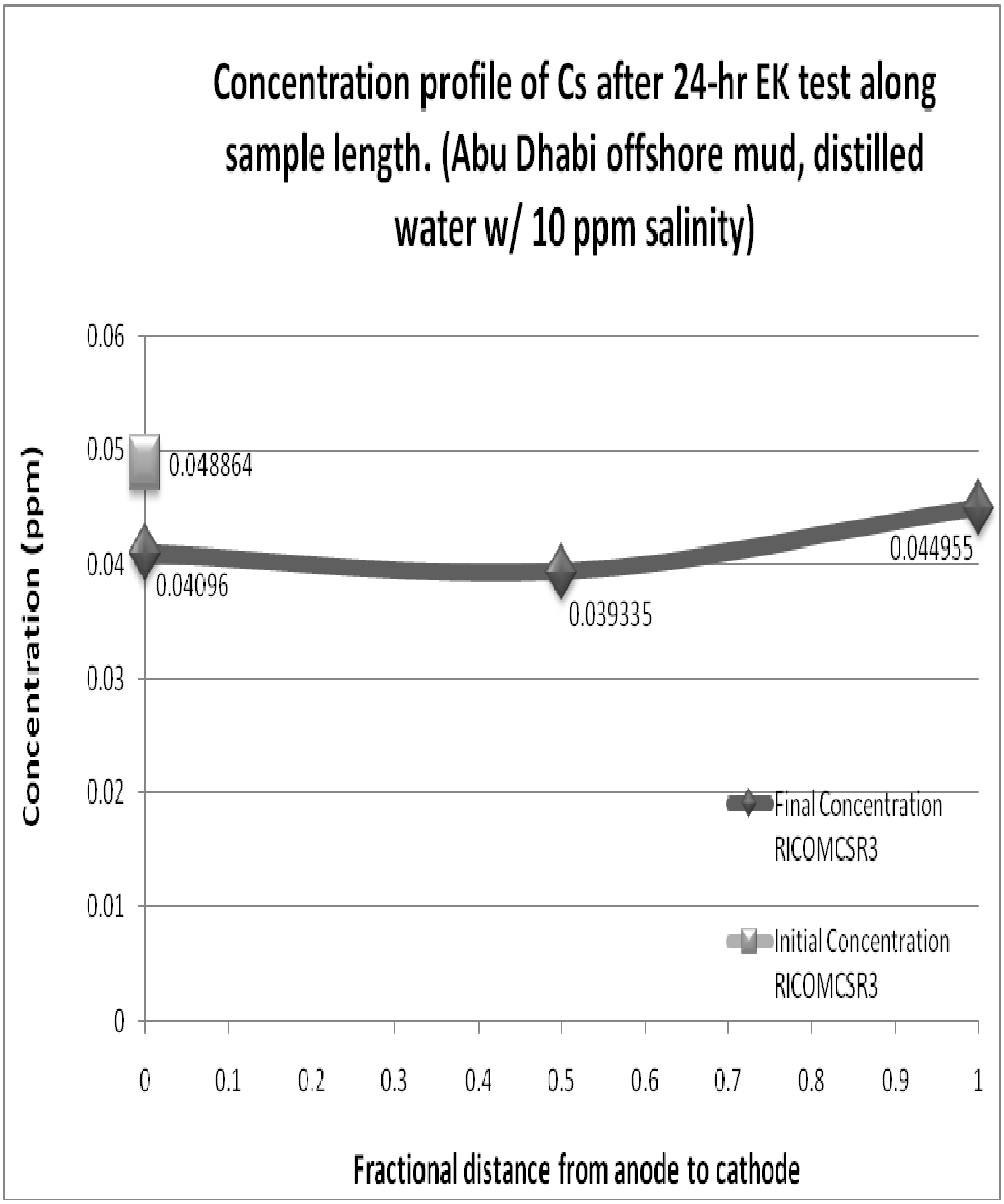

Figure 4-45: Concentration profile of Cs after 24-hr EK test a long sample length (Abu Dhabi offshore mud, distilled water 10 ppm salinity).

Cesium: Samples RICOMSWPHCS1 in Figure 4-46 using Abu Dhabi seawater with 26,000 ppm salinity and 450 ppm maleic acid

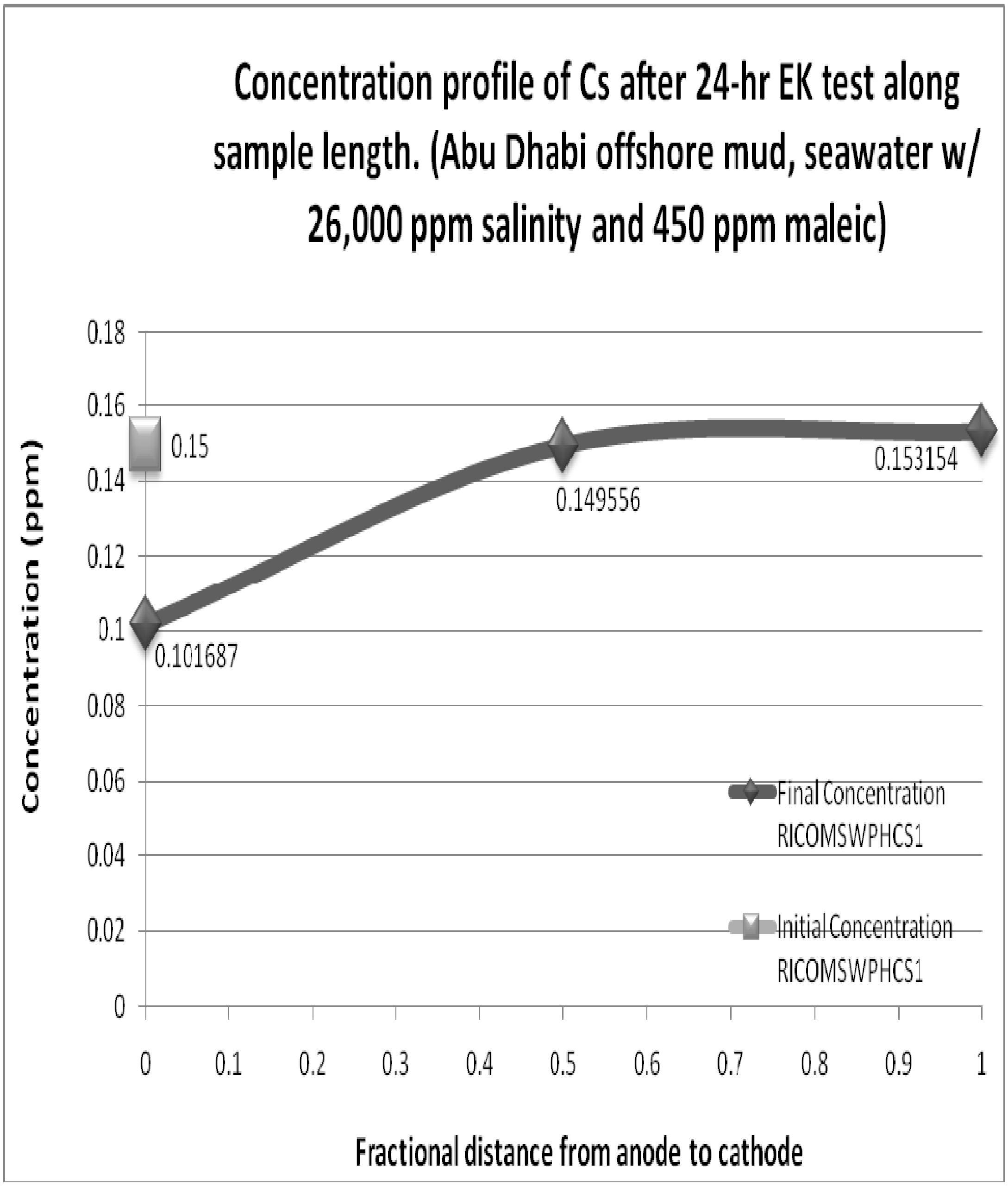

Figure 4-46: Concentration profile of Cs after 24-hr EK test a long sample length. (Abu Dhabi offshore mud, 26,000 ppm salinity & 450 ppm maleic acid)

Chromium: Figures 4-47 through 4-48 show the fraction of the Chromium found at three locations: anode side, center and cathode end of tested core after 24 hours of electrokinetic treatment. The initial concentrations were predetermined at the anode end of the contaminated offshore mud sample. The removal efficiency was calculated at the anode using equation 4-1 for all results obtained. After 24 hours, substantial reduction of chromium from its initial concentration at the anode region at the anode region using distilled water with 10 ppm salinity, was found to be 15.71 and 22.98% as shown in Figures 4-47 through 4-48 respectively. Electrokinetics was the main driving force of the Cr ion in the direction of the water flow. There was accumulation of metal at the discharge end (cathode end of the mud sample as can be seen in Figure 4-47 through 4-48). The shape of the curve in Figure 4-47 can be explained by the lack of pH control. (Pamukcu et al., 1993).

Chromium: 5, R3 samples in Figure 4-47 through 4-48 using Distilled water with 10 ppm salinity

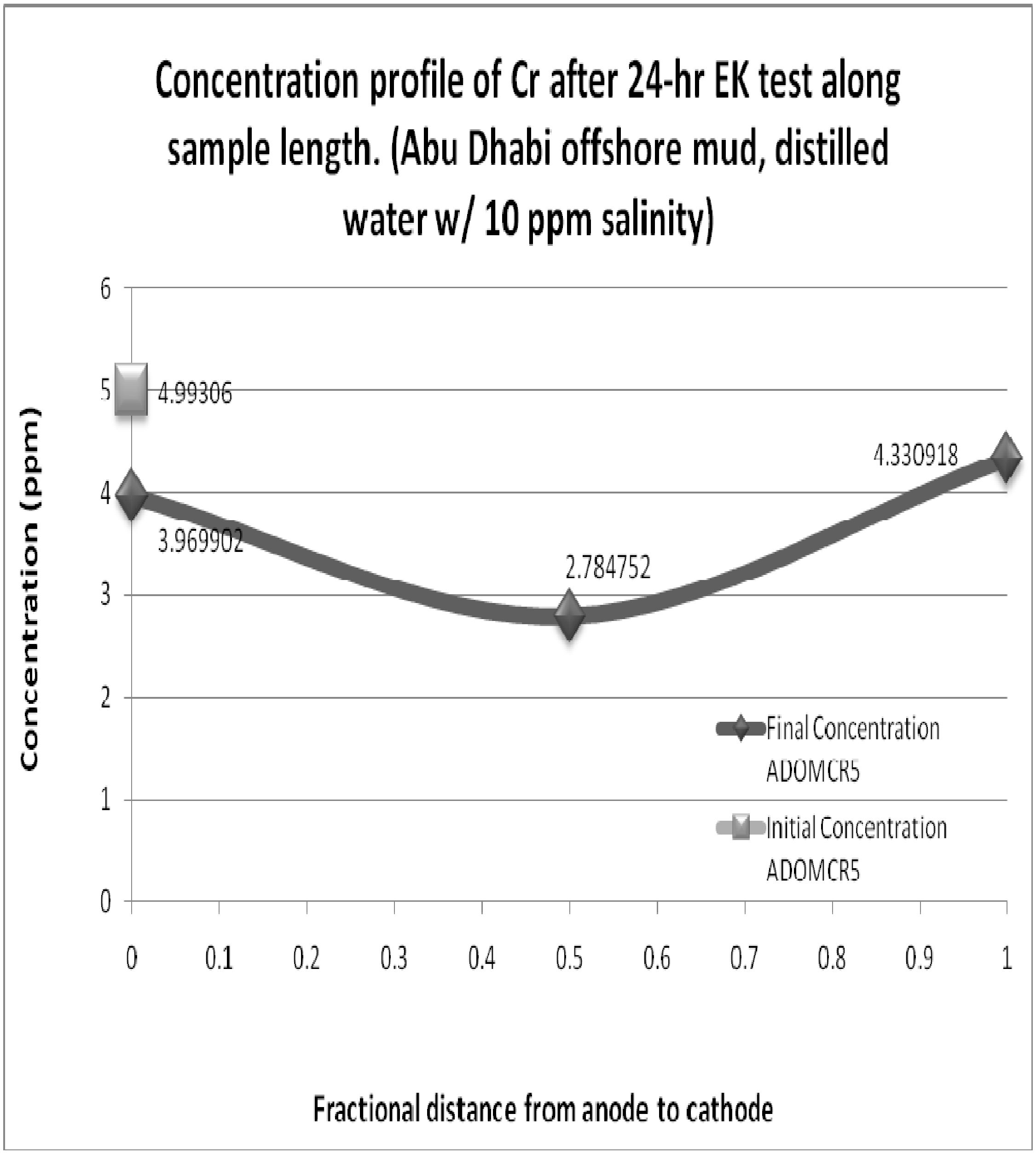

Figure 4-47: Concentration profile of Cr after 24-hr EK test a long sample length (Abu Dhabi offshore mud, distilled water 10 ppm salinity).

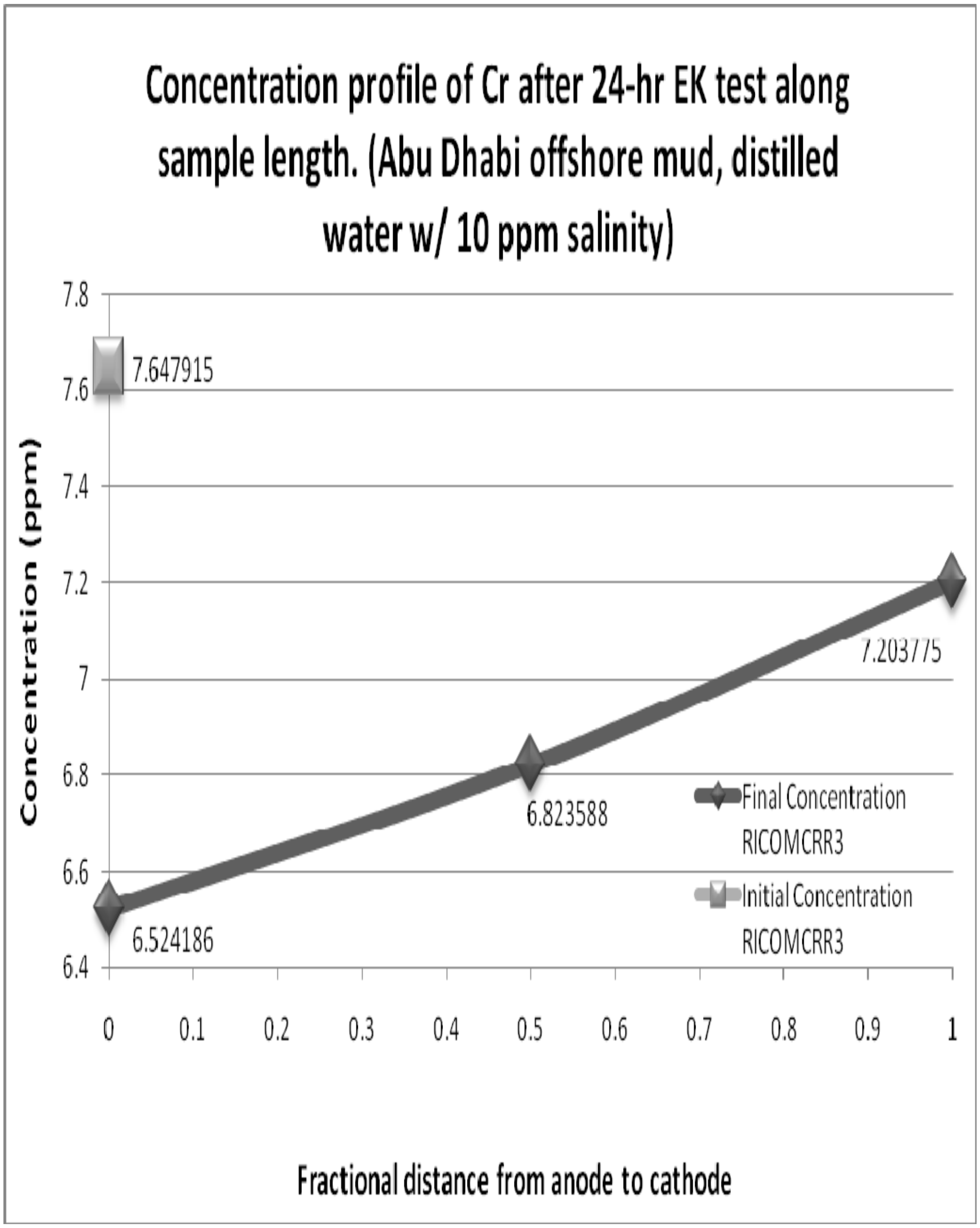

Figure 4-48: Concentration profile of Cr after 24-hr EK test a long sample length (Abu Dhabi offshore mud, distilled water 10 ppm salinity).

Copper: Copper can be present as both a monovalent and a divalent cation in its oxidation states under normal pH conditions. Figures 4-49 through 4-52 show the fraction of the copper found at three locations: anode side, center and cathode end of tested core after 24 hours of electrokinetic treatment. The initial concentrations were predetermined at the anode end of the contaminated offshore mud sample. The removal efficiency was calculated at the anode using equation 4-1 for all results obtained. After 24 hours, substantial reduction of beryllium from its initial concentration at the anode region using distilled water with 10 ppm salinity was found to be 52, 15.90, 9.57 and 37.58% as shown in Figures 4-49 through 4-52 respectively. Copper is a cation which carries two positive charges. Electrokinetics was the main driving force of the Cu ion in the direction of the water flow. There was accumulation of metal at the discharge end (cathode end of the mud sample) as can be seen in Figure 4-50 and 4-51. The shape of the curve in Figure 4-51 and 4-52 can be explained by the lack of pH control.

Figure 4-53 shows the results conducted with Abu Dhabi seawater having 26,000 ppm salinity, as well as 450 ppm of maleic acid added for pH control. The migration pattern was similar to that of Figure 4-50, however, the maximum removal efficiency of copper after 24 hours at the anode region here 26.032% as opposed to the 15.90%. This finding was interesting as it confirmed that the presense of both high salinity and pH control mechanism influenced all the samples tested here to consistently show higher removal efiiciencies at all the three locations analyzed. As you can see the bell shaped curve of figure 4-51 and 4-52, was eliminated here due to the pH control. The high salinity caused a higher conductivity in the bulk solution, where both the current and electrokinetic flow increased several fold. One explanation for this is that the electromigration force is now a dominat force allowing the ionic mobility to travel at 2-3 times faster than in the case of dominant electroosmosis, while another theory is the abundance of large volumes of cations in this high salinity carrying their waters of hydration further promoting ionic species velocity. The different valencies of this species having different electrokinetic velocity (Higher the charge, higher the EK velocity). This needs to be investigated further.

.

Copper: 1, 3, 5, R3 samples in Figure 4-49 through 4-52 using Distilled water with 10 ppm salinity

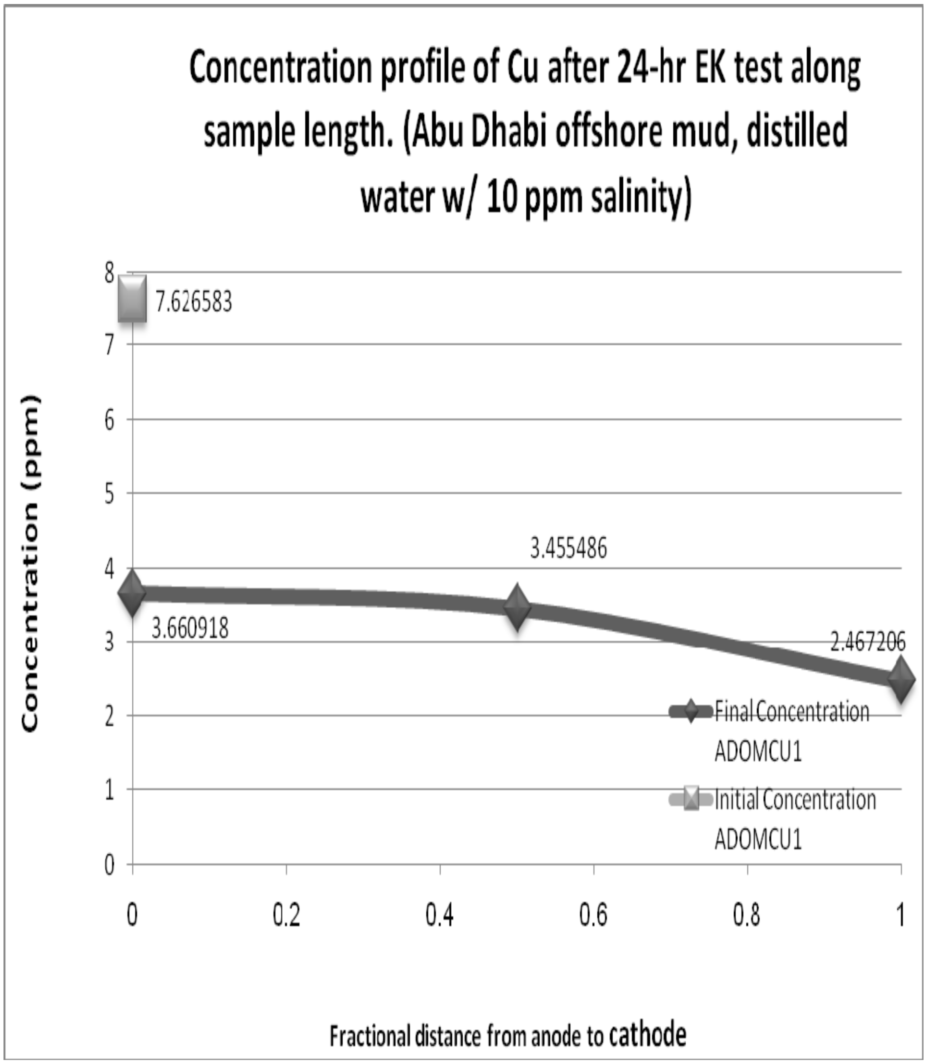

Figure 4-49: Concentration profile of Cu after 24-hr EK test a long sample length (Abu Dhabi offshore mud, distilled water 10 ppm salinity).

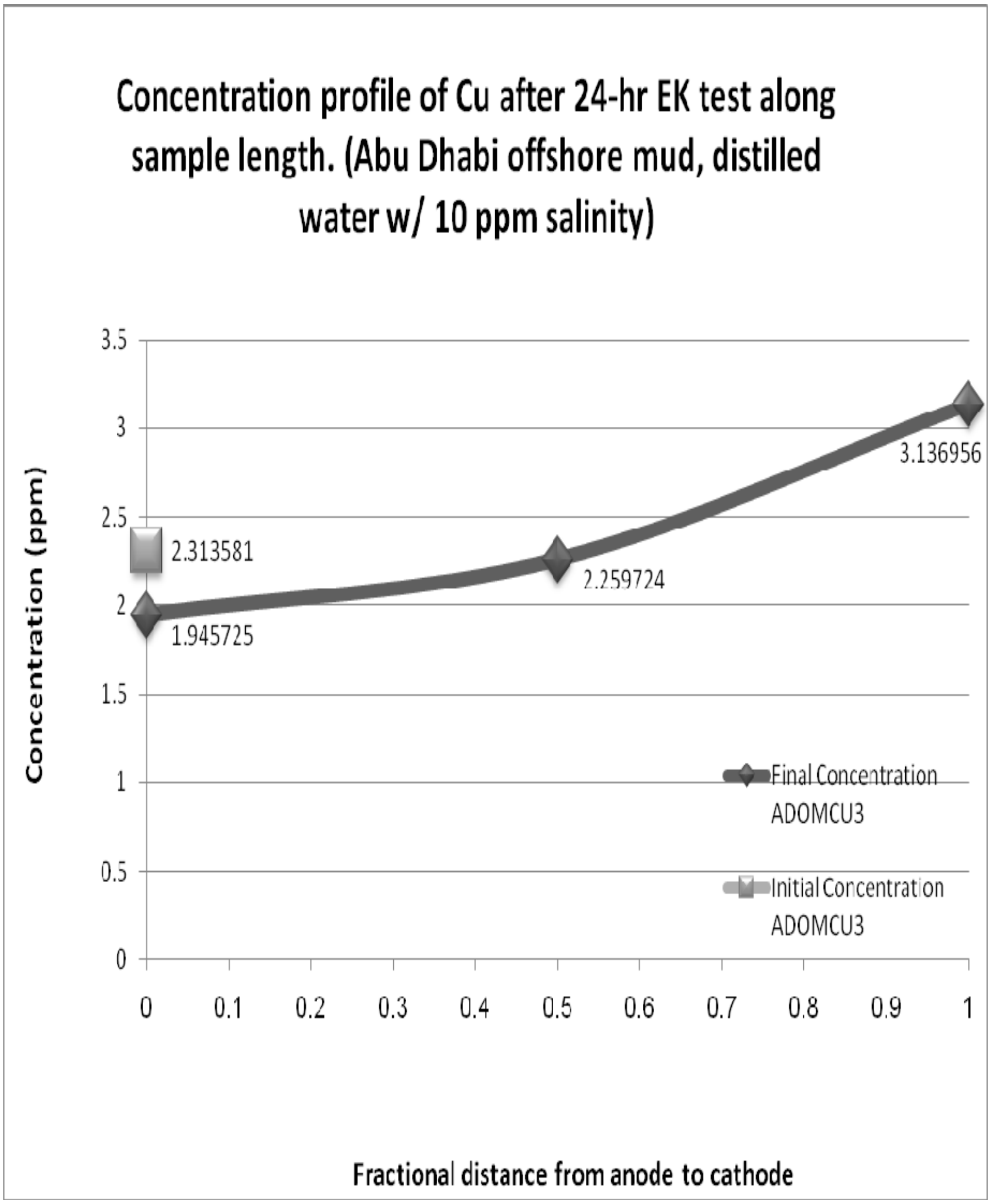

Figure 4-50: Concentration profile of Cu after 24-hr EK test a long sample length (Abu Dhabi offshore mud, distilled water 10 ppm salinity).

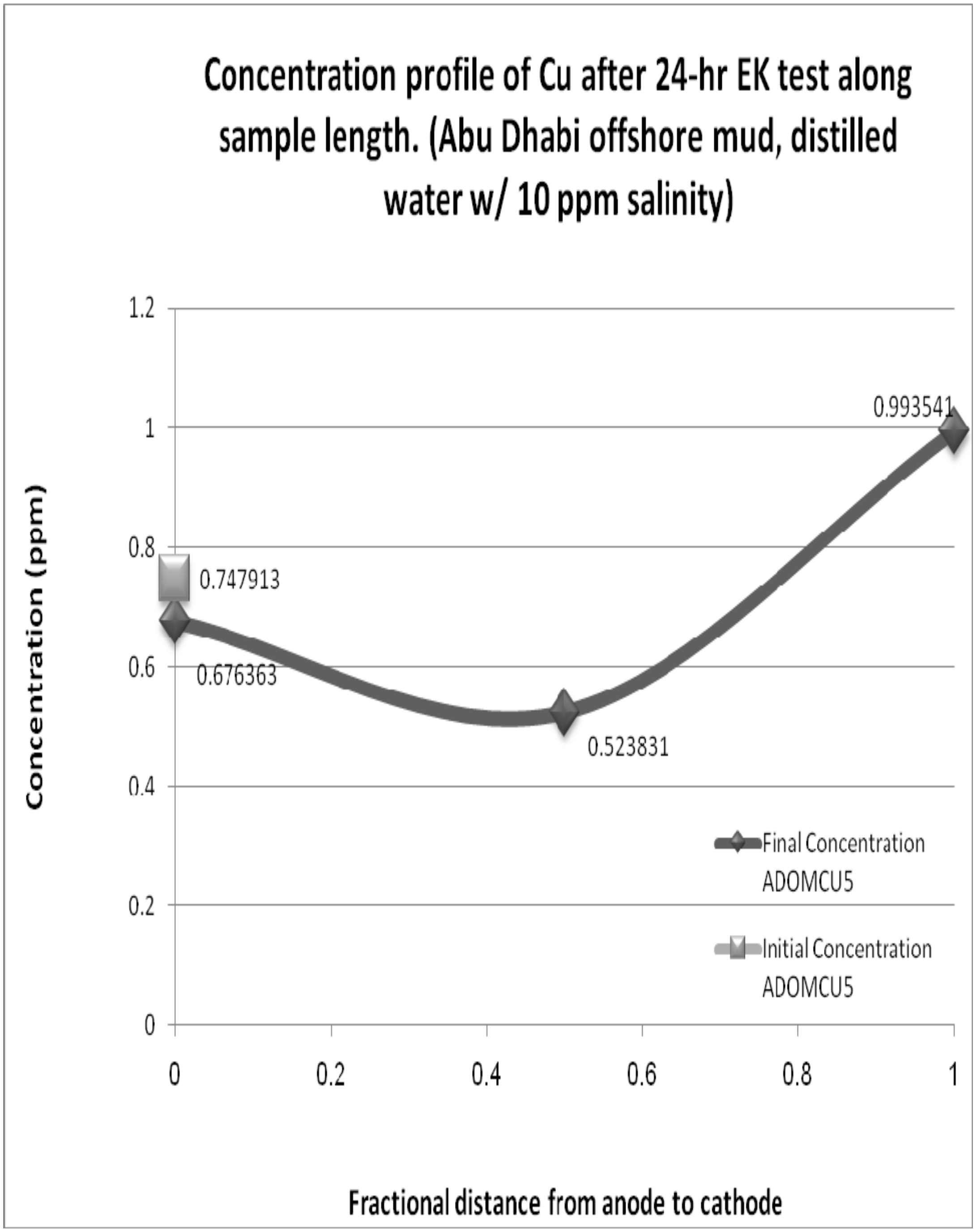

Figure 4-51: Concentration profile of Cu after 24-hr EK test a long sample length (Abu Dhabi offshore mud, distilled water 10 ppm salinity).

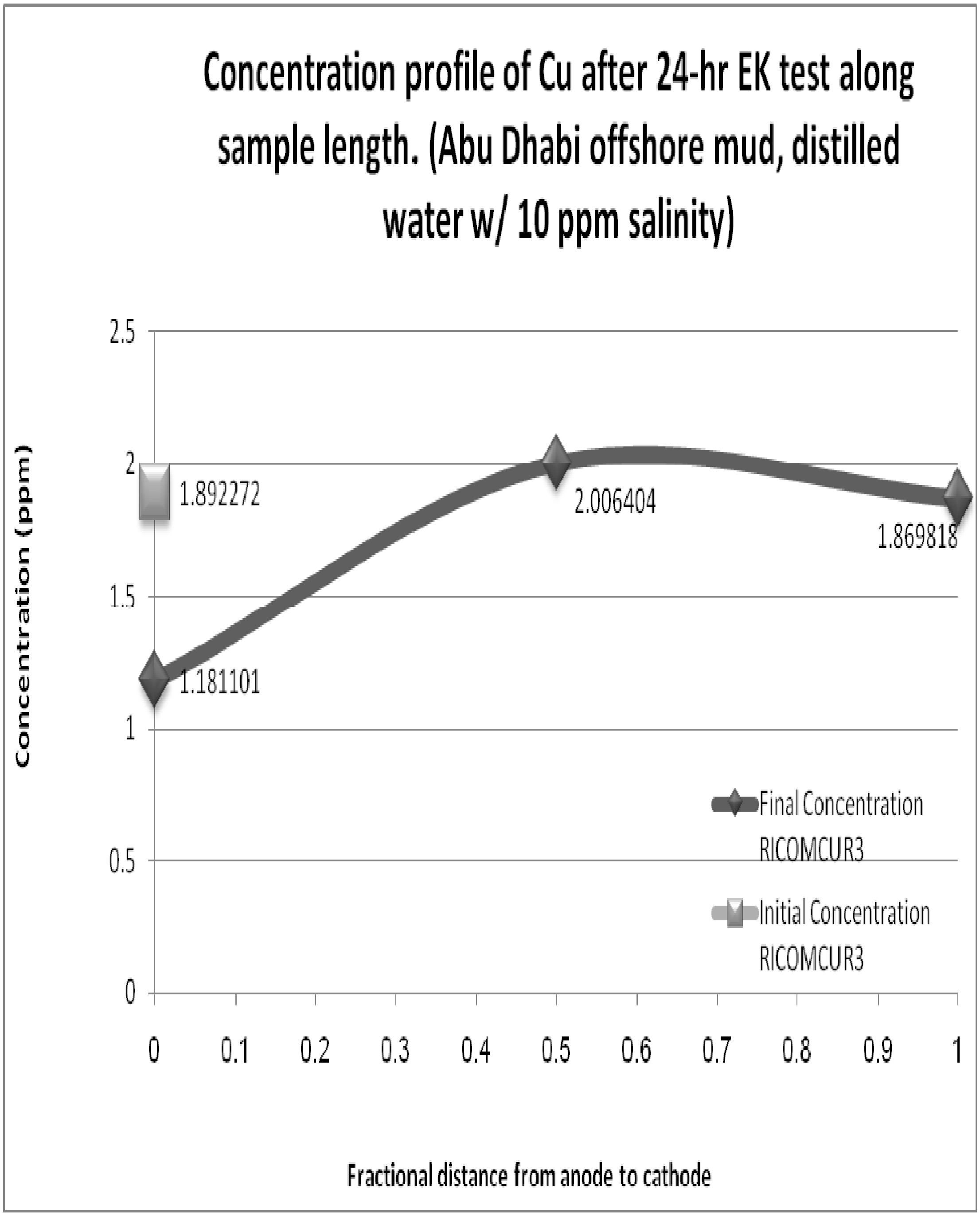

Figure 4-52: Concentration profile of Cu after 24-hr EK test a long sample length (Abu Dhabi offshore mud, distilled water 10 ppm salinity).

Copper: Sample RICOMSWPHCU2 in Figure 4-53 using Abu Dhabi seawater with 26,000 ppm salinity and 450 ppm maleic acid

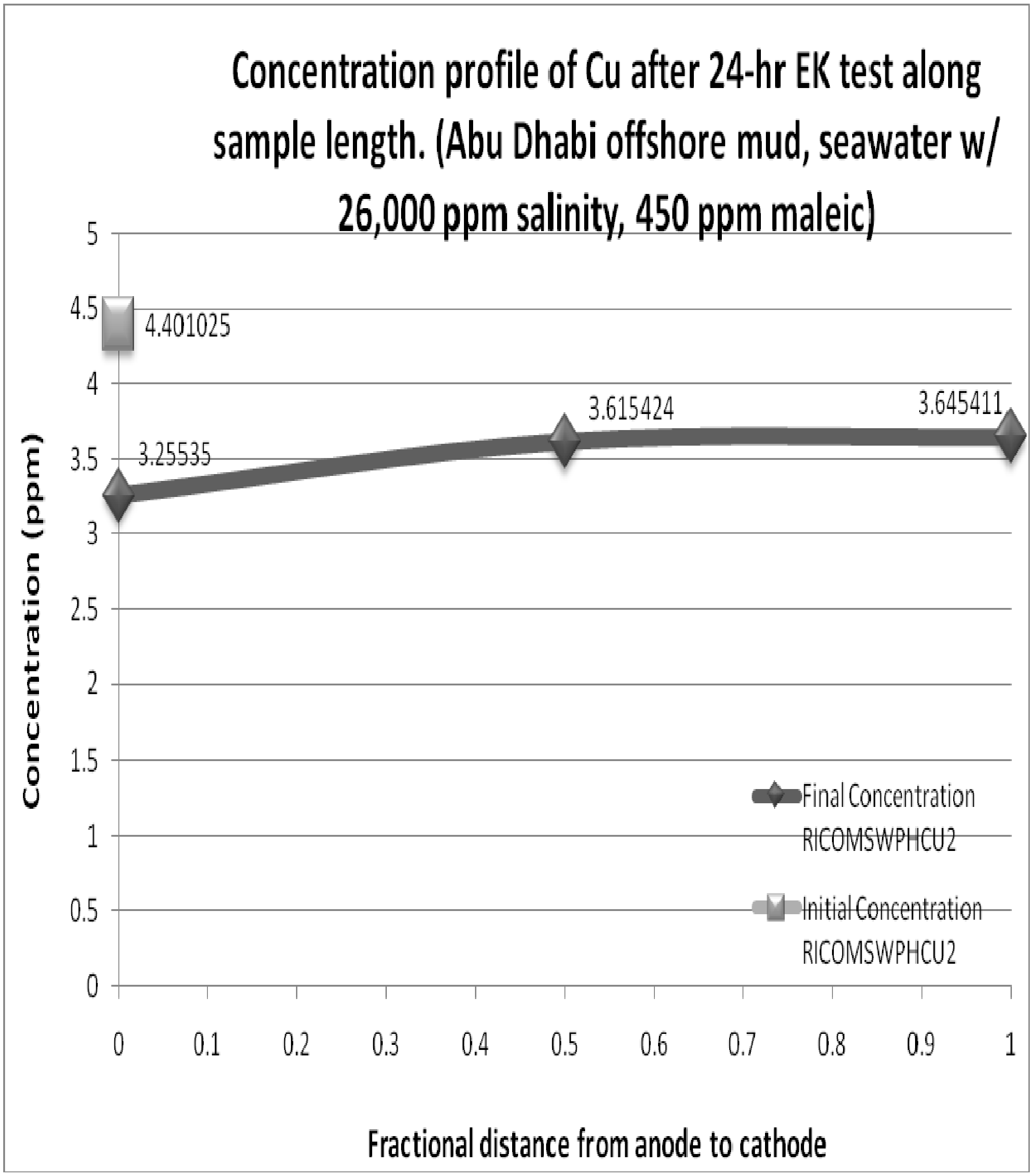

Figure 4-53: Concentration profile of Cu after 24-hr EK test a long sample length. (Abu Dhabi offshore mud, 26,000 ppm salinity & 450 ppm maleic acid)

Gallium: Gallium is a cation which carries three positive charges. Figure 4-54 show the fraction of the gallium found at three locations: anode side, center and cathode end of tested core after 24 hours of electrokinetic treatment. The initial concentrations were predetermined at the anode end of the contaminated offshore mud sample. The removal efficiency was calculated at the anode using equation 4-1 for all results obtained. Substantial reduction of bismuth from its initial concentration at the anode region was found to be 2.83 %. after 24 hours. Although the removal efficiency was quite low, long-term electroremediation tests would certainly increase the removal efficiency. Electrokinetics was the main driving force of the Ga ion in the same direction of the water flow. There was accumulation of metal at the discharge end as shown in both Figure 4-54 (cathode end of the mud sample).The shape of the curve can be explained by the lack of pH control.

Figure 4-55 shows the results conducted with Abu Dhabi seawater having 26,000 ppm salinity, as well as 450 ppm of maleic acid added for pH control. The maximum removal efficiency of Ga at the anode region here 29.36% as opposed to the 2.83%. This finding was interesting as it confirmed that the presense of both high salinity and pH control mechanism influenced all the samples tested here to consistently show higher removal efiiciencies at all the three locations analyzed. The high salinity caused a higher conductivity in the bulk solution, where both the current and electrokinetic flow increased several fold. One explanation for this is that the electromigration force is now a dominat force allowing the ionic mobility to travel at 2-3 times faster than in the case of dominant electroosmosis, while another theory is the abundance of large volumes of cations in this high salinity carrying their waters of hydration further promoting ionic species velocity. This needs to be investigated further.

Gallium: Sample ADOMGA5 in Figure 4-54 using Distilled water with 10 ppm salinity

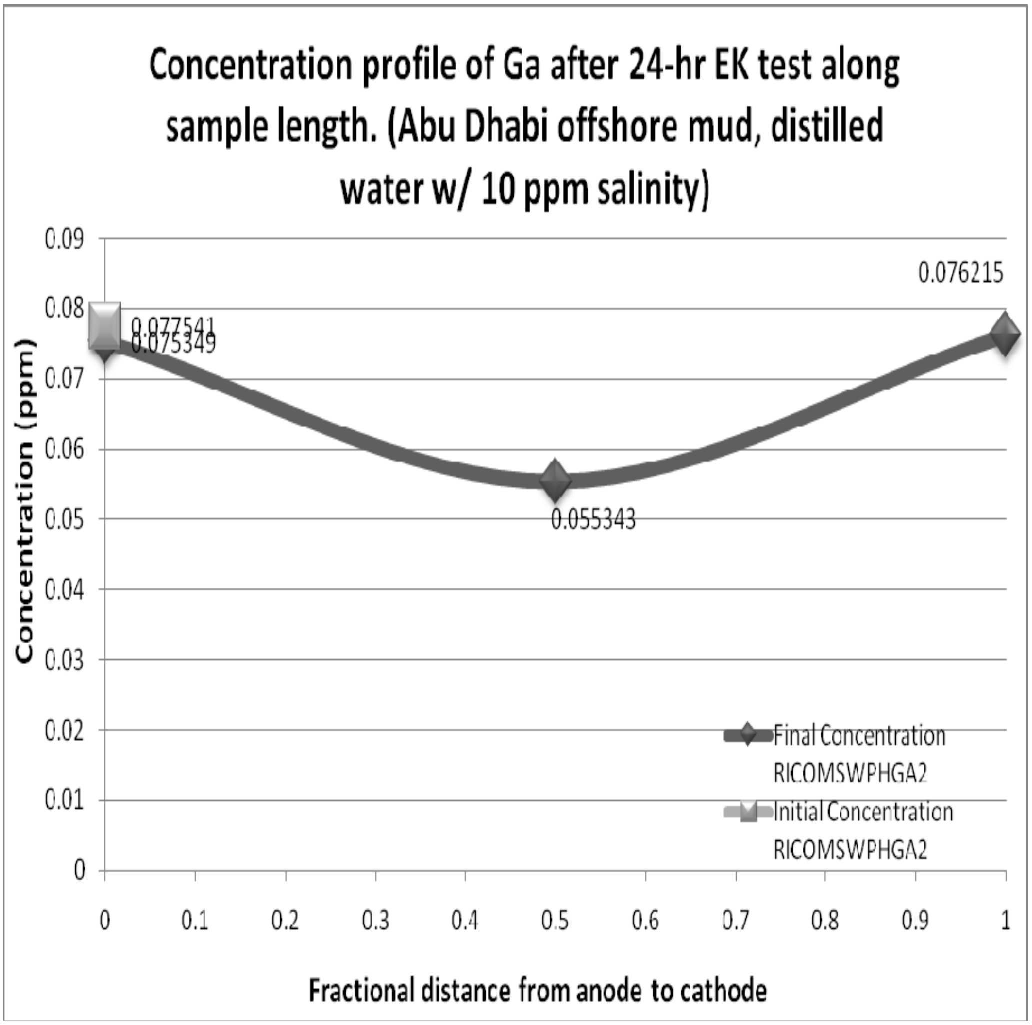

Figure 4-54: Concentration profile of Ga after 24-hr EK test a long sample length (Abu Dhabi offshore mud, distilled water 10 ppm salinity).

Gallium: Sample RICOMSWPHGA2 in Figure 4-55 using Abu Dhabi seawater with 26,000 ppm salinity and 450 ppm maleic acid

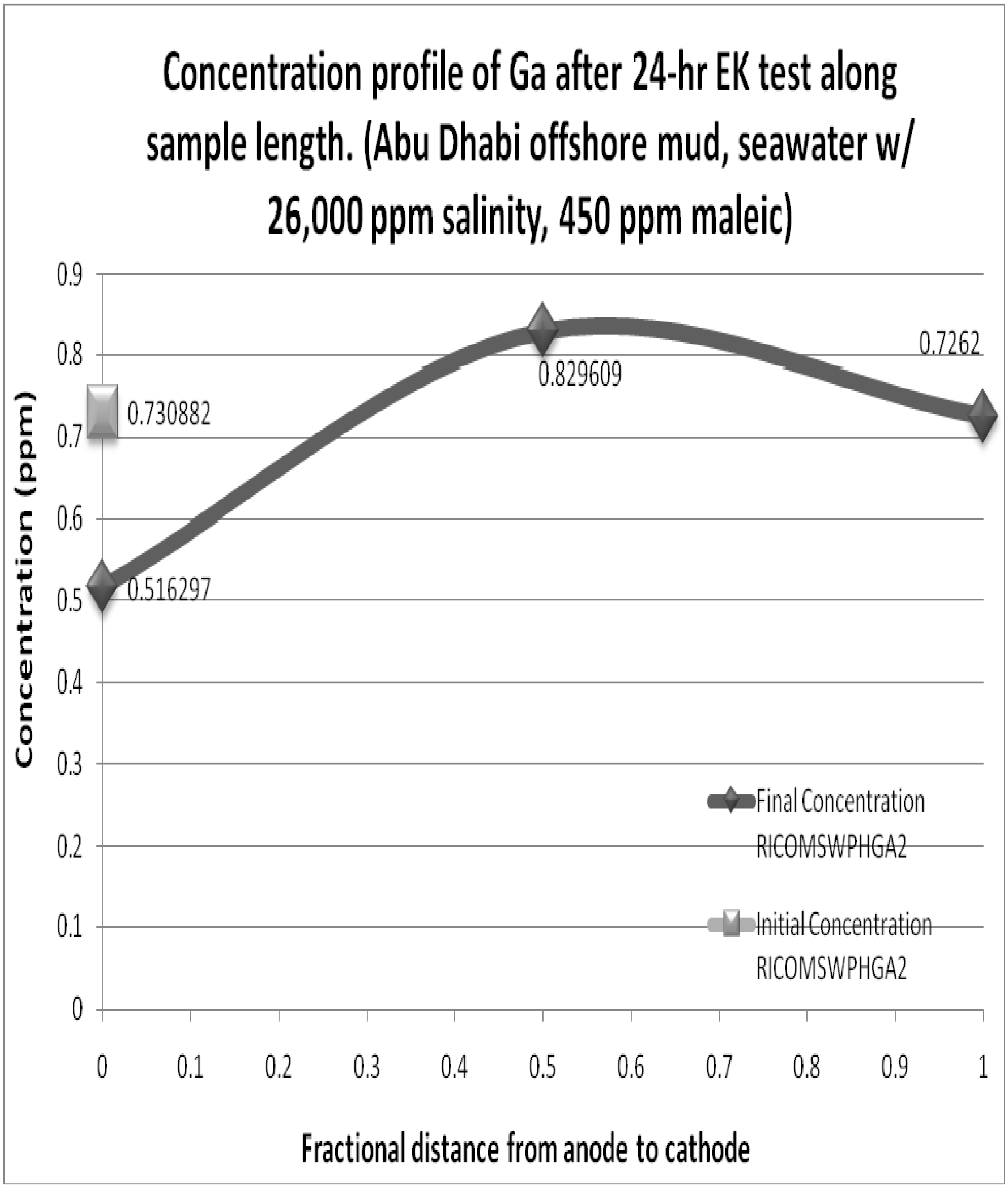

Figure 4-55: Concentration profile of Ga after 24-hr EK test a long sample length. (Abu Dhabi offshore mud, 26,000 ppm salinity & 450 ppm maleic acid)

Indium: Indium is a cation which carries three positive charges. Figure 4-56 show the fraction of the indium found at three locations: anode side, center and cathode end of tested core after 24 hours of electrokinetic treatment. The initial concentrations were predetermined at the anode end of the contaminated offshore mud sample. The removal efficiency was calculated at the anode using equation 4-1 for all results obtained. Substantial reduction of indium from its initial concentration at the anode region was found to be 18.0% after 24 hours. Electrokinetics was the main driving force of the indium ion in the same direction of the water flow. There was accumulation of metal at the discharge end as shown in both Figure 4-56 (cathode end of the mud sample).The shape of the curve can be explained by the lack of pH control.

Figure 4-57 shows the results conducted with Abu Dhabi seawater having 26,000 ppm salinity, as well as 450 ppm of maleic acid added for pH control. The maximum removal efficiency of indium at the anode region here 38.41% as opposed to the 18%. This finding was interesting as it confirmed that the presense of both high salinity and pH control mechanism influenced all the samples tested here to consistently show higher removal efiiciencies at all the three locations analyzed. The high salinity caused a higher conductivity in the bulk solution, where both the current and electrokinetic flow increased several fold. One explanation for this is that the electromigration force is now a dominat force allowing the ionic mobility to travel at 2-3 times faster than in the case of dominant electroosmosis, while another theory is the abundance of large volumes of cations in this high salinity carrying their waters of hydration further promoting ionic species velocity. This needs to be investigated further.

Indium: Sample RICOMINR3 in Figure 4-56 using Distilled water with 10 ppm salinity

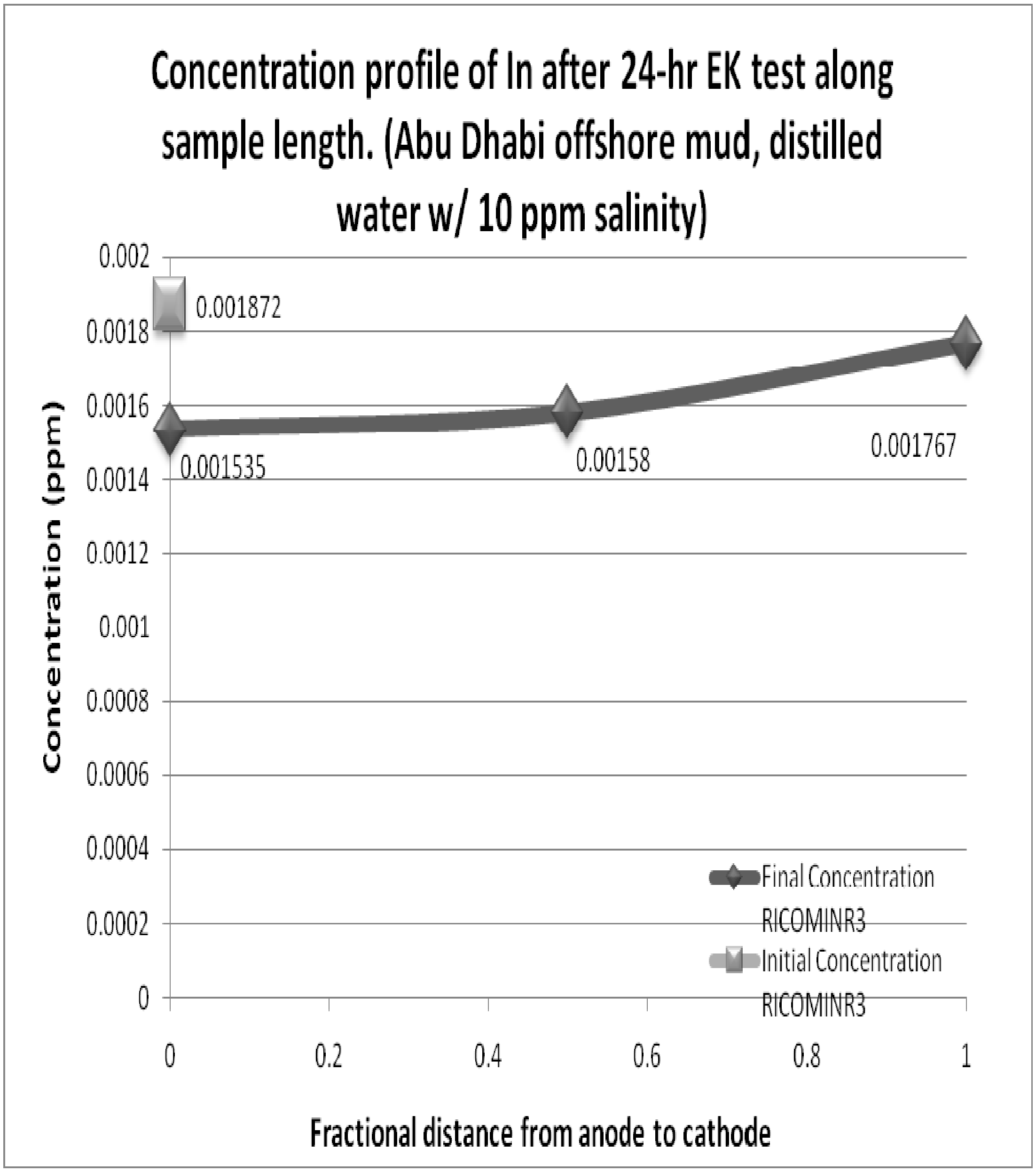

Figure 4-56: Concentration profile of In after 24-hr EK test a long sample length (Abu Dhabi offshore mud, distilled water 10 ppm salinity).

Indium: Sample RICOMSWPHIN1 in Figure 4-57 using Abu Dhabi seawater with 26,000 ppm salinity and 450 ppm maleic acid

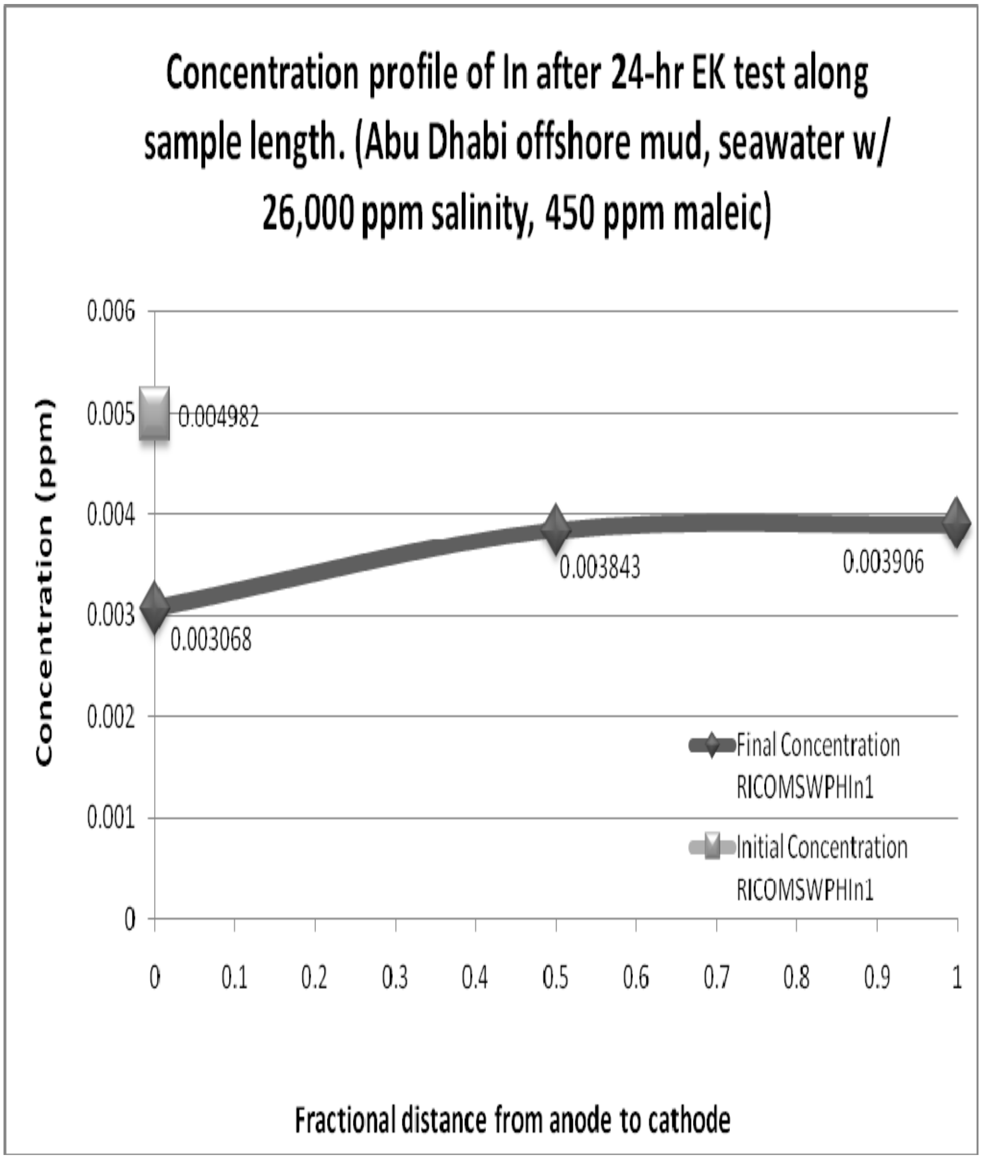

Figure 4-57: Concentration profile of In after 24-hr EK test a long sample length. (Abu Dhabi offshore mud, 26,000 ppm salinity & 450 ppm maleic acid)

Lead: Results are shown in Figure 4-58 through 4-62. Lead is one of the preferentially adsorbed metals by clay minerals (Basta and Tabatabal, 1992). It is mostly in the form of a divalent cation below pH of 9. Above pH 9, the PbO is the stable species (Dragun, 1988). At sufficiently high pH (>11) it forms an anionic species of hydrolysis product, $Pb(OH)_6^{-2}$, which is expected to migrate in the opposite direction of electrokinetic flow. Other hydrolysis products of lead which occur at pH levels greater than 6 are: $Pb_2(OH)_4^{+3}$, $Pb_4(OH)_4^{+4}$, $Pb_6(OH)_8^{+4}$. These species would exhibit increased ionic velocities due to their higher valances. The effect of high pH on the clay adsorption of metal becomes more significant at high concentrations of the metal, as shown in Fig. 4-62. This accumulation is attributed to: (i) precipitation and anion species formation, (ii) increased concentration of lead at the discharge end (cathode region of soil), (iii) increased adsorption and retention of lead on clay due to high pH and increased concentration at the cathode region of the soil (Pamukcu et al., 1993).

The removal efficiency was calculated at the anode using equation 4-1 for all results obtained. Figure 4-59, demonstrated 100% removal of Pb at the anode after just 24 hours of treatment, while figure 4-58 showed only 13% removal at the same location after 24 hours of electrotreatment. The shape of the curve on figure 4-58 and 4-62, can be explained by the lack of pH control.

Lead: 2, 3, 4, R3, R4 samples in Figure 4-58 through 4-62 using Distilled water with 10 ppm salinity

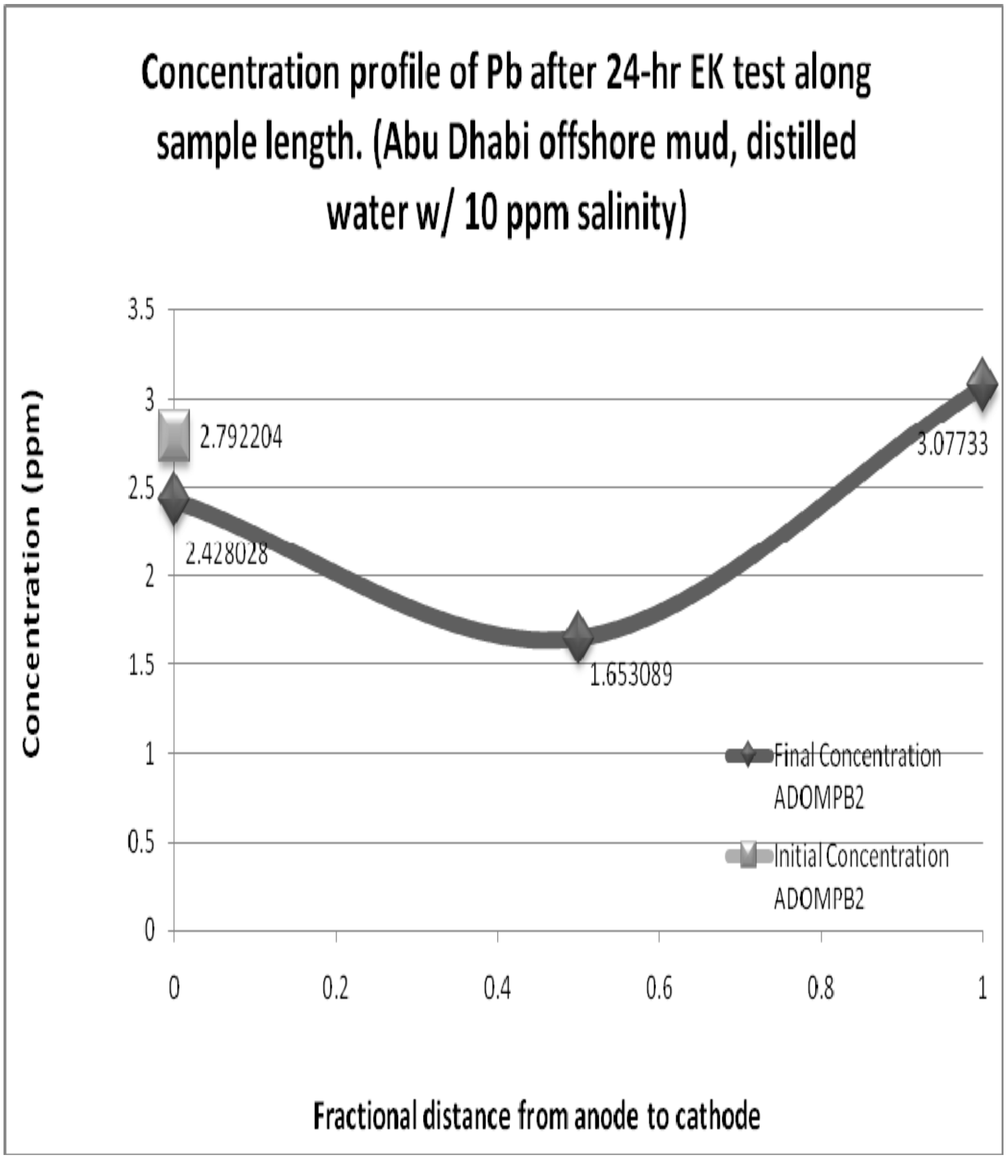

Figure 4-58: Concentration profile of Pb after 24-hr EK test a long sample length (Abu Dhabi offshore mud, distilled water 10 ppm salinity).

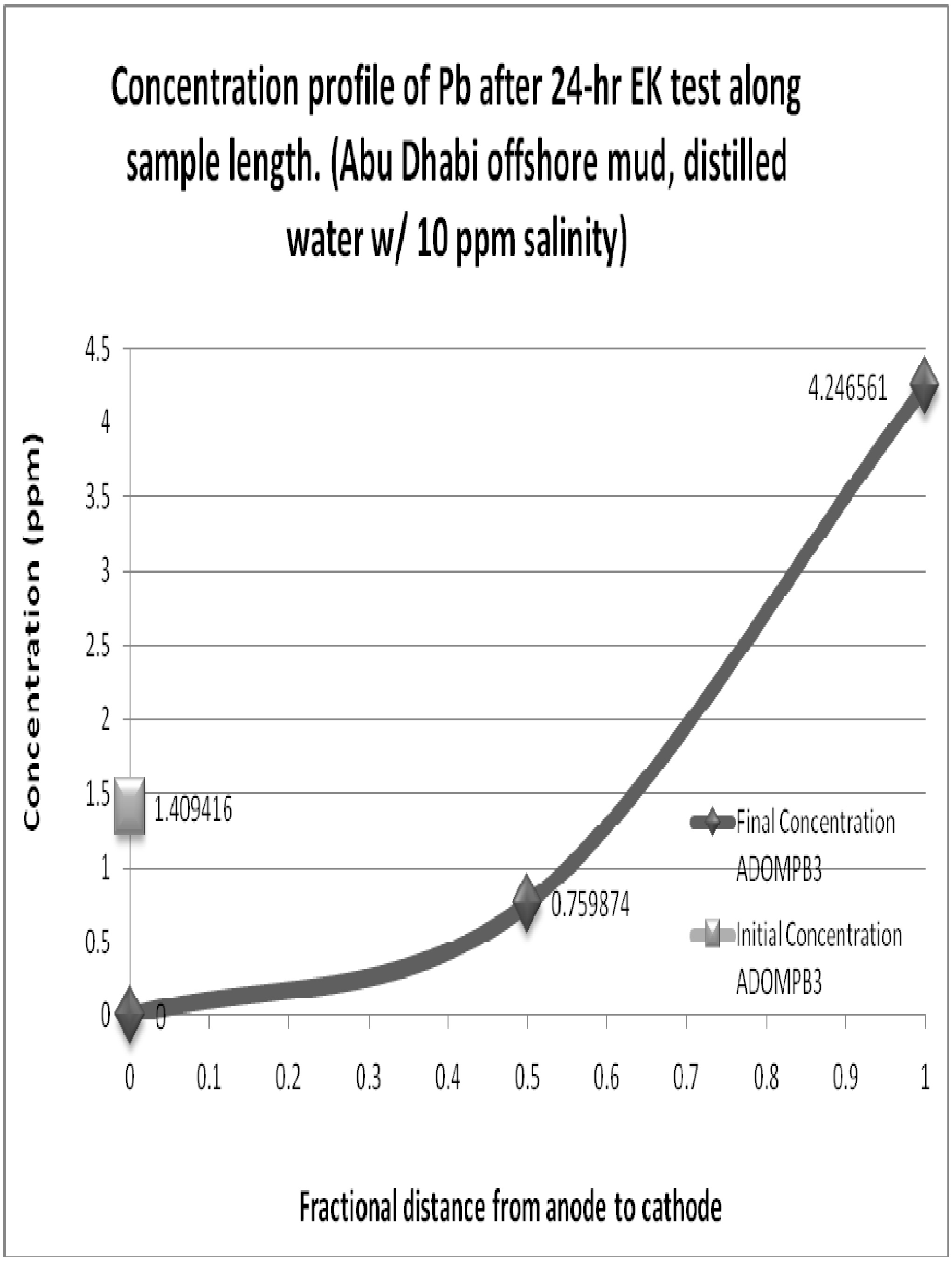

Figure 4-59: Concentration profile of Pb after 24-hr EK test a long sample length (Abu Dhabi offshore mud, distilled water 10 ppm salinity).

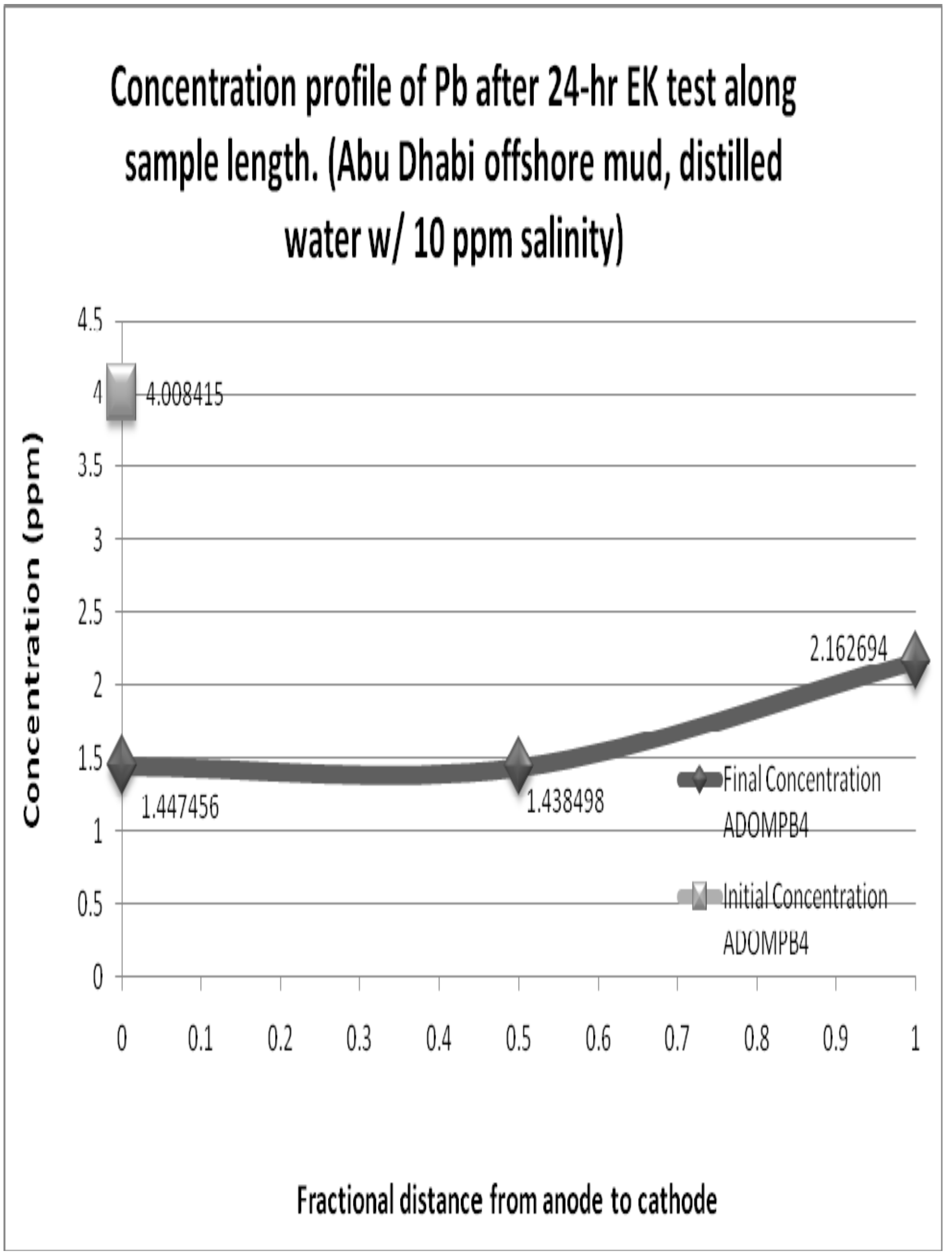

Figure 4-60: Concentration profile of Pb after 24-hr EK test a long sample length (Abu Dhabi offshore mud, distilled water 10 ppm salinity).

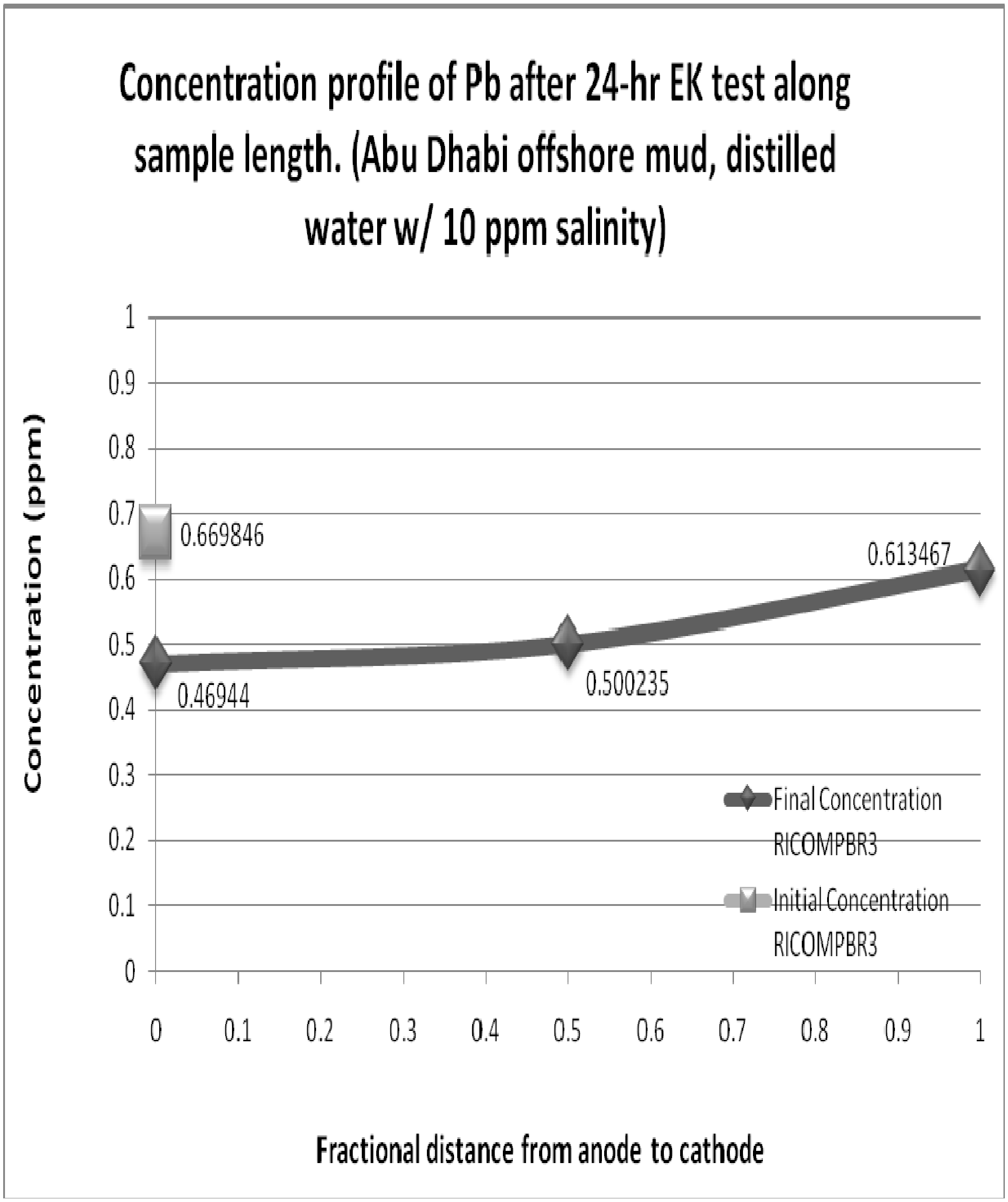

Figure 4-61: Concentration profile of Pb after 24-hr EK test a long sample length (Abu Dhabi offshore mud, distilled water 10 ppm salinity).

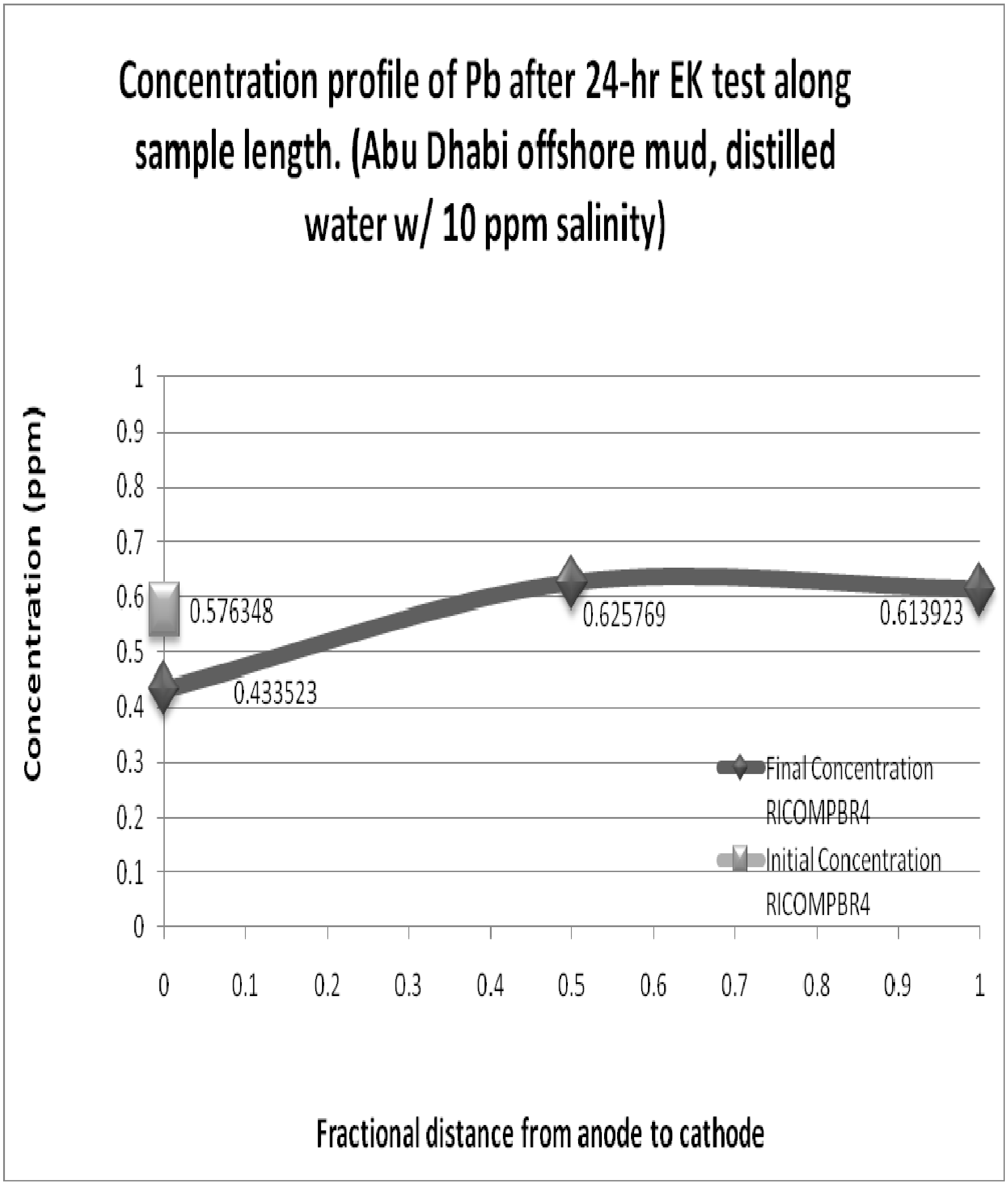

Figure 4-62: Concentration profile of Pb after 24-hr EK test a long sample length (Abu Dhabi offshore mud, distilled water 10 ppm salinity).

Lithium: Lithium exits as a monovalent ion throughout the pH range of 2 to 10. Lithium is a cation which carries three positive charges. Figure 4-63 through 4-65 show the fraction of the lithium found at three locations: anode side, center and cathode end of tested core after 24 hours of electrokinetic treatment. The initial concentrations were predetermined at the anode end of the contaminated offshore mud sample. The removal efficiency was calculated at the anode using equation 4-1 for all results obtained. Substantial reduction of lithium from its initial concentration at the anode region was found to be 6.80 and 23.51% after 24 hours using the distilled water with 10 ppm salinity as shown in Figures 4-63 and 4-64 respectively. Electrokinetics was the main driving force of the lithium ion in the same direction of the water flow. There was accumulation of metal at the discharge end as shown in both Figures 4-63 and 4-64 (cathode end of the mud sample). The shape of the curve can be explained by the lack of pH control.
Figure 4-65 shows the results conducted with Abu Dhabi seawater having 26,000 ppm salinity, as well as 450 ppm of maleic acid added for pH control. The maximum removal efficiency of lithium at the anode region here 19.097% as opposed to the 23.51%, however consistency was achieved using the seawater and pH control, where the lowest removal efficiency recored at the anode here was 14.102 as opposed to 6.80% as shown in Figure 4-65. This finding was interesting as it confirmed that the presense of both high salinity and pH control mechanism influenced all the samples tested here to consistently show higher removal efiiciencies at all the three locations analyzed. The high salinity caused a higher conductivity in the bulk solution, where both the current and

electrokinetic flow increased several fold. One explanation for this is that the electromigration force is now a dominat force allowing the ionic mobility to travel at 2-3 times faster than in the case of dominant electroosmosis, while another theory is the abundance of large volumes of cations in this high salinity carrying their waters of hydration further promoting ionic species velocity. This needs to be investigated further.

Lithium: ADOMLI5, RICOMLIR3 samples in Figure 4-63 through 4-64 using Distilled water with 10 ppm salinity

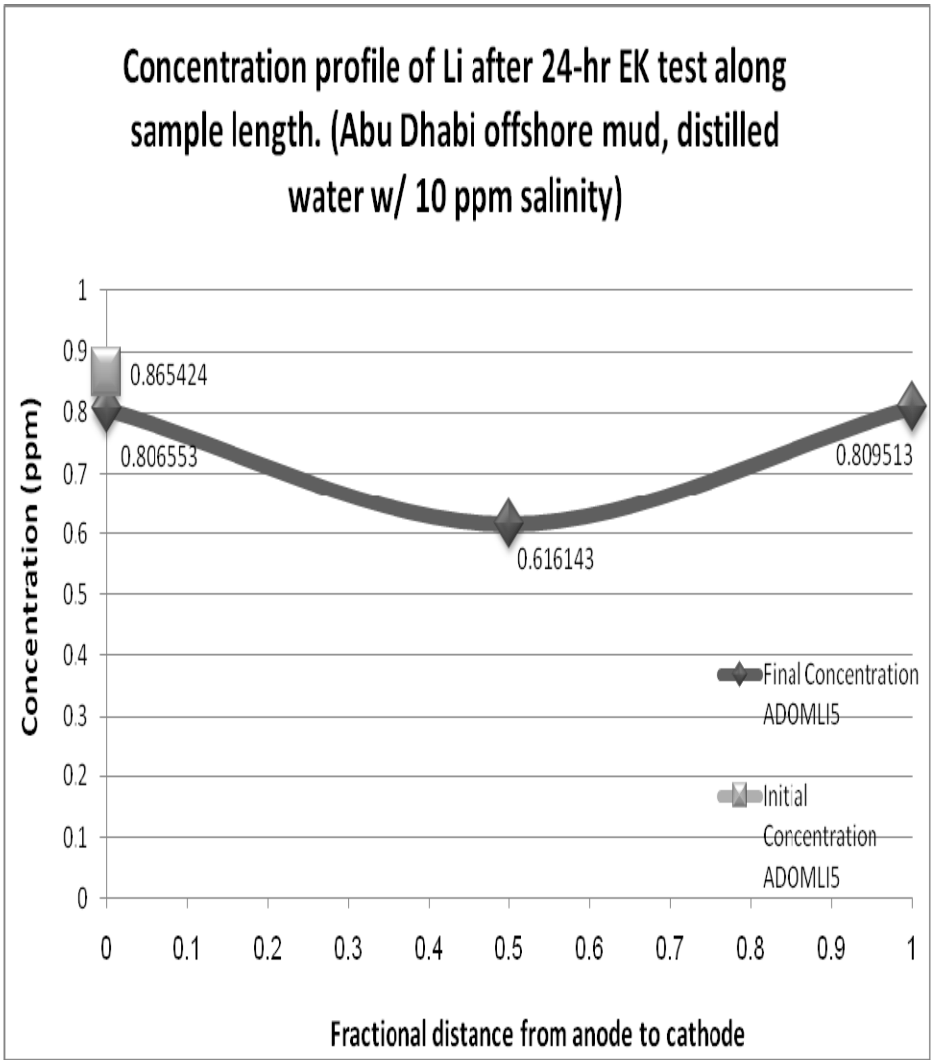

Figure 4-63: Concentration profile of Li after 24-hr EK test a long sample length (Abu Dhabi offshore mud, distilled water 10 ppm salinity).

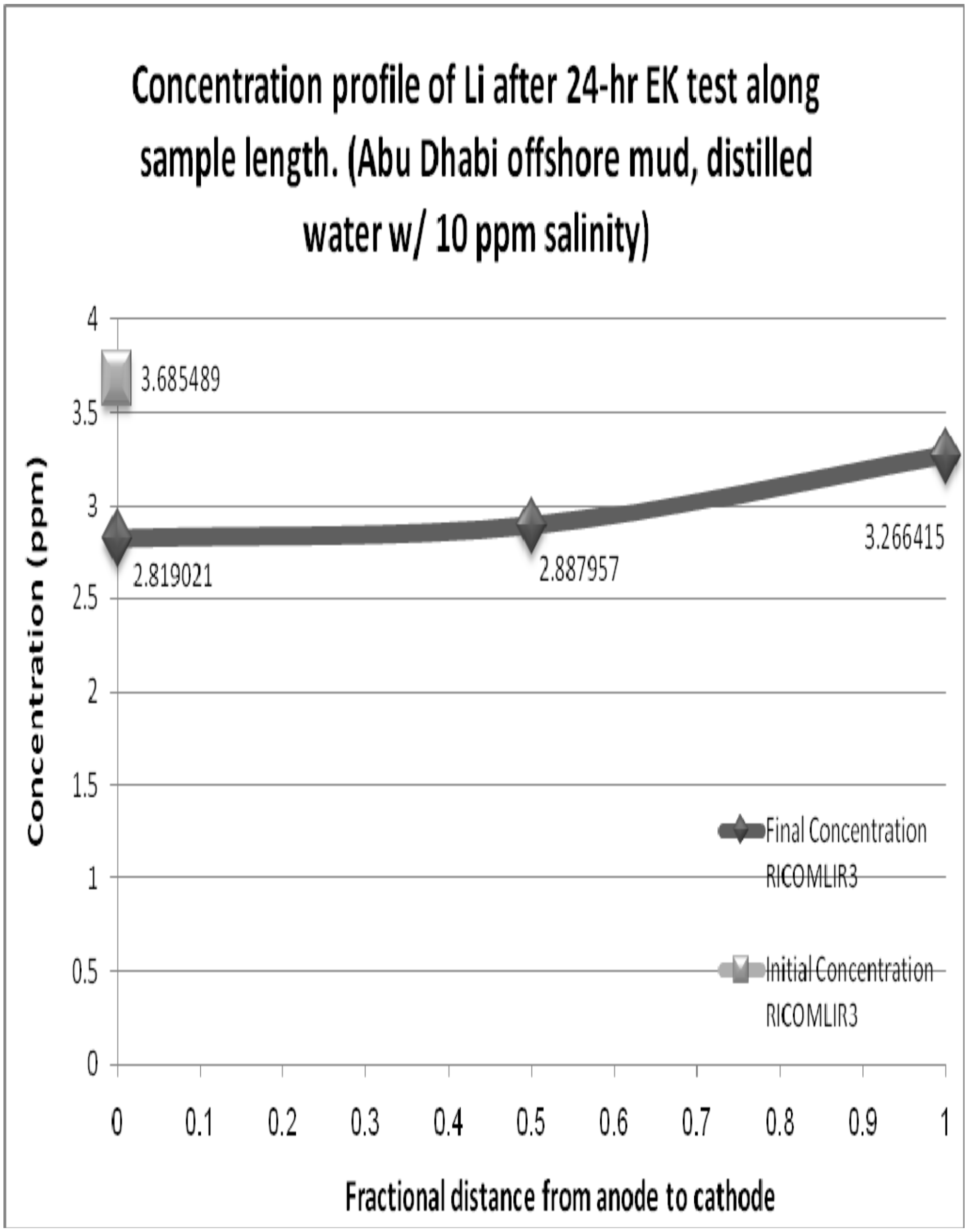

Figure 4-64: Concentration profile of Li after 24-hr EK test a long sample length (Abu Dhabi offshore mud, distilled water 10 ppm salinity).

Lithium: Sample RICOMSWPHLI2 in Figure 4-65 using Abu Dhabi seawater with 26,000 ppm salinity and 450 ppm maleic acid

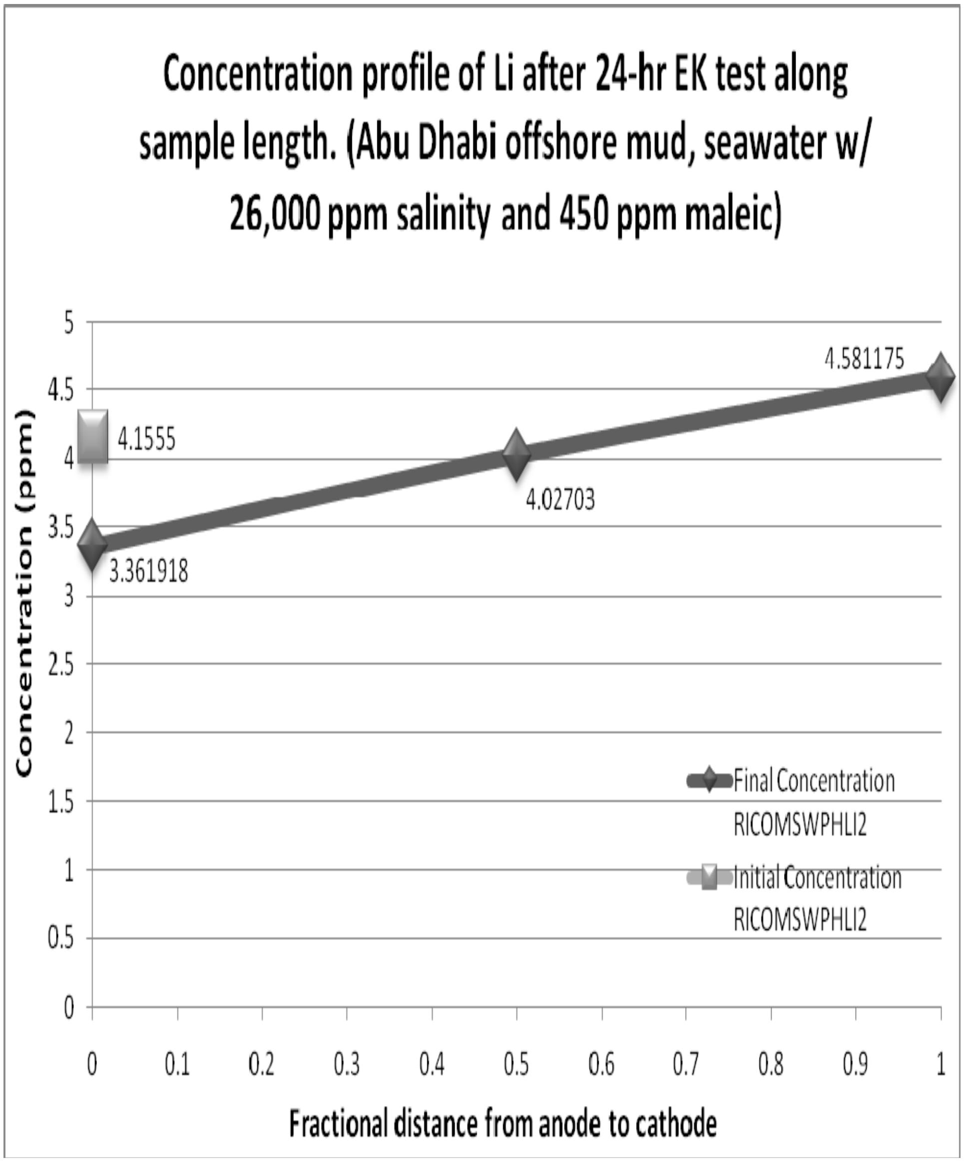

Figure 4-65: Concentration profile of Li after 24-hr EK test a long sample length. (Abu Dhabi offshore mud, 26,000 ppm salinity & 450 ppm maleic acid)

Rubidium: Rubidium exits as a monovalent cationic species throughout the pH range of 2 to 10. Rubidium is a cation which carries three positive charges. Figure 4-66 through 4-69 show the fraction of the indium found at three locations: anode side, center and cathode end of tested core after 24 hours of electrokinetic treatment. The initial concentrations were predetermined at the anode end of the contaminated offshore mud sample. The removal efficiency was calculated at the anode using equation 4-1 for all results obtained. Substantial reduction of rubidium from its initial concentration at the anode region was found to be 10.69, 24.31 and 20.47% after 24 hours using the distilled water with 10 ppm salinity as shown in Figures 4-66, 4-67 and 4-68 respectively. Electrokinetics was the main driving force of the rubidium ion in the same direction of the water flow. There was accumulation of metal at the discharge end as shown in both Figures 4-66 and 4-68 (cathode end of the mud sample). The shape of the curve can be explained by the lack of pH control.

Figure 4-65 shows the results conducted with Abu Dhabi seawater having 26,000 ppm salinity, as well as 450 ppm of maleic acid added for pH control. The maximum removal efficiency of rubidium at the anode region here 29.97% as opposed to the 24.31%, as shown in Figure 4-69. This finding was interesting as it confirmed that the presense of both high salinity and pH control mechanism influenced all the samples tested here to consistently show higher removal efiiciencies at all the three locations analyzed. The high salinity caused a higher conductivity in the bulk solution, where both the current and electrokinetic flow increased several fold. One explanation for this is that the electromigration force is now a dominat force allowing the ionic mobility to travel at

2-3 times faster than in the case of dominant electroosmosis, while another theory is the abundance of large volumes of cations in this high salinity carrying their waters of hydration further promoting ionic species velocity. This needs to be investigated further.

Rubidium: 2, 5, R3 samples in Figure 4-66 through 4-68 using Distilled water with 10 ppm salinity

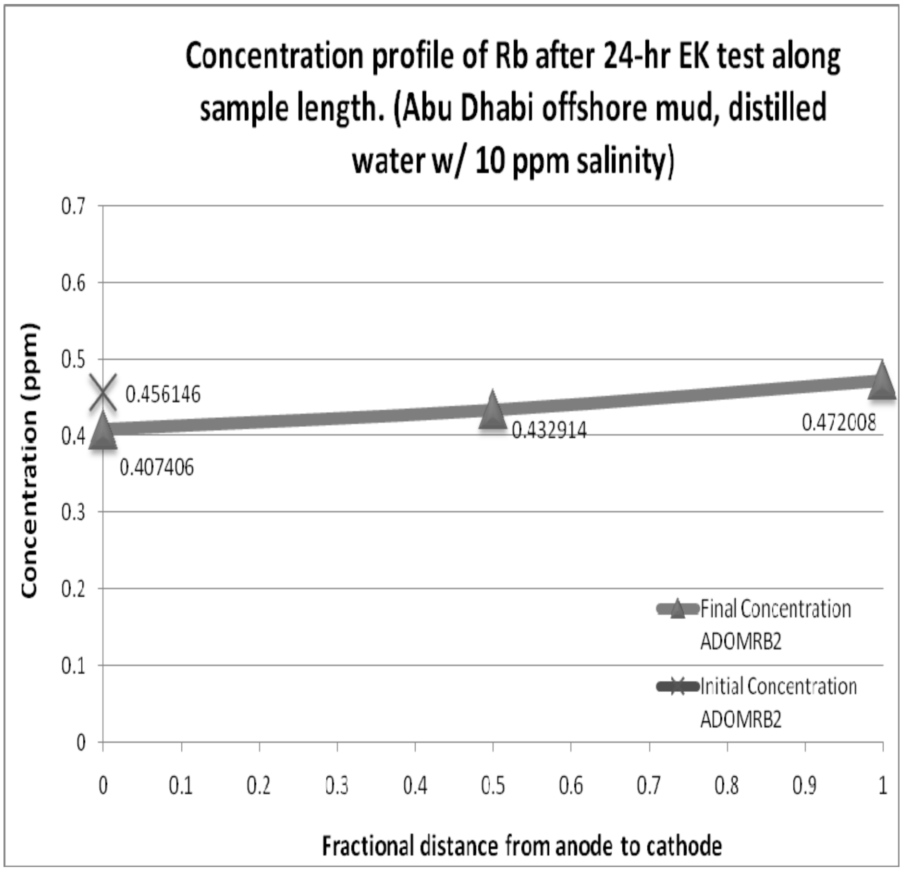

Figure 4-66: Concentration profile of Rb after 24-hr EK test a long sample length (Abu Dhabi offshore mud, distilled water 10 ppm salinity).

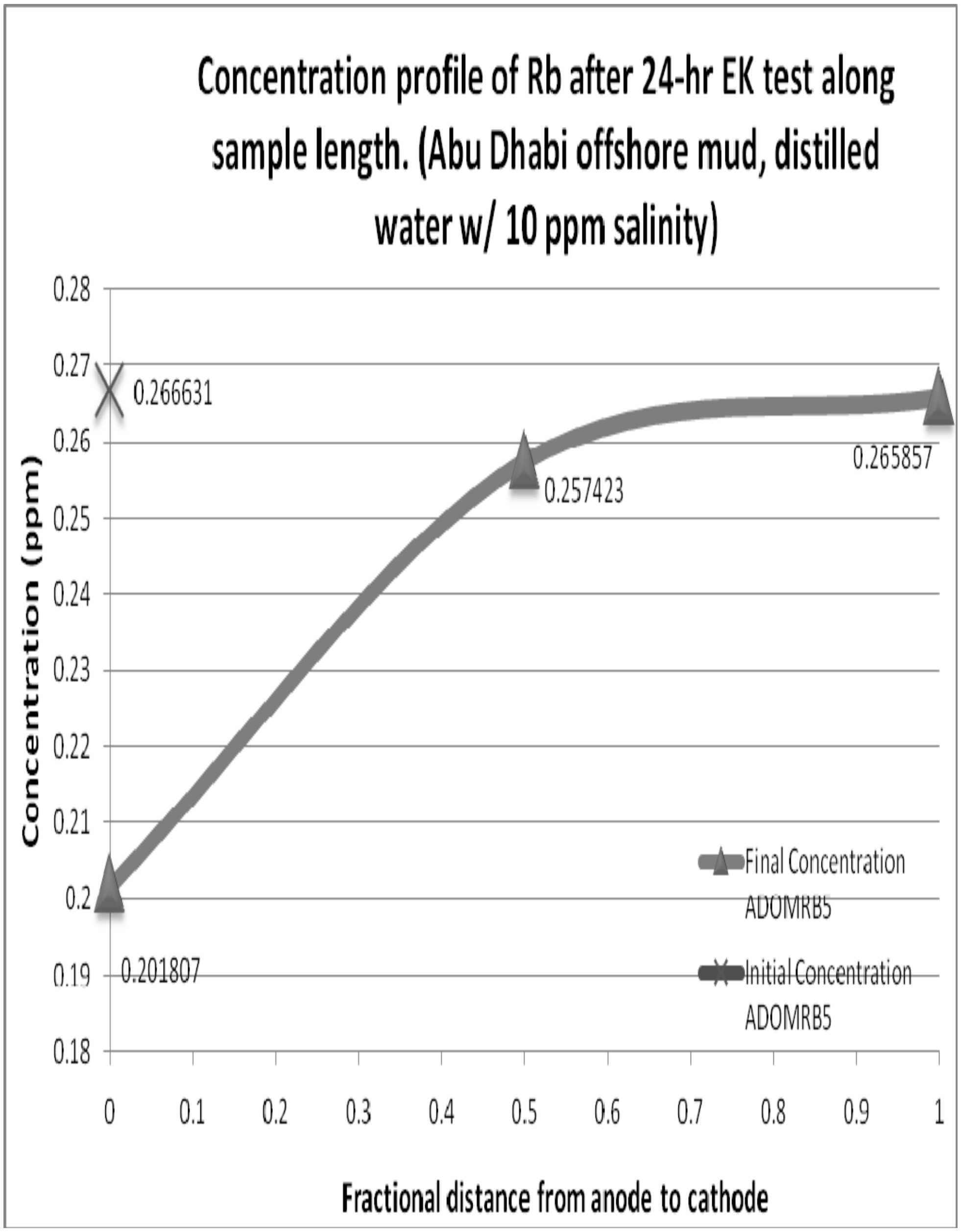

Figure 4-67: Concentration profile of Rb after 24-hr EK test a long sample length (Abu Dhabi offshore mud, distilled water 10 ppm salinity).

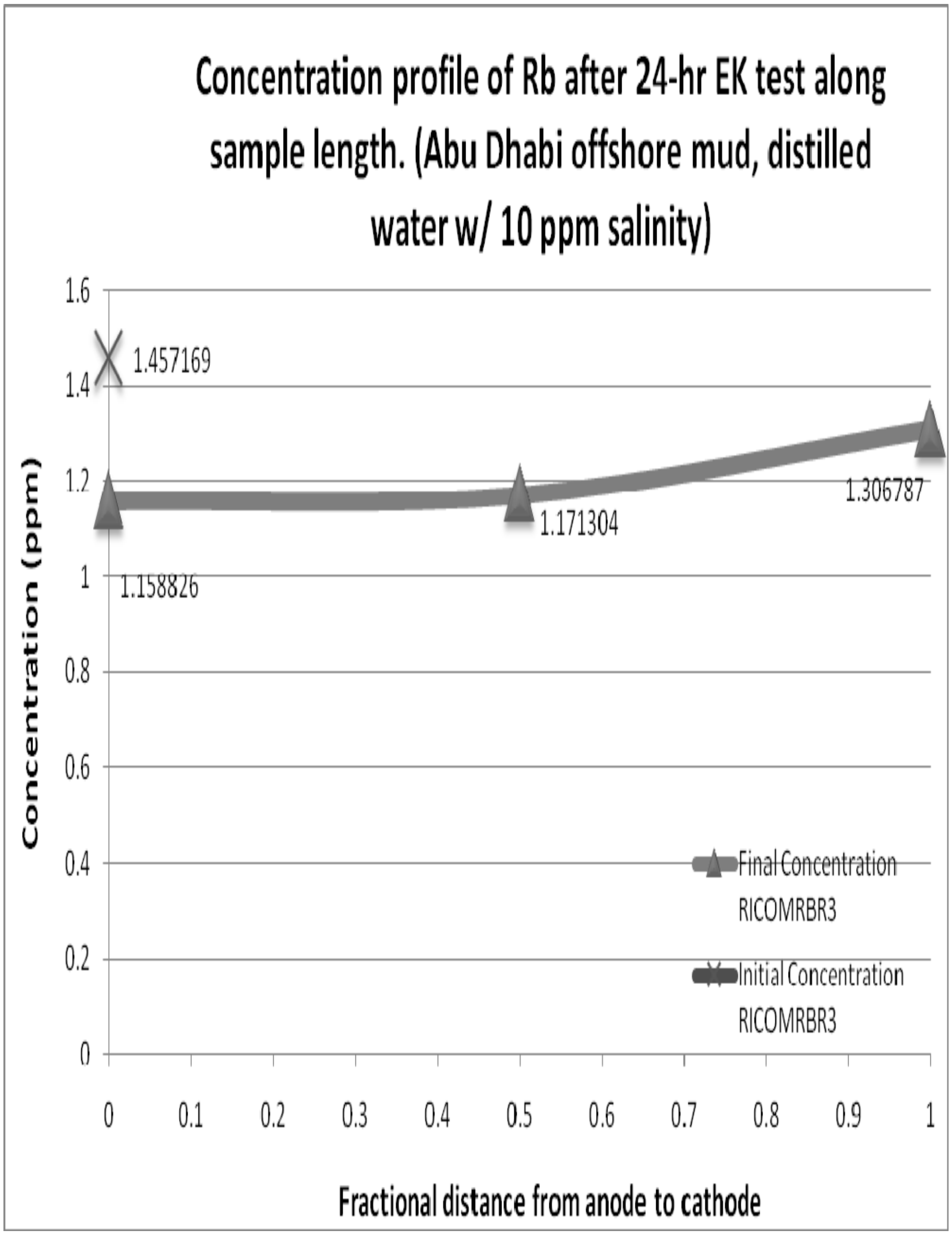

Figure 4-68: Concentration profile of Rb after 24-hr EK test a long sample length (Abu Dhabi offshore mud, distilled water 10 ppm salinity).

Rubidium: Sample RICOMSWPHRB2 in Figure 4-69 using Abu Dhabi seawater with 26,000 ppm salinity and 450 ppm maleic acid

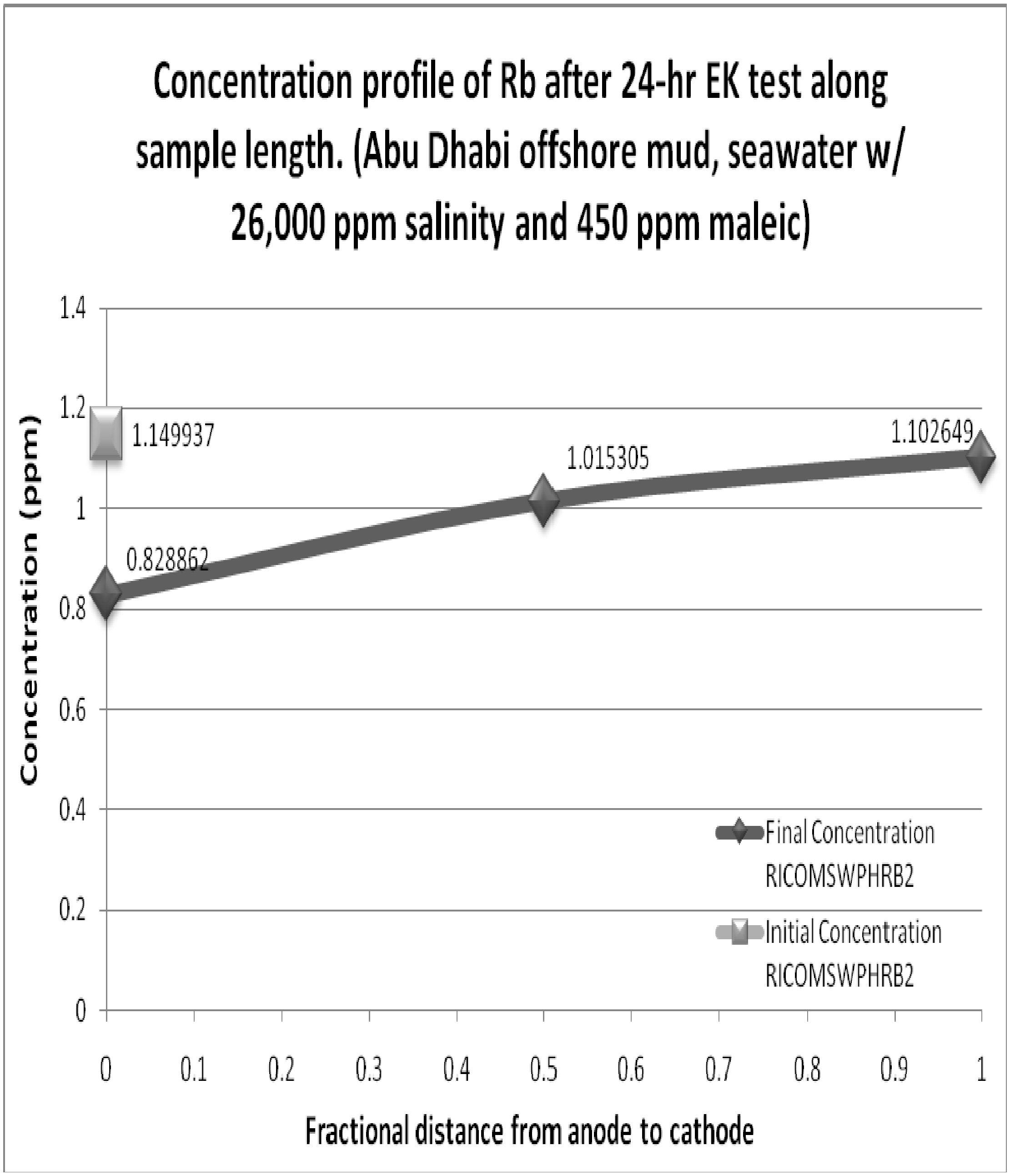

Figure 4-69: Concentration profile of Rb after 24-hr EK test a long sample length. (Abu Dhabi offshore mud, 26,000 ppm salinity & 450 ppm maleic acid)

Selenium: Selenium can be found in several cation forms, carrying two, four and six positive charges. Selenium exits as a monovalent ion throughout the pH range of 2 to 10. Selenium is a cation which carries three positive charges. Figure 4-70 through 4-75 show the fraction of the selenium found at three locations: anode side, center and cathode end of tested core after 24 hours of electrokinetic treatment. The initial concentrations were predetermined at the anode end of the contaminated offshore mud sample. The removal efficiency was calculated at the anode using equation 4-1 for all results obtained. Substantial reduction of selenium from its initial concentration at the anode region was found to be 41.35, 47.47, 24.24, 20.20, and 9.96% after 24 hours using the distilled water with 10 ppm salinity as shown in Figures 4-70 through 4-74 respectively. Electrokinetics was the main driving force of the selenium ion in the same direction of the water flow. There was accumulation of metal at the discharge end as shown in both Figures 4-70 through 4-74 (cathode end of the mud sample). The shape of the curve in Figures 4-71, 4-72 and 4-73 can be explained by the lack of pH control.

Figure 4-75 shows the results conducted with Abu Dhabi seawater having 26,000 ppm salinity, as well as 450 ppm of maleic acid added for pH control. The maximum removal efficiency of selenium at the anode region here 42.85% as opposed to the 47.47%, however consistency was achieved using the seawater and pH control, where the lowest removal efficiency recored at the anode here was 34.12% as opposed to 9.96% as shown in Figure 4-74. This finding was interesting as it confirmed that the presense of both high salinity and pH control mechanism influenced all the samples tested here to consistently show higher removal efiiciencies at all the three locations analyzed. The high salinity caused a higher conductivity in the bulk solution, where both the current and electrokinetic flow increased several fold. One explanation for this is that the electromigration force is now a dominat force allowing the ionic mobility to travel at 2-3 times faster than in the case of dominant electroosmosis, while another theory is the abundance of large volumes of cations in this high salinity carrying their waters of hydration further promoting ionic species velocity. This needs to be investigated further.

Selenium: ADOMSE1, ADOMSE4, RICOMSER1, RICOMSER3, RICOMSER4 samples in Figure 4-70 through 4-74 using Distilled water with 10 ppm salinity

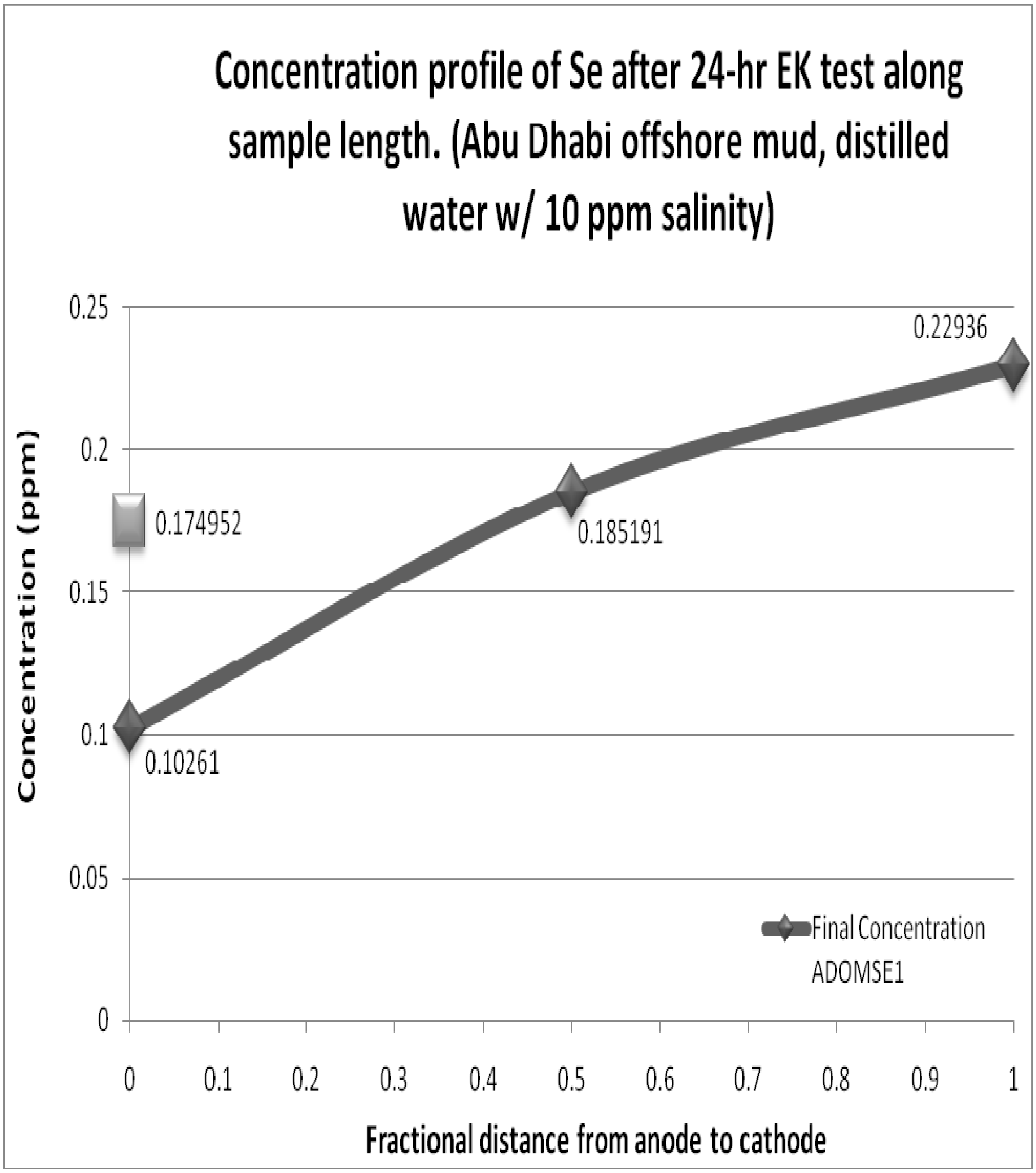

Figure 4-70: Concentration profile of Se after 24-hr EK test a long sample length (Abu Dhabi offshore mud, distilled water 10 ppm salinity).

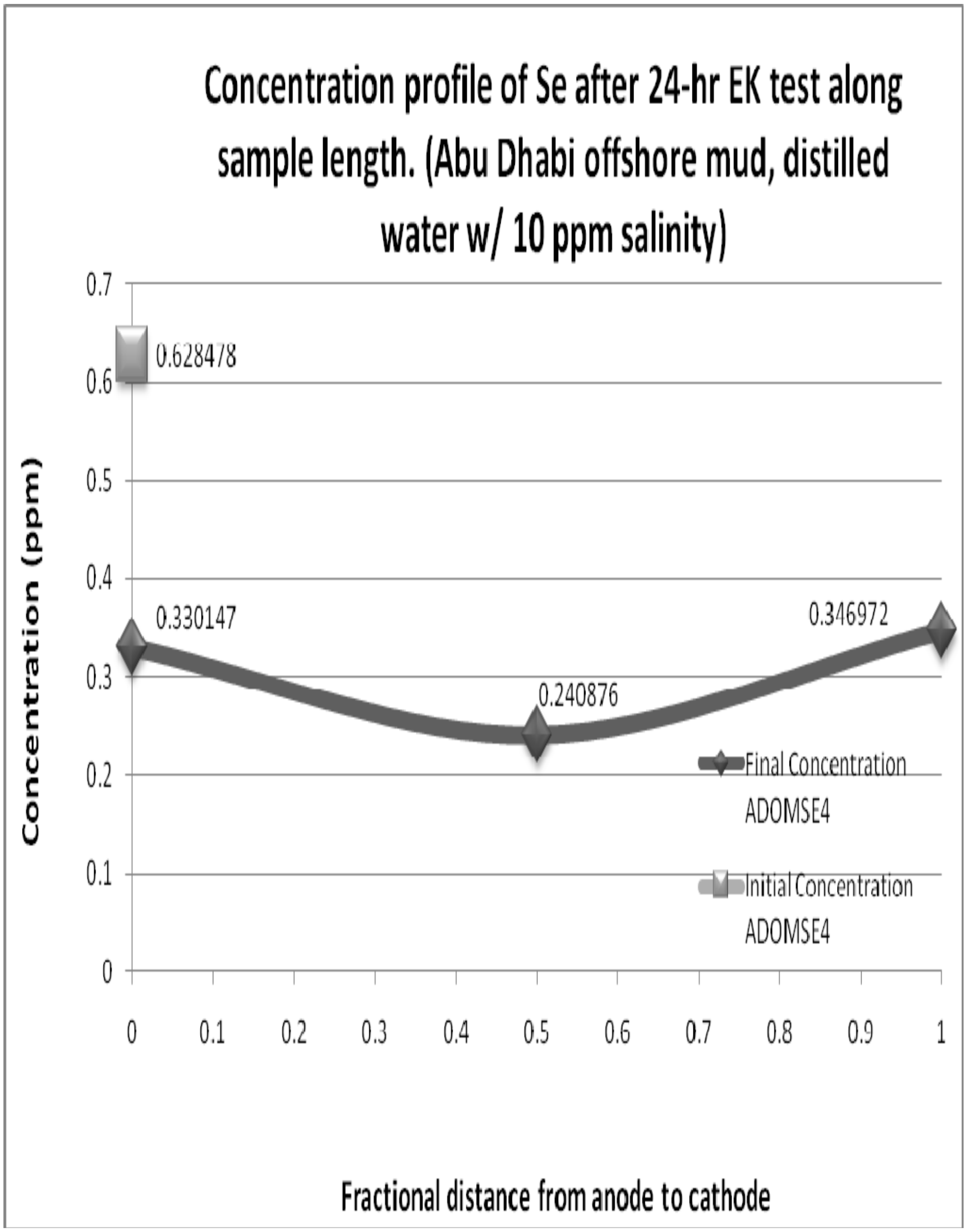

Figure 4-71: Concentration profile of Se after 24-hr EK test a long sample length (Abu Dhabi offshore mud, distilled water 10 ppm salinity).

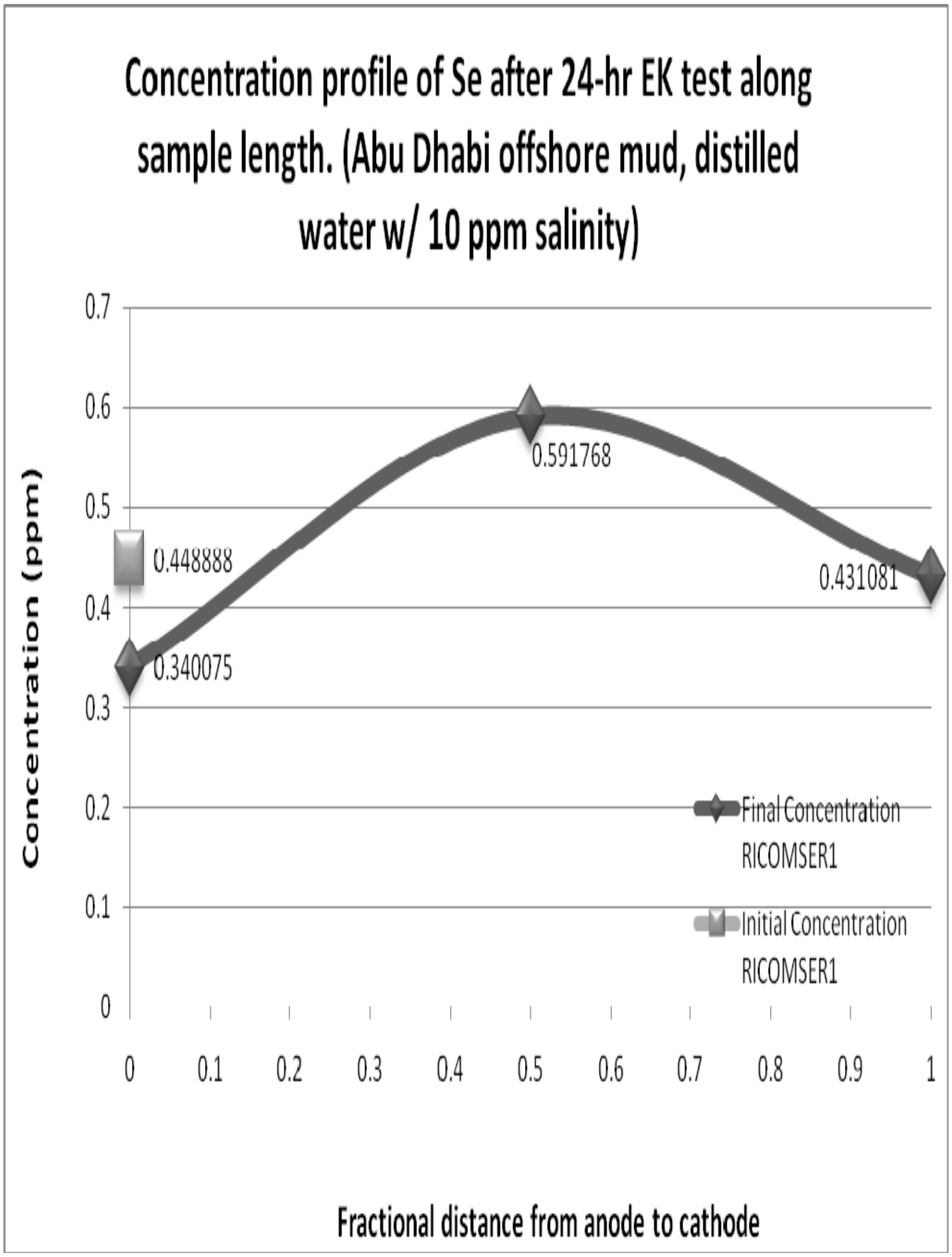

Figure 4-72: Concentration profile of Se after 24-hr EK test a long sample length (Abu Dhabi offshore mud, distilled water 10 ppm salinity).

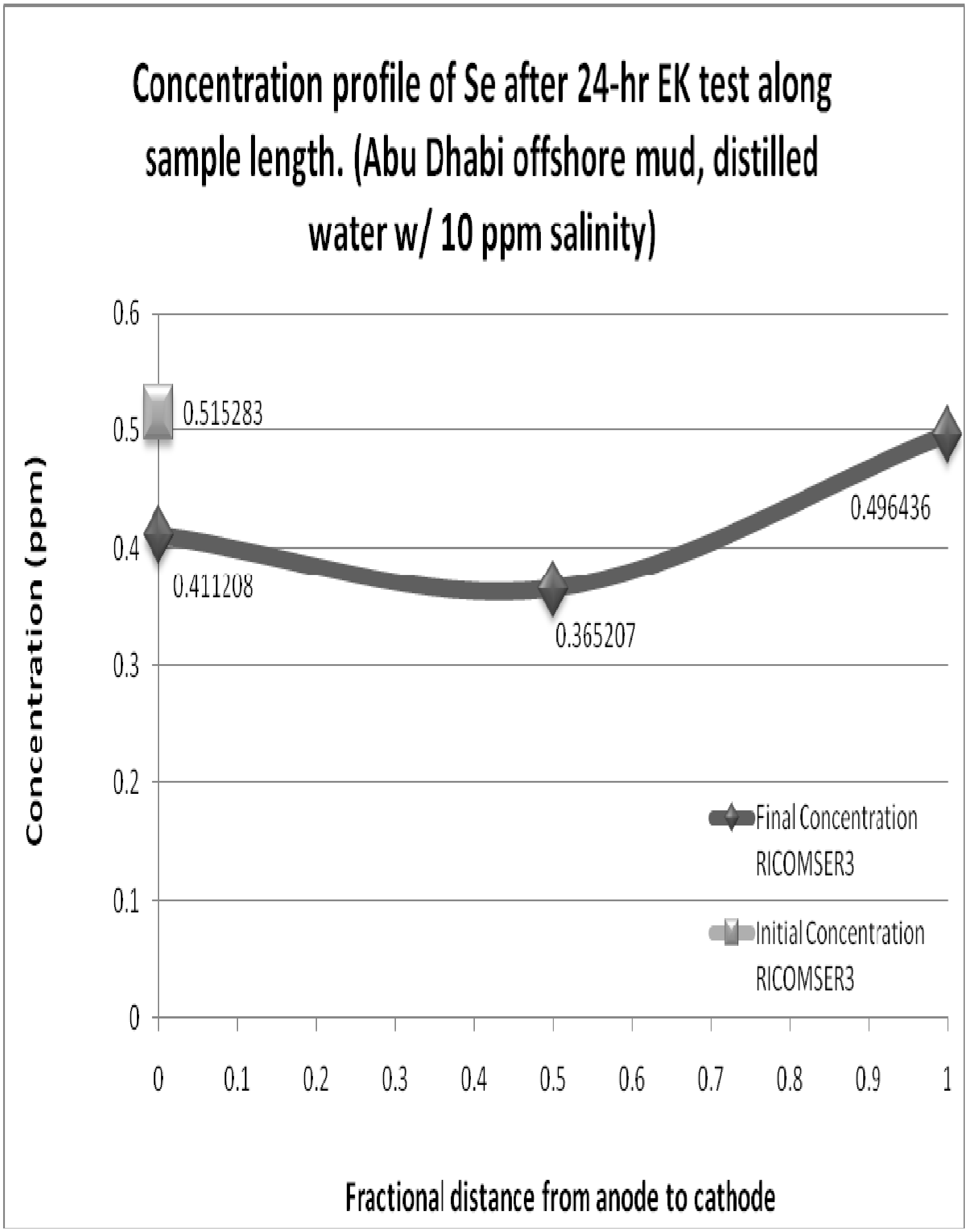

Figure 4-73: Concentration profile of Se after 24-hr EK test a long sample length (Abu Dhabi offshore mud, distilled water 10 ppm salinity).

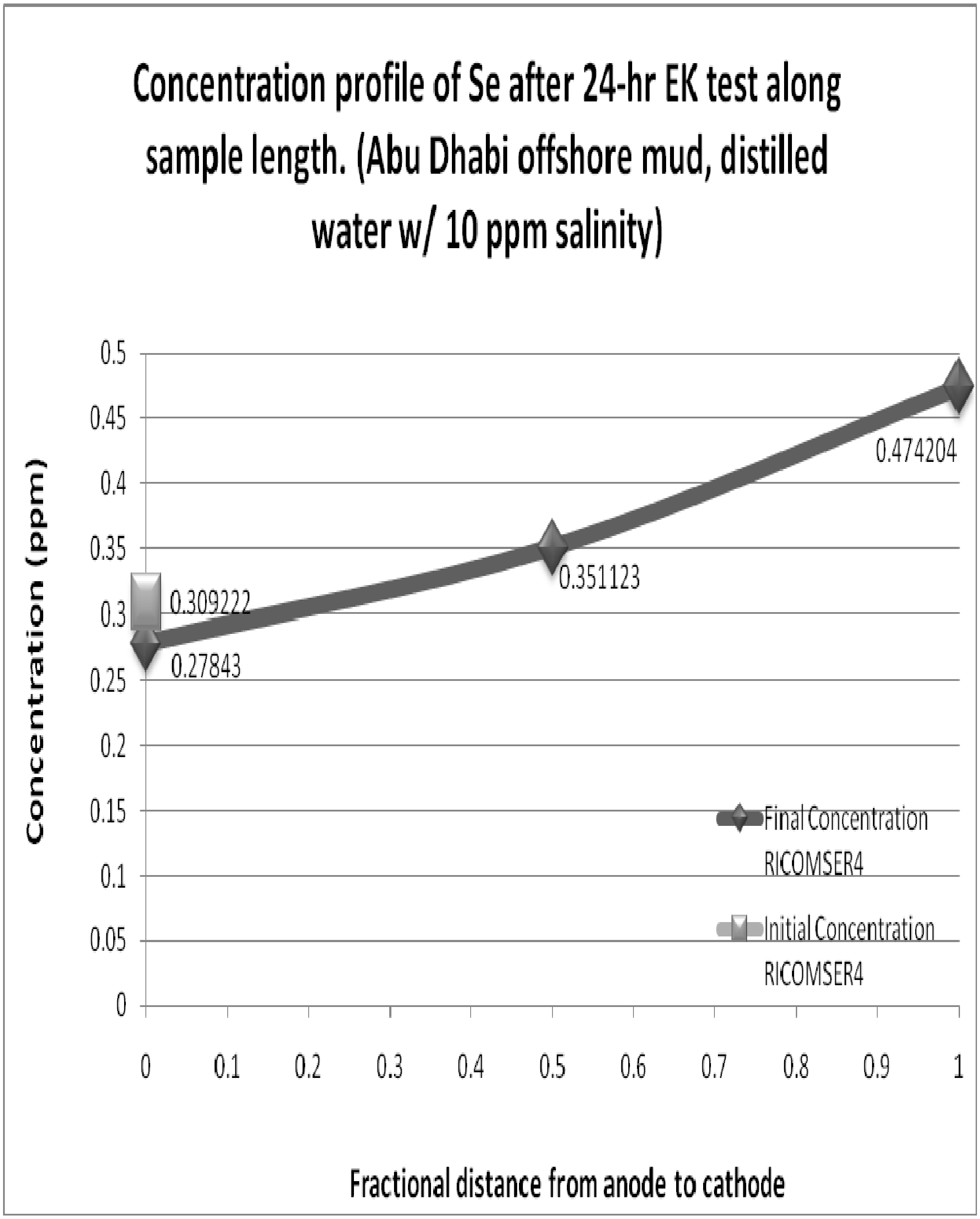

Figure 4-74: Concentration profile of Se after 24-hr EK test a long sample length (Abu Dhabi offshore mud, distilled water 10 ppm salinity).

Selenium: Sample RICOMSWPHSE3 in Figure 4-75 using Abu Dhabi seawater with 26,000 ppm salinity and 450 ppm maleic acid

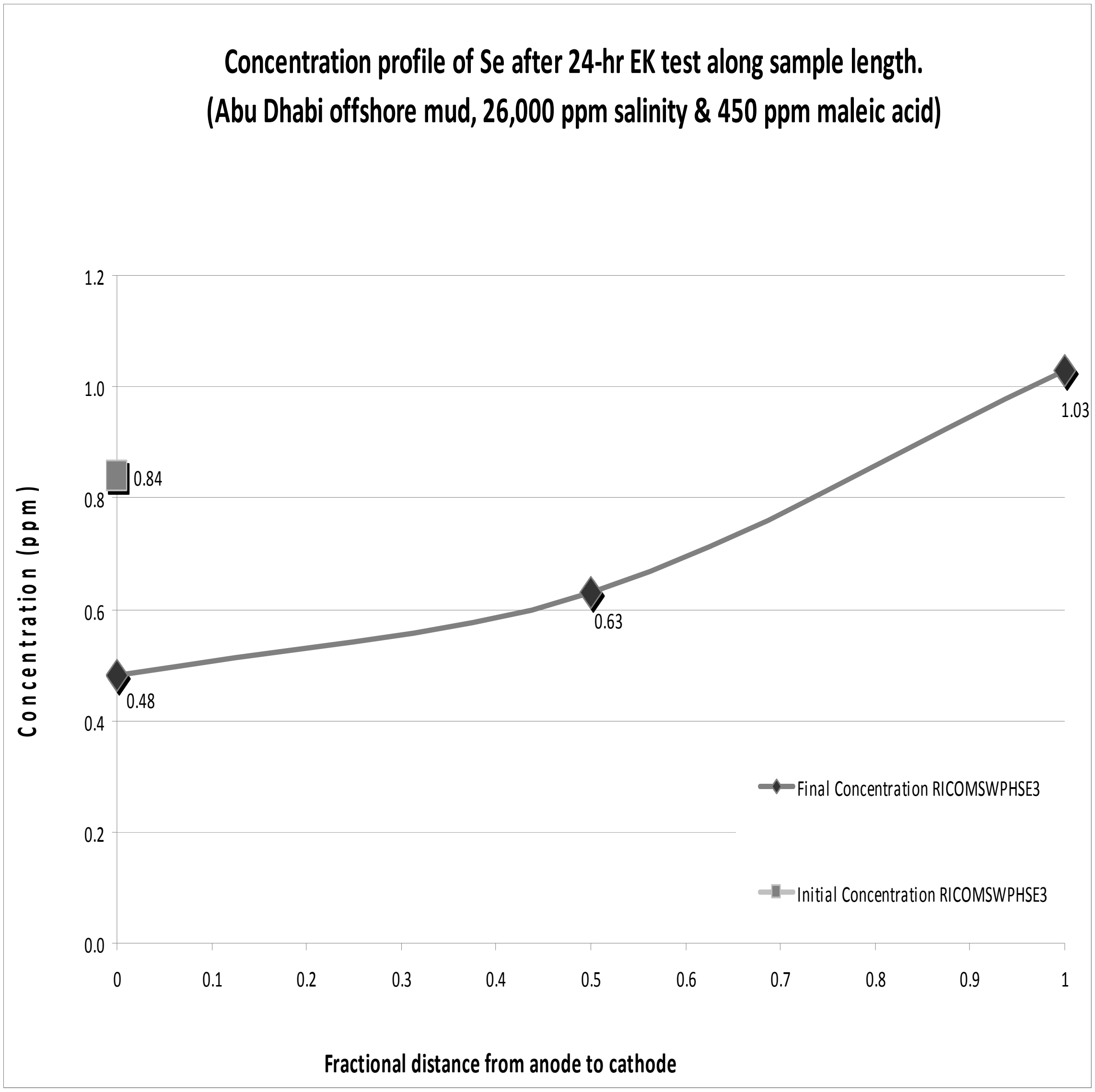

Figure 4-75: Concentration profile of Se after 24-hr EK test a long sample length. (Abu Dhabi offshore mud, 26,000 ppm salinity & 450 ppm maleic acid)

Silver: Silver can be found as a monovalent cationic metal. Silver exits as a monovalent ion throughout the pH range of 2 to 10. Silver is a cation which carries three positive charges. Figure 4-76 through 4-80 show the fraction of the silver found at three locations: anode side, center and cathode end of tested core after 24 hours of electrokinetic treatment. The initial concentrations were predetermined at the anode end of the contaminated offshore mud sample. The removal efficiency was calculated at the anode using equation 4-1 for all results obtained. Substantial reduction of silver from its initial concentration at the anode region was found to be 48.84, 20.77, 47.75, 40.85, and 11.88% after 24 hours using the distilled water with 10 ppm salinity as shown in Figures 4-76 through 4-80 respectively. Electrokinetics was the main driving force of the silver ion in the same direction of the water flow. There was accumulation of metal at the discharge end as shown in both Figures 4-76 through 4-80 (cathode end of the mud sample). The shape of the curve in Figures 4-77, 4-78 and 4-79 can be explained by the lack of pH control.

Ag: 2, 3, 4, 5, R3 samples in Figure 4-76 through 4-80 using Distilled water with 10 ppm salinity

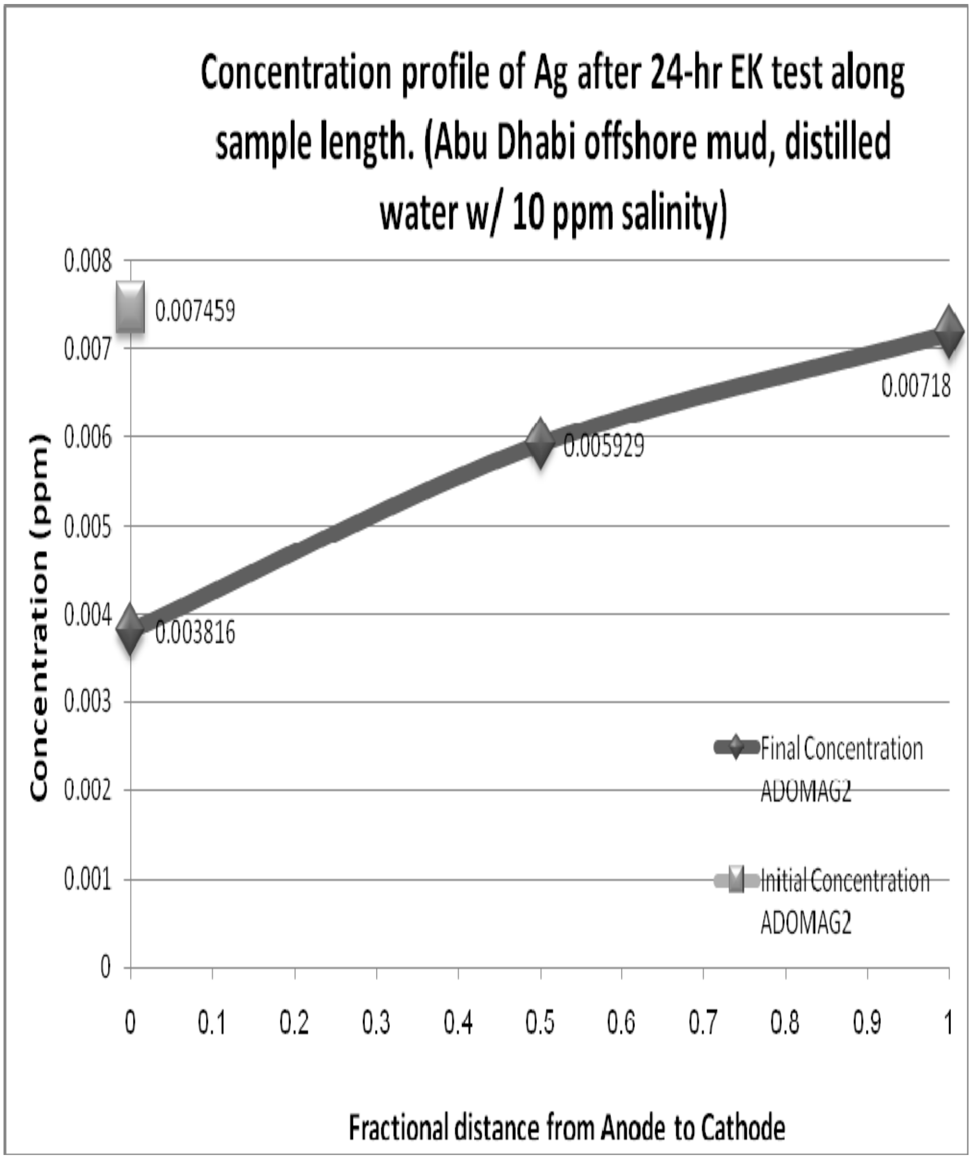

Figure 4-76: Concentration profile of Ag after 24-hr EK test a long sample length (Abu Dhabi offshore mud, distilled water 10 ppm salinity).

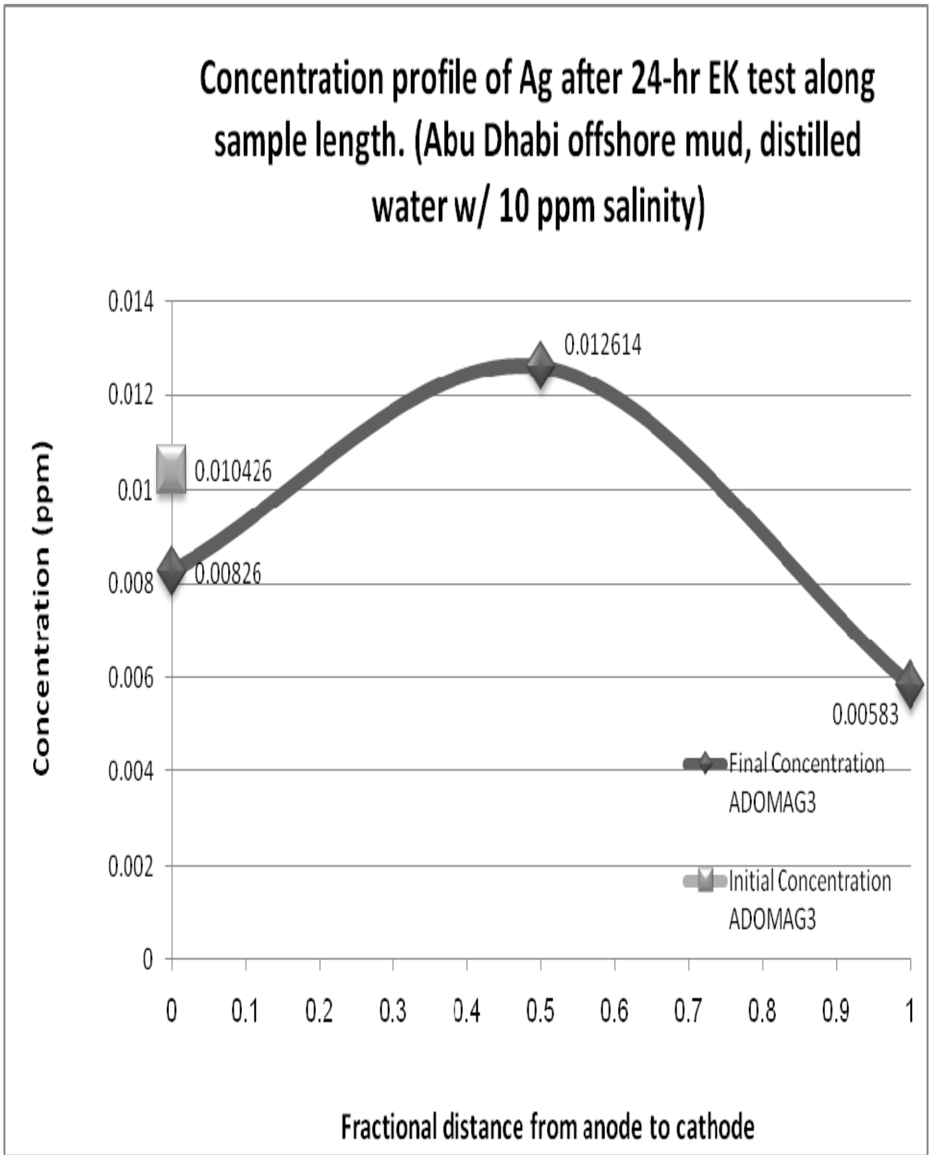

Figure 4-77: Concentration profile of Ag after 24-hr EK test a long sample length (Abu Dhabi offshore mud, distilled water 10 ppm salinity).

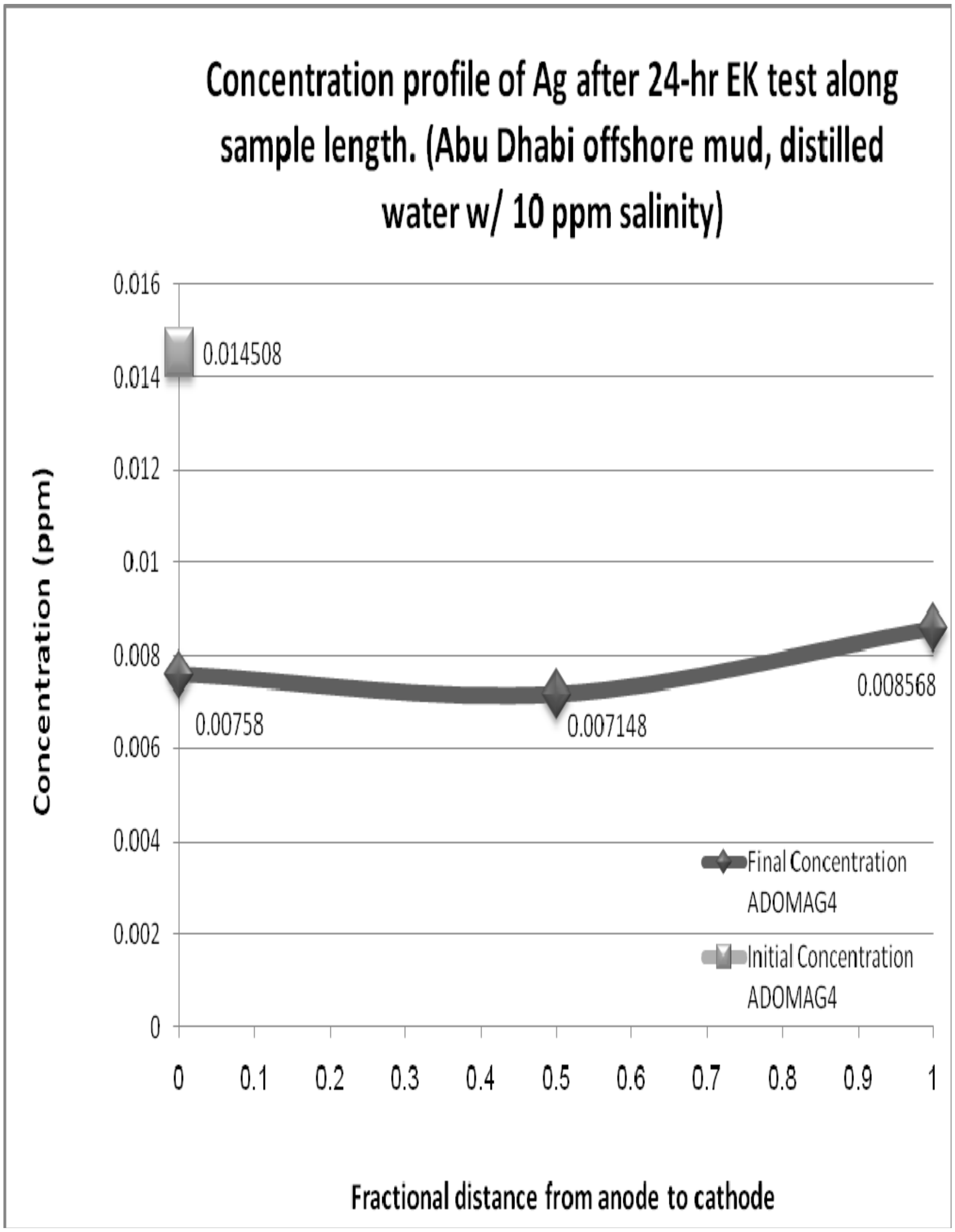

Figure 4-78: Concentration profile of Ag after 24-hr EK test a long sample length (Abu Dhabi offshore mud, distilled water 10 ppm salinity).

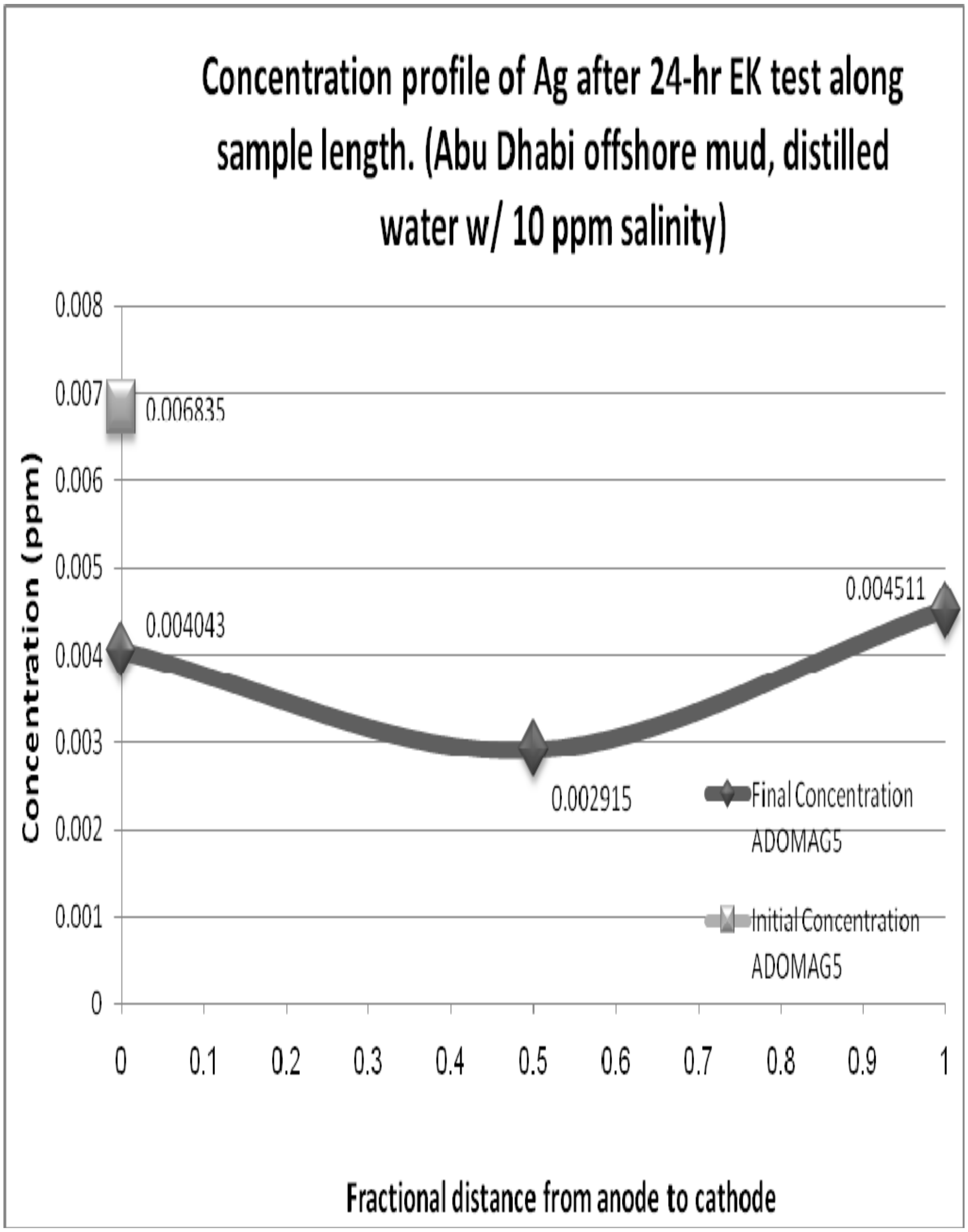

Figure 4-79: Concentration profile of Ag after 24-hr EK test a long sample length (Abu Dhabi offshore mud, distilled water 10 ppm salinity).

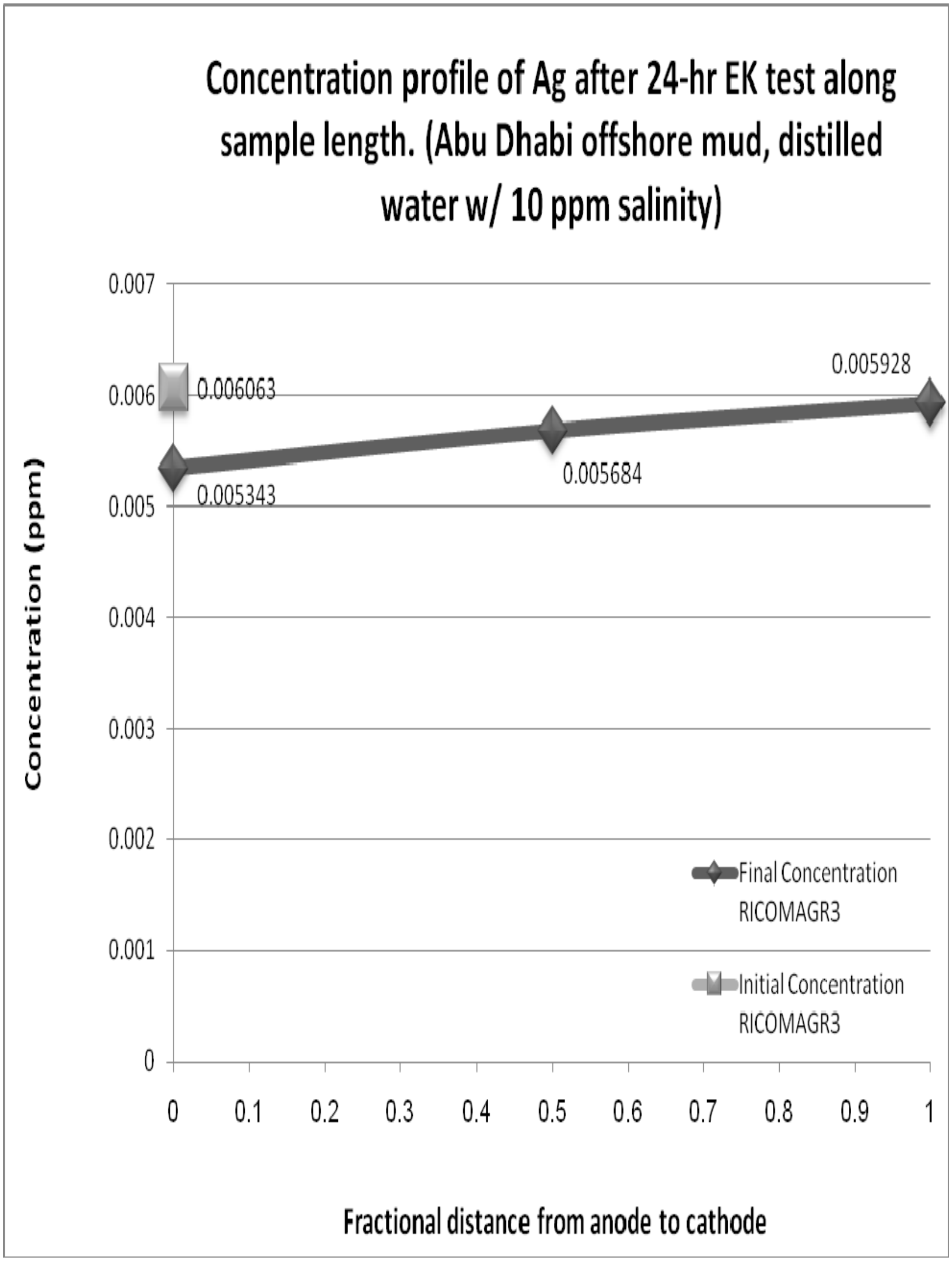

Figure 4-80: Concentration profile of Ag after 24-hr EK test a long sample length (Abu Dhabi offshore mud, distilled water 10 ppm salinity).

Aluminum: Aluminum can be found as a monovalent cationic metal. Aluminum exits as a monovalent ion throughout the pH range of 2 to 10. Aluminum is a cation which carries three positive charges. Figure 4-81 through 4-83 show the fraction of the aluminum found at three locations: anode side, center and cathode end of tested core after 24 hours of electrokinetic treatment. The initial concentrations were predetermined at the anode end of the contaminated offshore mud sample. The removal efficiency was calculated at the anode using equation 4-1 for all results obtained. Substantial reduction of aluminum from its initial concentration at the anode region was found to be 20.72, 32.84, and 21.72% after 24 hours using the distilled water with 10 ppm salinity as shown in Figures 4-81 through 4-83 respectively. Electrokinetics was the main driving force of the aluminum ion in the same direction of the water flow. There was accumulation of metal at the discharge end as shown in both Figures 4-81 through 4-83 (cathode end of the mud sample). The shape of the curve in Figures 4-81 and 4-82 can be explained by the lack of pH control.

Aluminum: 4, 5, R3 samples in Figure 4-81 through 4-83 using Distilled water with 10 ppm salinity

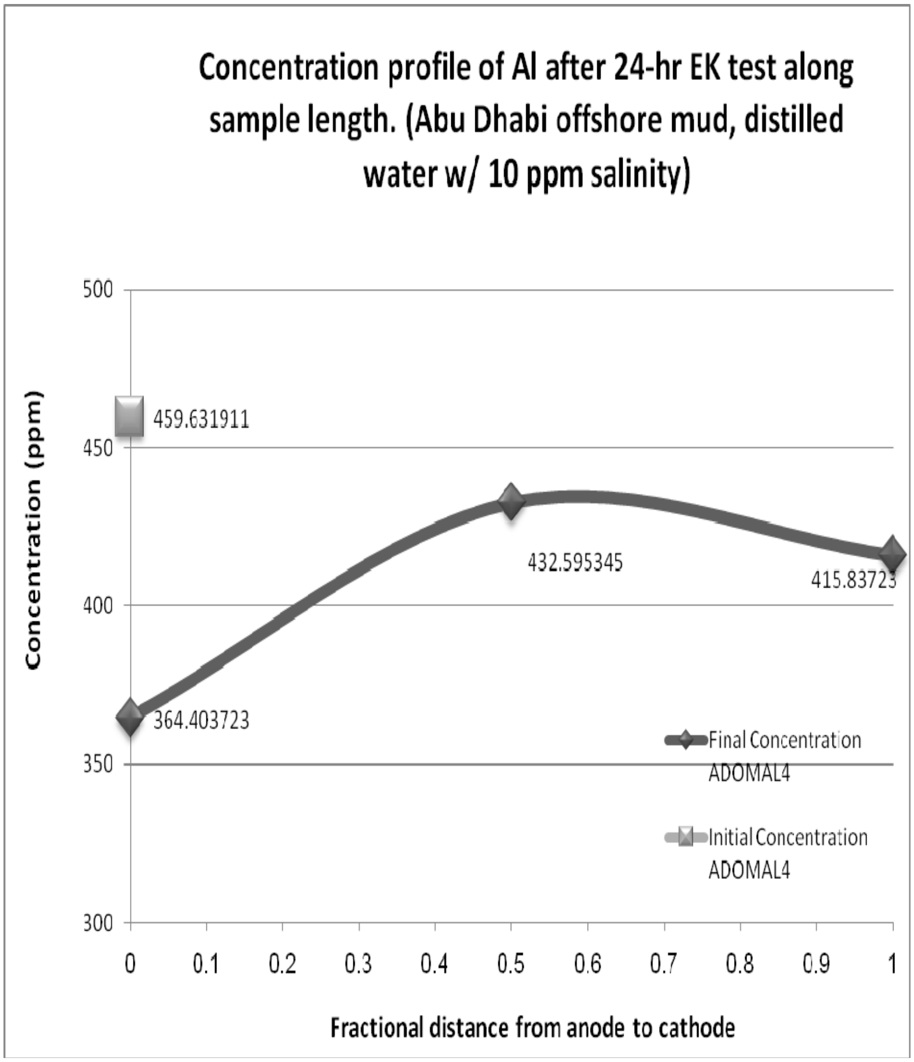

Figure 4-81: Concentration profile of Al after 24-hr EK test a long sample length (Abu Dhabi offshore mud, distilled water 10 ppm salinity).

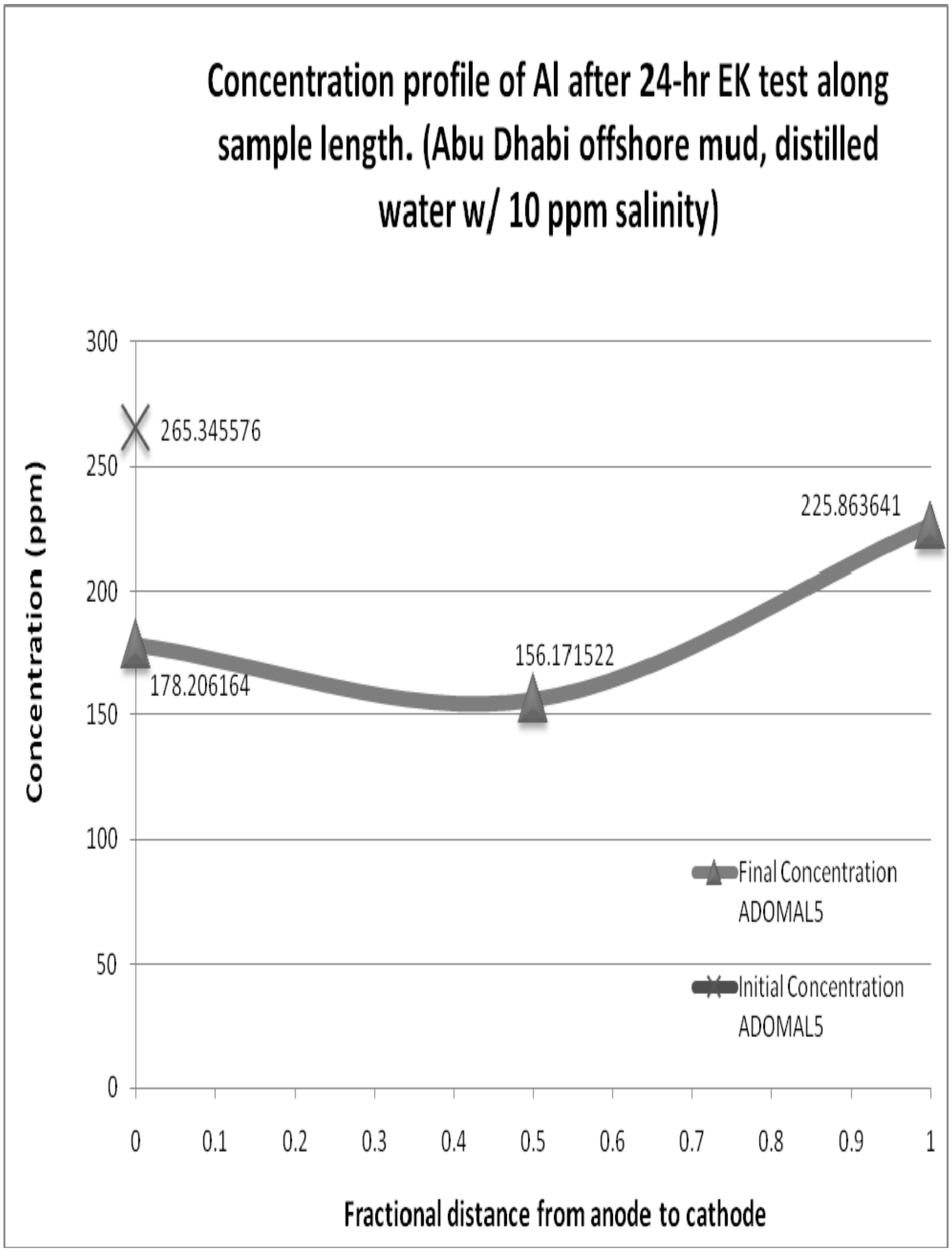

Figure 4-82: Concentration profile of Al after 24-hr EK test a long sample length (Abu Dhabi offshore mud, distilled water 10 ppm salinity).

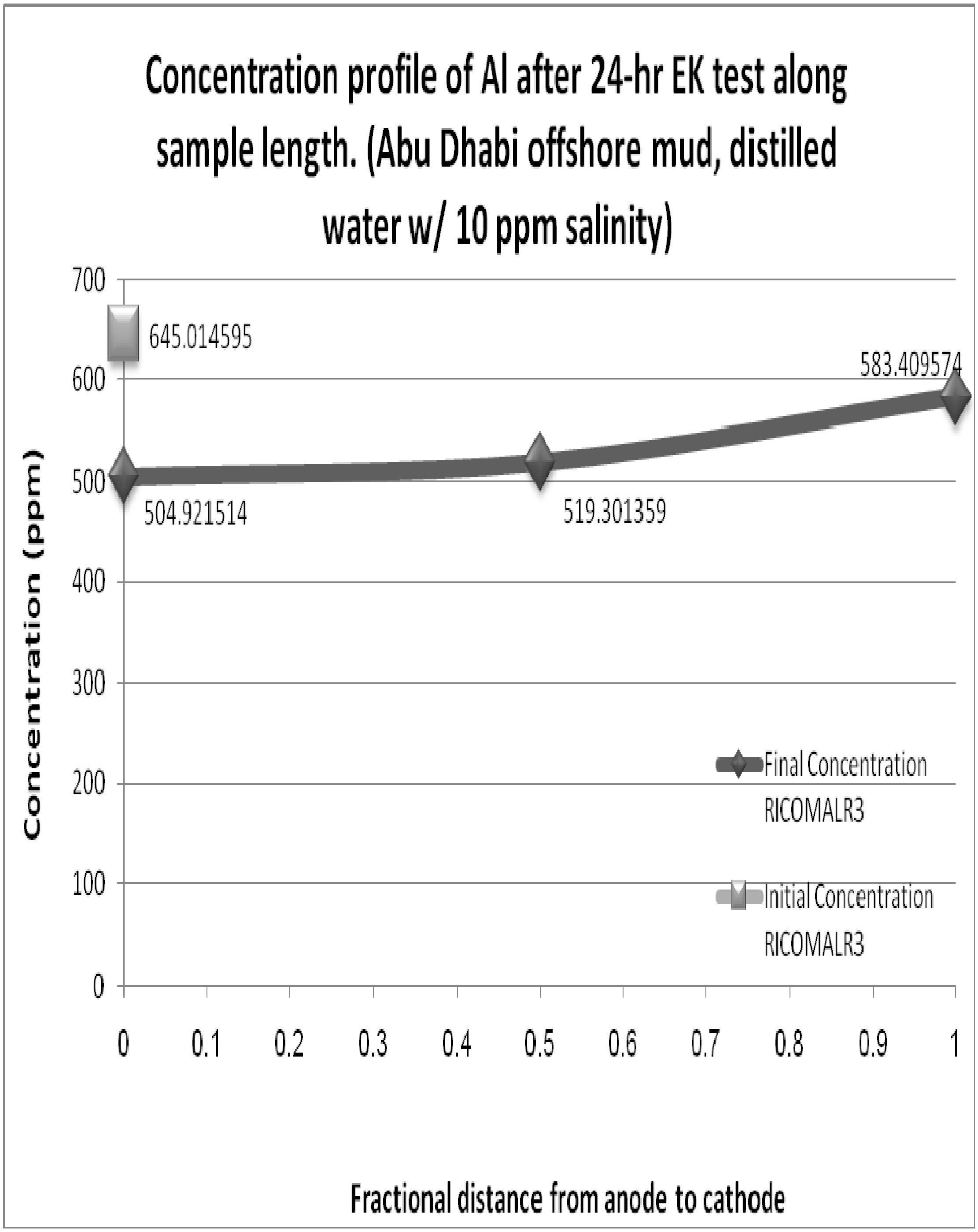

Figure 4-83: Concentration profile of Al after 24-hr EK test a long sample length (Abu Dhabi offshore mud, distilled water 10 ppm salinity).

Cobalt: Cobalt is a divalent cation which is in only oxidation state under normal pH conditions. Below pH of 9 it does not precipitate. The neutral species of $Co(OH)_2$ dominates above pH 9, and anionic species ($Co(OH)_3^-$, $Co(OH)_4^{2-}$) appear at pH>11 (Pamukcu et al., 1993).

Figure 4-84 through 4-85 show the fraction of the cobalt found at three locations: anode side, center and cathode end of tested core after 24 hours of electrokinetic treatment. The initial concentrations were predetermined at the anode end of the contaminated offshore mud sample. The removal efficiency was calculated at the anode using equation 4-1 for all results obtained. Substantial reduction of cobalt from its initial concentration at the anode region was found to be 15.90 and 34.10% after 24 hours using the distilled water with 10 ppm salinity as shown in Figures 4-84 through 4-85 respectively. Electrokinetics was the main driving force of the cobalt ion in the same direction of the water flow. There was accumulation of metal at the discharge end as shown in both Figures 4-81 through 4-83 (cathode end of the mud sample). The shape of the curve in Figures 4-81 and 4-82 can be explained by the lack of pH control.

Cobalt: 5, R3 samples in Figure 4-84 through 4-85 using Distilled water with 10 ppm salinity

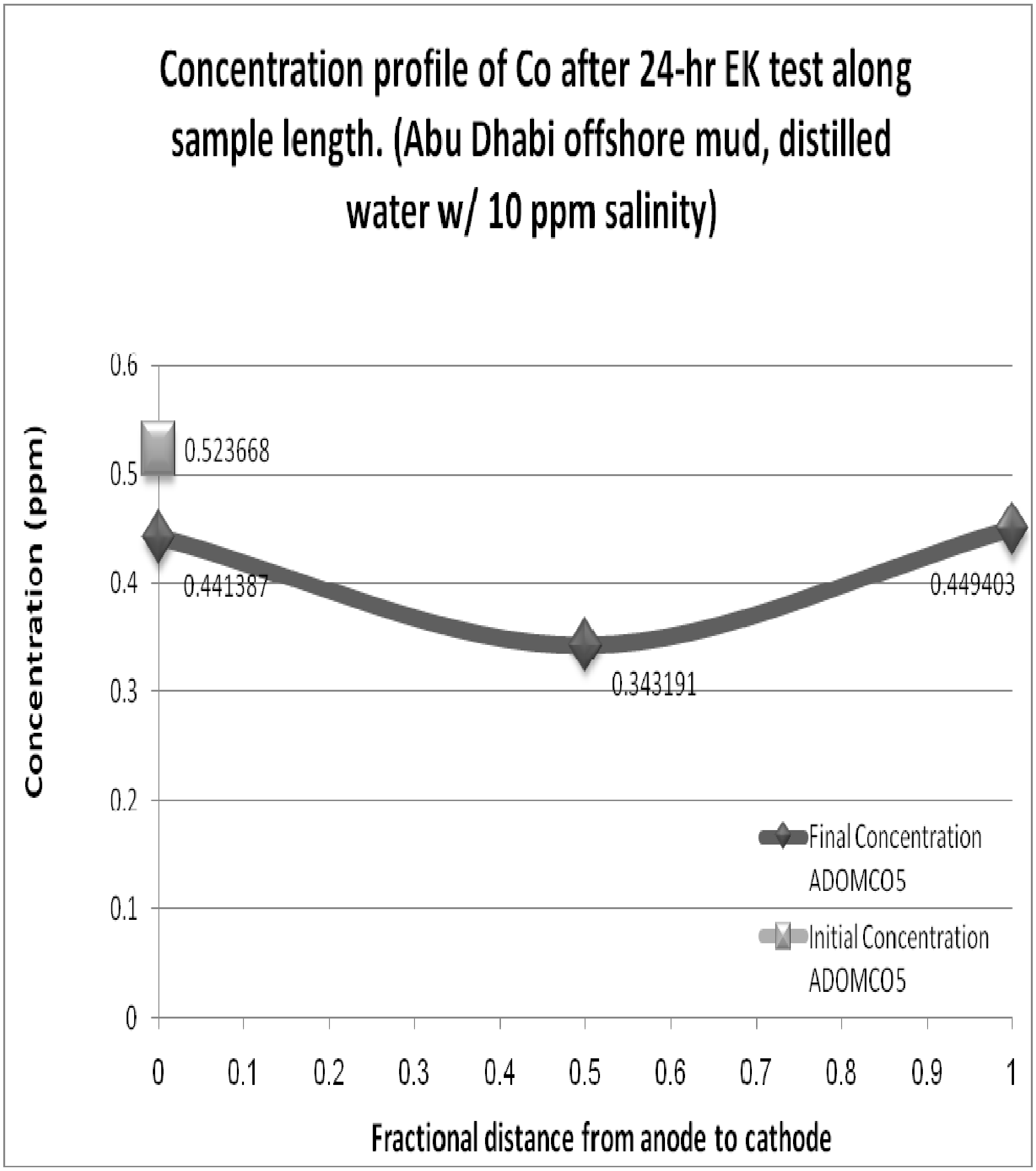

Figure 4-84: Concentration profile of Co after 24-hr EK test a long sample length (Abu Dhabi offshore mud, distilled water 10 ppm salinity).

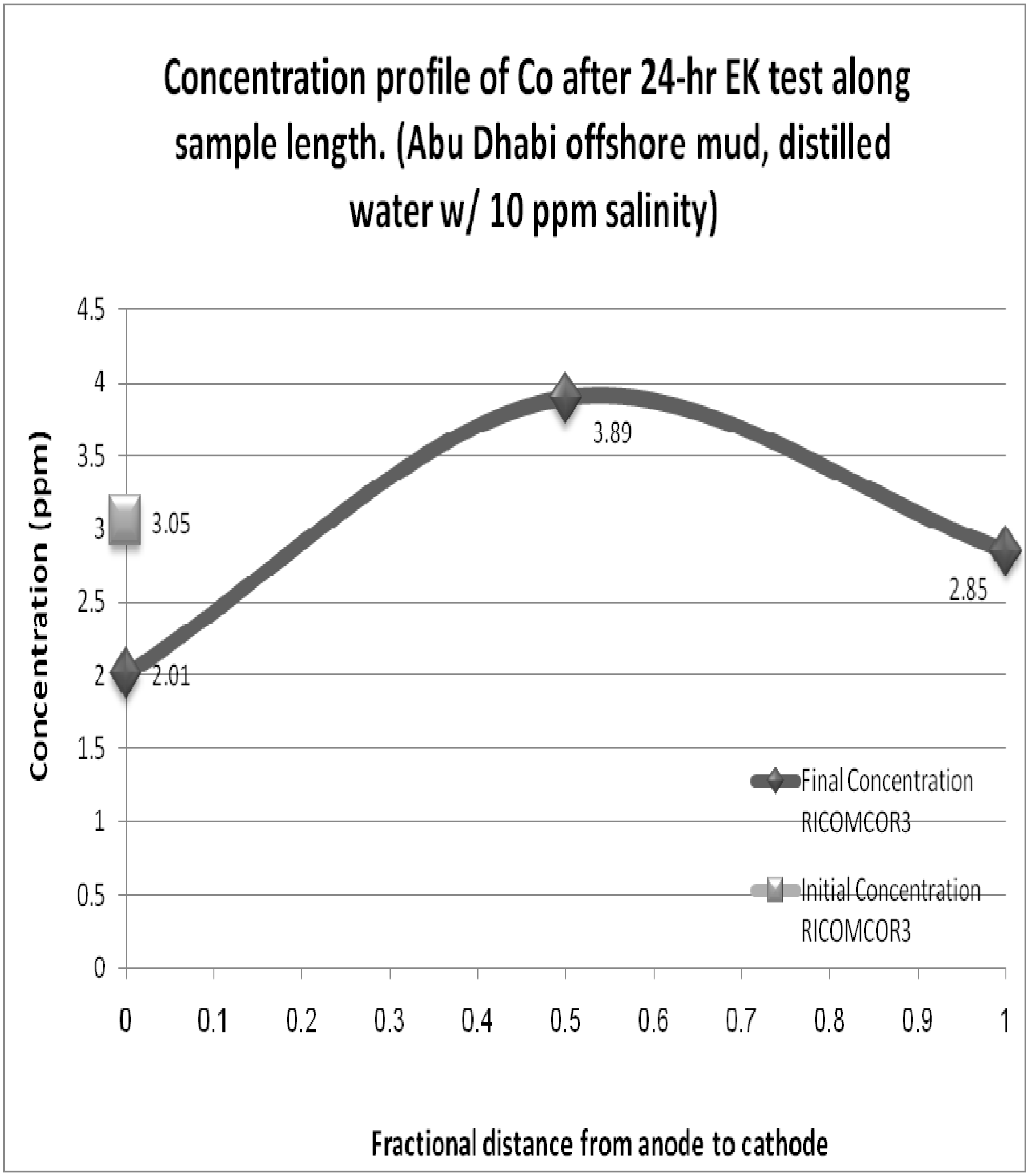

Figure 4-85: Concentration profile of Co after 24-hr EK test a long sample length (Abu Dhabi offshore mud, distilled water 10 ppm salinity).

Strontium: Strontium remains as a divalent ion for a large range of pH values and is stable to precipitation throughout the pH range of 2 to 10. The accumulation of the metal at the cathode region is due to retardation effects of electrophoresis and relaxation as the concentration of the cation increases at the cathode region (Kortum and Bockris, 1951). The mechanism which triggers the accumulation is probably the increased cation retention capacity of the clay at high pH levels (Pamukcu et al., 1993).

Figure 4-86 through 4-88 show the fraction of the strontium found at three locations: anode side, center and cathode end of tested core after 24 hours of electrokinetic treatment. The initial concentrations were predetermined at the anode end of the contaminated offshore mud sample. The removal efficiency was calculated at the anode using equation 4-1 for all results obtained. Substantial reduction of strontium from its initial concentration at the anode region was found to be 8.44 and 2.960% after 24 hours using the distilled water with 10 ppm salinity as shown in Figures 4-86 through 4-87 respectively. Electrokinetics was the main driving force of the strontium ion in the same direction of the water flow. There was accumulation of metal at the discharge end as shown in both Figure 4-86 through 4-87 (cathode end of the mud sample). The shape of the curve in Figures 4-86 and 4-87 can be explained by the lack of pH control.

Figure 4-88 shows the results conducted with Abu Dhabi seawater having 26,000 ppm salinity, as well as 450 ppm of maleic acid added for pH control. The maximum removal efficiency of strontium at the anode region here 9.746% as opposed to the 8.44%, as shown in Figure 4-88. This finding was interesting as it confirmed that the presense of both high salinity and pH control mechanism influenced all the samples tested here to consistently show higher removal efiiciencies at all the three locations analyzed. The high salinity caused a higher conductivity in the bulk solution, where both the current and electrokinetic flow increased several fold. One explanation for this is that the electromigration force is now a dominat force allowing the ionic mobility to travel at 2-3 times faster than in the case of dominant electroosmosis, while another theory is the abundance of large volumes of cations in this high salinity carrying their waters of hydration further promoting ionic species velocity. This needs to be investigated further. Another important factor to consider is that the sea water and formation water in the U.A.E. are very rich in strontium. Thus, more complex strategies must be deployed to isolate each treatment section along the coastline. In addition, maybe a long-term electroremediation strategy will be required.

Strontium: ADOMSR3, ADOMSR4 samples in Figure 4-86 through 4-87 using Distilled water with 10 ppm salinity

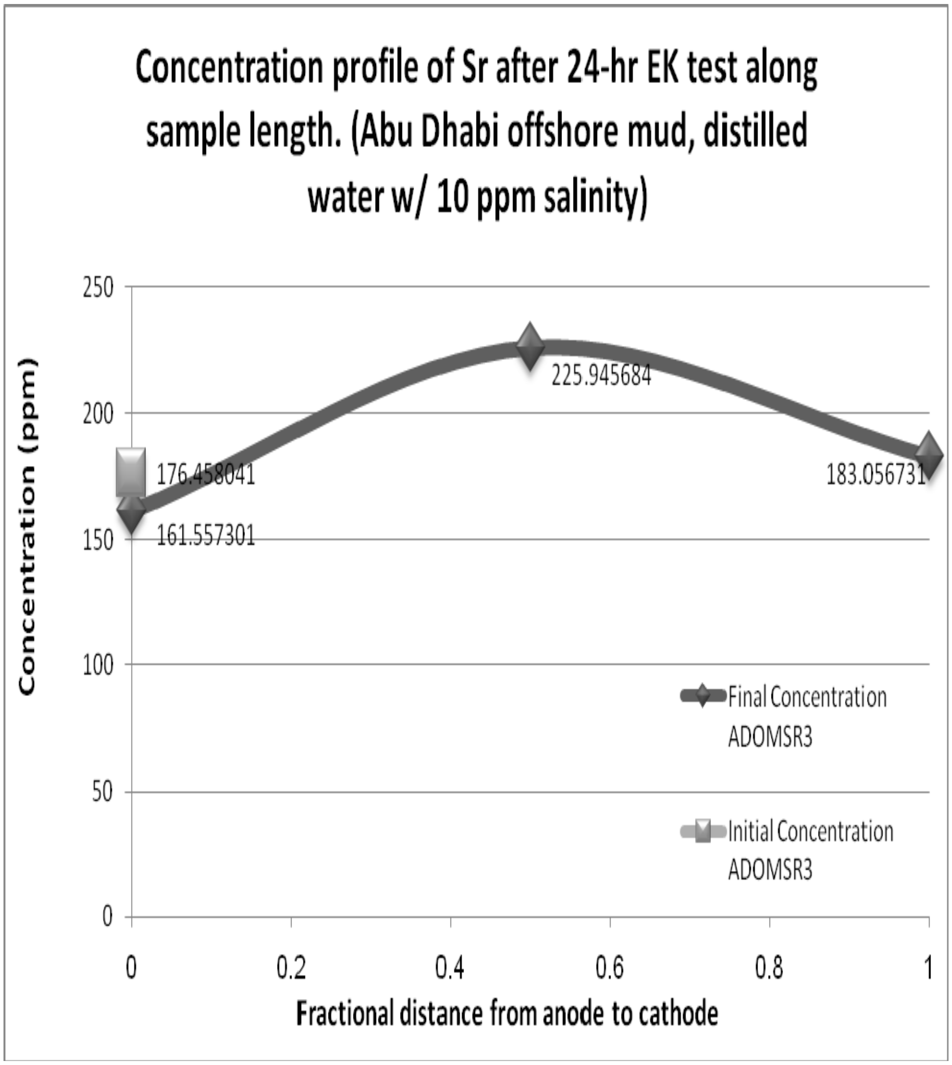

Figure 4-86: Concentration profile of Sr after 24-hr EK test a long sample length (Abu Dhabi offshore mud, distilled water 10 ppm salinity).

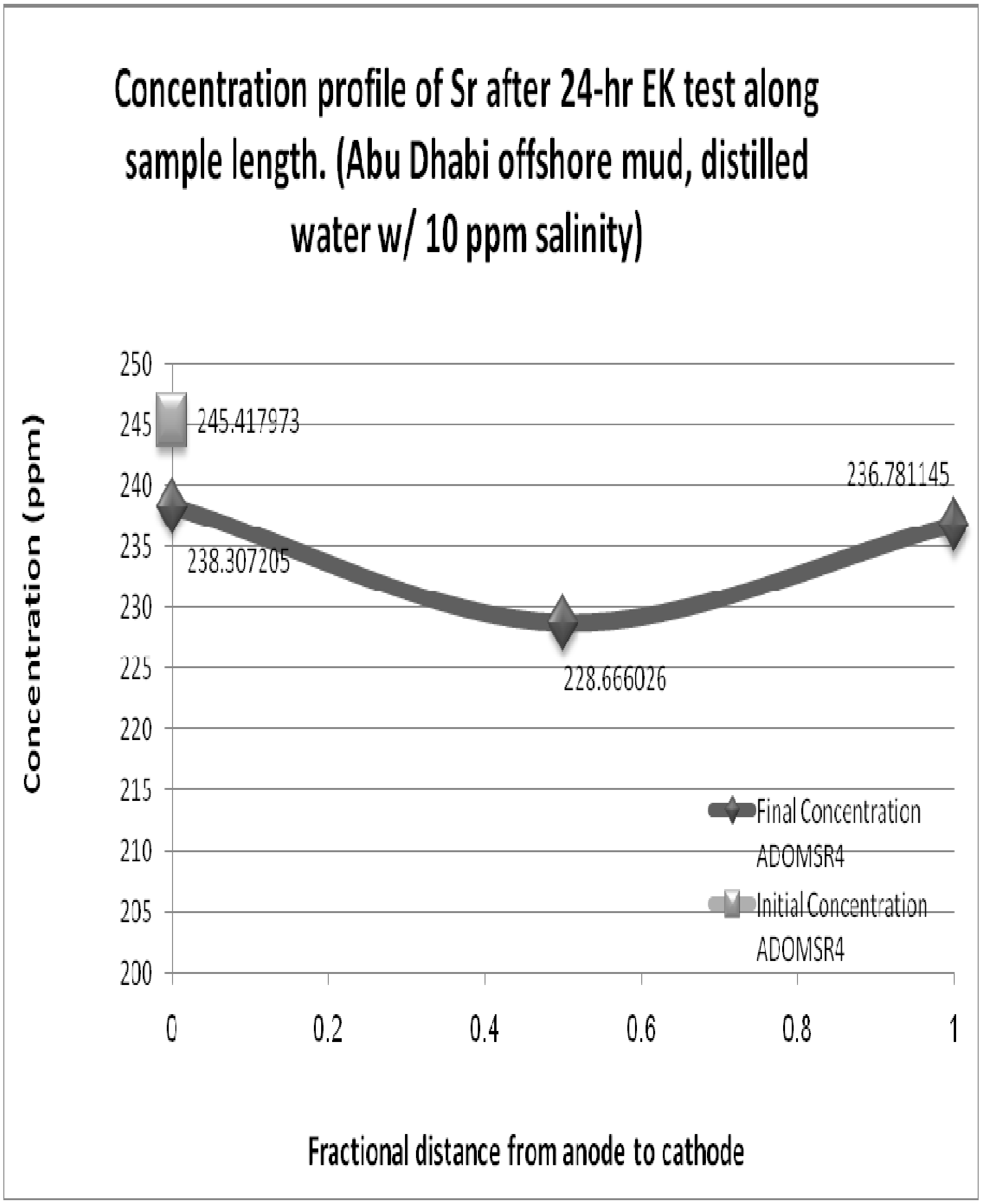

Figure 4-87: Concentration profile of Sr after 24-hr EK test a long sample length (Abu Dhabi offshore mud, distilled water 10 ppm salinity).

Strontium: Sample RICOMSWPHSR2 in Figure 4-88 using Abu Dhabi seawater with 26,000 ppm salinity and 450 ppm maleic acid

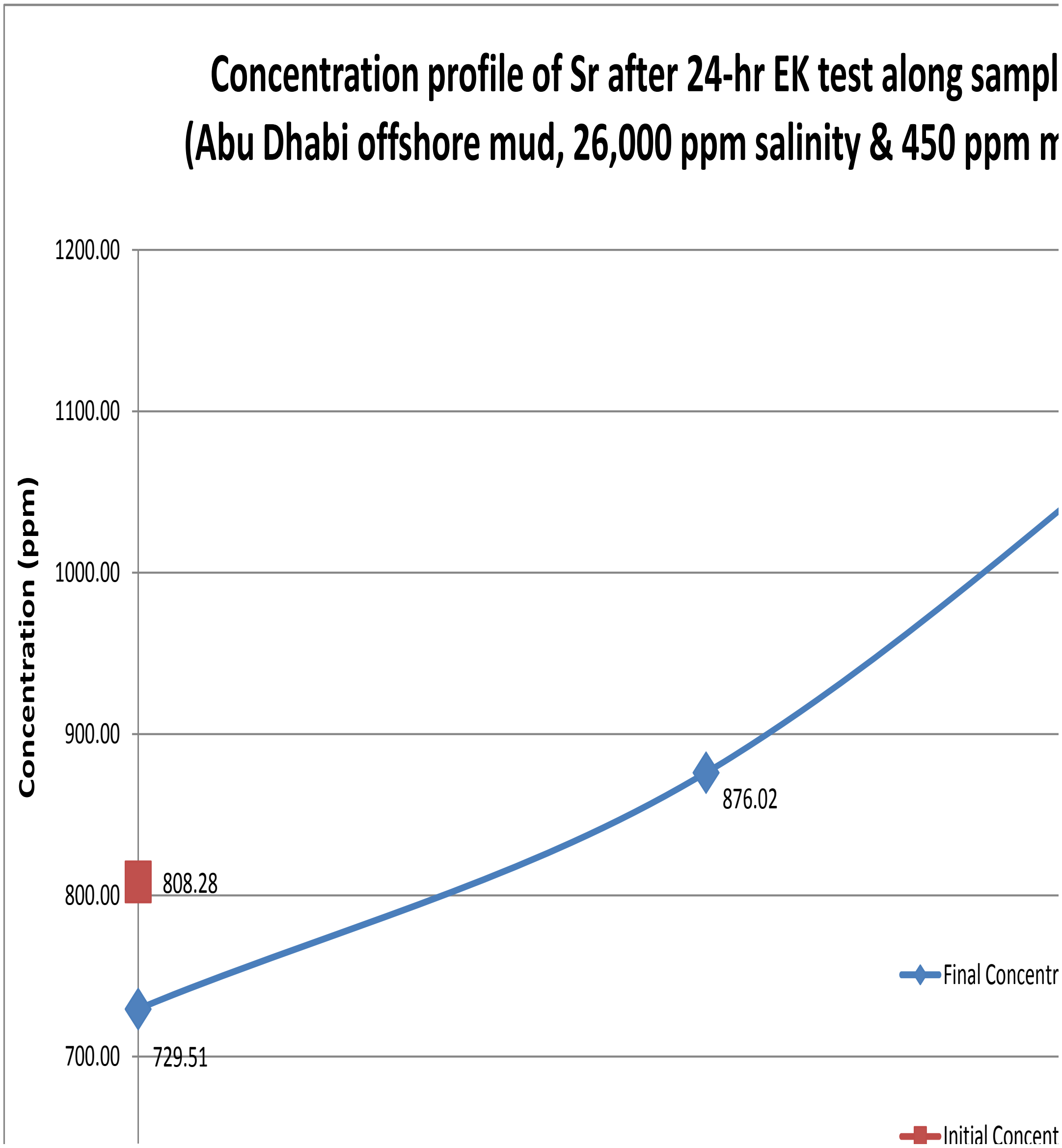

Figure 4-88: Concentration profile of Sr after 24-hr EK test a long sample length. (Abu Dhabi offshore mud, 26,000 ppm salinity & 450 ppm maleic acid)

Titanium: Titanium exits as divalent ionic species throughout the pH range of 2 to 10. Figure 4-89 through 4-92 show the fraction of the titanium found at three locations: anode side, center and cathode end of tested core after 24 hours of electrokinetic treatment. The initial concentrations were predetermined at the anode end of the contaminated offshore mud sample. The removal efficiency was calculated at the anode using equation 4-1 for all results obtained. Substantial reduction of titanium from its initial concentration at the anode region was found to be 21.61, 12.22 and 19.49% after 24 hours using the distilled water with 10 ppm salinity as shown in Figures 4-89 through 4-91 respectively. Electrokinetics was the main driving force of the titanium ion in the same direction of the water flow. There was accumulation of metal at the discharge end as shown in both Figures 4-89 through 4-91 (cathode end of the mud sample). The shape of the curve in Figures 4-89 and 4-90 can be explained by the lack of pH control. Figure 4-92 shows the results conducted with Abu Dhabi seawater having 26,000 ppm salinity, as well as 450 ppm of maleic acid added for pH control. The maximum removal efficiency of titanium at the anode region here 25.04% as opposed to the 19.49%, as shown in Figure 4-92. This finding was interesting as it confirmed that the presense of both high salinity and pH control mechanism influenced all the samples tested here to consistently show higher removal efiiciencies at all the three locations analyzed. The high salinity caused a higher conductivity in the bulk solution, where both the current and electrokinetic flow increased several fold. One explanation for this is that the electromigration force is now a dominat force allowing the ionic mobility to travel at 2-3 times faster than in the case of dominant electroosmosis, while another theory is the abundance of large volumes of cations in this high salinity carrying their waters of hydration further promoting ionic species velocity. This needs to be investigated further.

Titanium: ADOMTI2, ADOMTI3, RICOMTIR3 samples in Figure 4-89 through 4-91 using Distilled water with 10 ppm salinity

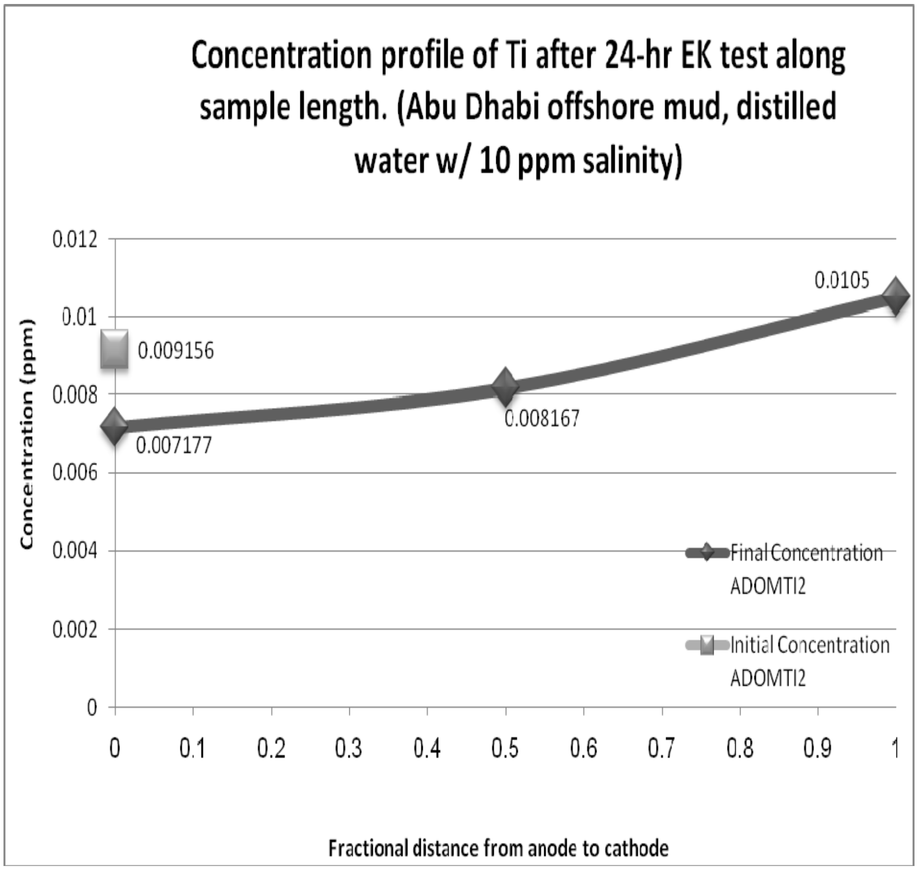

Figure 4-89: Concentration profile of Ti after 24-hr EK test a long sample length (Abu Dhabi offshore mud, distilled water 10 ppm salinity).

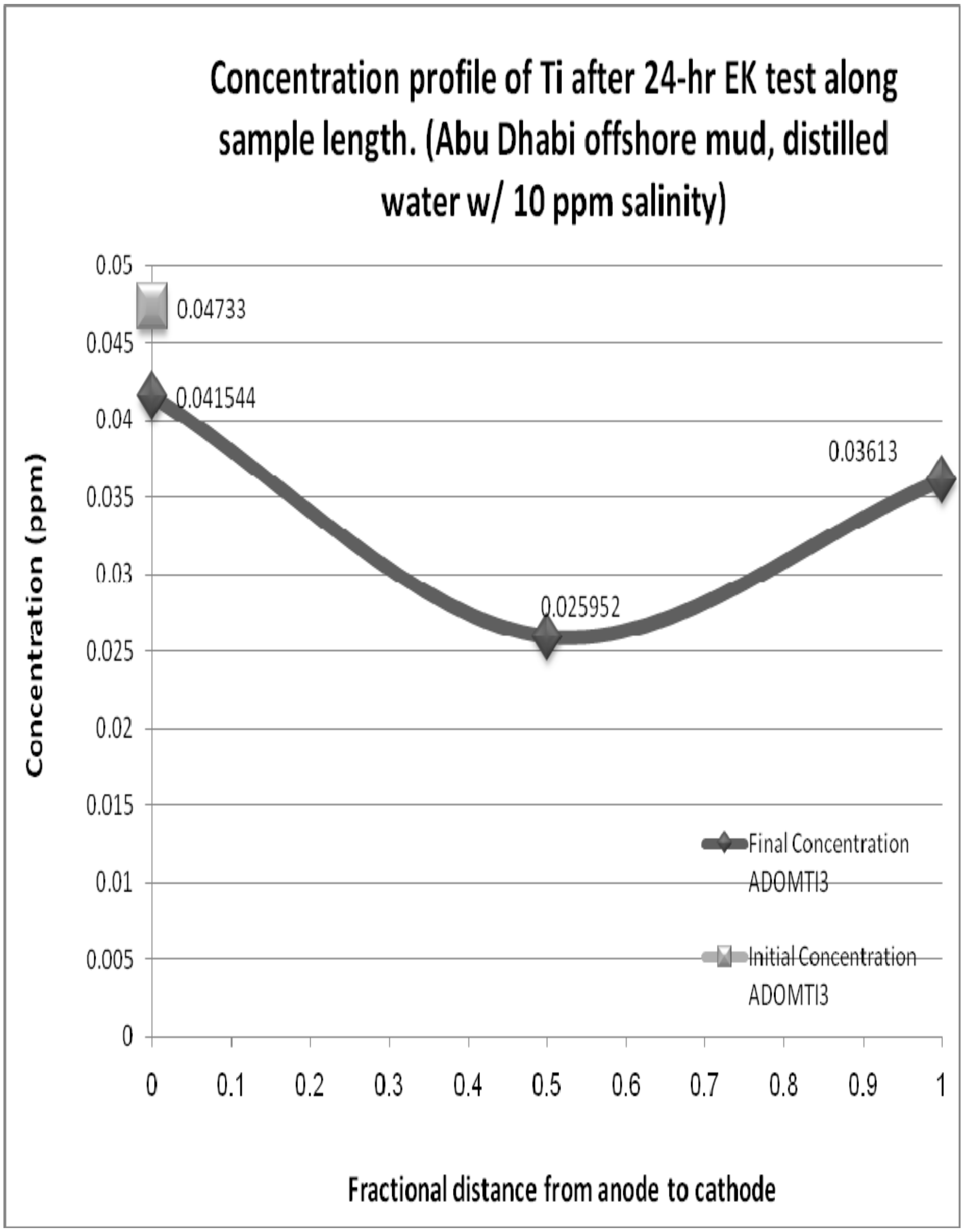

Figure 4-90: Concentration profile of Ti after 24-hr EK test a long sample length (Abu Dhabi offshore mud, distilled water 10 ppm salinity).

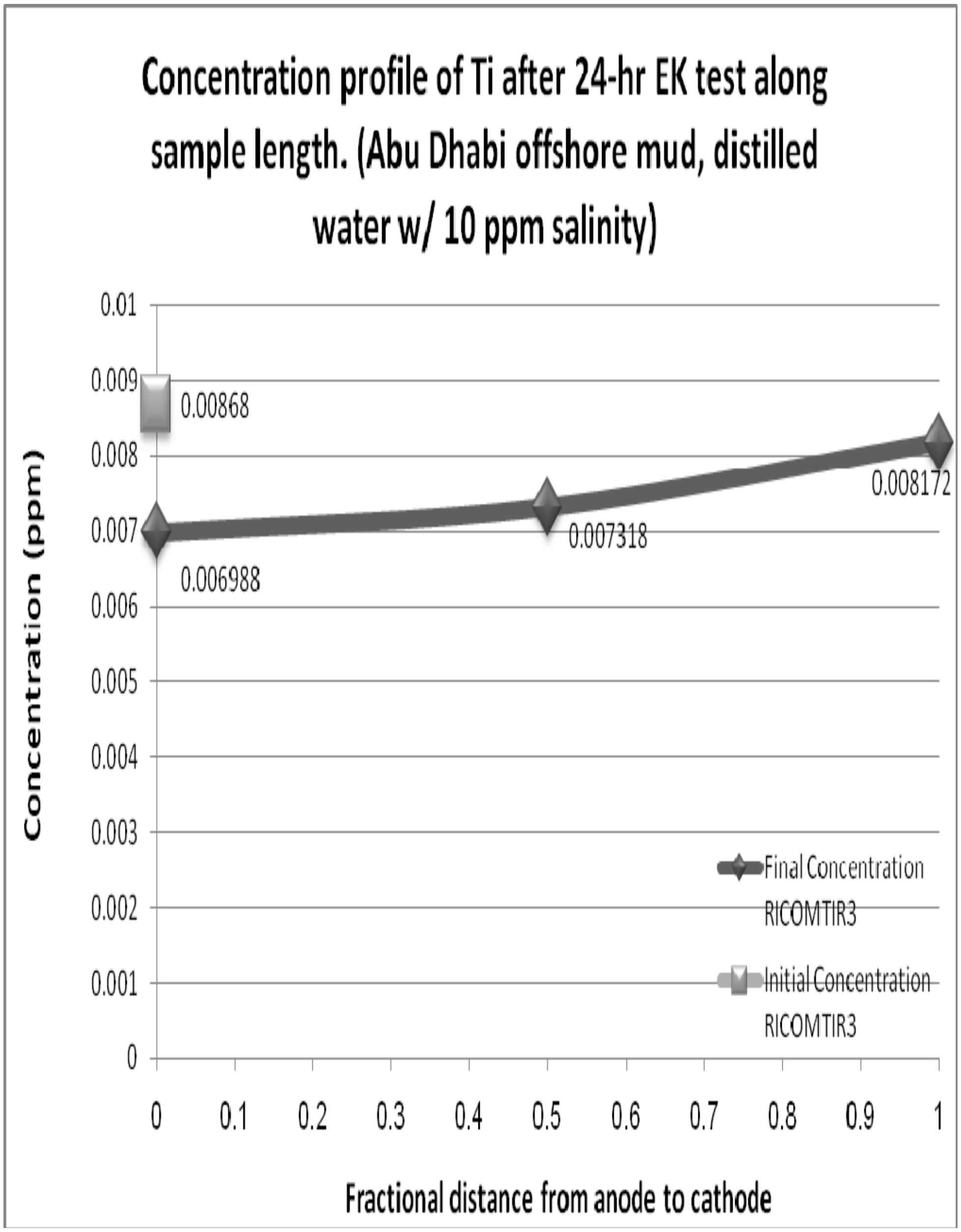

Figure 4-91: Concentration profile of Ti after 24-hr EK test a long sample length (Abu Dhabi offshore mud, distilled water 10 ppm salinity).

Titanium: Sample RICOMSWPHTI2 in Figure 4-92 using Abu Dhabi seawater with 26,000 ppm salinity and 450 ppm maleic acid

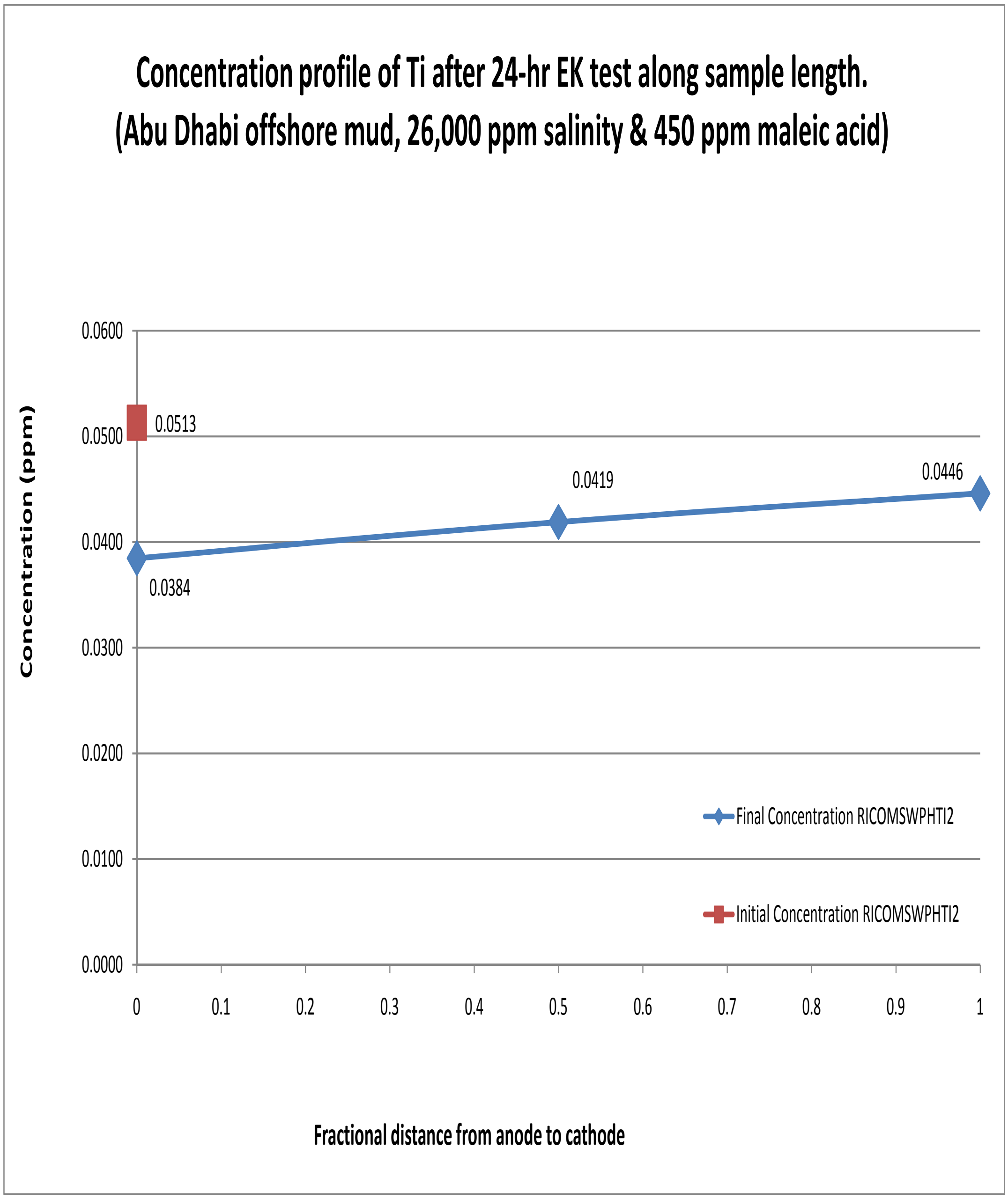

Figure 4-92: Concentration profile of Ti after 24-hr EK test a long sample length. (Abu Dhabi offshore mud, 26,000 ppm salinity & 450 ppm maleic acid)

Uranium: Uranium is a complex ionic species. Below pH of 6, Ur exits as a cation species in nature. At approximately pH of 6, the $UO_2(OH)_2.H_2O$ precipitates (Brovec, 1981). At higher pHs, the anion hydroxide species such as $UO_2(OH)_3^-$ and $UO_2(OH)_4^{2-}$ occurs, which would migrate in the opposite direction of flow. This is due to electromigration, which occurs 2 to 3 times faster than electrokinetics. These species may never be able to travel back to the anode chamber since they encounter low pH environment on the way and tend to change back to cationic form and, therefore, change direction back towards the cathode again. Diffusion of the metal would then allow this metal to precipitate at both ends of the mud sample. (Pamukcu et al., 1993).

Figure 4-93 through 4-94 show the fraction of the Ur found at three locations: anode side, center and cathode end of tested core after 24 hours of electrokinetic treatment. The initial concentrations were predetermined at the anode end of the contaminated offshore mud sample. The removal efficiency was calculated at the anode using equation 4-1 for all results obtained. Substantial reduction of uranium from its initial concentration at the anode region was found to be 6.67 and 10.01% after 24 hours using the distilled water with 10 ppm salinity as shown in Figures 4-93 through 4-94 respectively. Electrokinetics was the main driving force of the uranium ion in the same direction of the water flow. There was accumulation of metal at the discharge end as shown in both Figures 4-93 through 4-94 (cathode end of the mud sample). The wide range of removal efficiency and the shape of the curve in Figures 4-93 through 4-94 can be attributed to:

(i) The different valencies of this species having different electrokinetic velocity. (Higher the charge, higher the EK velocity).

(ii) Lack of pH control.

Uranium: ADOMUR3, RICOMURR3 samples in Figure 4-93 through 4-94 using Distilled water with 10 ppm salinity

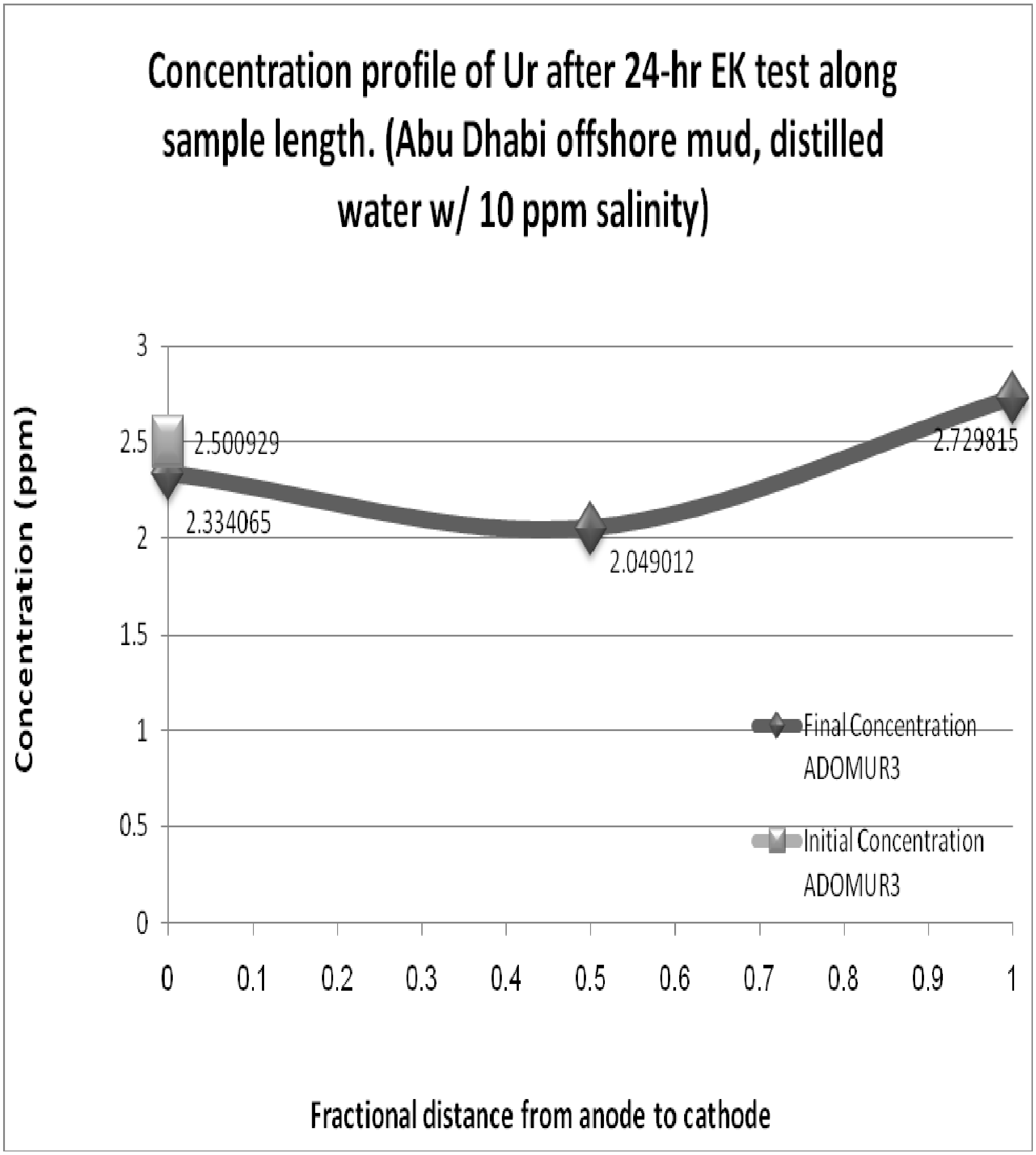

Figure 4-93: Concentration profile of Ur after 24-hr EK test a long sample length (Abu Dhabi offshore mud, distilled water 10 ppm salinity).

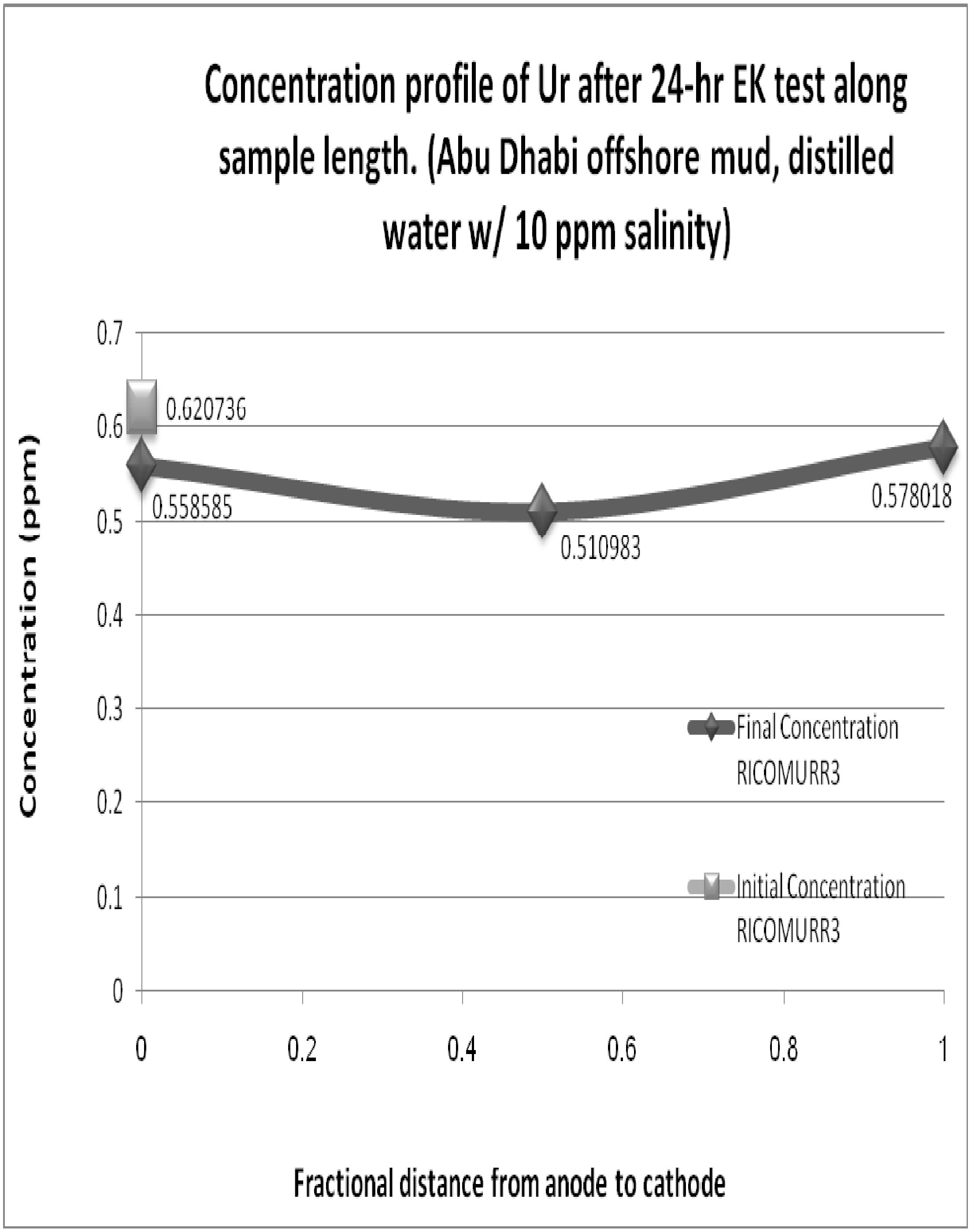

Figure 4-94: Concentration profile of Ur after 24-hr EK test a long sample length (Abu Dhabi offshore mud, distilled water 10 ppm salinity).

Vanadium: Vanadium exits as divalent, trivalent, quadravalent and pentavalent ionic species throughout the pH range of 2 to 10. The mechanism which triggers the accumulation has probably increased the cation retention capacity of the clay at high pH levels.

Figure 4-95 through 4-100 show the fraction of the vanadium found at three locations: anode side, center and cathode end of tested core after 24 hours of electrokinetic treatment. The initial concentrations were predetermined at the anode end of the contaminated offshore mud sample. The removal efficiency was calculated at the anode using equation 4-1 for all results obtained. Substantial reduction of vanadium from its initial concentration at the anode region was found to be 13.73, 14.48, 5.59, 23.86 and 19.18% after 24 hours using the distilled water with 10 ppm salinity as shown in Figures 4-95 through 4-99 respectively. Electrokinetics was the main driving force of the vanadium ion in the same direction of the water flow. There was accumulation of metal at the discharge end as shown in both Figures 4-95 through 4-100 (cathode end of the mud sample). The shape of the curve in Figures 4-96 and 4-98 can be explained by the lack of pH control.

Figure 4-100 shows the results conducted with Abu Dhabi seawater having 26,000 ppm salinity, as well as 450 ppm of maleic acid added for pH control. The maximum removal efficiency of vanadium at the anode region here 18.40% as opposed to the 23.86%, however consistency was achieved using the seawater and pH control, where the lowest removal efficiency recored at the anode here was 12.37% as opposed to 5.59% as shown in Figure 4-97. This finding was interesting as it confirmed that the presense of both high salinity and pH control mechanism influenced all the samples tested here to consistently show higher removal efiiciencies at all the three locations analyzed. The high salinity caused a higher conductivity in the bulk solution, where both the current and electrokinetic flow increased several fold. One explanation for this is that the electromigration force is now a dominat force allowing the ionic mobility to travel at 2-3 times faster than in the case of dominant electroosmosis, while another theory is the abundance of large volumes of cations in this high salinity carrying their waters of hydration further promoting ionic species velocity. This needs to be investigated further.

Vanadium: 2, 3, 4, 5, R3 samples in Figure 4-95 through 4-99 using Distilled water with 10 ppm salinity

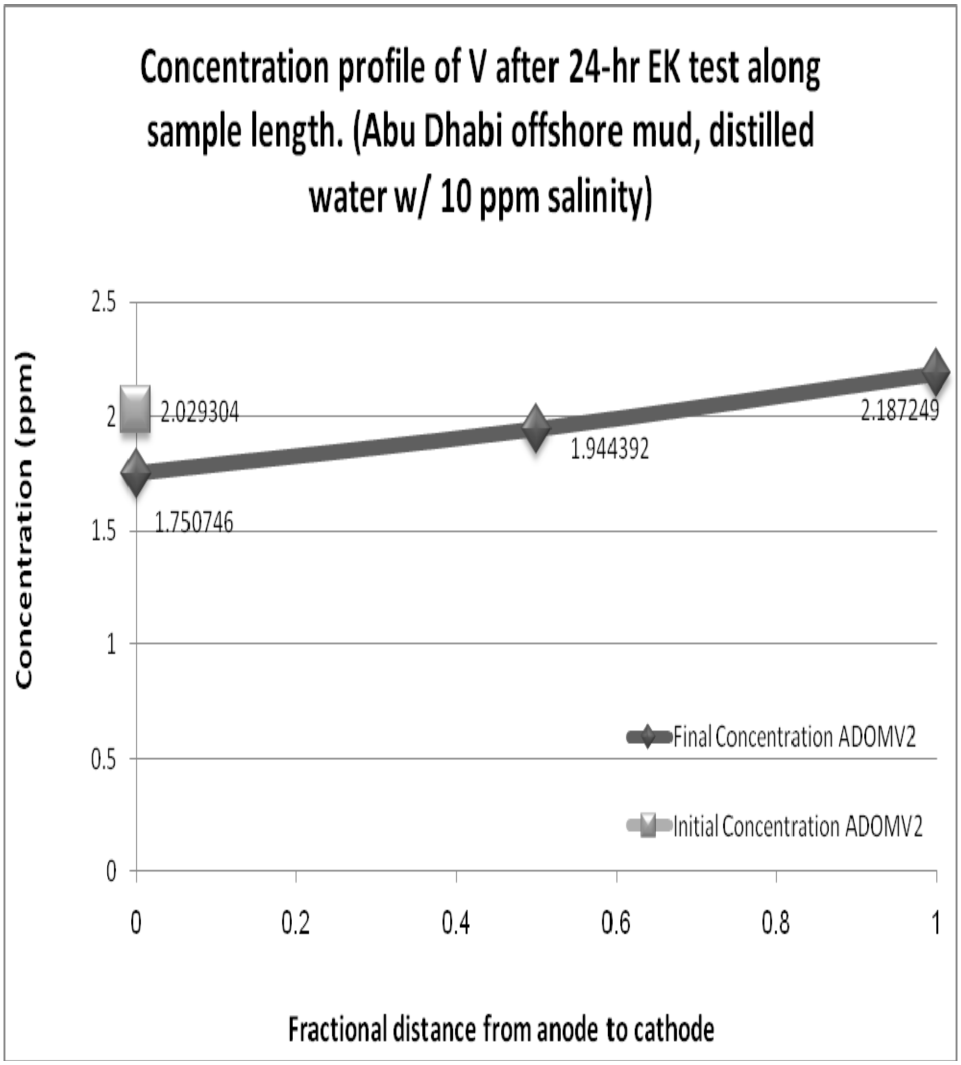

Figure 4-95: Concentration profile of V after 24-hr EK test a long sample length (Abu Dhabi offshore mud, distilled water 10 ppm salinity).

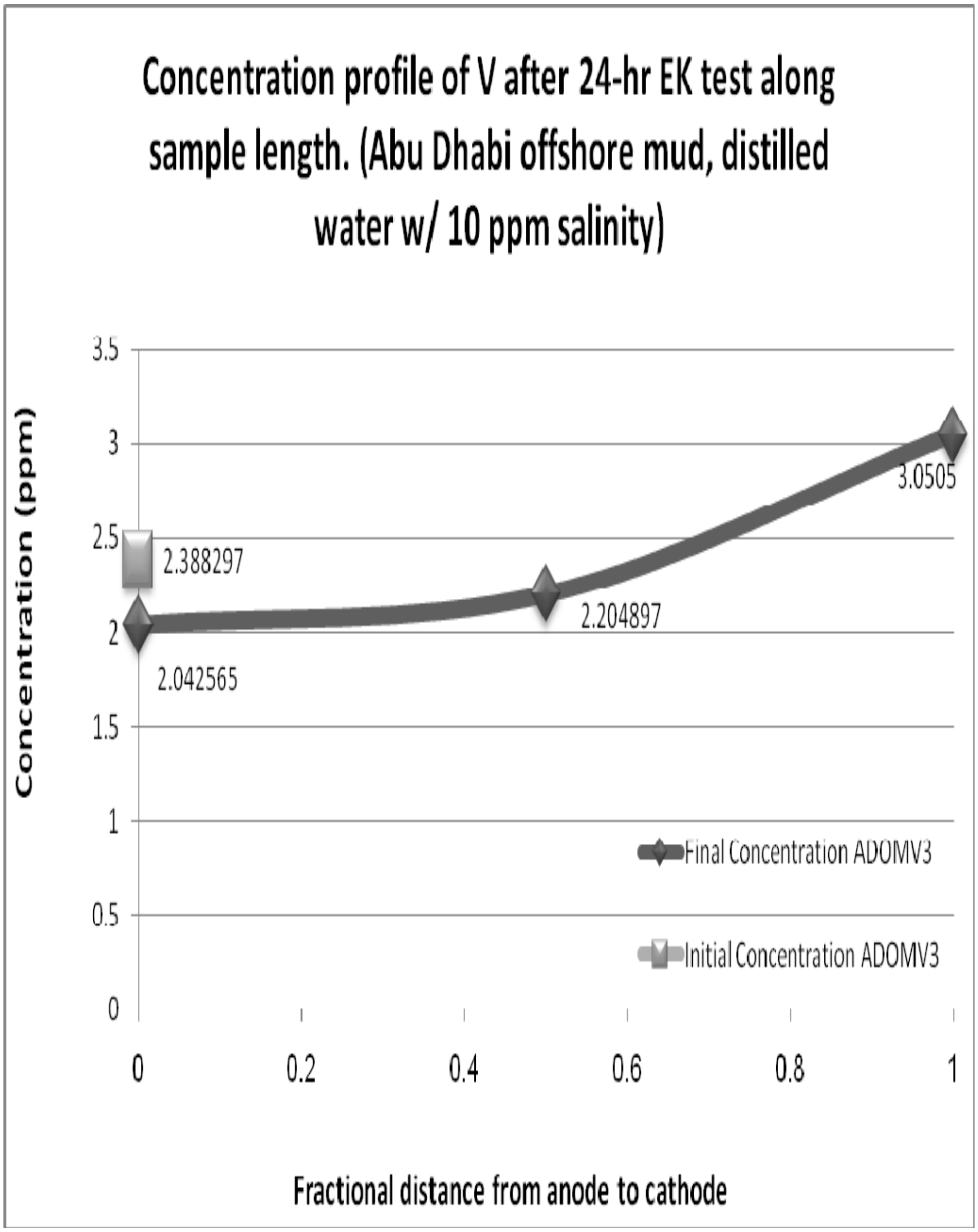

Figure 4-96: Concentration profile of V after 24-hr EK test a long sample length (Abu Dhabi offshore mud, distilled water 10 ppm salinity).

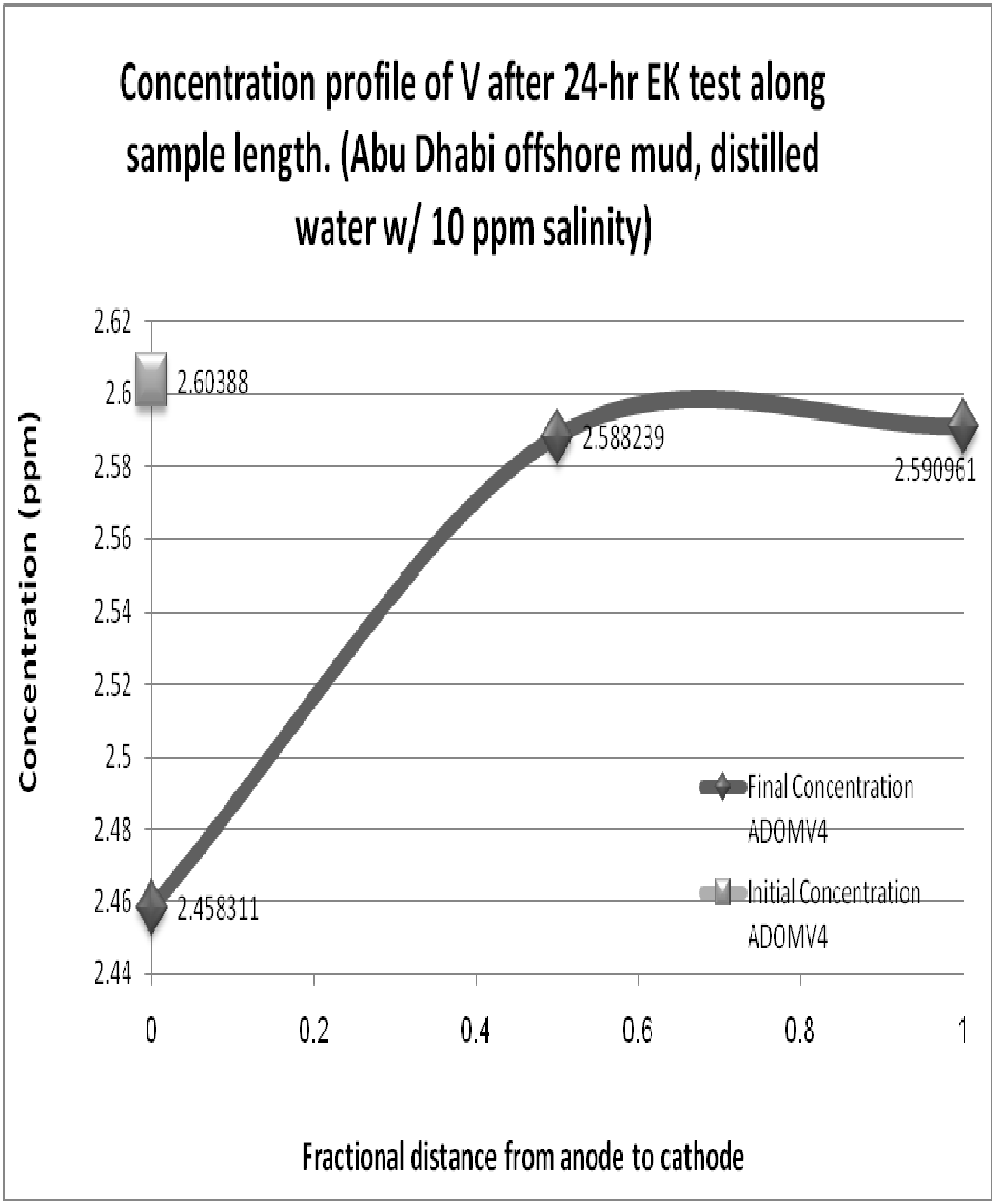

Figure 4-97: Concentration profile of V after 24-hr EK test a long sample length (Abu Dhabi offshore mud, distilled water 10 ppm salinity).

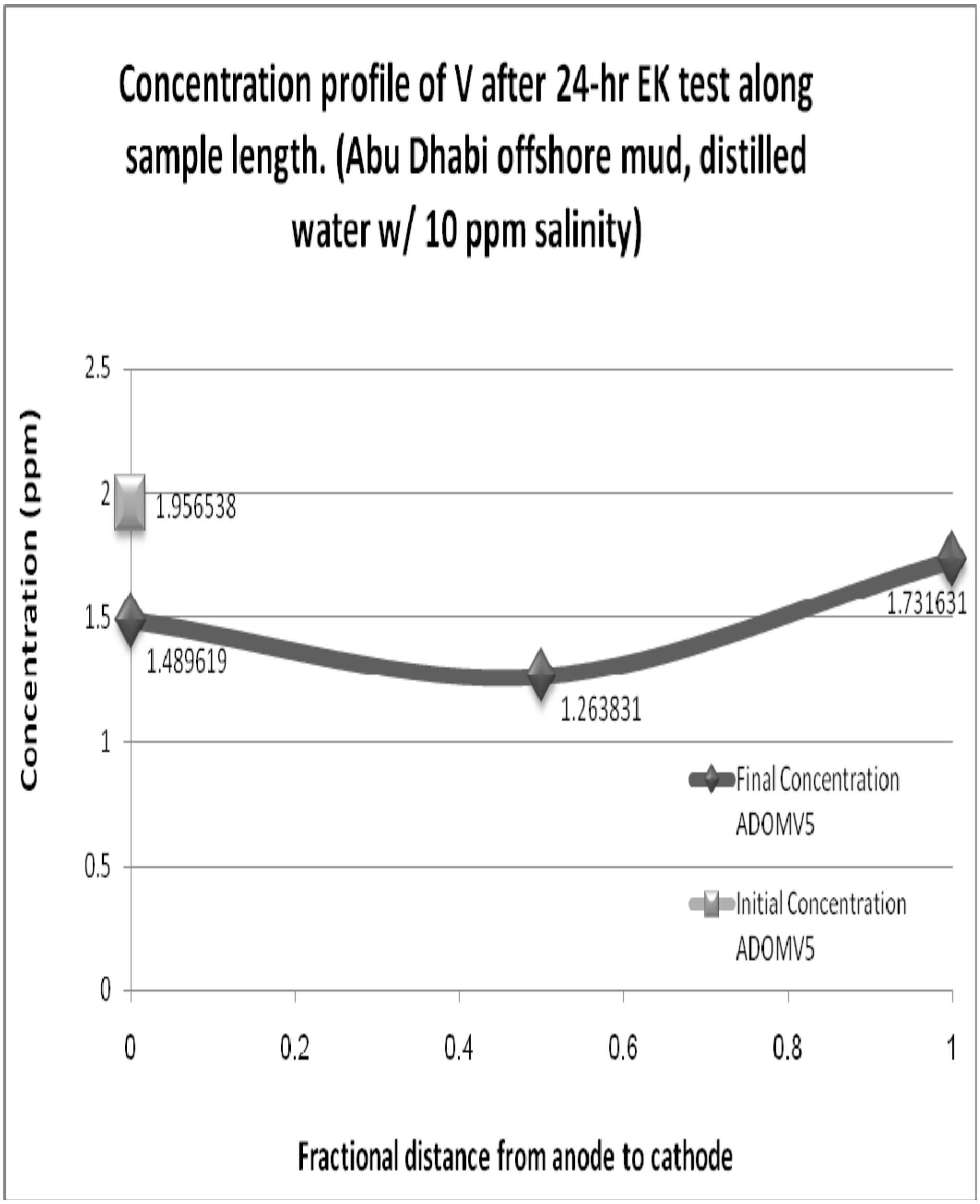

Figure 4-98: Concentration profile of V after 24-hr EK test a long sample length (Abu Dhabi offshore mud, distilled water 10 ppm salinity).

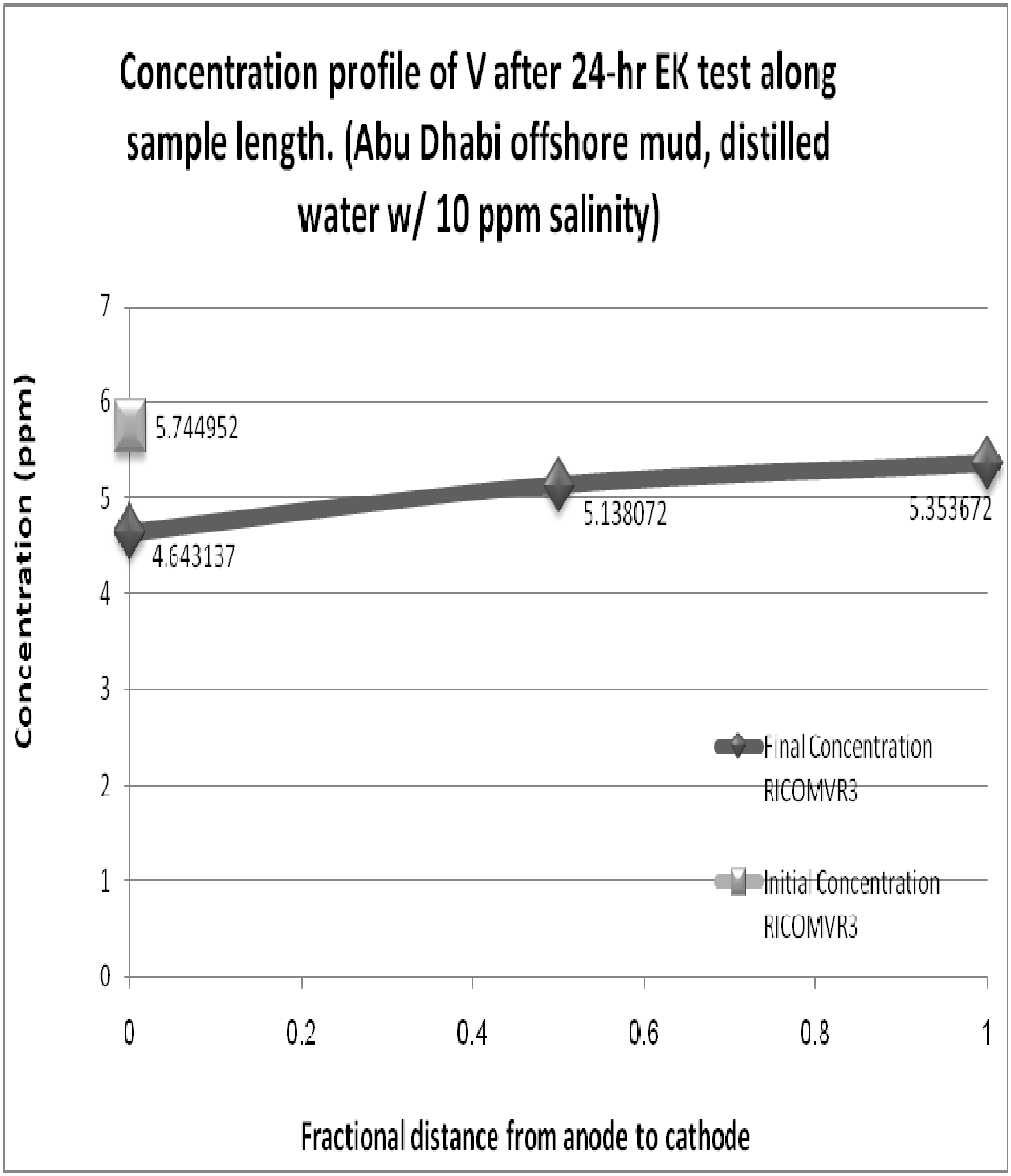

Figure 4-99: Concentration profile of V after 24-hr EK test a long sample length (Abu Dhabi offshore mud, distilled water 10 ppm salinity).

Vanadium: Sample RICOMSWPHV2 in Figure 4-100 using Abu Dhabi seawater with 26,000 ppm salinity and 450 ppm maleic acid

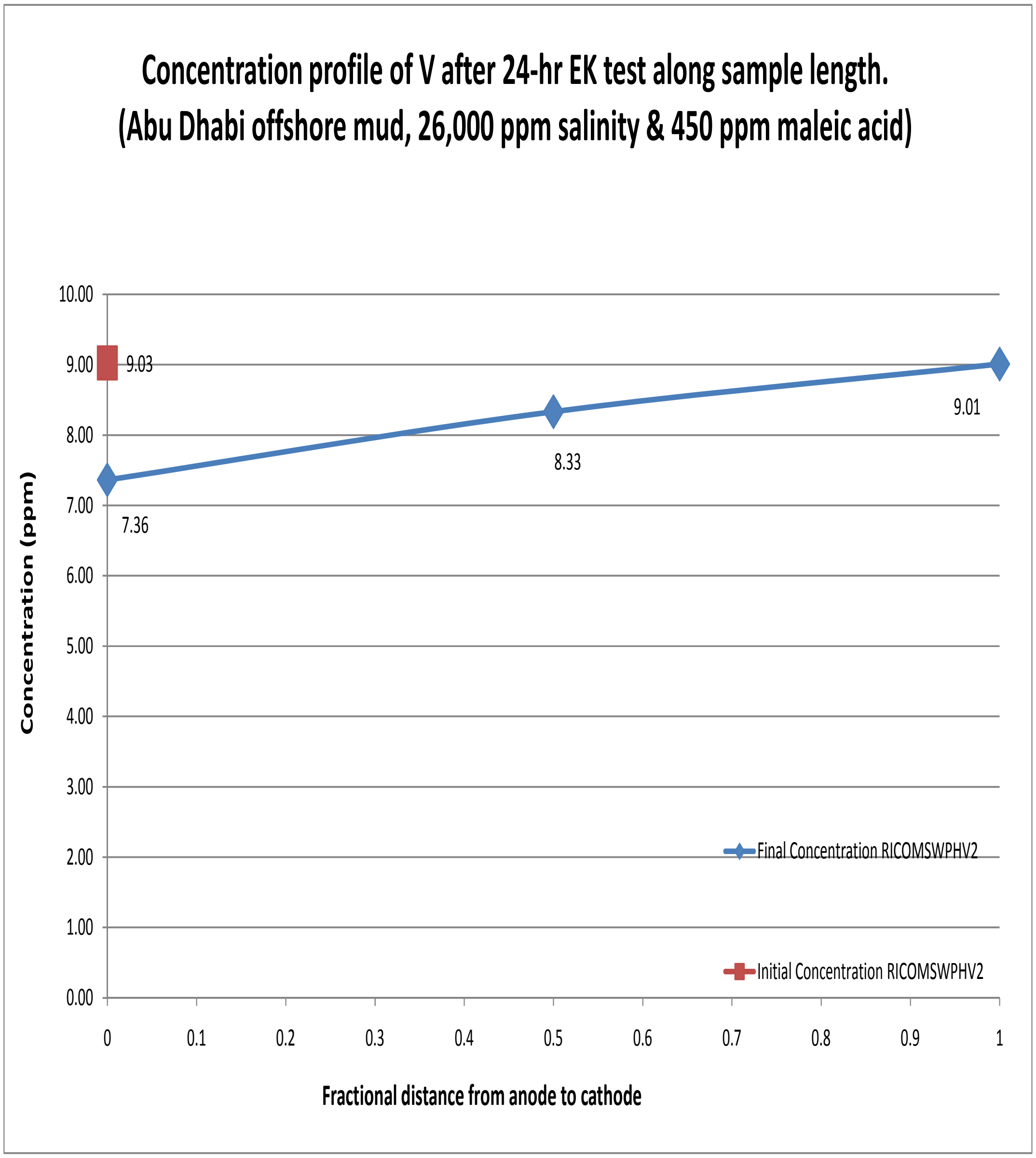

Figure 4-100: Concentration profile of V after 24-hr EK test a long sample length. (Abu Dhabi offshore mud, 26,000 ppm salinity & 450 ppm maleic acid)

Zinc: Zinc is amphoteric for which the divalent cation is stable below the pH of 7.7. The neutral species ($Zn(OH)_2$) predominates above pH 9.1. The anionic species, ($Zn(OH)_3^-$ and $Zn(OH)_4^{2-}$) become significant after pH 11. Due to the amphoteric nature of zinc and its tendency to form polynuclear hydrolysis species, similar removal fractions were obtained at the anode and cathode. (Pamukcu et al., 1993).

Figure 4-101 through 4-104 show the fraction of the zinc found at three locations: anode side, center and cathode end of tested core after 24 hours of electrokinetic treatment. The initial concentrations were predetermined at the anode end of the contaminated offshore mud sample. The removal efficiency was calculated at the anode using equation 4-1 for all results obtained. Substantial reduction of zinc from its initial concentration at the anode region was found to be 13.44, 7.40 and 44.17% after 24 hours using the distilled water with 10 ppm salinity as shown in Figures 4-101 through 4-103 respectively. Electrokinetics was the main driving force of the zinc ion in the same direction of the water flow. There was accumulation of metal at the discharge end as shown in both Figures 4-101 through 4-104 (cathode end of the mud sample). The shape of the curve in Figures 4-101 and 4-102 can be explained by the lack of pH control.

Figure 4-100 shows the results conducted with Abu Dhabi seawater having 26,000 ppm salinity, as well as 450 ppm of maleic acid added for pH control. The maximum removal efficiency of zinc at the anode region here 53.045% as opposed to the 44.17%, however consistency was achieved using the seawater and pH control, where the lowest removal efficiency recored at the anode here was 11.67% as opposed to 7.40% as shown in Figure 4-102. This finding was interesting as it confirmed that the presense of both high salinity and pH control mechanism influenced all the samples tested here to consistently show higher removal efiiciencies at all the three locations analyzed. The high salinity caused a higher conductivity in the bulk solution, where both the current and electrokinetic flow increased several fold. One explanation for this is that the electromigration force is now a dominat force allowing the ionic mobility to travel at 2-3 times faster than in the case of dominant electroosmosis, while another theory is the abundance of large volumes of cations in this high salinity carrying their waters of hydration further promoting ionic species velocity. This needs to be investigated further.

Zinc: 2, 5, R3 samples in Figure 4-101 through 4-103 using Distilled water with 10 ppm salinity

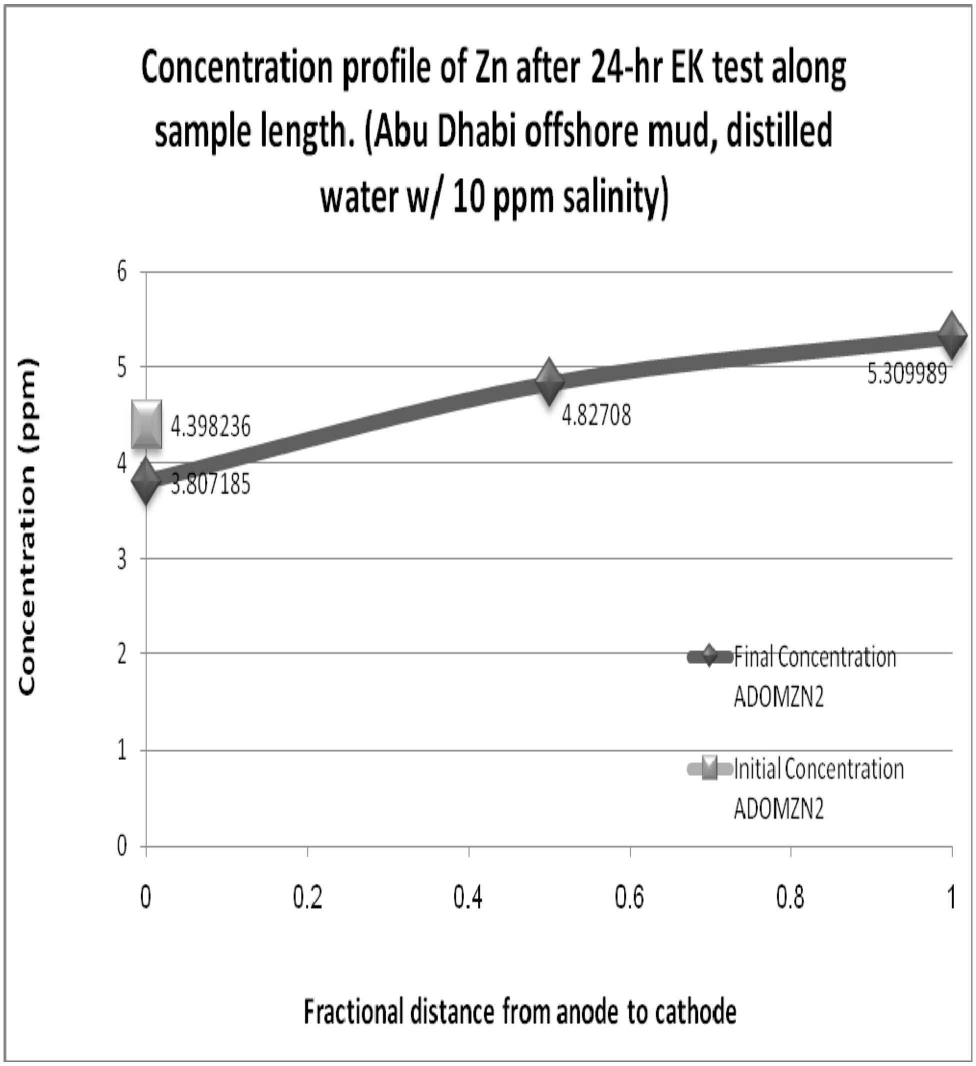

Figure 4-101: Concentration profile of Zn after 24-hr EK test a long sample length (Abu Dhabi offshore mud, distilled water 10 ppm salinity).

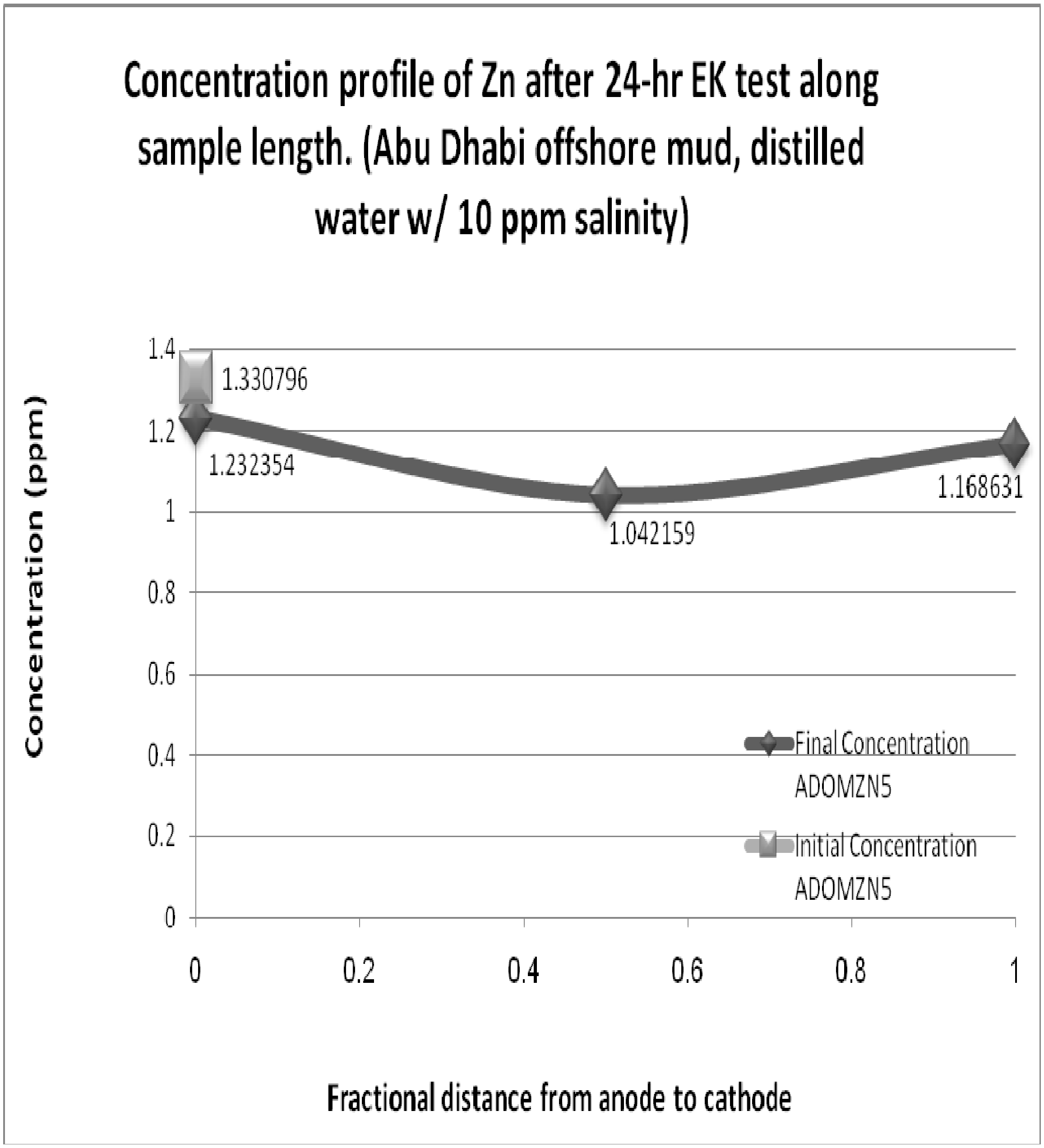

Figure 4-102: Concentration profile of Zn after 24-hr EK test a long sample length (Abu Dhabi offshore mud, distilled water 10 ppm salinity).

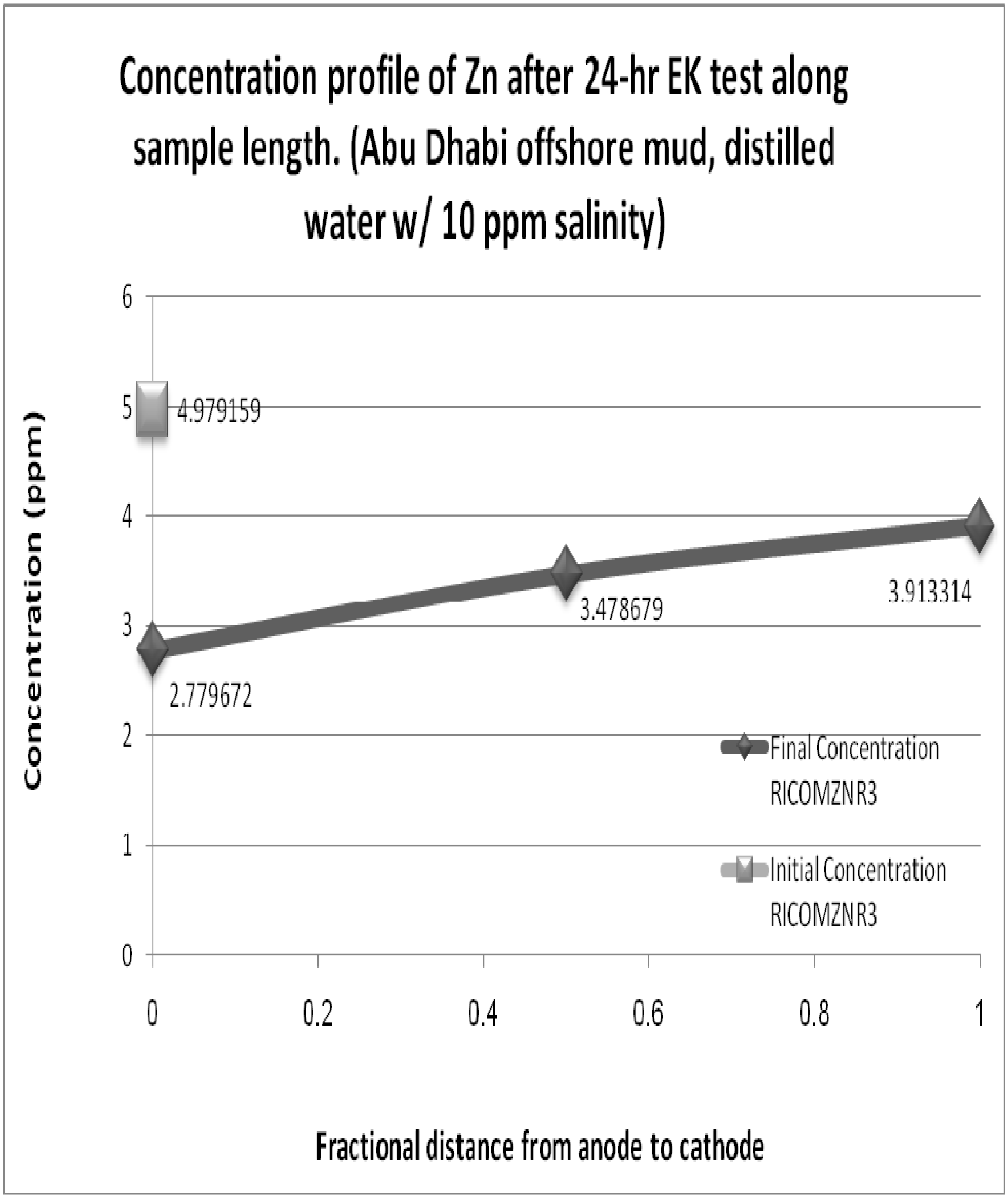

Figure 4-103: Concentration profile of Zn after 24-hr EK test a long sample length (Abu Dhabi offshore mud, distilled water 10 ppm salinity).

Zinc: Sample RICOMSWPHZN3 in Figure 4-104 using Abu Dhabi seawater with 26,000 ppm salinity and 450 ppm maleic acid

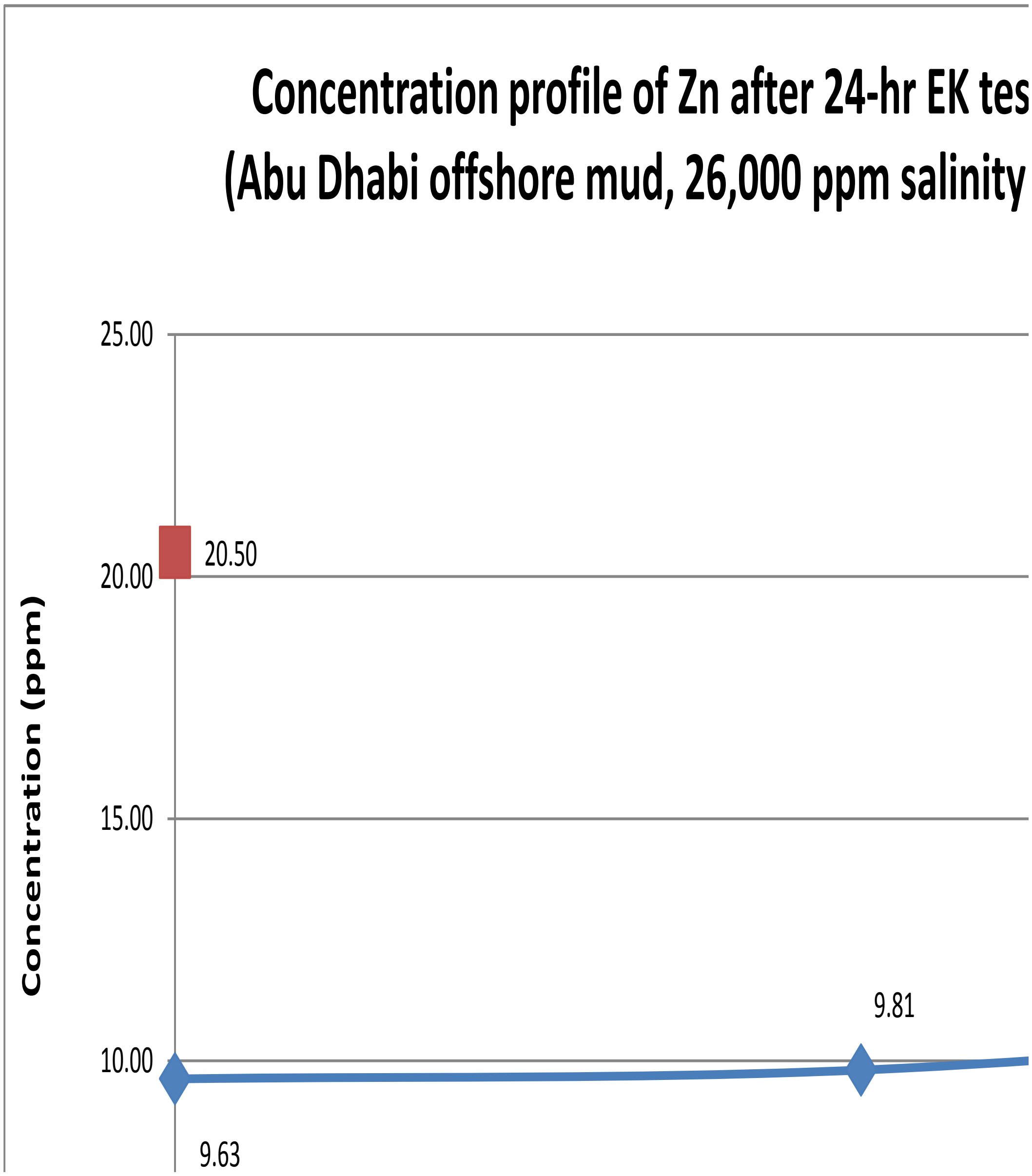

Figure 4-104: Concentration profile of Zn after 24-hr EK test a long sample length. (Abu Dhabi offshore mud, 26,000 ppm salinity & 450 ppm maleic acid).

Manganese: Manganese exits as divalent and trivalent ionic species throughout the pH range of 2 to 10.

The mechanism which triggers the accumulation is probably the increased cation retention capacity of the clay at high pH levels. Figure 4-105 through 4-106 show the fraction of the manganese found at three locations: anode side, center and cathode end of tested core after 24 hours of electrokinetic treatment. The initial concentrations were predetermined at the anode end of the contaminated offshore mud sample. The removal efficiency was calculated at the anode using equation 4-1 for all results obtained. Substantial reduction of manganese from its initial concentration at the anode region was found to be 15.38 and 18.75% after 24 hours using the distilled water with 10 ppm salinity as shown in Figures 4-105 through 4-106 respectively. Electrokinetics was the main driving force of the manganese ion in the same direction of the water flow. There was accumulation of metal at the discharge end as shown in both Figures 4-105 through 4-106 (cathode end of the mud sample). The shape of the curve in Figures 4-105 can be explained by the lack of pH control.

Manganese: 5, R3 samples in Figure 4-105 through 4-106 using Distilled water with 10 ppm salinity

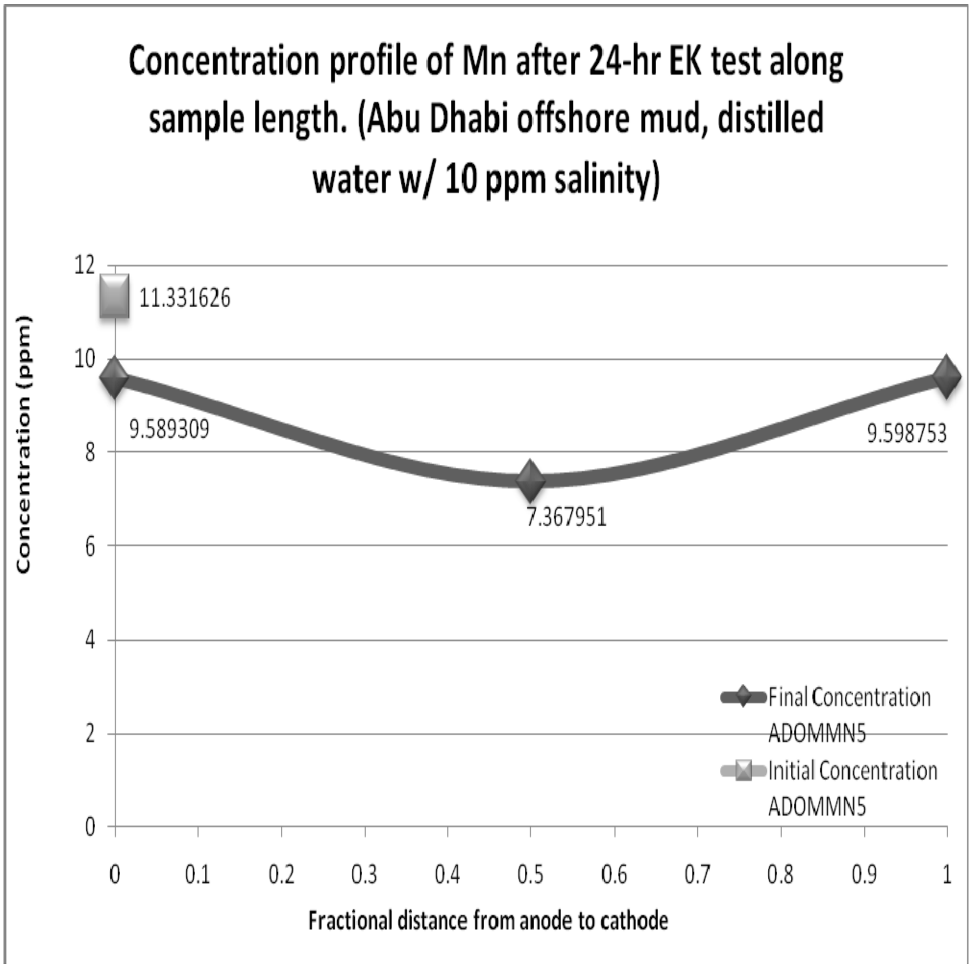

Figure 4-105: Concentration profile of Mn after 24-hr EK test a long sample length (Abu Dhabi offshore mud, distilled water 10 ppm salinity).

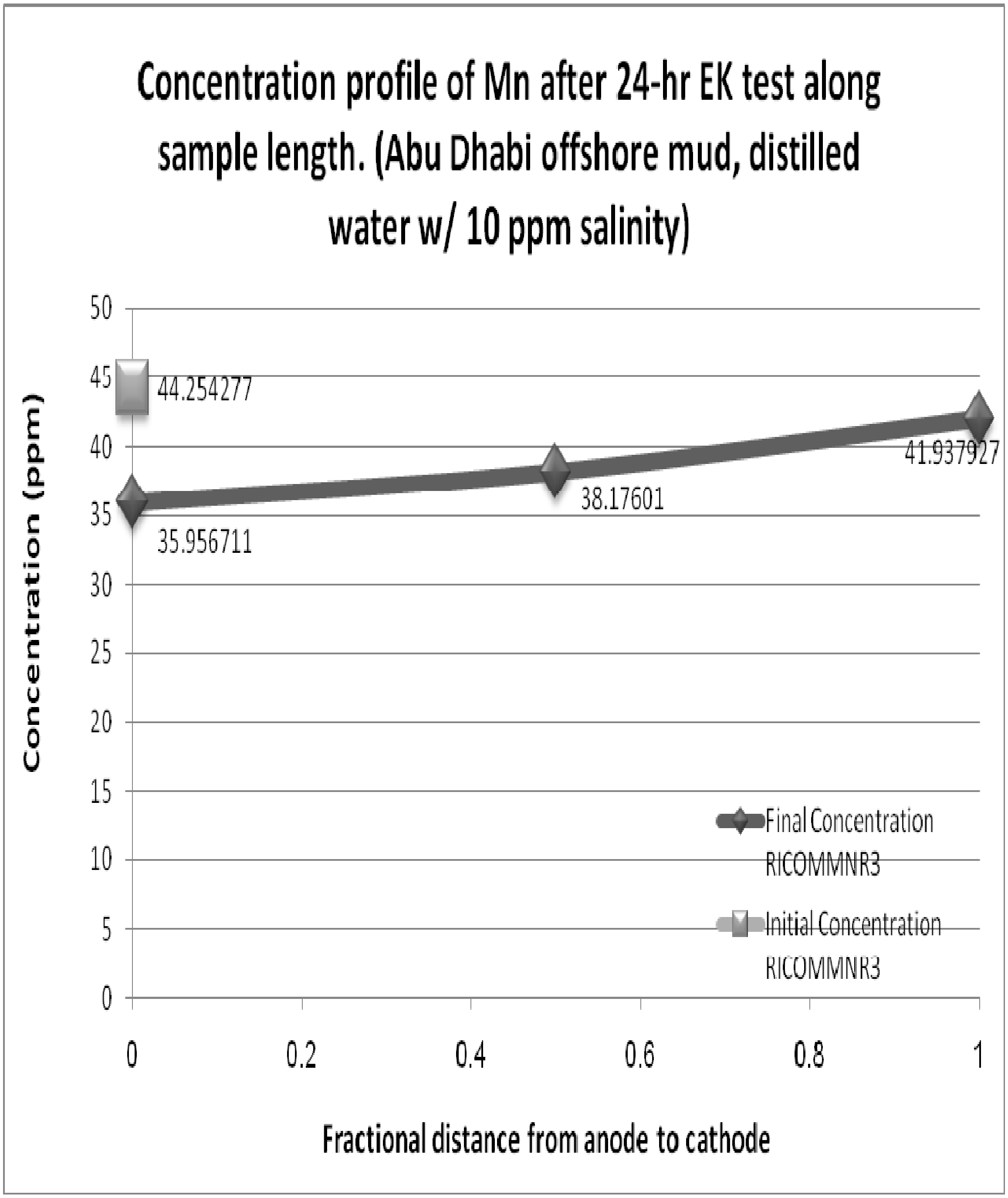

Figure 4-106: Concentration profile of Mn after 24-hr EK test a long sample length (Abu Dhabi offshore mud, distilled water 10 ppm salinity).

Nickel: Nickel exits as divalent ionic species throughout the pH range of 2 to 8, whereas, at pH>8 both $Ni(OH)^+$ and Ni^{2+} are present. At pH levels higher than 9, anionic ($Ni(OH)_3^-$ and $Ni(OH)_4^{2-}$) and aqueous neutral ($Ni(OH)_2$) species of Ni(II) appear. At high concentrations of Ni(II), $Ni(OH)_2$ precipitates. The removal trend of nickel was similar to that of cobalt. (Pamukcu et al., 1993).

Figure 4-107 through 4-108 show the fraction of the nickel found at three locations: anode side, center and cathode end of tested core after 24 hours of electrokinetic treatment. The initial concentrations were predetermined at the anode end of the contaminated offshore mud sample. The removal efficiency was calculated at the anode using equation 4-1 for all results obtained. Substantial reduction of nickel from its initial concentration at the anode region was found to be 18.66 and 26.56% after 24 hours using the distilled water with 10 ppm salinity as shown in Figures 4-107 through 4-108 respectively. Electrokinetics was the main driving force of the manganese ion in the same direction of the water flow. There was accumulation of metal at the discharge end as shown in both Figures 4-107 through 4-108 (cathode end of the mud sample). The wide range of removal efficiency and the shape of the curve in Figures 4-107 through 4-108 can be attributed to:

(iii) The different valencies of this species having different electrokinetic velocity. (Higher the charge, higher the EK velocity).

(iv) Lack of pH control.

(v) The formation of the complex anionic species migrating to the anode.

Nickel: 5, R3 samples in Figure 4-107 through 4-108 using Distilled water with 10 ppm salinity

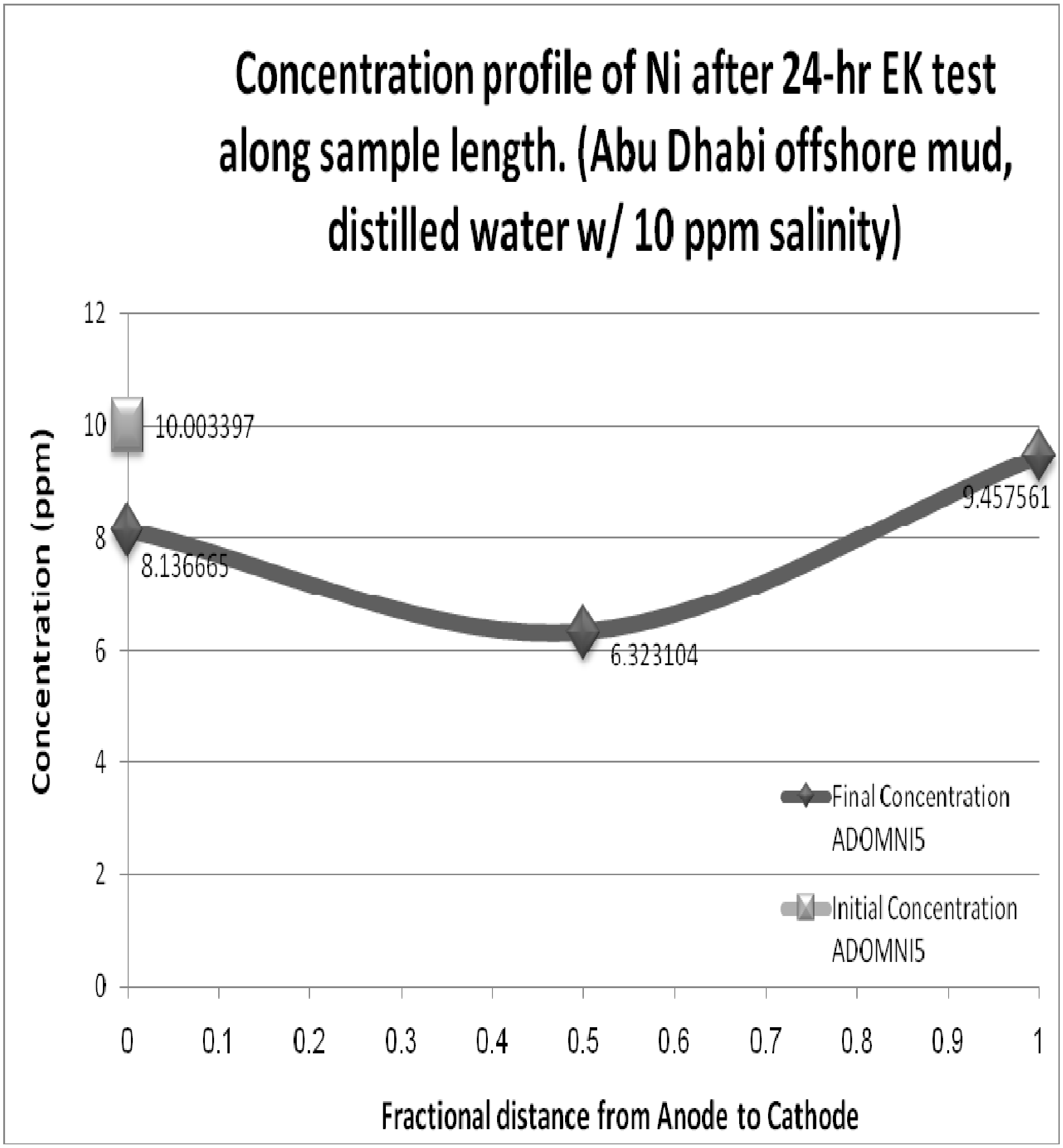

Figure 4-107: Concentration profile of Ni after 24-hr EK test a long sample length (Abu Dhabi offshore mud, distilled water 10 ppm salinity).

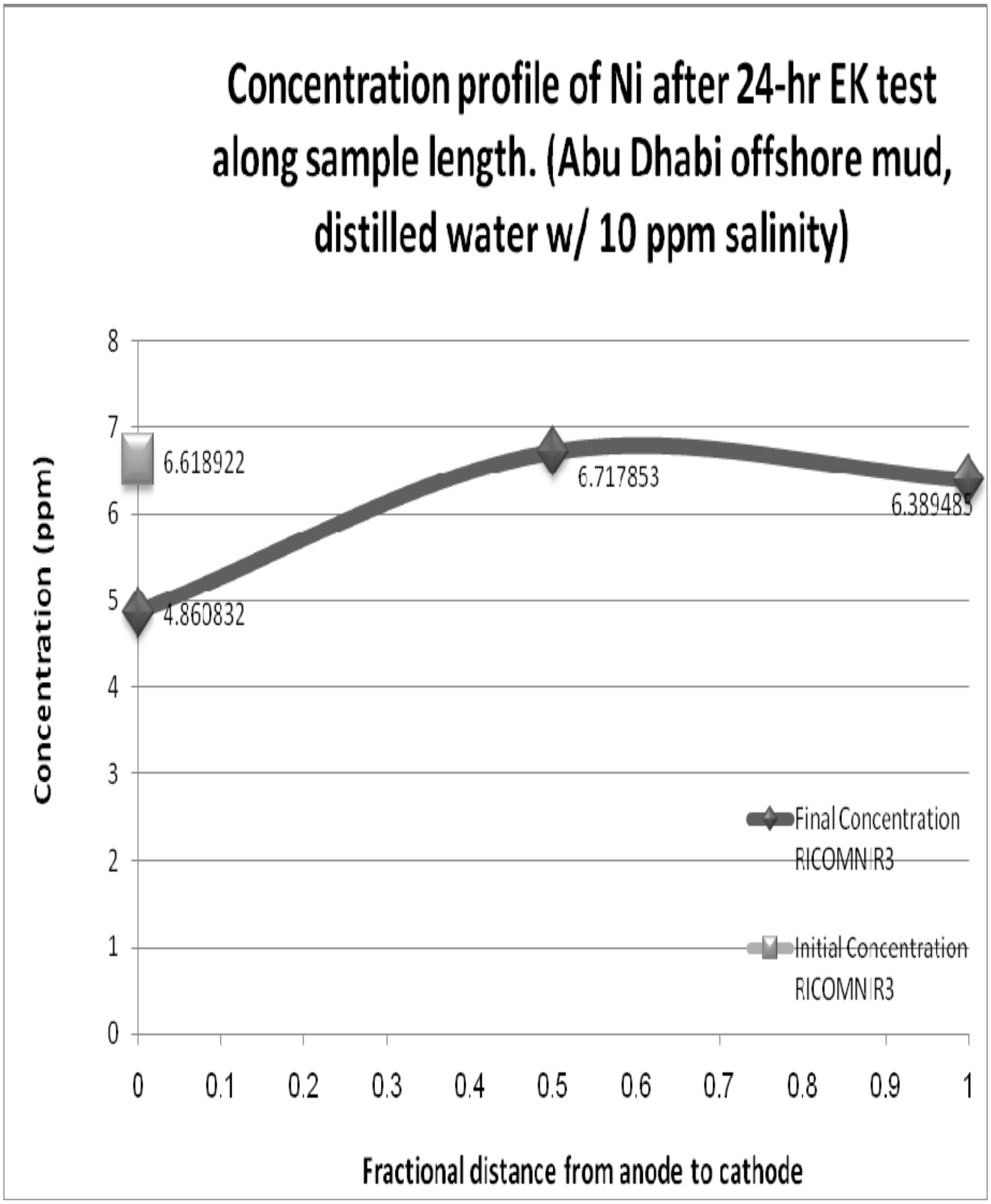

Figure 4-108: Concentration profile of Ni after 24-hr EK test a long sample length (Abu Dhabi offshore mud, distilled water 10 ppm salinity).

Figure 4-109 shows the electrokinetic flow potential, where cumulative volumetric flow is plotted against total electron transfer as columbs. Here we see that in both distilled water containing 10 ppm salinity and Abu Dhabi seawater (26,000 ppm salinity), the electrokinetic flow follows a similar pattern, with the slope of the seawater curve having 1.5 times larger response. This allows one to possibly conclude that the electrokinetic flow efficiency is in the same order of magnitude as far as short term electrokinetic test.

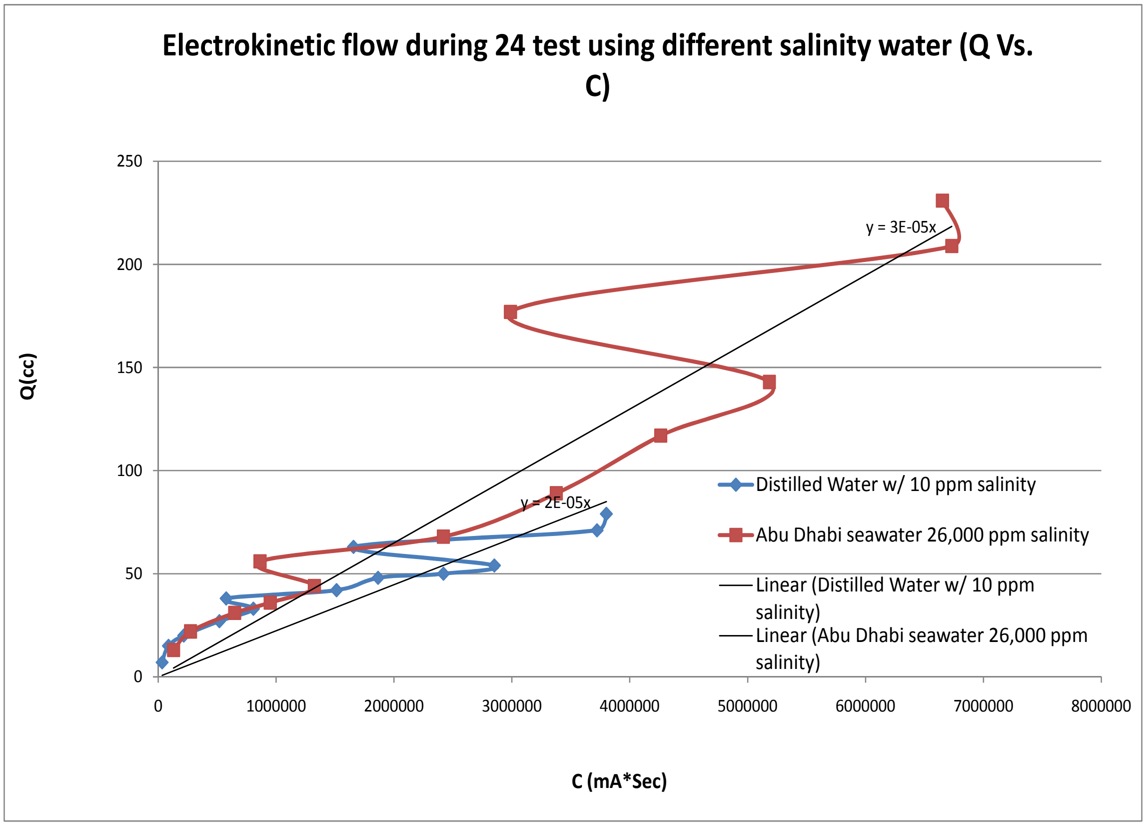

Figure 4-109: 24 – Electrokinetic flow during the 24 hour test using different salinity water on offshore mud samples of Abu Dhabi having varying concentrations of heavy metals.

Summary of removal efficiency (R.E.) at the anode region after 24 hours of electrokinetic treatment using distilled water having 10 ppm salinity and no pH control

$$\text{R.E.} = 100 - 100\,(\text{Final C}/\text{Initial C})\ \% \qquad (4-1)$$

The following table is a brief selection of some contaminants and physical conditions that may be present in drinking water. A dash (-) indicates that there is no information available regarding possible limits.

Units are in milligrams per liter (mg/L) unless otherwise noted. Milligrams per liter are equivalent to parts per million.

Table 4-3a: Removal efficiencies vs Canadlian limit, U.S. limit, WHO limit and Gulf limit of heavy metals at anode location after 24-hr EK test using distilled water with 10 ppm salinity and no pH control.

Heavy Metal	Sample	Ci(ppm)	Cf(ppm)	Removal Efficiency (%) at Anode	Canadian Limit (ppm)	US limit (ppm)	WHO limit (ppm)	Gulf limit (ppm)
Silver	2	0.0075	0.00382	48.84	0.05	0.1	no limit	
	3	0.0104	0.00826	20.77	0.05	0.1	no limit	
	4	0.0145	0.00758	47.75	0.05	0.1	no limit	
	5	0.0068	0.00404	40.85	0.05	0.1	no limit	
	R3	0.0061	0.00534	11.88	0.05	0.1	no limit	
Aluminum	4	459.63	364.404	20.72	0.1	0.05 - 0.2	no limit	
	5	265.35	178.206	32.84	0.1	0.05 - 0.2	no limit	
	R3	645.01	504.922	21.72	0.1	0.05 - 0.2	no limit	
Arsenic	4	1.2847	0.84463	34.25	0.01	0.01	0.01	
	5	0.5097	0.41963	17.67	0.01	0.01	0.01	
	R3	0.4509	0.4055	10.07	0.01	0.01	0.01	
Barium	2	6.3671	5.66415	11.04	1	2	0.7	
	4	3.0842	2.65835	13.81	1	2	0.7	
Beryllium	4	0.019	0.01732	8.66	no limit	0.004	no limit	
	5	0.0121	0.00941	22.16	no limit	0.004	no limit	
	R3	0.0488	0.03723	23.77	no limit	0.004	no limit	
Bismuth	3	0.01	0.00601	40.06				
	R3	0.0064	0.00554	12.75				
Cadmium	2	0.015	0.01023	31.70	0.005	0.005	0.003	
	3	0.0187	0.01407	24.91	0.005	0.005	0.003	
	5	0.0076	0.00695	8.74	0.005	0.005	0.003	
	R3	0.0139	0.01221	12.40	0.005	0.005	0.003	
Cesium	R3	0.0489	0.04096	16.18				

Chromium	**5**	**4.9931**	**3.9699**	**15.71**	**0.05**	**0.01**	**0.05**	Table 4-3a Continued
	R3	**7.6479**	**6.52419**	**22.98**	**0.05**	**0.01**	**0.05**	
Cobalt	**5**	**0.5237**	**0.44139**	**15.90**	**no limit**	**no limit**	**no limit**	
	R3	**3.05**	**2.01**	**34.10**	**no limit**	**no limit**	**no limit**	
Copper	**1**	**7.6266**	**3.66092**	**52.00**	**1**	**1.3**	**2**	
	3	**2.3136**	**1.94573**	**15.90**	**1**	**1.3**	**2**	
	5	**0.7479**	**0.67636**	**9.57**	**1**	**1.3**	**2**	
	R3	**1.8923**	**1.1811**	**37.58**	**1**	**1.3**	**2**	
Iron	**5**			**2.83**	**0.3**	**0.3**	**no limit**	
	R3			**18.00**	**0.3**	**0.3**	**no limit**	
	2			**95.20**	**0.3**	**0.3**	**no limit**	
Gallium	**4**	**0.0775**	**0.07535**	**2.83**				
In	**5**	**0.0019**	**0.00154**	**18.00**				
Potassium	**R4**			**53.25**				
	5			**6.80**				
	R3			**23.51**				
	4			**7.84**				
Lithium	**5**	**0.8654**	**0.80655**	**6.80**				
	R3	**3.6855**	**2.81902**	**23.51**				
Magnesium	**R3**			**18.75**	**50**	**-**	**-**	
	1			**35.00**	**50**	**-**	**-**	
Manganese	**5**	**11.332**	**9.58931**	**15.38**	**0.05**	**0.03**	**0.4**	
	R3	**44.254**	**35.9567**	**18.75**	**0.05**	**0.03**	**0.4**	
Sodium	**4**			**54.51**	**200**	**no limit**	**no limit**	
	5			**32.04**	**200**	**no limit**	**no limit**	
	R4			**85.90**	**200**	**no limit**	**no limit**	
	5			**18.66**	**200**	**no limit**	**no limit**	
	R3			**26.56**	**200**	**no limit**	**no limit**	
	2			**13.04**	**200**	**no**	**no**	

						limit	limit	
Nickel	5	10.003	8.13667	18.66	no limit	no limit	0.02	Table 4-3a Continued
	R3	6.6189	4.86083	26.56	no limit	no limit	0.02	
Lead	2	2.7922	2.42803	13.04	0.01	0	0.001	
	3	1.4094	0	100.00	0.01	0	0.001	
	4	4.0084	1.44746	63.89	0.01	0	0.001	
	R3	0.6698	0.46944	29.92	0.01	0	0.001	
	R4	0.5763	0.43352	24.78	0.01	0	0.001	
Rubidium	2	0.4561	0.40741	10.69				
	5	0.2666	0.20181	24.31				
	R3	1.4572	1.15883	20.47				
Selenium	1	0.175	0.10261	41.35				
	4	0.6285	0.33015	47.47				
	R1	0.4489	0.34008	24.24				
	R3	0.5153	0.41121	20.20				
	R4	0.3092	0.27843	9.96				
Strontium	3	176.46	161.557	8.44	no limit	no limit	no limit	
	4	245.42	238.307	2.90	no limit	no limit	no limit	
Titanium	2	0.0092	0.00718	21.61	no limit	no limit	no limit	
	3	0.0473	0.04154	12.22	no limit	no limit	no limit	
	R3	0.0087	0.00699	19.49	no limit	no limit	no limit	
Uranium	3	2.5009	2.33407	6.67	0.02	no limit	0.009	
	R3	0.6207	0.55859	10.01	0.02	no limit	0.009	
Vanadium	2	2.0293	1.75075	13.73	no limit	no limit	no limit	
	3	2.3883	2.04257	14.48	no limit	no limit	no limit	
	4	2.6039	2.45831	5.59	no limit	no limit	no limit	
	5	1.9565	1.48962	23.86	no limit	no limit	no limit	
	R3	5.745	4.64314	19.18	no limit	no limit	no limit	
Zinc	2	4.3982	3.80719	13.44	5	5	no limit	

	5	1.3308	1.23235	7.40	5	5	no limit	
	R3	4.9792	2.77967	44.17	5	5	no limit	

* As per Canadian or BC Health Act Safe Drinking Water Regulation BC Reg 230/92, & Sch 120, 2001. Task force of the Canadian Council or Resource and Environment Ministers Guidelines for Canadian Drinking Water Quality, 1996. See their website for more information.

** As per the U.S. Environmental Protection Agency Drinking Water Standards. See their website for more information.

*** As per the WHO (1998) Guidelines for drinking water quality, 2nd edition. Geneva, World Health Organization. See their website for more information.

^ TCU = true colour unit

^^ Individual limits for some of the individual trihalomethanes & haloacetic acids:

- Trihalomethanes: bromodichloromethane (zero); bromoform (zero); dibromochloromethane (0.06 mg/L). Chloroform is regulated with this group but has no MCLG.
- Haloacetic acids: dichloroacetic acid (zero); trichloroacetic acid (0.3 mg/L). Monochloroacetic acid, bromoacetic acid, and dibromoacetic acid are regulated with this group but have no limits.

^^^ NTU = nephelometric turbidity unit. Based on conventional treatment/slow sand or diatomaceous earth filtration/membrane filtration

Summary of removal efficiency (R.E.) at the anode region after 24 hours of electrokinetic treatment using Abu Dhabi seawater having 26,000 ppm salinity and maleic acid for pH control

Table 4-3b: Removal efficiencies vs Canadlian limit, U.S. limit, WHO limit and Gulf limit of heavy metals at anode location after 24-hr EK test using Abu Dhabi seawater with 26,000 ppm salinity and pH control.

using seawater with 26,000 ppm salinity

					Removal Efficiency (%) at:	
Heavy Metal	**Sample**	**Ci (ppm) Anode**	**Cf (ppm) Anode**	**Anode**	**Center**	**Cathode**
Silver	2	0.02	0.0153	0.312329	0.205088	0.159333
Aluminum	1	1569.91	1105.390505	0.29589	-0.0101	-0.05891
	2	1176.02	806.006221	0.31463	0.153545	0.063857
	3	1247.50	1064.159659	0.146969	-0.2437	-0.01595
Barium	1	17.48	14.834	0.151143	-0.21087	-0.02056
	2	8.42	6.112244	0.274047	-0.3641	0.005672
	3	7.05	4.462181437	0.366799	-0.12155	0.151556
Berelium	1	0.10	0.077603	0.24669	0.012066	0.057855
	2	0.06	0.042306	0.278252	0.178552	-0.09143
	3	0.06	0.048850547	0.244501	-0.1597	0.06558
Bismuth	1	0.03	0.018518	0.289355	0.230793	0.291772
	2	0.01	0.009562	0.219301	0.225669	-2.97069
Cadmium	2	0.06	0.054842	0.152797	0.018368	0.002642
	3	0.07	0.058072843	0.168452	-0.13767	-0.00937
Cesium	1	0.15	0.101687	0.314514	-0.00818	-0.03243
	2	0.12	0.0853	0.26532	0.10792	0.049731
	3	0.13	0.112243229	0.12933	-0.12939	0.021436

						Table 4-3b Continued
Chromium	**1**	**15.45**	**12.524895**	**0.189572**	**-0.04652**	**--0.04095**
	2	**11.54**	**9.292712**	**0.194436**	**0.078758**	**-0.01524**
	3	**11.56**	**9.411847286**	**0.186115**	**-0.05472**	**0.108137**
Cobalt	**1**	**2.08**	**1.74735**	**0.161542**	**-0.06359**	**-0.01128**
	2	**2.06**	**1.626463**	**0.209952**	**0.123827**	**0.06263**
Copper	**2**	**4.92**	**4.065371**	**0.174375**	**0.143097**	**0.081368**
	3	**3.65**	**2.696437466**	**0.26032**	**0.178504**	**0.17169**
Gallium	**1**	**1.37**	**1.021954**	**0.255372**	**-0.13709**	**-0.03392**
	2	**0.73**	**0.516297**	**0.293597**	**-0.13508**	**0.006406**
	3	**0.74**	**0.555350912**	**0.248343**	**-0.16689**	**0.071563**
Indium	**1**	**0.005**	**0.003068**	**0.384183**	**0.228623**	**0.215978**
	2	**0.002**	**0.00175**	**0.164678**	**0.155609**	**0.100716**
	3	**0.002**	**0.001930208**	**0.130145**	**-0.04665**	**-0.0047**
Lithium	**1**	**3.46**	**2.969554**	**0.141021**	**-0.06007**	**-0.07562**
	3	**4.027**	**3.257982106**	**0.190971**	**-0.10244**	**0.030916**
Manganese	**2**	**88.46**	**80.35690006**	**0.091651**	**-0.08695**	**0.020217**
	3	**0.13**	**0.118433902**	**0.103738**	**-0.07249**	**0.033254**
Nickel	**1**	**14.67**	**13.149394**	**0.103493**	**-0.12766**	**-0.13935**
	2	**25.59**	**20.77246**	**0.188357**	**0.149285**	**0.088135**
Lead	**3**	**1.17**	**0.6357161**	**0.456228**	**0.125249**	**0.340742**
Rubidium	**1**	**2.33**	**1.62825**	**0.299708**	**-0.01811**	**-0.02973**
	2	**1.15**	**0.828862**	**0.279211**	**0.117078**	**0.041122**
	3	**1.24**	**0.897687775**	**0.27877**	**0.000135**	**0.168975**
Selenium	**2**	**1.04**	**0.685253**	**0.341235**	**0.356514**	**0.382645**
	3	**0.63**	**0.360745034**	**0.428473**	**0.252165**	**-0.21977**
Strontium	**2**	**808.28**	**729.508784**	**0.09746**	**-0.0838**	**-0.418**
Titanium	**2**	**0.05**	**0.038449**	**0.250434**	**0.183332**	**0.130598**
	3	**0.05**	**0.03966132**	**0.128284**	**-0.0004**	**-0.00373**
Uranium	**2**	**2.71**	**2.50308**	**0.077016**	**0.041859**	**-0.01674**
Vanadium	**2**	**9.03**	**7.361849**	**0.184314**	**0.076917**	**0.00191**
	3	**9.67**	**8.472572847**	**0.123703**	**0.031452**	**-0.12645**
Zinc	**1**	**12.77**	**11.280571**	**0.116668**	**-0.01532**	**0.016889**
	2	**9.66**	**8.512559**	**0.119164**	**0.046321**	**-0.03907**
	3	**9.81**	**4.608141018**	**0.530452**	**0.521252**	**0.471604**

Chapter 5: Summary and Conclusions

Recent publications demonstrate the effectiveness of electroremediation of soils and sludges. Although electrokinetic purging was not successful in all cases, the character, number, scope, and results of conducted research demonstrate that it can be recommended as a convenient and cost-effective cleaning technology in offshore muds. The results of modeling and laboratory experiments have identified the causes of incomplete removal of contaminants to allow for the development of procedures for achieving a high degree of decontamination. Assessing the possible extent of electrotreatment, one needs to consider carefully the wide range of related constraints that can considerably reduce the expected effect of this remediation.

Necessary information regarding these constraints must be obtained during the pilot study. Analysis of the published literature shows that considerable knowledge regarding particular aspects of electroremediation have been collected for the past couple of decades. This information allows one to identify, analyze, and eliminate (or mitigate) the causes of insufficient performance of electrorestoration *in-situ*.

It is necessary to emphasize that the best remediation results are achieved *in situ* using a combination of various cleaning technologies. Only a few publications attempt to integrate the results of various disciplines (geology, geochemistry, chemistry, physics, etc.) into integrated study on industrial application of electrokinetics for decontamination of metals and hydrocarbons (Chilingar et al., 1997).

The main role in such a study must be given to the procedures of gathering and classifying the necessary data and procedures of decision making aimed at identification and selection of the best combination of remediation technologies (Chilingar et al., 1997).

The writer achieved up to 99% removal efficiencies in decontaminating artificially contaminated kaolinite clay samples from heavy metals. Depending on the heavy metals and ability to control pH, 2.83 to 100 % removal efficiencies were achieved for the field-collected offshore mud samples with 20 V DC application after only 24 hours.

The experiments conducted by the writer on field-collected offshore mud samples demonstrate that electroremediation is an efficient and promising solution. pH control was very critical and was acheived using a solution containing organic humic substances or maleic acids.

Chapter 6: Suggested Future Research Work

1 The main thrust of future research work should be concentrated on determining the feasibility of using DC technology (EEOR) in various carbonate formations:

  a) Porous and permeable limestones containing clays and those devoid of clays.

  b) Dolomized limestone (dolomitization gives rise to porosity, of ≈ 13.1%). (Asmari Formation)

2 Modifying the experimental apparatus to include:

Adding 3 probes for measuring pH, pressure and voltage/current along the core samples on a real time basis. Modifying the electrode chamber to increase the surface area to avoid the accumulation of gas generated due to the reactions at the electrodes — O_2 at the anode and H_2 at the cathode. This would allow for higher voltage applications for testing in the laboratory while reducing the volume of gas bubbles that cause insulation and, thus, reduce the electokinetics performance.

3 Upscaling and optimizing voltage, current and electrode configuration, including investigating the optimum critical distance between electrodes for field applications.

4 Solving the PDE for contaminant mass transport to include 2-D and 3-D flow for all heavy metal species with control of pH and salinity.

References

Acar, Y. B., R. W. Gale, J. Hamed, and G. Putman. 1990. Transportation Research Record,1288, pp. 23-24. Transportation Research Board, National Research Council, Washington,D.C.

Adamson, L. G., S. A. Amba,. G. V. Chilingar, and C. M. Beeson. 1963a. Possible use of electric current for increasing volumetric rate of flow of oil and water during primary or secondary recovery. *Chimika Chronika* 28(1):1-4.

Adamson, *L.* G., G. V. Chilingar, and C. M. Beeson. 1963b. Some data on electrokinetic phenomena and their possible application on petroleum production. *Chimika Chronika* 28(10):121-127.

Adamson, L. G., G. V. Chilingar, C. M. Beeson, and R. A. Armstrong. 1966. Electrokinetic dcwatering, consolidation and stabilization of soils. *Engineering Geology* 1:291-304.

Al-Sharhan, A.S. and A.A.El-Sammak, 2004, Grain size analysis and characterization of sedimentary environments of the United Arab Emirates coastal area, Journal of coastal research, 20 (2), pp: 464-477.

Alsharhan, A.S., Kendall, C.G.St.C., 2002. Holocene carbonate/ evaporites of Abu Dhabi, and their Jurassic ancient analogs. In: Barth, H.J., Boer, B.B. (Eds.), Sabkha Ecosystems. Kluwer Academic Publishers, pp. 187–202.

Amba, S. A., G. V. Chilingar, and C. M. Beeson. 1964. Use of direct electrical current for increasing the flow rate of reservoir fluids during petroleum recovery. *Journal of Canadian Petroleum Technology* 3(1):8-14.

Amba, S. A,, G. V. Chilingar, and C. M. Beeson. 1965. Application of electrical current for increasing the flow rate of oil and water in a porous medium. *Journal of Canadian Petroleum Technology* 4(2): 81-85.

Amba, S. A,, G. V. Chilingar, and C. M. Beeson. 1965. Application of electrokinetic phenomena in civil and petroleum engineering. *Annals NewYork Academy of Sci. 118(14):585-602*
Petroleum Technology 4(2):81-85.

Atlas, R. M. 1977. Stimulated petroleum biodegradation. *Critical Reviews in Microbiology*
5:371-386.

Atlas, R. M. 1981. Microbial degradation of petroleum hydrocarbons. *Microbiological Reviews* 45:180-209.

Bcar, J. 1973. *Dynamics of Fluids in Porous Media,* 764 pp. Elsevier, Amsterdam.

Bhandari, A., C. D. Dennis, and J. Novak. 1994. Soil washing and biotreatment of petroleum-contaminated soils. *Journal of Environmental Engineering* 120(5):1151-1169.

Blacker, S., and D. Goodman. 1994. Risk-based decision making ease study: Application at a Superfund cleanup. *Environmental Science and Technology* 28(11):471-477.
Briant, J. 1961. Theses: Les phenomenes electrocinetiques en milieu hydrocarbure et l'epaissuer de la double couche. La revue de l'institut Francais du petrole et annals des combustibles liquids. Vol. XVI, no. 6, p. 1 – 48, no. 7-8, p. 49 – 75.

Burnett, W. E., and W. W. Loo. 1994. In-situ bioremediation of gasoline in soil and groundwater: A case history. Paper presented at the Superfund XV Conference, Washington, D. C.

Chilingar, G. V. 1952. Possible utilization of electrophoretic phenomenon for separation of fine sediments into grades. *Journal of Sedimentary Petrology* 22(1): 29-32.

Chilingar, G. V., L. G. Adamson, R. A. Armstrong, and C. M. Beeson. 1964. Soils stabilized through electroosmosis. *Southwest Builder and Contractor* 145(24): 100-102.

Chilingar, G. V., L. G. Adamson, and H. H. Rieke 111. 1966. Notes on application of electrokinetic phenomena in soil stabilization. In *Proceedings of the International Clay Conference, Jerusalem,* Vol. *1,* pp. 81 -89.

Chilingar, G. V., L. G. Adamson, H. H. Rieke, and R. R. Gray. 1968b. Electrochemical treatment of shrinking soils. *Engineering Geology* 2(3): 197-203.

Chilingar, G. V., S. A. Amba, and C. M. Beeson. 1965. Application of electrokinetic phenomena in civil engineering and petroleum engineering. *Annals of the New York Academy of Science* 118(14): 585-602.

Chilingar, G. V., C. M. Beeson, and S. A. Amba. 1968a. Uso de corriente electrica directa para aumentar la proportion del fluxo de fluidos en 10s yacimientos: Effecto del tipo de arcilla sobre la produccion de flujo. *Ingenieria Petrolera* 5(3): 22-32.

Chilingar, G. V., K. S. Chang, J. E. Davis, H. J. Farhanghi, L. G. Adamson, and S. Sawabini.1968c. Possible use of direct electrical current for augmenting reservoir energy during petroleum production. *Compass of Sigma Gamma Epsilon* 45(4): 272-285.

Chilingar, G. V., A. El-Nassir, and R. G. Stevens. 1970. Effect of direct electrical current on permeability of sandstone cores. *Journal of Petroleum Technology* 22(7): 830-836.

Chilingar, G. V., W.W. Loo, L.F. Khilyuk, and S. A. Katz. 1997. Electrobioremediation of soils contaminated with hydrocarbons and metals: progress report. Energy sources, 19:129-146.

Chilingar, G. V., Buryakovsky, L.A., Eremenko, N.A., and Gorfunkel, M.V., 2005. Geology and Geochemistry of Oil and Gas, Elsevier, 370 pp.

Cozzarelli, I. M., J. S. Herman, and M. J. Baedecker. 1995. Fate of microbial metabolites of hydrocarbons in a coastal plain aquifer: The role of electron acceptors. *Environmental Science and Technology* 29: 458-469.

El Gawad, E. A., Lotfy, M.M., Sadooni, F.N., 2008, Sedimentology and hydrocarbon potentiality of arid Sabkha, UAE., Journal of Applied Sciences Research, 4 (9), pp:1124-1130.

Fairless, B. 1990. Applying total quality principles to Superfund planning, Part 11: DQOS in Superfund-A dioxin case study. In *Proc. American Society of Quality Control 17th Annual Meeting, Enew Division Session L, Tucson, Arizona,* pp. 17-21.

Halbert, P. F. 2006. *Handbook of Construction Cost*.

Harton, J. H., S. Hamid, E. Abi-Chedid, and G. V. Chilingar. 1967. Effect of electrochemical treatment on selected physical properties of clayey silt. *Engineering Geology* 2(3): 191-196.

Hicks, R. E., and S. Tondorf. 1994. Electrorestoration of metal contaminated soils. *Environmental Science and Technology* 28(12): 2203-2210.

Hinchee, R. E., D. C. Downey, R. R. Dupont, P. K. Aggarwal, and R. Miller. 1991. Enhancing biodegradation of petroleum hydrocarbons through soil venting. *Journal of Hazardous Materials* 27: 315-325.

Hopper, D. R. 1989. Cleaning up contaminated sites. *Chemical Engineering* (August): 94-110.

Huesemann, M. H. 1994. Guidelines for landtreating petroleum hydrocarbon contaminated soils. *Journal Soil Contamination* 3:299-318.

Huesemann, M. H. 1995. Predictive model for estimation of extent of petroleum hydrocarbon biodegradation in contaminated soils. *Environmental Science and Technology* 29(1): 7-18.

Katz, S. A., L. F. Khilyuk, and G. V. Chilingar. 1996. Sensitivity analysis and multivariant modeling for formation pressure and temperature fields in inhomogeneous media. *Journal of Petroleum Science and Engineering* 1695-108.

Kendall, C. G., Alsharhan, A.S. and Whittle, G.L., 1995, Holocene carbonate/evaporites of Abu Dhabi, United Arab Emirates-Field trip guidebook, International conference on "Quaternary deserts and climatic change,"published by the united Arab Emirates University.

Lageman, R., W. Pool, and G. Seffings. 1989. *Chem. Ind.* 18575.

Lancelot, F., H. Londiche, and G. De Marsily. 1987. Experimental results on the influence of electric fields on the migration of oil, ionic species and water in porous media. *Journal of Petroleum Science and Engineering*, 4(1990): 67-74.

Langnes, G.I., Robertson, J.O., and Chilingar, G.V., 1972. *Secondary Recovery and Carbonate Reservoirs*, Elsevier, 304 pp.

Leahy, J. G., and R. R. Colwell. 1990. Microbial degradation of hydrocarbons in the environment. *Microbiology Review* (54): 305-315.

Lee, M. D., J. M. Thomas, R. S. Borden, P. B. Bedient, C. H. Ward, and T. J. Wilson. 1988. Biorestoration of aquifers contaminated with organic compounds. *CRC Critical Reuiews in Environmental Control* 18: 29-89.

Loo, W. W. 1991. Heat enhanced bioremediation of chlorinated solvents and toluene in soil.
Pmc. of HMCRI R & D Conf., Anaheim, Calif., pp. 133-136.

Loo, W.W. 1993. Biotreatment of chlorinated solvents in soil and groundwater utilizing glucose as the co-substrate. Paper presented at the Hazmacon Conf., San Jose, Calif.

Loo, W. W. 1994. Electrokinetic enhanced passive in situ bioremediation of soil and groundwater containing gasoline, diesel and kerosene. Paper presented at the Hazmacon Conf., San Jose, Calif.

Loo, W. W., I. S. Wang, and K. T. Fan. 1994. Electrokinetic enhanced bioventing of gasoline in clayey soil: A case history. Paper presented at the Superfund XV Conference, Washington, D. C.

Mahaffey, W. R., G. Compeau, M. Nelson, and J. Kinsella. 1991. Developing strategies for PAH and TCE bioremediation. *Wafer and Environmental Technology* 3233-86. McCarty, P. L. 1991. Engineering concepts for in situ bioremediation. *Journal of Hazardous Materials* 28: l-10.

Morgan, P., and R. J. Watkinson. 1989. Hydrocarbon degradation in soils and methods for biotreatment. *Critical Reuiews in Biotechnology* 8:305-333.

Nash, J. H., and R. P. Traver. 1988. Field application of pilot soil-washing system. EPA Document EPA/68-03-3450. Office of Research and Development, US. Environmental Protection Agency, Cincinnati, Ohio.

Nelson, M. J. K., et al. 1987. Biodegradation of TCE and involvement of an aromatic biodegradative pathway. *Applied Environmental Microbiology* 5:949-954.

Nunno, T. J., J. A. Hyman, and T. H. Pheiffer. 1988. Assessment of international technologies for Superfund applications. EPA Document EPA/540/2-88/003, 37 pp. Office of Solid Waste and Emergency Response. U.S. Environmental Protection Agency, Washington, D.C.

Pamukcu, S., Wittle, J.K. 1993. Electronically enhanced *in-situ* soil decontamination.

Pamukcu, S., Wittle, J.K. 1993. Electrokinetic treatment of contaminated soils, sludges and lagoons. *DOE Contract No. 02112406.*

Pamukcu, S., Wittle, J.K. 1994. Electrokinetic removal of coal tar constituents from contaminated soils. *EPRI TR-103320, Project 2879-21.*

Pamukcu, S., Weeks, A., Wittle, J.K. 1997. Electrochemical extraction and stabilization of selected inorganic species in porous media. *Journal of hazardous materials, 55, 305 – 318.*

Pamukcu, S., Weeks, A., Wittle, J.K. 2004. Enhanced reduction of Cr(VI) by direct electrical current in a contaminated clay. *Environmental Science Technology, 38, 1236 – 1241.*

Pamukcu, S. Personal communication 2008.

Pheiffer, T. H. 1990. EPA's assessment of European contaminated soil treatment techniques.*Environmental Progress* 49582-587.

Pollard, S. J. T., S. E. Hmdey, and P. M. Fedorak. 1994. Bioremediation of petroleum and creosote-contaminated soils: A review of constraints. *Waste Management and Research* 12:173-194.

Pheiffer, T. H. 1990. EPA's assessment of European contaminated soil treatment techniques.*Environmental Progress* 49582-587.

Probstein, R. F., P. S. Renaud, and A. P. Shapiro. 1991. Electroosmosis techniques for removing hazardous materials from soil. US. Patent 5074986.

Raymond, R. L., J. 0 Hudson, and V. W. Jamison. 1976. Oil degradation in soil. *Applied Environmental Microbiology* 31: 522-535.

Renaud, P. S., and R. F. Probstein. 1987. Electroosmotic control of hazardous waste. *PhysicoChemical Hydrodynamics* 9(1/2): 345.

Shapiro, A. P., and R. F. Probstein. 1993. Removal of contaminants from saturated clay by electroosmosis. *Environmental Science Technology* 27(2): 283-291.

Shapiro, A. P., P. S. Renaud, and R. F. Probstein. 1989. Preliminary studies on the removal of chemical species from saturated porous media by electroosmosis. *PhysicoChemical Hydrodynamics* 11(5/6):785.

Sims, R. S. 1990. Soil remediation techniques at uncontrolled hazardous waste sites: A critical review. *Journal of the Air Waste Management Association* 40: 704-732.

Smoluchowski, von M. 1921. Handbuch der Electrizitat und des Magnetismus, 11. Translated by P. E. Bocque. In *Engineering Research Bulletin* 33:47-158.

Stinson, M. K., H. S. Skovronek, and W. D. Ellis. 1992. EPA Site demonstration of the BioTrol soil washing process. *Journal of the Air and Waste Management Association* 42:96-103.

Ungcrcr, *P.,* J. Burrus, B. Doligez, P. Y. Chenet, and F. Bessis. 1990. Basin evaluation by integrated two-dimensional modeling of heat transfer, fluid flow, hydrocarbon generation, and migration. *Petroleum Geology Bulletin* 74(3):309-335.

Visschcr, K., J. Brinkman, and E. R. Soczo. 1990. Biotechnology in hazardous waste management in the Netherlands. In *Biotechnology and Biodegradation: Advances in Applied Biotechnology,* Vol. 4, pp. 389-403. Gulf Publ. Co., Tx.

Wittle, J.K.; D.G. Hill, and G.V. Chilingar. SPE 114012, 2008, Direct current electrical enhanced oil recovery in heavy-oil reservoirs to improve recovery, reduce water cut, and reduce H_2S production while increasing API gravity.

Wilson, J. T., 1985. Biotransformation of TCE in soil. *Applied Environmental Microbiology,*
1:242-243.

Appendix A: Nomenclature

Nomenclature used for specimen ID:

KS: Kaolinite in distilled water

KG: Kaolinite in ground water

KH: Kaolinite in water containing 900 ppm of humic substances in solution.

As: Arsenic

Cd: Cadmium

Cr: Chromium

Pb: Lead

H: High concentration

L: Low concentration

Nomencalture for Abu Dhabi offshore mud sample IDs electroremediated for 24 hour period:

ADOM:Abu Dhabi Offshore Mud
RICOM: Ruwais Industrial Complex Offshore Mud
L: Low Concentration
H: High Concentration
SW: Abu Dhabi seawater with 26,000ppm
PH: 450 ppm of Maleic acid for pH control
AG: Silver
AL: Aluminum
AS: Arsenic
BA: Barium
BE: Berellium
BI: Bismuth
CD: Cadmium
CR: Chromium
CO: Cobalt
CU: Copper
CS: Cesium

GA: Gallium
IN: Indium
LI: Lithium
MN:Manganese
NI: Nickel
PB: Lead
RB: Rubidium
SE: Selenium
SR: Strontium
TI: Titanium
UR: Uranium
V: Vanadium
ZN:Zinc